



UNIVERSITÀ DELLA
CALABRIA

UNIVERSITY OF CALABRIA

Department of Pharmacy, Health and Nutritional Sciences

PhD in “Traslational Medicine”

CYCLE XXXII

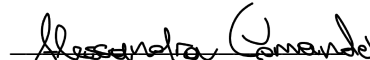
“Synthetic strategies towards short-chain peptides for potential biomedical applications and tumor-targeted mesoporous silica-based drug delivery systems development”

Research Area: CHIM/06

Coordinator: Ch.mo Prof. Sebastiano Andò

Supervisor: Prof.ssa Antonella Leggio

PhD Student: Dott.ssa Alessandra Comandé



Abstract

My PhD research project was focused on the design and development of short-chain peptides with biomedical applications and on the identification of new peptide synthesis strategies.

Briefly, the specific objectives of my research work were the following:

- Design and synthesis of novel methylated tetrapeptides acting as leptin antagonists with potentially improved stability and pharmacokinetic properties compared to the non-methylated analogue leptin antagonist LDFI.
- Identification and synthesis of a novel peptide ligand able to recognize CD38, a marker overexpressed on multiple myeloma (MM) cells, for the targeted delivery of bortezomib, the drug of choice for this type of cancer.
- Design and synthesis of new peptide entities to use as inhibitors linked to chelators to produce new molecular probes for prostate cancer imaging via PET.
- Identification of new and efficient peptide synthesis strategies aimed at obtaining small peptides in the solution phase. The developed strategies can prove useful for obtaining biologically active peptides.
- Development of a targeted MSN-based nanocarrier bearing the anticancer drug doxorubicin and grafted, on the external surface, with folic acid (FOL-MSN-DOXO). The system developed in this study provides an attractive template to develop more selective DOXO delivery systems by using peptides as targeting ligands.

The present thesis consists of published work (papers) and work in progress (ongoing works) that must still be completed in order to be published in the future.

Peptide sequences and their structural characterizations have been omitted in ongoing work 1 and in ongoing work 2 since a patent application is going to be filed for both products.

Table of contents

1. General Introduction	1
1.1. Strategies to overcome the limitations of peptides	2
1.2. <i>N</i> -methylation approach	4
1.3. Therapeutic peptides in cancer treatment: a brief overview	5
1.4. The aim of the work	7
References.....	16
2. Solid-phase synthesis of <i>N</i>-methylated analogues of the leptin antagonist tetrapeptide LDFI	22
Abstract.....	22
2.1. Introduction.....	23
2.2. Results and Discussion.....	27
2.3. Experimental Section	32
2.3.1. Materials	32
2.3.2. Synthesis of <i>N</i> -Fmoc- <i>N</i> -methyl- α -aminoacids.....	32
2.3.3. Peptide Synthesis	33
2.4. Outlook	35
References.....	36
3. Synthesis of a new peptide ligand for targeting CD38 receptor on multiple myeloma cells	38
Abstract.....	38
3.1. Introduction.....	39
3.2. Results and Discussion.....	46
3.3. Experimental Section	50
3.3.1. Materials	50
3.3.2. Microwave assisted peptide synthesis protocol.....	50
3.3.3. Peptide analysis.....	51
3.3.4. Mesoporous silica nanoparticles analysis.....	51
3.3.5. Synthesis of Mesoporous Silica Nanoparticles.....	52
3.3.6. Transmission electron microscopy (TEM) and electron immunocytochemistry.....	53
3.4. Conclusion and future work	54
References.....	55
4. Synthesis of novel PSMA-targeted tracers as diagnostic tools for prostate cancer	57
Abstract.....	57

4.1. Introduction.....	58
4.2. Results and Discussion.....	61
4.3. Experimental.....	75
4.3.1. Material and instrumentation.....	75
4.3.2. Synthesis of THP-PSMA ligands.....	76
4.3.2.1. Synthesis of Resin bound PSMA.....	76
4.3.2.2. Synthesis of bidentate pyridinone.....	77
4.3.2.3. Synthesis of Tripodal tris(hydroxypyridinone) ligands.....	80
4.4. Conclusions and outlook.....	88
References.....	89
5. Formation of amides: One-pot condensation of carboxylic acids and amines mediated by TiCl₄.....	91
Abstract.....	91
5.1. Introduction.....	92
5.2. Results and discussion.....	95
5.3. Experimental.....	104
5.3.1. General experimental details.....	104
5.3.2. General procedure for the synthesis of amides 1-28.....	104
5.4. Conclusion.....	110
References.....	111
6. A titanium tetrachloride-based effective methodology for the synthesis of dipeptides.....	113
Abstract.....	113
6.1. Introduction.....	114
6.2. Results and discussion.....	116
6.3. Experimental.....	123
6.3.1. General experimental details.....	123
6.3.2. General procedure for the synthesis of dipeptides 1-18.....	123
6.4. Conclusions.....	132
Notes and references.....	133
7. Alternative formation of amides and β-enaminones from aroyl chlorides using the TiCl₄-trialkylamine reagent system.....	136
Abstract.....	136
7.1. Introduction.....	137
7.2. Results and discussion.....	139
7.3. Experimental.....	146

7.3.1. General experimental details	146
7.3.2. General procedures for the synthesis of amides and β -enaminones.	146
7.4. Conclusions	152
Notes and references	153
8. Synthesis and Characterization of Large Pore MSU-Type Mesoporous Silica	155
Abstract.....	155
8.1. Introduction.....	156
8.2. Materials and methods	157
8.3. Results and Discussion.....	159
8.4. Conclusions.....	161
References.....	162
9. Mesoporous silica-based nanocarriers for pH-triggered doxorubicin delivery in cancer therapy	163
Abstract.....	163
9.1. Introduction.....	165
9.2. Results and Discussion.....	167
9.2.1. MSNs conjugated with DOXO via pH-sensitive imine bond.	169
9.2.2. MSNs conjugated with DOXO via pH-sensitive hydrazone bond.....	174
9.3. Experimental	178
9.3.1. Materials and experimental details	178
9.3.2. General synthesis of Folic acid-targeted MSNs (FOL-MSN).....	179
9.3.2.1. Synthesis of Mesoporous Silica Nanoparticles (MSNs).....	179
9.3.2.2. Synthesis of AP-MSN.....	179
9.3.2.3. Synthesis of FOL-MSN	179
9.3.3. Synthesis of MSNs conjugated with DOXO via pH-sensitive imine bond (FOL-MSN-IM-DOXO).....	180
9.3.3.1. Synthesis of MSN-AP _{in} (inner surface functionalization)	180
9.3.4. Synthesis of MSNs conjugated with DOXO via pH-sensitive hydrazone bond (FOL-MSN-HYD-DOXO)	181
9.3.5. <i>In vitro</i> experiments	183
9.3.6. <i>In vitro</i> release studies.....	184
9.4. Conclusion and Outlook.....	185
References.....	186

1

General Introduction

The therapeutic application of peptides is constantly increasing because of their versatility for the development of molecules for both diagnostics and therapy.¹ Nowadays, approximately 60 peptide drugs are approved by the FDA and more than 600 are in preclinical and clinical trials, and different diseases are treated using peptide-based drugs.²⁻³

Peptides are involved in a wide variety of physiological and biochemical processes as they act as neurotransmitters,⁴ hormones,⁵⁻⁶ growth factors,⁷ and signaling molecules.⁸ Besides, peptides also have an interesting pharmacological profile as they are used as antibiotics,⁹⁻¹⁰ antimicrobials,¹¹⁻¹² anticancer,¹³ gastroprotection,¹⁴ opioids,¹⁵ and in recent decades are successfully employed as target molecules.¹⁶

The use of peptides and short sequences of peptides in the pharmacological field results in significant advantages such as high selectivity and effective, high potency, excellent safety with low adverse effects, biological and chemical variety (Table 1).¹⁷⁻²¹ On the other hand, the main drawbacks of peptides are their proteolytic degradation by enzymes, poor oral bioavailability, risk of immunogenic effects (Table 1).²²

Table 1. Advantages and disadvantages of therapeutic peptides (adapted from 21).

Advantages	Disadvantages
High potency	Metabolic instability
High selectivity	Short circulating half-life
Wide range of targets	Poor oral bioavailability
Low toxicity	Poor solubility
Less toxic degradation products	Rapid body clearance
Low accumulation in tissues	Possible immunogenic effects
High biological and chemical variety	High manufacturing cost

As potential therapeutics, peptides have several advantages over small molecules, proteins and antibodies. In fact, small molecules are less specific than peptides, proteins, and antibodies are more complicated to synthesize, have poor delivery to the tumor because of their large size, have dose-limiting toxicity and are not able to penetrate the cell membranes.²³⁻²⁴

1.1. Strategies to overcome the limitations of peptides

The potential of peptides as drugs is limited by their unfavorable ADME (absorption, distribution, metabolism, and excretion) properties. The major part of peptides has less than 1% oral bioavailability,²⁵ very short *in vivo* half-life, low cell membrane permeability due to the high hydrogen-bonding capacity, low lipophilicity, fast proteolytic degradation and a rapid renal clearance (Table 1).²⁶

The short half-life is the main issue of peptides, in fact they are cleared from the bloodstream within minutes to hours, due to fast renal clearance and enzymatic degradation in blood, kidneys and liver, so this reduces the exposure time in the target tissue.²⁷ In fact, peptides with a molecular mass below 5kDa and unbound to plasma proteins have a fast renal clearance.²⁸ Enzymatic degradation is due to soluble enzymes present in the blood and membrane-bound enzymes and to a broad variety of peptidases.²⁹

Over the years, various strategies have been developed to achieve improvement in their pharmacokinetic properties and many of these are chemical modifications (Figure 1).

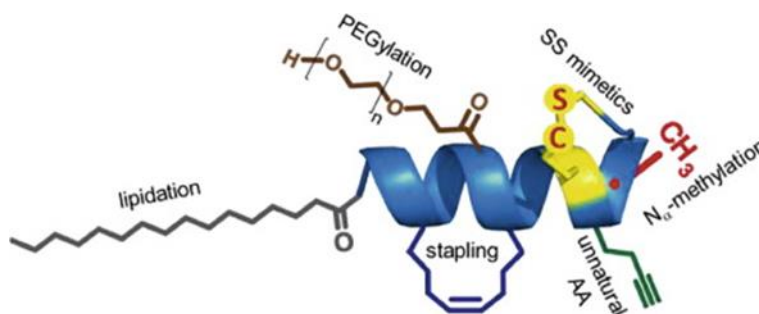


Figure 1. Different chemical modifications on the peptide structure (adapted from 26)

An important strategy, to extend half-life time, consists in replacing natural amino acids with non-natural analogues (*N*-methylation, D-amino acids, β -amino acids) in sites susceptible to enzymatic cleavage (Table 2).³⁰ These replacements decrease the substrate recognition and binding affinity of proteolytic enzymes and increase stability. Cyclization is another interesting approach, there are different type of cyclizations such as head-to-tail, side-chain with side-chain, head/end to side-chain.³¹ These modifications can also decrease the hydrogen-bonding potential and so improve the oral bioavailability and intestinal permeability.

Table 2. Peptide backbone modifications

Modification	Effects
-C α -alkylated amino acid	-Increased hydrophobicity.
-N α -alkylated amino acid	-Reduction of flexibility.
- β^3 amino acids	-Decrease of hydrogen-bonds potential.
-D-amino acids	-Conformational constraints. -Enzymatic stabilization. -Improve half-life. -Improve stability.
-backbone cyclization	-Increase membrane permeability.
-modification of amide bonds	-Decrease of hydrogen-bonds potential. -Increased hydrophobicity.

The introduction of PEG molecules on the peptide sequence can lead to considerable advantages.³² PEG is often conjugated to N or C termini of peptides and can protect them from the action of peptidases thus increasing their stability. Furthermore, PEG increases the size of the peptide thereby preventing renal filtration, and increasing the hydrodynamic radius of the peptide improving thus renal clearance.³³

The approach of lipid conjugation to the peptides can increase the half-life by stabilizing the structure of the peptides.³⁴ Lipidated peptides can bind to human serum albumin, which has a protective effect and ensures a prolonged time of circulating peptide.²⁶

Another strategy is the introduction of differently sized polymers, which make peptides soluble both in water and organic solvents, and can prevent the proteolytic action and increase the size over improving the renal clearance.³⁵

1.2. *N*-methylation approach

The methylation of nitrogen atoms in peptide backbone is a very useful manipulation that allows improving properties such as intestinal and cellular permeability,³⁶ stability to enzymatic proteolysis,³⁷ lipophilicity,³⁸ and binding affinity.³⁹

This chemical modification is often found in natural peptides including the immunosuppressor cyclosporin A with seven *N*-methylated peptide bonds (Figure 2),⁴⁰ omphalotin,⁴¹ natural cyclic peptides etc.⁴²

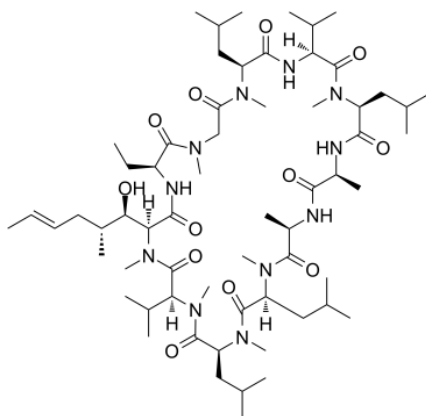


Figure 2. Cyclosporin A structure

N-methylation is mainly used to protect the peptide from enzymatic degradation. However, *N*-methylation causes conformational constraint because it limits the predominance of *trans* versus *cis* bond configuration.⁴³ In addition, the methyl group can sterically interact with the side chain of the adjacent residue.⁴⁴

The introduction of the methyl group has also effects on the hydrogen-bonding potential as the replacement of the proton-donator NH-group reduces the number of inter and intramolecular hydrogen bonds.⁴⁵

1.3. Therapeutic peptides in cancer treatment: a brief overview

The discovery of a wide variety of protein/peptide receptors and tumor-related peptides and proteins made therapeutic peptides interesting and promising anticancer agents. Commonly, peptides can be directly used as cytotoxic agents or as carriers of cytotoxic agents and radioisotopes by selectively targeting cancer cells.⁴⁶

The introduction of recombinant display technologies (phage, yeast, bacteria, DNA/RNA) has made it possible to detect high-affinity peptides against most protein targets.⁴⁷

Anticancer effects of different peptides involve the inhibition of angiogenesis ($\alpha\beta$ peptides),⁴⁸ protein-protein interactions (β -peptides),⁴⁹ signal transduction pathways⁵⁰ and apoptosis induction (RGD peptides),⁵¹ moreover, they can act as agonist and antagonist of a specific receptor.^{46, 52}

Among peptides with antitumor activity, very interesting and promising are peptides that permeabilize membranes with cytotoxic effects.⁵³ This peptide class could be classified into three major groups:

antimicrobial peptides, cell-permeable peptides and tumor targeting peptides (Figure 1).

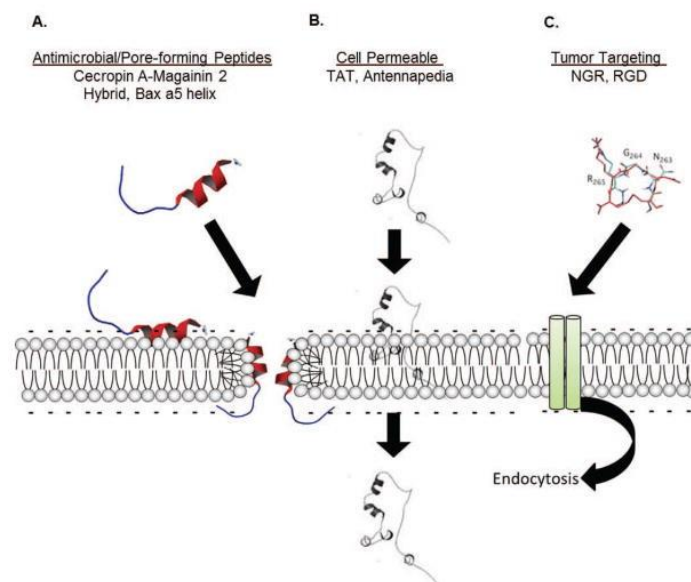


Figure 1. Illustration of action mechanisms of antimicrobial/pore-forming peptides, cell permeable peptides and tumor targeting (adapted from 31).

Anti-microbial peptides(AMPs), such as Cecropins, Defensins, Magainins, are made up of about 10-14 amino acids and have a cationic amphipathic structure thanks to which they can interact with anionic lipid membranes.⁵⁴ They are naturally part of the innate immune response to microbes in many organisms.

Lipid membranes are the main target of the major part of AMPs, and they induce the cytotoxic effect through apoptosis or necrosis. Because of their mechanism of action, these peptides can be used as anti-cancer agents.⁵⁵

Cell permeable peptides are short amino acid oligomers (5–30 residues) that can permeate the cell membrane via endocytosis and direct translocation.⁵⁶ The conjugation of these peptides with cell-impermeable substances such as proteins, antibodies, antisense oligonucleotides drugs, and nanoparticles is a very useful strategy for intracellular delivery.⁵⁷⁻⁵⁸ HIV-Tat peptide,⁵⁹ penetratin (Antp),⁶⁰ and Tat⁶¹ are the most studied examples of cell permeable peptides.

The recent discovery of tumor biomarkers allowed the introduction of targeted therapies in which specific molecular targets present only on tumor cells are exploited for drug delivery. The presence of these target receptors is crucial, as peptide-binding can induce high levels of internalization by endocytosis processes. This mechanism can, therefore, be exploited for the intracellular delivery of drugs.⁶²

Cancer cell surface targets are usually identified rationally through structure-activity studies.⁶³ Peptides are promising alternative targeting molecules due to their smaller size, and they can also bind to their targets with high specificity and affinity.

One of the best examples of receptor-targeted peptide, for active targeting strategies, is the Integrins. These proteins are heterodimers transmembrane receptors overexpressed in endothelial cells of the tumor.⁶⁴⁻⁶⁵

1.4. The aim of the work

My PhD research project was aimed to design and develop small peptides for biomedical applications and smart drug delivery systems in targeted anti-cancer therapy.

Firstly, the peptide Leu-Asp-Phe-Ile (LDFI), a leptin-receptor antagonist we previously developed,⁶⁶ and its pegylated analogue (LDFI-PEG) were synthesized in order to investigate and evaluate their efficacy in antagonizing leptin actions in human testicular seminoma cancer by using *in vitro* and *in vivo* experimental models.

Leptin, is a hormone consisting of 146 amino acids, involved in the control of several physiological processes, e.g. body weight regulation and appetite, fertility modulation, that performs its functions after interacting with its membrane receptor (LepR).⁶⁷

Leptin is involved in the control of several physiological processes (e.g. body weight regulation and appetite, fertility modulation, bone formation, angiogenesis and insulin secretion).⁶⁸⁻⁷¹ Moreover, *in vitro* and *in vivo* studies have shown leptin has also a role in the pathogenesis of various tumor forms: testicular, breast, prostate, colon and pancreatic cancers.⁷²⁻⁷⁶ In hormone-dependent cancers, such as breast and colon cancer, leptin and ObR are overexpressed and therefore proposed as prognostic markers.⁷⁷⁻⁷⁹

The LDFI peptide acts as a full leptin antagonist, in fact *in vitro* studies on mammary tumor cells, showed the inhibitory effects on the leptin-induced growth of ER α -positive (MCF-7) and ER α -negative (SKBR3) breast cancer cells.⁸⁰

In prostatic cancer, LDFI has suppressed leptin's effect on JAK2, ERK1/2 and Akt/PKB phosphorylation as well as activation of apoptotic proteins.⁸¹

Our results showed that the treatment with the leptin antagonist LDFI significantly reduced the leptin-induced growth and motility in seminoma tumor cells (TCam-2 cells). Furthermore, the *in vivo* xenograft experiments showed that LDFI-PEG treatment markedly decreased seminoma tumor growth (A. Comandè *et al.* 2019, *Am J Pathol*).⁷²

The use of peptides and short peptide sequences in the pharmacological field has significant advantages such as high efficacy and selectivity, high target specificity, low toxicity and low accumulation in tissues. However, factors as metabolic instability, limited bioavailability and reduced half-life limit their use as therapeutic agents.⁸² Peptide

poor bioavailability is mainly due to rapid enzymatic degradation by peptidase, which occurs both in the gastro-intestinal tract and in the circulatory stream.⁸³

The introduction of methylated amino acids into the peptide chain is a widely used strategy to improve the pharmacokinetic profile of peptides in terms of increased lipophilicity, metabolic stability and bioavailability.⁸⁴

Based on these considerations, two tetrapeptides (**peptide a** and **peptide b**) analogues of the LDFI peptide methylated on selected amide bonds in order to enhance the proteolytic stability and the therapeutic potential of LDFI, were synthesized (*Ongoing work 1*).

The *N*-methylated peptides were easily prepared by solid phase synthesis methods starting from *N*-Fmoc-*N*-methyl amino acids for the purpose synthesized.

In vitro studies of the as-synthesized methylated peptides on leptin induced breast cancer cell proliferation, showed that they inhibit effectively the leptin-induced growth as well as migration in both ER α -positive and ER α - negative breast cancer cells.

Stability assays of the methylated peptides to study peptide degradation and evaluate the stabilization of the leptin antagonist by *N*-methylation are ongoing. The study of the proteolytic degradation in the blood of the two methylated peptides will be performed by incubating in parallel LDFI and its methylated analogues in plasma and comparing their degradation profiles. The remaining peptides and degradation products will be identified through mass spectrometry.

In the last years, peptides have attracted great interest in the field of drug delivery and nanomedicine. Peptide-conjugates in fact, are able to direct therapeutic agents selectively towards specific biological targets.⁸⁵

In these applications, peptides can act by crossing the cytoplasmic membrane and allowing the internalization of structurally disadvantaged molecules (CPP) or acting as cell-targeting peptides (CTP).⁸⁶ Peptides are particularly suitable for this purpose since they are small, easy to synthesize and generally non-immunogenic furthermore they have high affinities and specificities for their receptors.

Cell-targeting peptides (CTP), interacting with high affinity with the target receptor overexpressed on cancer cells allow the internalization of the peptide-conjugates selectively into cancer cells thus reducing the side effects associated with anticancer therapies.⁸⁷

My research activity in the field of targeted drug delivery was aimed to the development of a highly selective delivery system of Bortezomib (BTZ), a drug of choice for the treatment of multiple myeloma (*Ongoing work 2*).⁸⁸

Multiple myeloma (MM) is a B-cell malignancy characterized by an abnormal proliferation of plasma cells. Due to the high accumulation of misfolded or unfolded proteins in the endoplasmic reticulum (ER), the use of proteasome inhibitors constitutes the main therapeutic choice for this malignancy. Proteasome inhibition generates an accumulation of these proteins, activating apoptotic pathways and consequent cell death.

Bortezomib, a dipeptide boronic acid, is an antineoplastic agent that acts by inhibiting the chemotrypsin-like activity of proteasome 26S. Although bortezomib is a potent proteasome inhibitor, it has many associated side effects such as chronic peripheral neuropathy that limit its use as an anticancer drug.⁸⁹

Therefore, the development of new and highly efficient BTZ delivery systems represents a particularly attractive goal.

Recently, exploiting the high biocompatibility and versatility of mesoporous silica nanoparticles (MSNs), we developed a new MSN-based delivery system of Bortezomib (FOL-MSN-BTZ).⁹⁰

The MSN-based nanodevice (FOL-MSN-BTZ) employs a receptor-specific ligand (folic acid, FOL) on the external surface of MSNs while the antitumor drug Bortezomib is linked, mainly on the pore walls, through a pH-sensitive bond thus, it preferentially delivers the drug to FOL-expressing target tissues, protecting the drug from premature release and avoiding undesired side effects.

Folic acid was chosen as targeting function since it has a high affinity for folate receptor (FR), a tumor associated protein, which is overexpressed in a large number of tumours⁹¹ while it is present at low levels in most normal tissues.

The *in vitro* tests of FOL-MSN-BTZ on cancer cells overexpressing the folate receptor (FR+ cells) including the human FR α -/FR β - multiple myeloma cells lines and on FR-normal cells showed that it induces death in FR+ cancer cells but not in FR- normal cells while free BTZ was toxic for all cell lines tested, independently on their FR expression. Finally, the biocompatibility of FOL-MSN-BTZ at increasing concentrations and its antitumor activity was demonstrated in mouse xenograft models. However, the *in vivo* experimentation indicated that our system affects moderately the mouse neuronal cells

functionality. Most likely this effect is due to the FR+ receptor expression in the nervous system.

In this regard, encouraged also by the remarkable results obtained with FOL-MSN-BTZ prototype we studied the possibility to improve the technology functionalizing our BTZ MSN-based delivery system with a ligand able to interact with the CD38 receptor that is a biomarker overexpressed on MM cells in order to enhance the potency and efficacy of BTZ in MM cells.

CD38 is a multifunctional cell surface protein that is expressed at very high levels on plasma cell tumors as multiple myeloma.⁹² We decided then to develop a more selective MSN-based prototype with BTZ conjugated inside the pores via pH-sensitive bond and a peptide ligand on the surface able to recognize the more specific CD38 receptor. This approach required the identification and synthesis of a peptide sequence able to bind CD38 and induce its internalization. To this aim, the interaction between CD38 receptor and specific antibodies was investigated.⁹³

On the base of the binding site of the antibody SAR650984 (Isatuximab) to CD38,⁹⁴ some short peptide chains mimicking the identified antibody paratope and that could be able to interact with CD38 receptor were hypothesized. Then the interactions of the hypothesized peptides with the CD38 receptor have been simulated and evaluated by *in silico* studies. The results obtained from these computational studies have allowed us to define a pool of short amino acid sequences to synthesize and conjugate to the carrier.

We started with the synthesis of a small peptide (CD38-PEP) that was prepared using solid phase synthesis (SPPS) methodologies based on Fmoc-Chemistry. CD38-PEP is an heptapeptide containing an *N*-terminal cysteine unit, important residue for the internalization process. CD38-PEP was obtained in 68% yield, and characterized by nuclear magnetic resonance (¹H-NMR and ¹³C-NMR) and chromatographic separation techniques combined with mass spectrometry (HPLC-MS).

The conjugation of the peptide (CD38-PEP) to the nanoparticles (MSNs) was carried out through the formation of an amide bond between the amino function grafted on the nanocarrier external surface and the carboxyl function of the peptide C-terminal residue. The obtained system without BTZ inside the pores (CD38-PEP-MSN) was analyzed via transmission electron microscopy (TEM) analysis to assess the uptake of the nanocarrier

by MM RPMI-8626 cells expressing the CD38 receptor. TEM images confirmed that the recognition of CD38-PEP-MSN depends on CD-38.

These preliminary data obtained with CD38-PEP-MSN system are encouraging thus, the new synthesized CD38 peptide ligand might be an excellent substitute of folic acid for the development of a more selective CD38-PEP-MSN-BTZ prototype, since CD38 receptor is highly expressed on MM cells.

During my doctoral course, I spent a 6 month period research at King's College London, where I worked on a project centred on peptide synthesis and (bio)-conjugation of peptide inhibitors to metal chelators (*Ongoing work 3*).

I developed a library of PSMA small peptide inhibitors related to a tris-hydroxypyridinone (THP) chelator to produce a total of four new THP-PSMA molecular probes for prostate cancer imaging via PET.

Prostate cancer is the second most prevalent cancer for men worldwide. The progression of this type of cancer is very slow and can take up to 15 years for its full development into metastatic lesions.⁹⁵ However, due to the little symptoms it expresses, its diagnosis at an early stage is difficult to perform. Therefore, screening for early signs of prostate cancer is of clinical importance to detect it before it metastases and spreads to areas where it will be too difficult to eradicate. This has lead research to develop pharmaceutical therapies personalized around individuals with prostate cancer. Prostate-Membrane Specific Antigen (PSMA) is a protease overexpressed in almost all types of prostate cancer cells and has been the target of a lot of researches for this type of cancer.⁹⁶

PSMA is a type II transmembrane glycoprotein (100-120 kDa) that consists of three distinct domains: an intracellular domain (1-18 amino acids), a transmembrane domain (19-43 amino acids), as well as a large extracellular domain (44-750 amino acids).⁹⁷ PSMA has unique enzymatic functions where it is responsible for glutamate production by cleaving *N*-acetylaspartylglutamate (NAAG) to generate glutamate and *N*-acetylaspartate (NAA). Peptide inhibitors are able to be conjugated to a radioactive metal, such as gallium-68, lesions containing this peptide will be detectable via Positron Emission Tomography (PET).⁹⁸⁻¹⁰⁰

New ⁶⁸Ga-Tris(hydroxypyridinone)-PSMA ligands useful for the prostate cancer diagnosis were designed and synthesized. Two final compounds with a longer chain have

been synthesized, and will be purified through semi-preparative HPLC, characterized and then will be performed *in vitro* experiments to evaluate the cellular uptake and binding affinity. The characterization of the two ligands consisting of a shorter chain is currently underway. The systems thus composed may act as ^{68}Ga radiotracer for imaging PSMA expression.

Within the scope of peptide synthesis, my research activity also concerned the identification of new and efficient synthetic strategies to obtain small peptide systems in solution phase with the aim to extend afterward the developed methodologies also to the solution and solid phase synthesis of modified and biologically active peptides.

The most general way for obtaining peptides involves the activation of the carboxylic function of the *N*-terminal amino acid by means its conversion into the corresponding acid chloride¹⁰¹⁻¹⁰² or by using coupling reagents.¹⁰³⁻¹⁰⁴ The direct formation of amide bond by condensing the non activated carboxylic component and the amine component by using metal-mediated procedures represents an alternative to coupling reagent.¹⁰⁵⁻¹⁰⁶

Since titanium tetrachloride (TiCl_4) manifests a strong affinity for the oxygen atom and increases, the susceptibility of carbonyl-containing compounds towards nucleophiles, also promoting dehydration reactions, the use of titanium tetrachloride (TiCl_4) as condensing agent in the direct reaction between carboxylic acids and amines was proposed (*Paper I*).¹⁰⁷

Firstly, the TiCl_4 -mediated amidation reaction was investigated for the synthesis of secondary and tertiary amides starting from a series of aliphatic and aromatic carboxylic acid and amines precursors.

The amidation reaction was performed at 85 °C in pyridine, and using an excess of TiCl_4 to accelerate the reaction. The reaction was tested with a wide range of substrates providing the corresponding amide products in moderate to excellent yields and high purity. The reaction proceeds with low yields when both the carboxylic acid and the amine are sterically hindered. The process takes place with nearly complete preservation of the stereochemical integrity of chiral substrates. The synthesis involves the activation of the carboxylic function by TiCl_4 , thus facilitating the attack of the amine and the formation of a good leaving group. Titanium tetrachloride therefore acts as a condensing agent.

Solution phase peptide synthesis is the method of choice for preparing dipeptides and more generally small peptides. This strategy, although is not well suited for making longer peptides, is much more scalable, and allows to produce larger quantities of high-quality peptides, and at a lower cost than solid phase. The formation of amide bond is of particular importance for the purposes of stereochemistry preservation of the chiral centres of the amino acids that participate in the condensation reaction. Therefore, the development of new methods of peptide bond formation in liquid phase is particularly attractive in order to obtain dipeptides or small peptides since this methodology can also be used with non-natural or unusual amino acids.

In this context, and considering the successful results above described concerning the use of titanium tetrachloride as condensing agent in the amidation reaction, the applicability of titanium tetrachloride for the formation of peptide systems was investigated.

The use of titanium tetrachloride (TiCl_4) for the formation of the peptide bond was by no means obvious. In fact, TiCl_4 could deprotect not only the amino functions of *N*-protected amino acids as it occurs with other Lewis acids¹⁰⁸⁻¹¹⁰ but also the amino acid side chain functional groups. Accordingly, we tested the reaction in a pyridine-buffered medium.

A series of dipeptide systems have been synthesized in high yields through a TiCl_4 -assisted condensation reaction of *N*-protected α -amino acids with α -amino acid methyl ester hydrochlorides in pyridine (*Paper 2*).¹¹¹ Using pyridine as reaction solvent has proved useful not only to convert the ammonium group of amino acid methyl ester hydrochloride into the free amino function able to react as nucleophile in the condensation reaction, but also to preserve the protecting groups on the masked functionalities. The reaction was applied successfully to amino acids protected on the α -amino function with different protecting groups (Fmoc, Boc, Cbz and Nosyl groups). The recovery of the dipeptide products has been achieved by simple filtration through a silica gel column, which greatly simplifies the reaction work-up and avoids the formation of emulsions and product losses. Furthermore, the preservation of the stereochemical integrity at the amino acid chiral centres was evaluated. The maintenance of amino acids stereochemical integrity is almost complete for dipeptides protected on the amino function with urethane protecting groups (Fmoc, Cbz, Boc). A nonnegligible loss of stereochemical integrity was instead observed in *N*-nosyl-protected dipeptides.

Currently, the developed synthesis method has also been applied to tripeptide systems by exploiting the ability of titanium tetrachloride to remove acid-labile groups in side chains on amino acids and peptides subjected to coupling for the formation of the peptide bond, this new extension is still under investigation.

An alternative synthesis of tertiary amides was carried out by treating acyl chlorides, lacking of hydrogen atoms at the carbon atom alpha to the carbonyl group, with TiCl_4 in the presence of a tertiary amine (NR_3) (*Paper 3*).¹¹² By using the reagent system $\text{TiCl}_4/\text{NR}_3$ two different ways of performing the reaction were established leading to the formation of completely different main products as the result of two diverse reaction pathways (Method A and Method B). The reactions of variously substituted benzoyl chlorides with the $\text{TiCl}_4/\text{NR}_3$ reagent system according to method A and method B, both modulated by the presence of TiCl_4 , afforded alternatively the corresponding amides and β -enaminones as unique or major products. The two developed protocols were investigated with a series of tertiary amines

Titanium tetrachloride forms with the alkyl tertiary amine an ammonium ion adduct. In the presence of an excess of amine this adduct generates, through an elimination process, the amide (Method A). The formation of the amide with the proposed method A is quite general.

When the molar ratio of the amine and TiCl_4 is 1:1, the produced ammonium ion is oxidized generating an organotitanium compound that leads to the formation of β -enaminone (Method B). This mechanism operates when the amine is not in excess and is added slowly. The reported study represents a new example of reactivity of $\text{TiCl}_4\text{-NR}_3$ reagent system with aroyl chlorides involving carbon-carbon bond formation.

Lastly, as part of my research project I also worked on the development of a MSN-based anticancer prodrug systems for active targeting delivery of doxorubicin (*Ongoing work 4*).

The development of the system started with the identification of a new synthesis protocol for obtaining nanoparticles with ideal features for the transport of the drug (*Paper 4*).¹¹³ Doxorubicin is an antineoplastic drug clinically used in different type of malignancies but with serious limitations due to an undesired systemic toxicity.¹¹⁴

The use of carrier systems e.g. polymeric nanoparticles, liposomes, micelles and more able to control DOXO release and lower down the administered dose represents an important approach to overcome these limits.¹¹⁵⁻¹¹⁷

In the last few years among drug delivery systems, mesoporous silica-based nanoparticles (MSNs) have gained considerable interest thanks to their attractive structural and morphological properties. Furthermore, due to their biocompatibility and the presence on their surfaces of silanol groups (SiOH) that can be appropriately functionalized, they have been extensively investigated for therapeutic and diagnostic purposes, especially in oncology.¹¹⁸⁻¹²²

The target was the development of devices having stimuli-responsive properties and able to release the drug, exploiting the pH difference between the circulatory stream and the tumor intracellular microenvironment.

The developed FOL-MSN-HYD-DOXO nanocarrier, consists of nanometric silica frame that presents, folic acid (FOL) covalently linked to the external surface of particles as targeting function (folate receptor specific ligand) and doxorubicina (DOXO) linked within the pores by means of hydrazone acid-labile bond.

For our purpose, we have used folic acid as targeting molecule to mediate specific uptake by cancer cells.

The effect of FOL-MSN-HYD-DOXO on cell proliferation was evaluated on FR+ and FR- cell lines.

FOL-MSN-HYD-DOXO gave interesting results since it showed a good FR+ cancer cell killing efficacy and consequently an enhanced cellular uptake by FR positive cancer cells and a negligible cytotoxicity to FR- negative cells.

The developed system FOL-MSN-HYD-DOXO represents a versatile drug delivery system useful as template for the development of a highly selective and efficient targeted DOXO delivery systems in which the targeting function is a peptide molecule that, interacting with specific receptors overexpressed on cancer cells, addresses the drug exclusively to cancer cells avoiding the normal ones.

References

1. S. Galdiero, P.A. C. Gomes, *Molecules*, **2017**, *22*, 2185-2190.
2. M. Erak, K. Bellmann-Sickert, S. Els-Heindl, A. G. Beck-Sickinger, *Bioorganic & Medicinal Chemistry*, **2018**, *26*, 2759–2765.
3. B.G. de la Torre, and F. Albericio, *Molecules*, **2019**, *24*, 809;
4. L. A. Devi, L. D. Fricker, **2016**, *Transmitters and Peptides: Basic Principles*. In: Pfaff D., Volkow N. (eds) *Neuroscience in the 21st Century*. Springer, New York, NY
5. J. A. Hutchinson, S. Burholt, I. W. Hamley, *J. Pept. Sci.*, **2017**, *23*: 82–94.
6. Y. Nakagawa, T. Nishikimi, K. Kuwahara, *Peptides*, **2019**, *111*, 18-25.
7. R. R. Beerli, N. E. Hynes, *J. Biol. Chem.*, **1996**, *271*, 6071-6076.
8. A. Polykratis, P. Katsoris, J. Courty, E. Papadimitriou, *J. Biol. Chem.*, **2005**, *280*, 22454-22461.
9. R.E.W. Hancock, A. Patrzykat, *Curr. Drug Targets*, **2002**, *2*, 1: 79-83.
10. R.D. Joerger, *Poultry Science*, **2003**, *82*, 4, 640–647.
11. H. Jenssen, P. Hamill, R. E.W. Hancock, *Clin Microbial. Rev*, **2006**, *19*, 3, 491–511.
12. A. A. Bahar and D. Ren, *Pharmaceuticals*, **2013**, *6*(12), 1543-1575.
13. D.L. Vesely, *J. Invest. Med.*, **2005**, *53*:360-365.
14. E Al-azzeh, O Dittrich, J Vervoorts, N Blin, P Gött, B Lüscher, *Gut*, **2002**, *51*:685-690.
15. J. Shook, J.T. Pelton, V.J. Hruby and T.F. Burks, *JEPT*, **1987**, *243*, 2, 492-500.
16. A. Falanga & S. Galdiero, *FutureMed. Chem.*, **2018**, *10*(16), 1877–1880.
17. J.L. Lau, M.K. Dunn, *Bioorganic & Medicinal Chemistry*, **2018**, *26*, 2700–2707.
18. Y. A. Haggag, A. A. Donia, M.A. Osman, S. A. El-Gizawy, *Biomed J Sci & Tech Res*, **2018**, *8*, 4, 6659-6662.
19. A. Loffet, *J. Peptide Sci.*, **2002**, *8*: 1–7.
20. A. C-L. Lee, J. L. Harris, K. K. Khanna and Ji-H. Hong, *Int. J. Mol. Sci.* **2019**, *20*, 2383.
21. V. Mäde, S. E-Heindl and A.G. Beck-Sickinger, *Beilstein J. Org. Chem.* **2014**, *10*, 1197–1212.
22. P. Vlieghe, V. Lisowski, J. Martinez and M. Khrestchatisky, *Drug Discovery Today*, **2010**, *15*, 40-56.
23. S. Marqus, E. Pirogova and T. J. Piva, *J Biomed Sci*, **2017**, *24*:21.
24. A.K Sato, M. Viswanathan, R.B Kent and C.R Wood, *Curr Opin Biotechnol*, **2006**, *17*:638–642.
25. X.H. Zhou, A. Li Wan Po, *Int J Pharm.* **1991**, *75*, 2–3, 117–30.
26. M.Erak, K. Bellmann-Sickert, S. Els-Heindl, A.G. Beck-Sickinger, *Bioorganic & Medicinal Chemistry*, **2018**, *26*, 2759–2765.
27. M. Werle and A. Bernkop-Schnürch, *Amino Acids*, **2006**, *30*: 351–367.

28. H. Akizawa, T. Uehara, Y. Arano, *Adv Drug Deliv Rev*, **2008**, 60, 12, 1319-1328.
29. C. Adessi, C. Soto, *Curr Med Chem.*, **2002**, 9, 16, 963-978.
30. J.S. Davies, *J. Peptide Sci.*, **2003**, 9, 471-501.
31. R. Rink, A. Arkema-Meter, I. Baudoin, E. Post, A. Kuipers, S.A. Nelemans, M. Haas, J. Akanbi, G.N. Moll, *J Pharmacol Tox Met*, **2010**, 61, 2, 210-218.
32. F.M. Veronese, G. Pasut, *Drug Discov Today*, **2005**, 10:1451-1458.
33. I.W. Hamley, *Biomacromolecules* **2014**, 15, 5, 1543-1559.
34. B.P. Ward, N.L. Ottaway, D. Perez-Tilve, D. Ma , V.M. Gelfanov , M.H. Tschöp, R.D. Dimarchi, *Mol Metab.*, **2013**;2:468-479.
35. J.Y. Shu, B. Panganiban, T. Xu, *Annual Review of Physical Chemistry*, **2013**, 64:631-657.
36. O. Ovadia, S. Greenberg, J. Chatterjee, B. Laufer, F. Opperer, H. Kessler, C. Gilon, and A. Hoffman, *Mol. Pharmaceutics*, **2011**, 8, 479-487.
37. J. Shaji and V. Patole, *Indian J Pharm Sci.*, **2008**, 70, 3: 269-277.
38. D.P. Fairlie, G. Abbenante, D.R March, *Curr. Med. Chem.*, **1995**, 2, 654-686.
39. M.A. Dechantsreiter, E. Planker, B. Matha, E. Lohof, G. Holzemann, A. Jonczyk, S. Goodman, H. Kessler, *J. Med. Chem.*, **1999**, 42,16, 3033-3040.
40. Y. In, T. Ishida, K. Takesado, *J. Pept. Res.*, **1999**, 53, 492.
41. A. Mayer, H. Anke, O. Sterner, *Natural Product Letters*, **1997**, 10:1, 25-32.
42. Y. Hamada, T. Shioiri, *Chem. Rev.*, **2005**, 105, 4441-4482.
43. H. Kessler, *Angew. Chem.* **1970**, 82, 237 - 253.
44. S. Sagan, P. Karoyan, O. Lequin, G. Chassaing, S. Lavielle, *Current Medicinal Chemistry*, **2004**, 11, 2799-2822.
45. J. Deska, U. Kazmaier, *Current Organic Chemistry*, **2008**, 12: 355.
46. J. Thundimadathil, *Journal of Amino Acids*, **2012**, Article ID 967347.
47. C.G. Ullman, L. Frigotto and R.N. Cooley, *Brief Funct Genomics.*, **2011**, 10, 3:125-134.
48. D.Paris, K. Townsend, A. Quadros, J. Humphrey, J. Sun, S. Brem, M. Wotoczek-Obadia, A. DelleDonne, N. Patel, D.F. Obregon, R. Crescentini, L. Abdullah, D. Coppola, A.M. Rojiani, F. Crawford, S.M. Sebti, M. Mullan, *Angiogenesis*, **2004**, 7: 75.
49. J.A. Kritzer, O.M. Stephens, D.A. Guarracino, S.K. Reznika, A. Schepartz, *Bioorganic & Medicinal Chemistry*, **2005**, 13, 11-16.
50. C. Borghouts, C. Kunz, B. Groner, *Peptide Sci.*, **2005**, 11: 713-726.
51. C.D. Buckley, D. Pilling, N.V. Henriquez, G. Parsonage, K. Threlfall, D. Scheel-Toellner, D.L. Simmons, A.N. Akbar, J.M. Lord, M. Salmon, *Nature*, **1999**, 397, 534-539.
52. A. Leggio, S. Catalano, R. De Marco, I. Barone, S. Andò, A. Liguori. *Eur J Med Chem.* **2014**, 6, 78:97-105.
53. R.J. Boohaker, M.W. Lee, P. Vishnubhotla, J.M. Perez, A.R. Khaled, *Curr Med Chem.*, **2012**, 19(22): 3794-3804.
54. D. Gaspar, A.S. Veiga, M.A.R.B. Castanho, *Front. Microbiol.*, **2013**, 4:294.

55. D.W. Hoskin, A. Ramamoorthy, *Biochimica et Biophysica Acta*, **2008**, 1778, 357–375.
56. T. Tashima, *Bioorganic & Medicinal Chemistry Letters*, **2017**, 27, 121–130.
57. N. Tsomaia, *Eur J Med Chem*, **2015**, 94, 459470.
58. I. Nakase, Y. Konishi, M. Ueda, H. Saji, S. Futaki, *Journal of Controlled Release*, **2012**, 159, 2, 181-188.
59. U. Niesner, C. Halin, L. Lozzi, M. Günthert, P. Neri, H. Wunderli-Allenspach, L. Zardi, D. Neri, *Bioconjugate Chem.* **2002**, 13, 4, 729-736.
60. I. D. Alves, C. Bechara, A. Walrant, Y. Zaltsman, C-Y Jiao, S. Sagan, *PLoS ONE*, **2011**, 6, 9, 24096.
61. H. Brooks, B. Lebleu, E. Vivès, *Advanced Drug Delivery Reviews*, **2005**, 57, 4, 559-577.
62. D. Tesauro, A. Accardo, C. Diaferia, V. Milano, J Guillon, L. Ronga, F. Rossi, *Molecules*, **2019**, 24, 351.
63. D. Kwekkeboom, E.P. Krenning, M. de Jong, *J Nucl Med.* **2000**, 41, 10:1704-13.
64. D. Hallahan, L. Geng, S. Qu, C .Scarfone, T. Giorgio, E. Donnelly, X. Gao, J. Clanton, *Cancer Cell*, **2003**, 3, 1, 63-74.
65. K Chen, X Chen, *Theranostics*. **2011**, 1: 189–200.
66. A. Liguori, S. Andò, A. Leggio, S. Catalano, R. De Marco, I. Barone, **2014**, Italian Patent, CS2014A000016, 28/04/2014.
67. S. Margetic, C. Gazzola, G.G. Pegg, R.A. Hill, *International Journal of Obesity*, **2002**, 26, 1407-1433.
68. F. Peelman, K. Van Beneden, L. Zabeau, H. Iserentant, P. Ulrichs, D. Defeau, A. Verhee, D. Catteuw, D. Elewaut, J. Tavernier, *J. Biol. Chem.*, **2004**, 279, 41038-41046.
69. S. Margetic, C. Gazzola, G.G. Pegg, R.A. Hill, *Int J Obes*, **2002**, 26, 1407-1433.
70. H. Lu, C. Li, *Cell Res.*, **2000**, 10, 81- 92.
71. P. Ducy, M. Amling, S. Takeda, M. Priemel, A.F. Schilling, F.T. Beil, J. Shen, C. Vinson, J.M. Rueger, G. Karsenty, *Cell*, **2000**, 100, 197-207.
72. R.B. Ceddia, H.A. Koistinen, J.R. Zierath, G. Sweeney, *FASEB J.*, **2002**, 16:10, 1163-1176.
73. S. Panza, L. Gelsomino, R. Malivindi, V. Rago, I. Barone, C. Giordano, F. Giordano, A. Leggio, A. Comandè, A. Liguori, S. Aquila, D. Bonofiglio, S. Andò, S. Catalano, *Am. J. Pathol.*, **2019**, 189:3, 687-698.
74. H. Jensen, P. Hamill, R.E.W. Hancock, *Clin Microbial. Rev*, **2006**, 19, 3, 491–511.
75. S. Andò, S. Catalano, *S. Nat. Rev. Endocrinol.*, **2012**, 8, 263-275.
76. S. Andò, L. Gelsomino, S. Panza, C. Giordano, D. Bonofiglio, I. Barone, S. Catalano, *Cancers*, **2019**, 11, 62.
77. D. Housa, J. Housova, Z. Vernerova, M. Haluzik, *Physiol. Res.*, **2006**, 55, 233-244.

78. C. Garofalo, M. Koda, S. Cascio, M. Sulkowska, L. Kanczuga-Koda, J. Golaszewska, A. Russo, S. Sulkowski, E. Surmacz, *Clin Cancer Res*, **2006**, *12*(5), 1447-1453.
79. S. Samuel-Mendelsohn, M. Inbar, E. Weiss-Messer, L. NivSpector, A. Gertler, R.J. Barkey, *The Prostate*, **2011**, *71*, 929–945.
80. S. Catalano, A. Leggio, I. Barone, R. De Marco, L. Gelsomino, A. Campana, R. Malivindi, S. Panza, Cinzia Giordano, A. Liguori, D. Bonofiglio, A.Liguori, and S. Andò, *J Cell Mol Med*. **2015**, *19*, 5: 1122–1132.
81. C. Giordano, F. Chemi, S. Panza, I. Barone, D. Bonofiglio, M. Lanzino, A. Cordella, A. Campana, A. Hashim, P. Rizza, A. Leggio, B. Györffy, B.M. Simões, R.B. Clarke, A. Weisz, S. Catalano, S. Andò, *Oncotarget.*, **2016**, *7*(2):1262–1275.
82. Q. Liu, I.A. Kriksunov, R. Graeff, C. Munshi, H.C. Lee, Q. Hao, *Structure*, **2005**, *13*, 1331-1339.
83. E. Biron, J. Chatterjee, O. Ovadia, L. Langenegger, J. Brueggen, D. Hoyer, H. Schmid, R. Jelinek, C. Gilon, A. Hoffman, H. Kessler, *Angew. Chem., Int. Ed.*, **2008**, *47*, 2595-2599.
84. J. Chatterjee, F. Rechenmacher, H. Kessler, *Angew. Chem., Int. Ed.*, **2013**, *52*, 254.
85. M. Das, C. Mohanty, S. K Sahoo, *Expert Opin. Drug Deliv.*, **2009**, *6*, 3: 285-304.
86. E. Vivès, J. Schmidt, A. Pèlegri, *Biochimic Biophys Acta*, **2008**, *1786*, 126–138.
87. N. Tsomaia, *Eur J Med Chem.*, **2015**, *13*, 94:459-470.
88. K.A. Sarosiek, L.E. Cavallin, S. Bhatt, N.L. Toomey, Y. Natkunam, W. Blasini, A.J. Gentles, J.C. Ramos, E.A. Mesri, I.S. Lossos, *Proc. Natl. Acad. Sci. U. S. A.*, **2010**, *107*, 13069–13074.
89. T. Hideshima, P. Richardson, D. Chauhan, V.J. Palombella, P.J. Elliott, J. Adams, K.C. Anderson, *Cancer Res*, **2001**, *61*:3071-3076.
90. L. Pasqua, A. Leggio, A. Liguori, C. Morelli, S. Andò, (2016) "Bortezomib-Based Delivery System". EP3288955B1, Publication number, WO2016174693 A1. Application number PCT/IT2016/00011 Owned of NanoSilical Devices Srl, spin-off of the University of Calabria
91. L. Pasqua, F. Testa, R. Aiello, S. Cundari, J.B. Nagy, *Micropor Mesopor Mat*, **2007**, *103*, 166-173.
92. N.W. Van de Donk, M.L. Janmaat, T. Mutis, J.J Lammerts van Bueren, T. Ahmadi, A.K Sasser, H.M. Lokhorst, P.W. Parren, *Immunol Rev*, **2016**, *270*, 1: 95-112.
93. A. Chillemi, G. Zaccarello, V. Quarona, M. Ferracin, C. Ghimenti, M. Massaia, A.L. Horenstein, F. Malavasi, *Mol Med*, **2013**, *19*: 99-108.
94. M-K. Han, S-J Kim, Y-R. Park, Y-M. Shin, H-J Park, K-J. Park, K-H. Park, H-K. Kim, S-I. J., N-H. An, U-H. Kim, *J. Biol. Chem.*, **2002**, *277*:5315-5321.
95. N. Borley, M.R. Feneley, *Asian J. Androl*, **2009**, *103*, 356-387.

96. S.S. Chang, *Rev Urol.*, **2004**, 6 (Suppl 10): S13-S18.
97. A. Ghosh and W.D.W. Heston, *J Cell Bioch*, **2004**, 91:528–539.
98. C. Imberti, Y-L. Chen, C.A. Foley, M.T. Ma, B.M. Paterson, Y. Wang, J.D. Young, R.C. Hider and P.J. Blower, *Dalton Trans.*, **2019**, 48, 4299-4313.
99. J.D. Young, V. Abbate, C. Imberti, L. K. Meszaros, M.T. Ma, S.Y.A. Terry, R.C. Hider, G.E. Mullen, P.J. Blower, *J Nucl Med*, **2017**, 58: 1270-1277.
100. R. Cusnir, C. Imberti, R. C. Hider, P. J. Blower and M. Ma, *Int. J. Mol. Sci.*, **2017**, 18, 116-139.
101. C.A.G.N. Montalbetti, V. Falque, *Tetrahedron*, **2005**, 61:10827–10852.
102. A. Leggio, M.L. Di Gioia, F. Perri, A. Liguori, *Tetrahedron*, **2007**, 63:8164–8173.
103. J.R. Dunetz, J. Magano, G.A. Weisenburger, *Org Process Res Dev*, **2016**, 20:140–177.
104. J.D. Goodreid, P.A. Duspara, C. Bosch, R.A. Batey, *J Org Chem*, **2014**, 79:943–954.
105. E. Valeur, M. Bradley, *Chem Soc Rev*, **2009**, 38:606–631.
106. C.L. Allen, A.R. Chhatwal, J.M.J. Williams, *Chem Commun*, **2012**, 48:666–668.
107. A. Leggio, J. Bagalà, E.L. Belsito, A. Comandè, M. Greco, A. Liguori, *Chemistry Central Journal*, **2017**, 11:87.
108. A. Leggio, A. Liguori, A. Napoli, C. Siciliano, and G. Sindona, *Eur. J. Org. Chem.*, **2000**, 5732575.
109. M.L. Di Gioia, A. Leggio, A. Le Pera, A. Liguori, F. Perri, C. Siciliano, *Eur. J. Org. Chem.*, **2004**, 4437-4441.
110. M.L. Di Gioia, A. Leggio, A. Le Pera, C. Siciliano, G. Sindona, A. Liguori, *J. Peptide Res.*, **2004**, 63, 383–387.
111. A. Comandè, M. Greco, E.L. Belsito, A. Liguori, A. Leggio, *RSC Adv.*, **2019**, 9, 22137-22142.
112. A. Leggio, A. Comandè, E.L. Belsito, M. Greco, L. Lo Feudo, A. Liguori, *Org. Biomol. Chem.*, **2018**, 16, 5677-5683.
113. N. Garofalo, A. Comandè, I. Perrotta, M. Davoli, G. Niceforo, L. Pasqua, *Advanced Science Letters*, **2017**, 23, 6026-6028.
114. T. Šimunek, M. Štirba, O. Popelová, M. Adamcová, R. Hrdina, V. Geršl, *Pharmacological Reports*, **2009**, 61, 154–171.
115. L. Brannon-Peppas, J.O. Blanchette, *Adv Drug Deliv Rev*, **2012**, 64, 206-212.
116. N. Zhao, M.C Woodle, and A.J. Mixson, *J Nanomed Nanotechnol.*, **2018**, 9, 5: 519.
117. D.N. Waterhouse, P.G. Tardi, L.D. Mayer, M.B. Bally, *Drug-Safety*, **2001**, 24: 903.
118. I. Slowing, J.L. Vivero-Escoto, C-W. Wu, VS-Y. Lin, *Adv. Drug Deliv.Rev.*, **2008**, 60, 1278-1288.

119. A. Nigro, M. Pellegrino, M. Greco, A. Comandè, D. Sisci, L. Pasqua, A. Leggio, C. Morelli, *Pharmaceutics*, **2018**, 10, 250.
120. L. Pasqua, I.E. De Napoli, A. Leggio, C. Morelli, A. Comandè, A. Nigro, M. Greco, G. Montera, “Engineered Stimuli-Responsive Nanoparticles for the Interaction With Biological Structures”, *Chemistry of Silica and Zelite-based Materials: Synthesis, Characterization and Applications*, Elsevier, Chapter 21, 399-412, **2019**.
121. S. Jafaria, H. Derakhshankhaha, L. Alaeib, A. Fattahia, B.S. Varnamkhastia, A.A. Sabouryb, *Biomed Pharmacother.*, **2019**, 109, 1100-1111.
122. R. Narayan, U.Y. Nayak, A.M. Raichur, and S. Garg, *Pharmaceutics*, **2018**, 10, 3: 118.

Solid-phase synthesis of *N*-methylated analogues of the leptin antagonist tetrapeptide LDFI

[Ongoing work 1]

Abstract

N-methylated analogues of the leptin antagonist peptide LDFI were designed and synthesized by solid phase methods using reagent systems and methodologies of Fmoc-chemistry. To this aim, specific *N*-Fmoc-*N*-methyl amino acids were synthesized and then used as building block for the solid-phase synthesis of LDFI peptide methylated on selected positions.

Their efficacy in antagonizing leptin actions in breast cancer was evaluated using in vitro experimental models. The obtained results have shown that the synthesized *N*-methylated derivatives inhibit leptin-induced proliferation and motility in human breast cancer cells.

2.1. Introduction

Leptin is a hormone belonging to the family of long-chain helical cytokines and it is encoded by the obese (*Ob*) *Lep* gene located on chromosome 7. The initial transcribed protein has a 16KD molecular weight and is composed of 167 amino acids with a 21-amino acids signal sequence at the amino-terminus, which is cleaved following the translocation of leptin into microsomes, the resulting hormone is a 146 amino acids peptide. The hormone performs its functions through the interaction with its membrane receptor (LepR or ObR) expressed both in the central nervous system and in the peripheral tissues and after binding to LepR, it allows its activation.¹

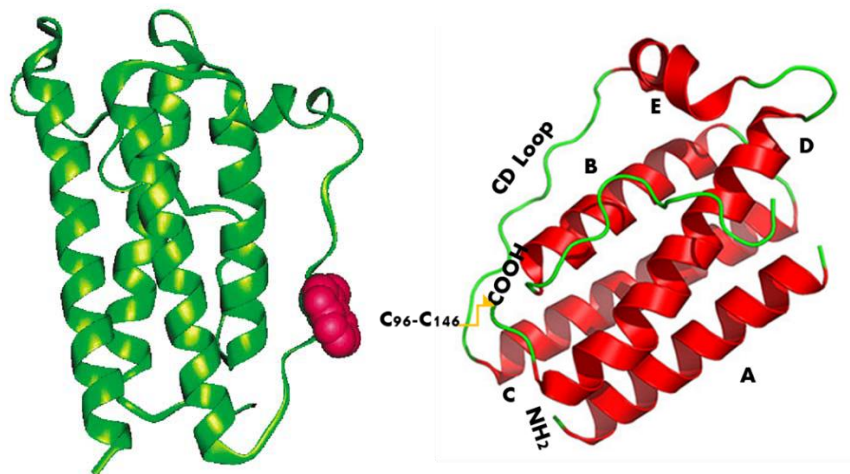


Figure 1. Three-dimensional structure of the Leptin.

Leptin is made up of four α -helices (A, B, C and D) interconnected by two long loops (AB and CD) and a shorter one (BC). The four helices are arranged in an "up-up-down-down" configuration, resulting in helices A and D being antiparallel to helices B and C. (Figure 1).²

Leptin interacts with its receptor via three different binding sites (I, II and III). Briefly, the binding site II consists of two fragments IIa and IIb formed by the residues of the helix A and helix C, while the binding site III is formed by the *N*-terminal residues of the helix D. Binding site I, that is formed by the connection loop between helices A and B, plays a key role in the formation of the leptin-leptin receptor complex and in the receptor activation.³

Leptin is involved in the control of several physiological processes, e.g. body weight regulation and appetite, fertility modulation, bone formation, angiogenesis and insulin secretion.⁴⁻⁷

Moreover, *in vitro* and *in vivo* studies have shown leptin is involved in the pathogenesis of various tumor forms: testicular, breast, prostate, colon and pancreatic cancers.⁸⁻¹²

In hormone-dependent cancers, such as breast and colon cancer, leptin and ObR are overexpressed and therefore were proposed as prognostic markers.¹³⁻¹⁵ It seems evident that leptin represents a novel therapeutic target and that its antagonists may constitute a new class of anticancer drugs.

The amino acid sequence 39-42, located in the loop that connects helices A and B, is essential for activation of the leptin receptor and represents the main target region that can be modified for obtaining ObR antagonists.²

Recently we designed and developed, based on the wild-type sequence of leptin binding site I, a leptin antagonist: the short-chain peptide LDFI, consisting of four amino acids (Leucine-Aspartic acid-Phenylalanine-Isoleucine, Figure 2).¹⁶⁻¹⁸

LDFI peptide and its pegylated analogue produced very interesting and promising results as they proved effective in antagonizing leptin actions in breast cancer by reducing breast tumor progression both *in vitro* and *in vivo*. The LDFI peptide acts as full leptin antagonist, in fact *in vitro* studies on mammary tumor cells, showed the inhibitory effects on the leptin-induced growth of ER α -positive (MCF-7) and ER α -negative (SKBR3) breast cancer cells. The peptide did not interfere with cell proliferation in the absence of leptin and did not produce any significant cytotoxic effects at all the doses tested.¹⁷

Moreover, using the same leptin receptor antagonist on breast cancer stem cells (BCSC) showed reduced mammosphere formation, blocking the stromal-tumor interactions driving BCSC-mediated disease progression.¹⁸

Recently, it was observed that the expression of leptin and its receptor was notably elevated in human testicular seminoma unlike to normal adult testis. Treatment of TCam-2 cells (Human seminoma cell line) with the peptide LDFI (leptin receptor antagonist) markedly decreased seminoma tumor growth and the expression of leptin-regulated genes (A. Comandè *et al.* 2019, *Am J Pathol*).⁸

The LDFI have been also used for the identification of specific exosome signatures and to find molecular effectors associated with cancer progression, to aim interrupt the

dangerous cell-to-cell communication in cancer; showing as leptin/leptin receptor/Hsp90 axis is as an important regulator of exosome generation in mammary carcinoma cells.¹⁹ Furthermore, since LDFI does not act as receptor agonists in the absence of leptin, it overcomes the therapeutic limit of other known peptide antagonists.

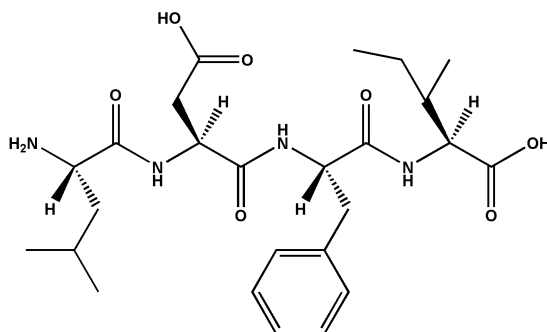


Figure 2. Primary structure of the Leptin antagonist LDFI

Intending to improve the pharmacokinetic properties of LDFI, we decided to explore the possibility of changing the structural properties of the peptide by replacing some amino acid residues of LDFI chain with modified amino acid analogues able to enhance the proteolytic stability and therefore also the biological activity of LDFI.

In general, peptides and short peptide sequences are considered promising therapeutic molecules thanks to their high efficacy and selectivity, high target specificity, low systemic toxicity and low tissue accumulation, furthermore they are easy and fast to synthesize.

However, many factors limit the use of peptides as therapeutic agents such as reduced half-life, metabolic instability, limited bioavailability and poor membrane permeability.²⁰

The low bioavailability of protein and peptide drug, caused by their instability and poor membrane permeation, constitutes a major drawback for the development of medicinal products since it leads to a poor control over plasma concentrations and as well as pharmacological effects.

The oral peptide delivery is limited by the low absorption and by the acid pH of the stomach that induces peptide ionization. The ionization is responsible for the secondary and tertiary structure alterations of larger peptides. The low bioavailability of peptides following oral administration is also attributed to their inactivation through enzymatic

degradation by peptidases present in the gastrointestinal tract.²¹ Administration by injection (parenteral administration) also has limitations due to the instability of peptides toward peptidases in the systemic blood circulation that causes rapid elimination (i.e., short half-life).²²

Proteolytic degradation of peptide-based drugs represents one of the major factors limiting systemic therapeutic applications. Hence, peptide sequences of drug candidates are modified to remove patterns recognized by proteases or to induce structural features preventing proteolysis.

Several strategies have been used to generate peptides with enhanced enzymatic stability and improved oral bioavailability. These include structural modifications such as covalent attachment of polyethylene glycol, lipidation and chemical modifications such as cyclization, D-amino acid substitution, and *N*-methylation of the peptide backbone.²³⁻²⁷

Backbone *N*-methylation restrains conformational freedom of peptides and also blocks potential intramolecular hydrogen bonding sites and proteolytic enzyme cleavage sites. These properties, together with the enhanced hydrophobicity, improve the bioavailability and the pharmacological properties of peptide drugs.^{20, 28}

In light of these evidence, we planned to improve the proteolytic stability and the therapeutic potential of LDFI modifying its backbone by *N*-methylation.

In this study, the synthesis and biological activity evaluation of two novel *N*-methylated analogues of LDFI is described.

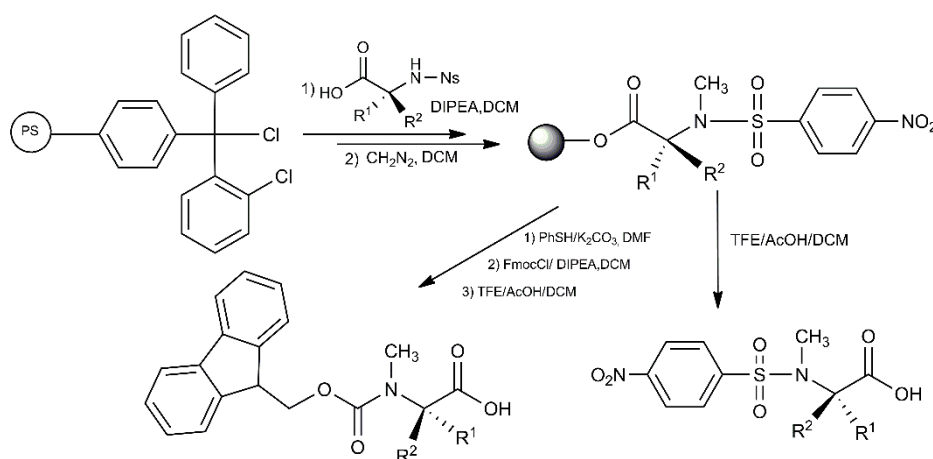
2.2. Results and Discussion

The synthesis of peptides containing *N*-methyl amino acids can be performed by using *N*-methyl amino acid derivatives as building blocks or by site-selective *N*-methylation of the peptide chain.

The *N*-methylated analogues of the leptin antagonist LDFI were synthesized by solid phase methods using reagent systems and methodologies of Fmoc-chemistry. This approach required the synthesis of *N*-Fmoc-*N*-Methyl- α -aminoacids.

Various synthetic procedures were developed for the preparation of *N*-methyl- α -amino acid derivatives²⁹ and among these, the most generally applicable approach is the *N*-methylation of *N*-arylsulfonamide-protected aminoacids.³⁰⁻³¹

For the preparation of the *N*-Fmoc-*N*-methyl- α -aminoacids we used an approach developed by our group³² based on the use of the highly acid-labile 2-chlorotrityl chloride solid support (Barlos) as carboxylic protecting group, also to exploit the advantages of solid-phase synthesis, and of α -amino acids protected on the amino function with the *p*-nitrobenzenesulfonyl (nosyl) group, while the methylation reaction is performed by using a solution of diazomethane in dichloromethane (Scheme 1)



Scheme 1. *N*-Fmoc-*N*-methyl- α -aminoacids synthesis

After the removal of nosyl group and re-protection of the amino function with the Fmoc group the *N*-Fmoc-*N*-methyl analogues of Leu, Asp, Phe and Ile were obtained in 65-75% yields.

Although the above-mentioned strategy successfully yields the *N*-Fmoc *N*-methylated amino acids in satisfactory yields, the biggest challenge is to assemble them into peptides. The coupling reactions onto the sterically hindered *N*-methyl amino acids is difficult and often unsuccessful. The couplings not only result in notoriously poor yields of the final peptide but also cause side reactions that become more problematic as coupling rates decrease.³³

Several coupling reagents have been reported to overcome these problems.³⁴

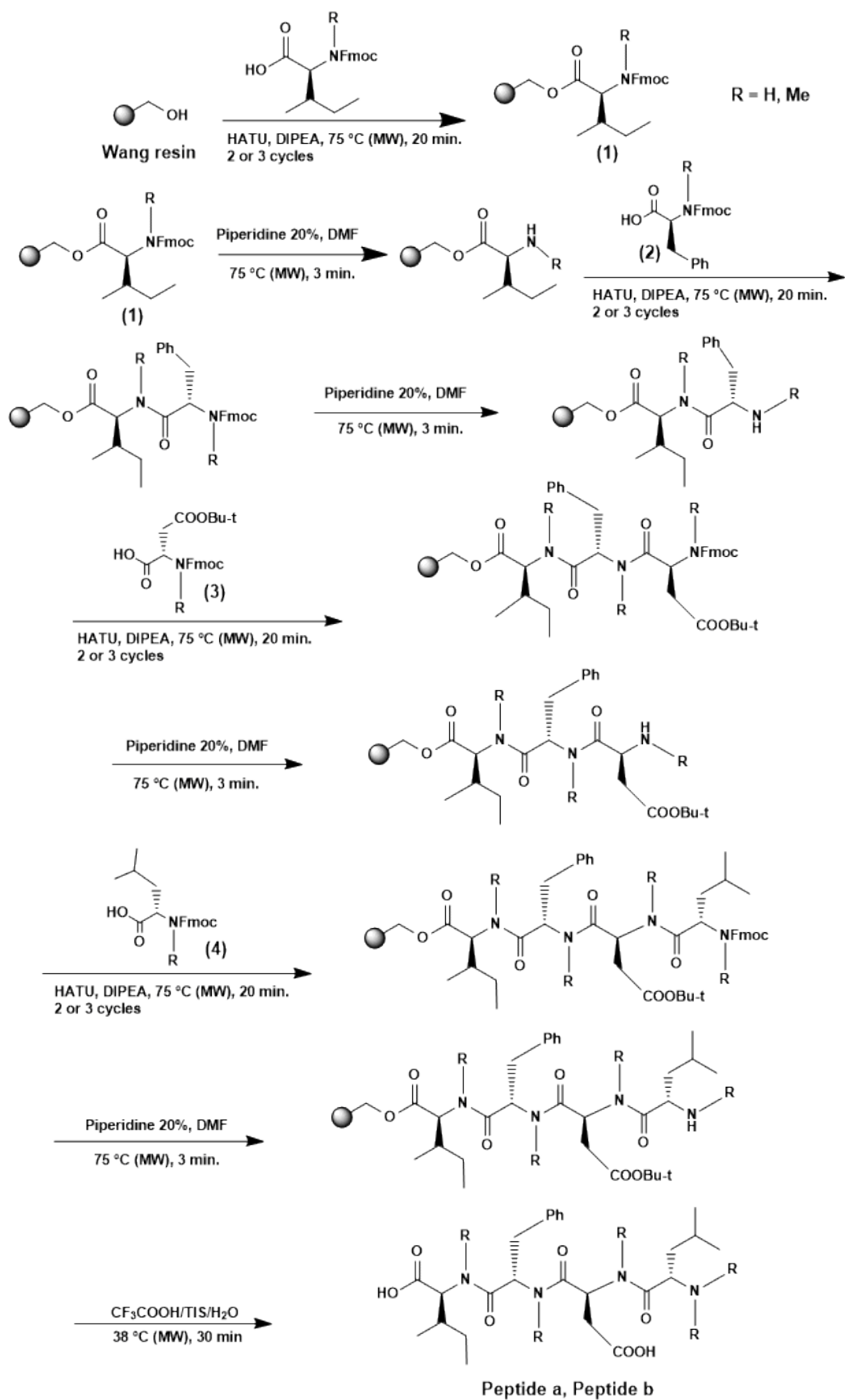
In the synthesis of the *N*-methylated LDFI analogues (Table 1), in order to improve the efficiency of couplings with *N*-methyl residues, we used the coupling reagent *O*-(7-azabenzotriazol-1-yl)-*N,N,N',N'*-tetramethyluronium hexafluorophosphate (HATU), an activating agent recommended for the acylation of *N*-Methyl amino acids in solid phase,³² and the microwave heating in addition to perform double or triple coupling cycles.

We designed and attempted the synthesis of various *N*-methylated LDFI analogues by incorporating different combinations of the synthesized *N*-methyl- α -amino acids. Then we focused our interest only onto two of them, peptide **a** and peptide **b**, that showed higher leptin antagonistic properties.

For the synthesis of peptide **a** and peptide **b** (Table 1) we used two similar protocols starting from Wang resin 100-200 mesh (0.7 mmol) or from *N*-Fmoc-L-Ile-OH anchored to the Wang resin (**1**) (0.1 mmoles, loading 0.6 mmoles/g) (Scheme 2).

Table 1. Solid phase synthesis of *N*-methylated LDFI analogues

Peptide	Yield
a	70%
b	60%



Scheme 2

Coupling reactions were performed in DMF with fivefold excess of *N*-Fmoc-*N*-Me-L-amino acids, and *N*-Fmoc-L-amino acids, and in the presence of HATU (5.0 equivalents) and DIPEA (10 equivalents) for 20 min. at 75°C. The Fmoc protecting group was removed by treatment of the resin with a 20% solution of piperidine in DMF at 75°C.

The peptide was cleaved from the resin using a mixture of TFA, water, and TIS (9.5/0.25/0.25 by volume) for 30 min. at 38 °C. Following cleavage the peptides **a** and **b** were obtained in 70% and 60% yield respectively by precipitation with cold diethyl ether (Scheme 2).

Both peptides (**a** and **b**) were characterized by ¹H NMR, ¹³C NMR and ESI-QTOF-MS analyses. ESI-MS/MS data were collected to elucidate the peptide structure.

The ¹H NMR spectra showed the incorporation of the *N*-methylated residues and confirmed the structure of the synthesized methylated derivatives. All signal assignments were made by decoupling experiments.

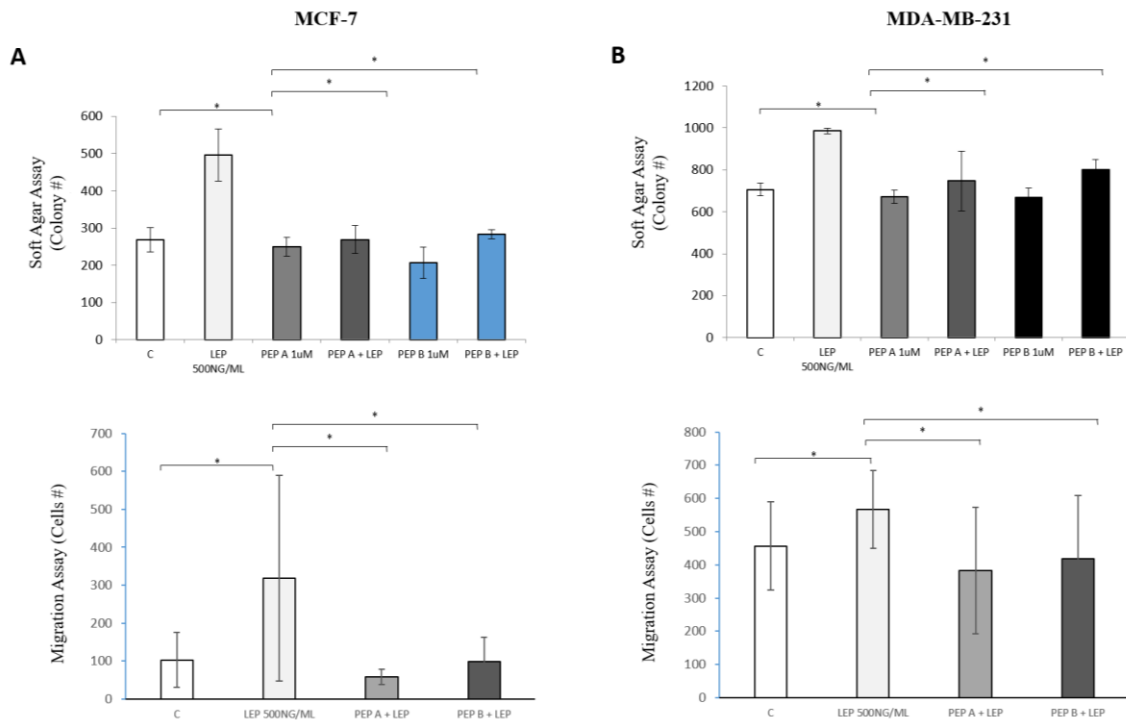
Furthermore, the ESI MS/MS spectra of the MH⁺ precursor ions showed the key fragmentations related to the analyzed peptide sequences.

The fragmentations of the two peptides (**a** and **b**) led to the formation of the typical ions that match the expected fragments from the precursor ions ([M+H]⁺) for the obtained methylated sequences.

The obtained results showed that performing three HATU-mediated couplings in a 5-fold excess of reagents allowed for the efficient coupling of the *N*-Fmoc-amino acids onto the hampered resin-bound *N*-methyl residues.

Finally, the ability of peptides **a** and **b** in antagonizing leptin activity in breast cancer cells was evaluated.

We tested the biological activity of the peptide **a** and **b** on anchorage-independent cell growth and cell motility using as experimental models ObR-positive and leptin-sensitive MCF-7 (Estrogen Receptor alpha-positive) and MDA-MB-231 (Estrogen Receptor alpha-negative) breast cancer cells. We found that treatment with leptin (500 ng/ml) increased cell proliferation and the peptides **a** and **b** at 1 μM concentration significantly reversed the leptin-induced cell growth in both cell lines (Figure 3 A and B, upper panel). Moreover, pretreatment with the peptides **a** and **b** counteracted leptin effects on cell motility (Figure 3 A and B, lower panel).



* P<0,05

Figure 3. Effects of *N*-methylated tetrapeptides on leptin induced breast cancer cell proliferation.

Our results suggest that the proposed *N*-methylated LDFI analogues, acting as full leptin antagonists, after further experiments and biological assessments, could represent promising therapeutic tools for breast cancer treatment and other leptin-related cancers.

2.3. Experimental Section

2.3.1. Materials

Reagents were commercially available with analytical grade and used as purchased without further purification. Solvents were purified according to well-known laboratory methods and freshly distilled prior to use.

Manual solid-phase synthesis of *N*-Fmoc-*N*-Methyl- α -amino acids was carried out in a peptide vessel. Commercially available 2-chlorotrityl chloride resin (purchased from Sigma-Aldrich) and α -amino acids of the L-series were used.

The peptide chain assembly was made on a CEM-Liberty microwave-assisted automated synthesizer.

N-Fmoc-*L*-amino acids, Wang resin (100-200 mesh), Fmoc-*L*-Ile-Wang resin (100-200 mesh), O-(7-azabenzotriazol-1-yl)-*N,N,N',N'*-tetramethyluronium hexafluorophosphate (HATU), diisopropylethylamine (DIPEA), trifluoroacetic acid (TFA), triisopropylsilane (TIS) and dimethyl sulfoxide- d_6 (DMSO- d_6) were purchased from Sigma-Aldrich. Ultrapure water was distilled with the MilliQ® water, Millipore.

N-methylpyrrolidone (NMP), Dichloromethane (DCM), *N,N*-dimethylformamide (DMF), diethyl ether were purchased from VWR.

2.3.2. Synthesis of *N*-Fmoc-*N*-methyl- α -aminoacids

N-Fmoc-*N*-methyl- α -aminoacids were prepared according to a previously developed protocol.³²

***N*-Fmoc-*N*-methyl-*L*-leucine** (70 %). ¹H NMR (300 MHz, DMSO- d_6), mixture of two rotational isomers A and B (60:40): δ 7.87-7.25 (m, 8H, ArH), 4.60 (dd, $J=11.4, 4.5$ Hz, 1H, α -CH), 4.45-4.20 (m, 3H, CH₂-Fmoc, CH-Fmoc), 2.72 (B) and 2.68 (A) (2s, 3H, CH₃), 1.75-1.22 (m, 3H, CH₂CH), 0.94-0.65 (m, 6H, CH(CH₃)₂); ¹³C NMR (75 MHz, DMSO- d_6), mixture of two rotational isomers A and B: δ 172.50, 156.51, 156.22, 144.21, 144.13, 128.14, 128.02, 127.54, 125.36, 125.26, 120.61, 67.33, 56.65, 56.43, 47.22, 37.53, 37.24, 30.42, 24.91, 23.62, 22.44, 21.37.

***N*-Fmoc-*N*-methyl- -*L*-Aspartic acid 4-tert-butyl ester** (75 %). ¹H NMR (300 MHz, DMSO- d_6), mixture of two rotational isomers A and B (62:38): δ 7.97-7.22 (m, 8H, ArH),

4.89 (B) and 4.76 (A) (2dd, $J=8.5, 6.2$ Hz, 1H, α -CH), 4.41-4.18 (m, 3H, CH₂-Fmoc, CH-Fmoc), 2.89-2.73 (m, 4H, CH₃, CH₂COOH), 2.69-2.54 (m, 1H, CH₂COOH), 1.38 (B) and 1.34 (A) (2s, 9 H, (CH₃)₃C); ¹³C NMR (75 MHz, DMSO-*d*₆), mixture of two rotational isomers A and B: δ 171.86, 169.98, 156.16, 144.17, 141.19, 129.22, 128.63, 126.57, 119.64, 80.41, 56.07, 47.82, 46.03, 35.68, 33.13, 28.78, 27.18, 25.41.

***N*-Fmoc-*N*-methyl-*L*-phenylalanine** (65 %). ¹H NMR (300 MHz, DMSO-*d*₆), mixture of two rotational isomers A and B (52:48): δ 7.94-6.97 (m, 13H, ArH), 4.79 (A) and 4.67 (B) (2dd, $J=11.8, 4.4$ Hz, 1H, α -CH), 4.33-4.07 (m, 3H, CH₂-Fmoc, CH-Fmoc), 3.28-2.95 (m, 2H, CH₂Ph), 2.691 (A) and 2.66 (B) (2s, 3H, CH₃); ¹³C NMR (75 MHz, DMSO-*d*₆), mixture of two rotational isomers A and B: δ 172.27, 156.27, 144.10, 141.03, 130.20, 129.07, 128.62, 128.15, 127.65, 126.48, 124.31, 119.57, 67.12, 59.62, 46.03, 34.53, 32.64.

***N*-Fmoc-*N*-methyl-*L*-isoleucine** (73%); ¹H NMR (300 MHz, DMSO-*d*₆) mixture of two rotational isomers A and B (80:20) δ 7.94-7.24 (m, 8H, ArH), 4.48-3.92 (m, 4H, α -CH, CH₂-Fmoc, CH-Fmoc), 2.71 (A) and 2.69 (B) (2s, 3H, CH₃), 1.80 (m, 1H, CHCH₃), 1.34-1.07 (m, 2H, CH₂CH₃), 0.93-0.72 (m, 6H, CHCH₃, CH₂CH₃); ¹³C NMR (75 MHz, DMSO-*d*₆) mixture of two rotational isomers A and B: δ 172.27, 156.42, 144.35, 144.26, 141.35, 128.16, 127.52, 125.41, 120.56, 67.26, 62.72, 59.91, 47.23, 33.12, 30.43, 25.12, 22.11, 16.21, 10.82.

2.3.3. Peptide Synthesis

Microwave assisted peptide synthesis protocol

The peptide chain assembly was made on a CEM-Liberty microwave-assisted automated synthesizer. The syntheses' scales were 0.10 mmol.

In the 50 mL bottles, the Fmoc-*L*-AA-OH (0.2 mmol) amino acids were dissolved in DMF. Subsequently, solutions containing 20% DIPEA in NMP, the HATU coupling reagent dissolved in DMF and 20% piperidine in DMF were prepared.

The Wang resin 100-200 mesh (0.7 mmol) was introduced into the reaction vessel and swollen in DMF (5 ml) for 30 min. Then, the reaction vessel was placed in the *Discovery microwave* and the temperature adjusted via optical fiber.

The loading of the resin with *N*-Fmoc- α -amino acids and all coupling steps were performed in DMF with fivefold excess of *N*-Fmoc-*N*-Me-L-amino acids, and *N*-Fmoc-L-amino acids, and in the presence of HATU (5.0 equivalents) and DIPEA (10 equivalents) for 20 min. at 75°C. Coupling steps were performed twice or three times.

The Fmoc protecting group was removed by treatment of the resin with a 20% solution of piperidine in DMF (v/v) (7 ml). Deprotection was performed in two stages with an initial deprotection of 30 sec. followed by 3 min. at 75°C.

Between each step, the resin was washed thoroughly with DMF. The completed peptide was washed with DMF and DCM.

The peptide was cleaved from the resin using a mixture of TFA, water, and TIS (9.5/0.25/0.25 by volume) for 30 min., the temperature was maintained at 38 °C via optical fiber.

The mixture with the resin was placed in a test tube with a porous septum and washed once with 1 mL of TFA, with TFA: DCM (2 mL, 1: 1 v/v) and then with DCM. TFA and DCM were removed under reduced pressure conditions. Then the peptides **a** and **b** were obtained in 70% and 60% yield respectively by precipitation with cold diethyl ether.

Peptide analysis

¹H NMR spectra were recorded on a Bruker Avance 300 instrument at 300 MHz. Spectroscopic analysis was performed at 293 K on diluted solutions of each compound by using DMSO-d₆ as the solvent. Chemical shifts (δ) are reported in ppm. Coupling constants (*J*) are reported in Hertz (Hz). ESI-QTOF mass spectra were recorded on a Agilent Quadrupole Time of Flight (QTOF) mass spectrometer fitted with an electrospray ionization source (ESI) operating in positive ion mode.

Peptide structures and all related experimental data are not reported since a patent application is being drafted

2.4. Outlook

Here, we synthesized two methylated analogues of the leptin antagonist tetrapeptide (LDFI). The *N*-methylated peptides were easily prepared by solid phase methods starting from *N*-Fmoc-*N*-methyl amino acids for the purpose synthesized.

The effects of both methylated peptides on leptin induced breast cancer cell proliferation were evaluated using *in vitro* experimental models.

Interestingly our results showed that the novel methylated peptides inhibit effectively the leptin-induced growth as well as migration in both ERa-positive and - negative breast cancer cells.

Stability assays of methylated peptides **a** and **b** are ongoing in order to study peptide degradation and evaluate the stabilization of the leptin antagonist by *N*-methylation.

The study of the proteolytic degradation in the blood of the two methylated peptides is performed by incubating in parallel LDFI and its methylated analogues in plasma and comparing their degradation profiles. The remaining peptides and degradation products will be identified using mass spectrometry.

References

1. H. Münzberg, C.D. Morrison, *Metabolism.*, **2015**, 64(1), 13–23.
2. A. Leggio, S. Catalano, R. De Marco, I. Barone, S. Andò, A. Liguori, *Eur J Med Chem.*, **2014**, 6, 78, 97-105.
3. F. Peelman, K. Van Beneden, L. Zabeau, H. Iserentant, P. Ulrichs, D. Defeau, A. Verhee, D. Catteuw, D. Elewaut, J. Tavernier, *J. Biol. Chem.*, **2004**, 279, 41038-41046.
4. S. Margetic, C. Gazzola, G.G. Pegg, R.A. Hill, *Int J Obes*, **2002**, 26, 1407-1433.
5. H. Lu, C. Li, *Cell Res.*, **2000**, 10, 81- 92.
6. P. Ducy, M. Amling, S. Takeda, M. Priemel, A. F. Schilling, F.T. Beil, J. Shen, C. Vinson, J.M. Rueger, G. Karsenty, *Cell*, **2000**, 100, 197-207.
7. R.B. Ceddia, H.A. Koistinen, J.R. Zierath, G. Sweeney, *FASEB J.*, **2002**, 16:10, 1163-1176.
8. S. Panza, L. Gelsomino, R. Malivindi, V. Rago, I. Barone, C. Giordano, F. Giordano, A. Leggio, A. Comandè, A. Liguori, S. Aquila, D. Bonofiglio, S. Andò, S. Catalano, *Am. J. Pathol.*, **2019**, 189:3, 687-698.
9. S. Andò, S. Catalano, *S. Nat. Rev. Endocrinol.*, **2012**, 8, 263-275.
10. S. Andò, L. Gelsomino, S. Panza, C. Giordano, D. Bonofiglio, I. Barone, S. Catalano, *Cancers*, **2019**, 11, 62.
11. C. Garofalo, E. Surmacz, *J. Cell. Physiol.*, **2006**, 207, 12-22.
12. D. Housa, J. Housova, Z. Vernerova, M. Haluzik, *Physiol. Res.*, **2006**, 55, 233-244.
13. C. Garofalo, M. Koda, S. Cascio, M. Sulkowska, L. Kanczuga-Koda, J. Golaszewska, A. Russo, S. Sulkowski, E. Surmacz, *Clin Cancer Res*, **2006**, 12(5), 1447-1453.
14. E. Surmacz, *Breast Cancer Res.*, **2007**, 9, 301.
15. P. Stattin, S. Derberg, G. Hallmans, A. Bylund, R. Kaaks, U-H. Stenman, A. Bergh, T. Olsson, *J. Clin. Endocrinol. Metab.*, **2001**, 86(3), 1341-1345.
16. A. Liguori, S. Andò, A. Leggio, S. Catalano, R. De Marco, I. Barone, **2014**, Italian Patent, CS2014A000016, 28/04/2014.
17. S. Catalano, A. Leggio, I. Barone, R. De Marco, L. Gelsomino, A. Campana, R. Malivindi, S. Panza, C. Giordano, A. Liguori, D. Bonofiglio, A. Liguori, S. Andò, *J Cell Mol Med.*, **2015**, 19(5): 1122–1132.
18. C. Giordano, F. Chemi, S. Panza, I. Barone, D. Bonofiglio, M. Lanzino, A. Cordella, A. Campana, A. Hashim, P. Rizza, A. Leggio, B. Györfy, B.M. Simões, R.B. Clarke, A. Weisz, S. Catalano, S. Andò, *Oncotarget.*, **2016**, 7(2):1262–1275.
19. C. Giordano, L. Gelsomino, I. Barone, S. Panza, G. Augimeri, D. Bonofiglio, D. Rovito, G. D. Naimo, A. Leggio S. Catalano and S. Andò, *J. Clin. Med.* **2019**, 8(7), 1027

20. D.J. Craik, D.P. Fairlie, S. Liras, D. Price, *Chem Biol Drug Des*, **2013**, *81*, 136–147.
21. A.L. Smart, S. Gaisford, A.W. Basit, *Expert Opin. Drug Deliv.*, **2014**, *11*(8), 1323-1335.
22. E. Biron, J. Chatterjee, O. Ovadia, L. Langenegger, J. Brueggen, D. Hoyer, H. Schmid, R. Jelinek, C. Gilon, A. Hoffman, H. Kessler, *Angew. Chem., Int. Ed.*, **2008**, *47*, 2595-2599.
23. M.F. Powell, T. Stewart, L.Jr Otvos, L. Urge, F.C.A. Gaeta, A. Sette, T. Arrhenius, D. Thomson, K. Soda, S.M. Colon, *Pharm Res*, **1993**, *10*: 1268.
24. M. Werle, A. Bernkop-Schnürch, *Amino Acids*, **2006**, *30*: 351–367.
25. J.G. Beck, J. Chatterjee, B. Laufer, M. Udaya Kiran, A.O. Frank, S. Neubauer, O. Ovadia, S. Greenberg, C. Gilon, A. Hoffman, and H. Kessler, *J. Am. Chem. Soc.* **2012**, *134*, 29, 12125-12133.
26. M. Erak, K. Bellmann-Sickert, S. Els-Heindl, A.G. Beck-Sickinger, *Bioorg. Med. C.*, **2018**, *26*, 2759–2765.
27. J. Chatterjee, F. Rechenmacher, H. Kessler, *Angew. Chem., Int. Ed.*, **2013**, *52*, 254.
28. S. Md, A. Rauf, P.I. Arvidsson, F. Albericio, T. Govender, G.E.M. Maguire, H.G. Kruger, B. Honarparvar, *Org. Biomol. Chem.*, **2015**, *13*, 9993-10006.
29. J.M. Collins, S.K. Singh, G.S. Vanier, *Chem. Today*, **2012**, 30.
30. A. Comandè, M. Greco, E.L. Belsito, A. Liguori, A. Leggio, *RSC Adv.*, **2019**, *9*, 22137-22142.
31. M.L Di Gioia, A. Leggio, A. Liguori, *J. Org. Chem.* **2005**, *70*, 3892.
32. M.L. Di Gioia, A. Leggio, A. Le Pera, A. Liguori, A. Napoli, C. Siciliano, G. Sindona, *J. Org. Chem.* **2003**, *68*, 7416.
33. M.L. Di Gioia, A. Leggio, A. Liguori, and F. Perri, *J. Org. Chem.* **2007**, *72*, 3723-3728.
34. H. Rodríguez, M.Suarez, F.Albericio, *J. Pept. Sci.*, **2010**, *16*: 136–140.
35. A. El-Faham, F. Albericio, *Chem. Rev.* **2011**, *111*, 6557–6602.

Synthesis of a new peptide ligand for targeting CD38 receptor on multiple myeloma cells

[Ongoing work 2]

Abstract

A short peptide chain (heptapeptide) able to interact with the CD38 receptor over-expressed by multiple myeloma cells was designed and synthesized. The developed peptide was conjugated, as targeting molecule, to the external surface of a MSN-based nanocarrier with the aim to achieve a more specific and efficient bortezomib delivery system (CD38-PEP-MSN-BTZ). TEM analysis of the CD38-PEP-MSN conjugate gave promising results in fact, TEM images showed that the system is internalized by CD38+ RPMI MM cells. The new synthesized CD38 peptide ligand might be an excellent substitute of folic acid for the MSN-BTZ prototype, since CD38 receptor is highly expressed on MM cells.

3.1. Introduction

Peptides regulate a wide range of physiological processes and interact with numerous biological targets involved in different pathologies, thus providing a vast opportunity for biomedical applications. The interest towards the synthesis of biologically active peptides has significantly increased since they are widely used as therapeutic agents against different types of diseases.

In recent years, peptides have also gained remarkable success in the field of drug delivery and nanomedicine. Peptide-conjugates in fact, are able to direct active pharmaceutical ingredients (APIs) selectively towards specific biological targets.¹

In these applications, peptides can act by crossing the cytoplasmic membrane and allowing the internalization of structurally disadvantaged molecules (CPP) or acting as cell-targeting peptides (CTP).²

Peptides are particularly suitable for this purpose since they are small, easy to synthesize and generally non-immunogenic furthermore they have high affinities and specificities for their receptors.

Oligopeptides also present the ability to penetrate the cell allowing the transport through the membrane of drugs that due to size, possible ionization and plasma protein bonds are hardly able to cross it.³

Importantly the carrier or drug does not necessarily have to be chemically conjugated to the peptide; the peptide activates a particular transport system of any molecule that is present in the blood.⁴

Cell-targeting peptides (CTP) show affinity and specificity towards a cellular or tissue targets, and by maintaining a conformation adequate to the interaction with the receptor they are able to bind the target receptor with high affinity, thus reducing the side effects associated with anticancer therapies.⁵

In the identification of new peptides to be used as targeting functions, computer modeling techniques are important to establish the possible interactions that occur between a receptor protein and peptides, and to improve binding affinities through optimization of

amino acid sequences in the peptide chains.⁶ Methods based on molecular docking strategies are essential tools for the structure-based design of optimized binding peptides.

Multiple myeloma (MM) is a B-cell malignancy characterized by an abnormal proliferation of plasma cells. It is the second most common hematologic malignancy accounting for more than 10,000 deaths annually in the USA.⁷

The disease is characterized by the presence of numerous genetic alterations and it is the results from the neoplastic transformation of B lymphocytes. MM causes a decrease in the production of blood cells and in the resistance to infection.⁸

Due to the high accumulation of misfolded or unfolded proteins in the endoplasmic reticulum (ER), the use of proteasome inhibitors constitutes the main therapeutic choice for this malignancy. Proteasome inhibition generates an accumulation of these proteins, activating apoptotic pathways and consequent cell death.

Bortezomib (BTZ, VELCADE®) is the first-in-class proteasome inhibitor approved by US FDA for the treatment of multiple myeloma (MM) patients.⁹

Bortezomib, a dipeptide boronic acid, (Figure 1) is an antineoplastic agent belonging to a class of new generation antineoplastic agents which acts by inhibiting the chemotrypsin-like activity of proteasome 26S. Bortezomib, by inhibiting the proteasome, blocks the cellular protein degradation system¹⁰⁻¹¹ and promotes the apoptotic process of the myeloma cells.¹²⁻¹⁵

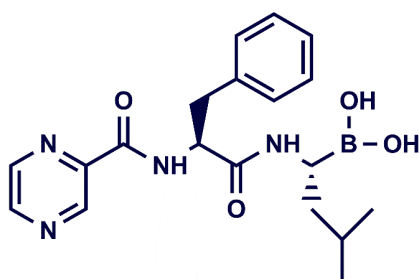


Figure 1 Structure of Bortezomib

Although bortezomib (BTZ) is one of the most potent proteasome inhibitors available, it still has a high number of associated undesired side effects, such as chronic peripheral neuropathy, that limit its use as anticancer drug.

The peripheral neuropathy is one of the most serious dose-limiting side effects that occur during BTZ treatment.⁹ Therefore, there is a great interest for the development of specific BTZ delivery systems in order to reduce its side effects in the normal tissues and to enhance its potency in the MM cells.¹⁶

Based on the above, the development of new and highly efficient BTZ delivery systems represents a particularly attractive goal.¹⁷

Unsoy *et al.* 2014 developed a drug delivery using Chitosan magnetic nanoparticles loaded with Bortezomib. The stimuli-responsive system allows pH-responsive release of Bortezomib, which can be targeted to tumor cells under a magnetic field. The magnetic targeting limits the side effects of chemotherapy, while the effective release from the nanoparticles may reduce the amount of Bortezomib required, and the frequency of drug administration.¹⁸

Moreover, it was also synthesized a system for the Bortezomib delivery based on liposomal nanoparticles. *In vitro* studies have demonstrated that the system has induced significant proteasome inhibition and cytotoxicity against multiple myeloma cell lines, in addition *in vivo* has showed a remarkable tumor growth inhibition with reduced systemic toxicity.¹⁹

Recently in our laboratory, a new system of BTZ administration has been developed exploiting the unique properties of mesoporous silica nanoparticles (MSNs) such as high biocompatibility and versatility.²⁰

The intrinsic properties of mesoporous silica nanoparticles (MSN) make them ideal delivery platforms.²¹ Their structural and chemical features as high surface area, tunable size, and easy surface modification permit to design versatile nanosystems able to encapsulate a variety of therapeutic agents and to host targeting molecules able to interact selectively with specific membrane receptors overexpressed in tumor cells.²² The use of these drug delivery systems composed of biocompatible nanomaterials allows minimizing toxic side effects and increasing the therapeutic efficacy of the drug.²³ The MSNs can be exploited as vehicles for targeting and release of biologically active molecules, to be employed in targeted therapy. MSNs have been tested for the delivery

of a variety of drugs including nonsteroidal anti-inflammatories (e.g., aspirin), antibiotics (e.g., vancomycin), and chemotherapeutics (e.g., doxorubicin and methotrexate).²⁴⁻²⁸

The patented MSN-based nanodevice (FOL-MSN-BTZ)²⁹ is totally engineered, it employs a receptor-specific ligand (folic acid) on the external surface of MSNs while the antitumor drug Bortezomib is linked, mainly on the pore walls, through a pH-sensitive bond (Figure 2). The drug is only anchored on the inner pore walls, in this way the pH-sensitive bond is protected from the hydrolysis during the plasmatic distribution, until when it penetrates inside the target cells.

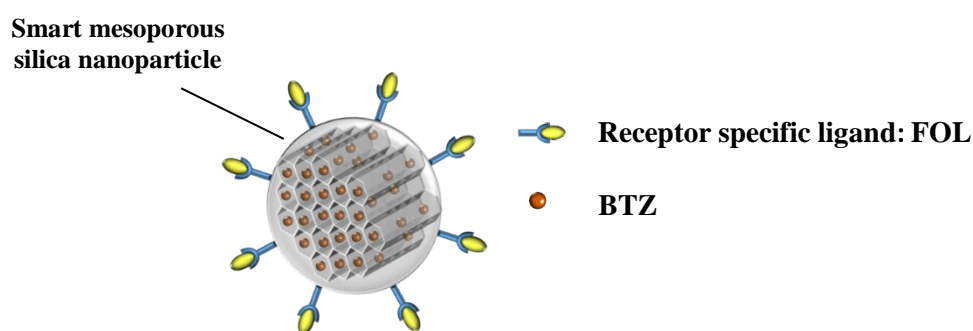


Figure 2. Schematization of our system FOL-MSN-BTZ.

The system works through three steps that are: cellular recognition; system internalization and intracellular drug release.

Mesoporous silica nanoparticles used were synthesized by modifying an interfacial synthesis procedure carried out at room temperature, introducing cyclohexane as the organic phase in which tetraethyl orthosilicate, silica source, (TEOS) is dissolved (1)³⁰

Folic acid (FOL) was used as targeting molecule since its use as tumour-homing agent is widespread recognized.³¹

Aminopropyl-functionalized particles (MSN-AP) were prepared by covalent grafting of aminopropyltriethoxysilane (APTES) on the external surface of MSNs. Folic acid functionalized particles (MSN-FOL) were synthesized through amide bond formation between the amino group of MSN-AP and folic acid. The following steps concern

surfactant removal and the conjugation of BTZ-prodrug via pH-sensitive bond to silica pore walls.³²

The BTZ boronic acid group forms, with a diol linker anchored on the MSNs pore surface, reversible cyclic boronate esters rather stable at neutral and alkaline pH, and that dissociate in acidic environments to release the free active drug (Figure 3).

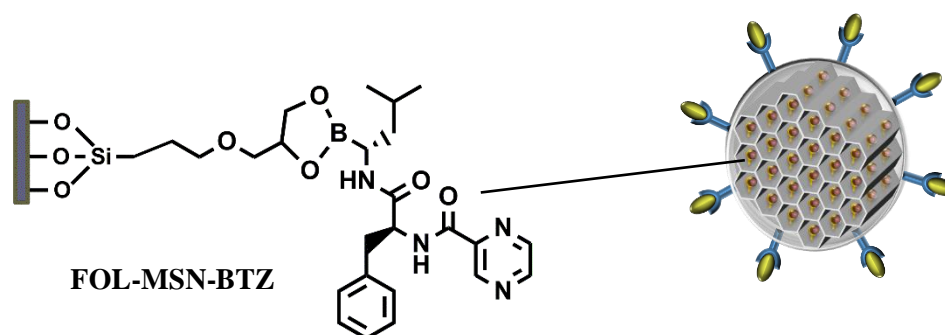


Figure 3. FOL-MSN-BTZ conjugate

The formation of boronic acid-diol conjugate is reversible in a pH-sensitive manner: at neutral or alkaline pH, BTZ and catechol form a stable boronate ester, in a low-pH environment, the BTZ-catechol ester conjugate dissociates and release BTZ, and catechol groups.³³

Drug release from FOL-MSN-BTZ as a function of time and at different pH values has been studied. Release experiments, carried out in media mimicking the physiological (pH=7.4) and endolysosomal compartments (pH = 5) proved the ability of the system to modulate drug release in relation to the variation of pH.

FOL-MSN-BTZ was tested on cancer cells overexpressing the folate receptor (FR+ cells) and on FR- normal cells including the human FR α -/FR β + MM cells lines, RPMI and U266B-1, being BTZ the treatment of choice for this type of cancer. Our experiments showed that FOL-MSN-BTZ induces death or inhibit proliferation in FR+ cancer cells but not in FR- normal cells while free BTZ resulted toxic for all cell lines tested, independently on their FR expression.

These results fit very well with our TEM observations on RPMI and BJhTERT cells treated with FOL-MSN-BTZ, which showed how MSNs uptake occurs in FR+ RPMI only and not in FR- BJhTERT cells, where they remain confined in the intercellular

spaces. Finally, the biocompatibility of FOL-MSN-BTZ at increasing concentrations and its antitumor activity was demonstrated in mouse xenograft models. However, the *in vivo* experimentation indicated that our system affects moderately the mouse neuronal cells functionality. Most likely this effect is due to the FR+ receptor expression in the nervous system.

In this regards encouraged by the remarkable results obtained we studied the possibility to improve the technology functionalizing our BTZ MSN-based delivery system with a ligand able to interact with the CD38 receptor that is specifically expressed on Multiple Myeloma cells in order to enhance the potency and efficacy of BTZ in MM cells.

CD38 is a multifunctional cell surface protein that has receptor as well as enzyme functions. The protein is generally expressed at low levels on various hematological and solid tissues, while plasma cells express particularly high levels of CD38. The protein is also expressed in a subset of hematological tumors, and shows especially broad and high expression levels in plasma cell tumors such as multiple myeloma (MM).³⁴

Numerous studies have shown an over-expression, in cells of multiple myeloma, of the CD-38 receptor.

We thought then that a peptide able to bind selectively CD38 receptor could allow to selectively target and deliver bortezomib to MM cancer cells.

CD38 consists of 300 amino acid residues pertaining to three domains: a short intracellular domain, a single transmembrane helix domain, and a large extracellular domain. The human CD38 molecule presents two separate domains.

The *N*-terminal domain (residues 45–118 and 144–200) is formed by a bundle of α helices (α 1, α 2, α 3, α 5, α 6) and two short β strands (β 1, β 3); and the *C*-terminal domain (residues 119–143 and 201–300) consists of a four-stranded parallel β sheet (β 2, β 4, β 5, and β 6) surrounded by two long helices (α 8 and α 9) and two short helices (α 4 and α 7). Two distinct domains are connected by a hinge region composed of three peptide chains, including residues 118–119, 143–144, and 200–201. A disulphide bond (Cys119-Cys201), which is unique in CD38, in addition to the other five pairs of disulphide bonds (Cys67-Cys82, Cys99-Cys180, Cys160-Cys173, Cys254-Cys275, and Cys287-Cys296) conserved in ADP-ribosyl cyclase family members, further stabilizes the relative conformations of two domains by linking peptides 118–119 and 200–201 together.^{35, 36}

The process of endocytosis of the human CD38 molecule has been studied in normal lymphocytes and in a number of leukemia- and lymphoma-derived cell lines by investigating the fate of CD38 after ligation to agonistic and non-agonistic specific antibodies.³⁷

Since CD38 is highly expressed in hematologic malignancies CD38, it represents an attractive therapeutic target and a highly interesting target for anticancer therapy in MM. Various CD38 antibodies have been identified that show strong preclinical and clinical potential. Different study demonstrated that CD38 undergoes internalization after ligation with agonistic or non-agonistic specific antibodies.³⁸

Based on the above, we investigated the interaction between CD38 receptor and specific antibodies in order to identify short amino acidic sequences able to bind CD38 and to induce its internalization. On the base of the binding site of the antibody SAR650984 (Isatuximab) to CD38, we identified a sequence of the Isatuximab paratope and hypothesized some short peptides mimicking the identified paratope and that could be able to interact with CD38 receptor. Finally, on the base of hypothesized peptides we defined some specific amino acid sequences incorporating also cysteine residues. It is reported in fact that cysteine residues play an important role in the internalization of CD38 through the formation of disulfide bonds.³⁹

The interactions of the hypothesized peptides with the CD38 receptor have been simulated and evaluated by *in silico* studies. The careful analysis and interpretation of the obtained results from these computational studies have allowed us to define a pool of short amino acid sequences to synthesize and conjugate to the carrier.

In this study, the solid phase synthesis of a short peptide chain (heptapeptide) and its conjugation to the external surface of a MSN-based nanocarrier is described. Furthermore, through transmission electronic microscopy (TEM) the uptake and localization of the obtained system CD38-PEP-MSN within MM cells is evaluated.

3.2. Results and Discussion

In our design, for the synthesis of the targeting peptide molecule (CD38-PEP) we use Fmoc-based Solid Phase Peptide Synthesis methodologies.

We designed and synthesized a small peptide (CD38-PEP) composed by 7 amino acids containing a cysteine residue as *N*-terminal unit, important for the nanocarrier uptake.

For the synthesis of peptide CD38-PEP we used the *N*-Fmoc protected C-terminal amino acid anchored to the Wang resin (**1**) (0.1 mmoles, loading 0.6 mmoles/g) (Scheme 1) and HBTU (*N,N,N',N'*-Tetramethyl-O-(1H-benzotriazol-1-yl)uronium hexafluorophosphate) as coupling agent.

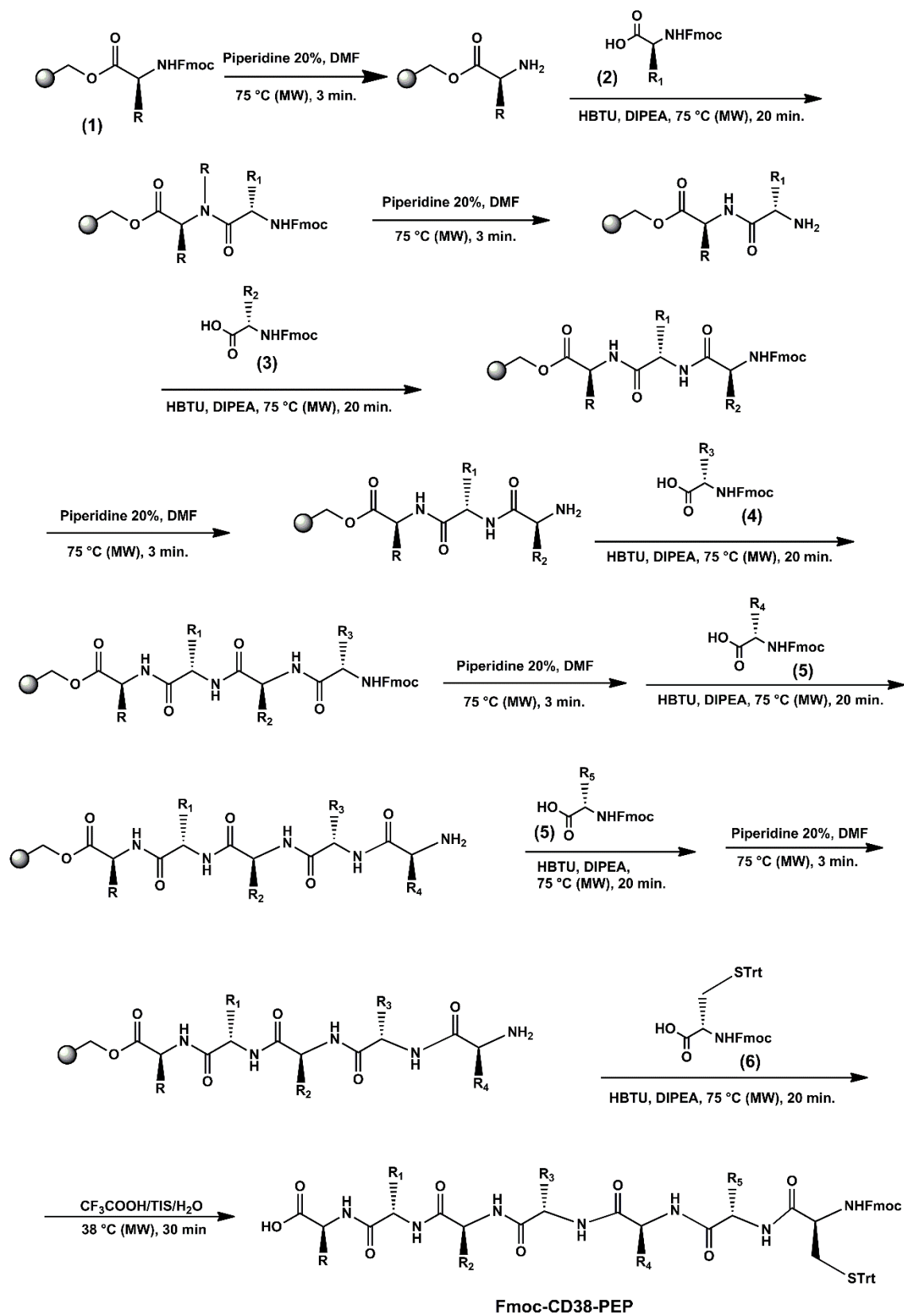
Coupling reactions were performed in DMF with fivefold excess of *N*-Fmoc-L-amino acids, and in the presence of HBTU (5.0 equivalents) and DIPEA (10 equivalents) for 20 min. at 75°C. The last coupling for the insertion of *N*-Fmoc-Cys(Trt)-OH was performed at 50°C for 20 minutes. Lowering the microwave coupling temperature from 75°C to 50°C limits the racemization of cysteine. The Fmoc protecting group was removed by treatment of the resin with a 20% solution of piperidine in DMF at 75°C. The deprotection of the amino function was carried out for all the amino acids of the sequence except for the *N*-terminal amino acid cysteine (Scheme 1). The protocol used for the conjugation of the peptide to the external surface of the nanoparticles required the presence of the protecting group on the cysteine amine function to avoid side reactions.

Cleavage and removal of the side-chain protecting group was carried out using a mixture of TFA (95% v/v), water (2.5% v/v), and TIS (2.5% v/v) for 30 min. at 38°C by microwave heating.

Following cleavage, the peptide Fmoc-CD38-PEP was obtained in 68% yield by precipitation with cold diethyl ether.

HPLC/MS analysis of the crude peptide showed that peptide ligand Fmoc-CD38-PEP was obtained with a high purity degree (> 90%) (Figure 4, *rt* = 18.0 min).

The peptide was characterized by ¹H NMR, ¹³C NMR and HPLC-ESI-QTOF-MS analysis. All ¹H NMR signal assignments were made by decoupling experiments and ESI-MS/MS data were collected to elucidate peptide structure. The structure of Fmoc-CD38-PEP derived from the NMR data was confirmed by LC-MS/MS analysis, in which the peptide bonds between the amino acid residues were sequentially cleaved.



Scheme 1

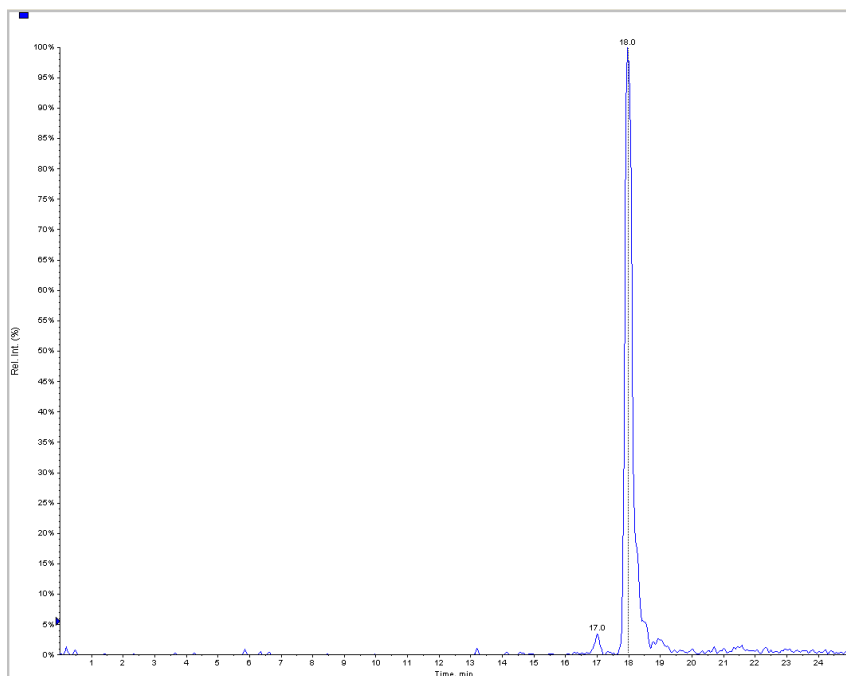


Figure 4. LC/MS analysis of Fmoc-CD38-PEP peptide

The Fmoc-CD38-PEP sequence was then conjugated to the external surface of the mesoporous silica nanoparticles in order to obtain the targeted nanocarrier CD38-PEP-MSN and evaluate its uptake by MM cells overexpressing CD38 receptor.

The nanoparticles (MSNs) were synthesized according to the published procedure, present in *Paper 5*, using Triton X-100 as a surfactant molecule, TEOS as a source of silica and cyclohexane. The synthesized nanoparticles were then characterized by SEM, XRD and TGA. The external surface of MSNs was then functionalized with APTES in order to incorporate on the surface aminopropyl functions useful to conjugate the targeting peptide molecule by means an amide bond.

The conjugation of the peptide to the nanoparticles was carried out through the formation of an amide bond between the amino function on the nanocarrier external surface and the carboxyl function of the peptide C-terminal residue.

Firstly, Fmoc-CD38-PEP (0.27 mmoles, 1 equivalent) was dissolved in 10 mL of a mixture of anhydrous DCM and DMF (1: 1 by volume), then DIC (0.27 mmoles, 1 equivalent) and DIPEA (0.54 mmol, 2 equivalents) were added. The reaction mixture was left under stirring for about 2 hours at room temperature. Subsequently, 0.1 g of MSNs were added and the reaction mixture was left stirring for 48 hours at room temperature.

The suspension was then filtered, washed three times with DMF and anhydrous DCM and dried to afford the nanocarrier Fmoc-CD38-PEP-MSN.

The following steps concern surfactant removal from the nanoparticles internal pores by extraction with distilled water and the deprotection of the amino function of the *N*-terminal cysteine. The removal of Fmoc group was performed using 10 mL of a solution of 20% piperidine in DMF. Two deprotection cycles of 30 minutes each were carried out. The CD38-PEP-MSN nanoparticles were recovered by filtration and washing with DMF and anhydrous DCM.

The effectiveness of nanomaterials for biomedical applications depends on successful ingestion/uptake by cells, and this was verified via transmission electron microscopy (TEM) images.

The CD38-PEP-MSN nanoparticles thus obtained, before Bortezomib loading, were analyzed by TEM to evaluate the uptake of the nanocarrier by MM RPMI-8626 cells expressing the CD38 receptor and consequently to evaluate the efficacy of the targeting peptide function against CD38 receptor.

Immunogold labeling experiments on RPMI cells demonstrate the recognition of CD38-PEP-MSN by CD-38. Interestingly, as depicted in Figure 5, after CD38 recognition at the cell membrane, CD38-PEP-MSN were internalized through the CD38-mediated endocytic process.

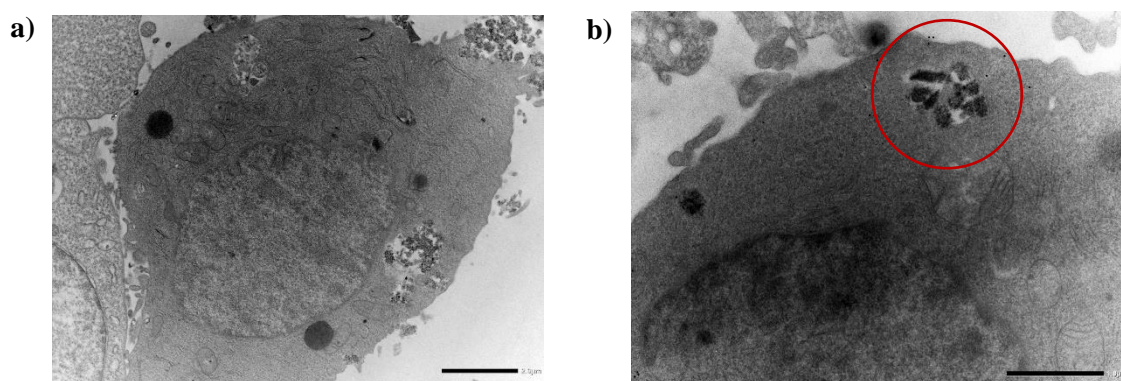


Figure 5. Colloidal-gold immunocytochemistry for CD-38 (black dots indicated by red circle) in RPMI cells exposed to CD38-MSN for 2h. (a) Scale bars 2μm, x 4.000 magnification (left panel); (b) scale bars 0.1μm, x10k magnification (left panel).

3.3. Experimental Section

3.3.1. Materials

Reagents were commercially available with analytical grade and used as purchased without further purification. Solvents were purified according to well-known laboratory methods and freshly distilled prior to use.

The peptide chain assembly was made on a CEM-Liberty microwave-assisted automated synthesizer.

N-Fmoc-*L*-amino acids, Wang resin (100-200 mesh), *N,N,N',N'*-Tetramethyl-*O*-(1*H*-benzotriazol-1-yl)uronium hexafluorophosphate (HBTU), diisopropylethylamine (DIPEA), trifluoroacetic acid (TFA), triisopropylsilane (TIS) and dimethyl sulfoxide-*d*₆ (DMSO-*d*₆), Triton X-100, neutral polyoxyethylene(10) octylphenyl ether, tetraethylorthosilicate (TEOS), (3-aminopropyl)-triethoxysilane (APTES), Diisopropylcarbodiimide (DIC) were purchased from Sigma-Aldrich. Ultrapure water was distilled with the MilliQ® water, Millipore. Diethyl ether, trifluoroacetic acid (TFA), *N*-methylpyrrolidone (NMP), Dichloromethane (DCM), *N,N*-dimethylformamide (DMF), hexane and Cyclohexane were purchased from VWR.

3.3.2. Microwave assisted peptide synthesis protocol

The peptide chain assembly was made on a CEM-Liberty microwave-assisted automated synthesizer. The syntheses' scales were 0.10 mmol.

In the 50 mL bottles, the Fmoc-*L*-AA-OH (0.2 mmol) amino acids were dissolved in DMF. Subsequently, solutions containing 20% DIPEA in NMP, the HBTU coupling reagent dissolved in DMF and 20% piperidine in DMF were prepared.

Fmoc-*L*-amino acid - Wang resin (0.6 mmol) was introduced into the reaction vessel and swollen in DMF (5 ml) for 30 min. Then, the reaction vessel was placed in the *Discovery microwave* and the temperature adjusted via optical fiber.

The loading of the resin with *N*-Fmoc- α - amino acids and all coupling steps were performed in DMF, and in the presence of HBTU (5.0 equivalents) and DIPEA (10 equivalents) for 20 min at 75°C for all amino acids, and for 20 min at 50°C for cysteine. The Fmoc protecting group was removed by treatment of the resin with a 20% solution of piperidine in DMF (v/v) (7 ml). Deprotection was performed in two stages with an initial deprotection of 30 sec. followed by 3 min. at 75°C.

Between each step, the resin was washed thoroughly with DMF. The completed peptide was washed with DMF and DCM.

The peptide was cleaved from the resin using a mixture of TFA, water, and TIS (9.5/0.25/0.25 by volume) for 30 min., the temperature was maintained at 38°C via optical fiber.

The mixture with the resin was placed in a test tube with a porous septum and washed once with 1 mL of TFA, with TFA: DCM (2 mL, 1: 1 v/v) and then with DCM. TFA and DCM were removed under reduced pressure conditions. Then the peptide was obtained in 68% yield by precipitation with cold diethyl ether.

3.3.3. Peptide analysis

¹H and ¹³C NMR spectra were recorded on a Bruker Avance 300 instrument at 300 MHz and 75 MHz, respectively. Spectroscopic analysis was performed at 293 K on diluted solutions of each compound by using DMSO-d₆ as the solvent. Chemical shifts (δ) are reported in ppm. Coupling constants (J) are reported in Hertz (Hz). LC-MS analysis was carried out using a UHPLC instrument coupled to a QTOF mass spectrometer fitted with an ESI operating in positive ion mode. Chromatographic separation was achieved using a C18 RP analytical column (Eclipse Plus C18, 50 \times 9.21 mm, 1.8 μ m) at 50°C with an elution gradient from 5% to 50% of B over 15 min., A being H₂O (0.1% FA) and B CH₃CN (0.1% FA). Flow rate was 0.5 ml/min. ESI-QTOF mass spectra were recorded on an Agilent Quadrupole Time of Flight (QTOF) mass spectrometer fitted with an electrospray ionization source (ESI) operating in positive ion mode.

3.3.4. Mesoporous silica nanoparticles analysis

Fourier transform infrared (FTIR) spectra were recorded with an infrared spectrometer (FT/IR-4600 FT-IR, Jasco; Germany). The ordered mesoporous framework of the synthesized materials was studied by small angle powder X-ray diffraction (XRD) on a MiniFlex 600 Rigaku diffractometer operating at 40 kV and 15 mA, employing Ni b-filtered Cu K α radiation in the 2θ range of 0.3–10° with a scan speed of 0.3 deg per min. The TG analysis were carried out with a Netzsch STA 409 instrument between 20°C and 850°C at a ramp of 10°C/min in air with a flow rate of 10 ml/min.

3.3.5. Synthesis of Mesoporous Silica Nanoparticles

MSU-type MSNs were synthesized through an assembly mechanism at neutral pH of non-ionic poly(ethylene oxide)-based surfactants and silica sources we developed (*Paper 5*).⁴⁰ The surfactant Triton X-100 (21 g) was dissolved in ultrapure water (230 g) in about four hours at room temperature. In order to create two phases, along the vessel it was slowly added a solution of TEOS (22 g) in cyclohexane (9.8 g) (molar composition TEOS: Cyclohexane: Triton X-100: H₂O 1: 1.08: 0.32: 120).

The synthesis was carried out at room temperature and aged for 15 days. The upper phase was removed and the resulting precipitate was collected by filtration and washed three times with ultrapure water. Finally, the sample was dried in the oven at 70 °C for 24 h thus a white powder was obtained.

Synthesis of AP-MSN

The external surface of the nanoparticles was functionalized with aminopropyl groups necessary for the subsequent reaction. For the purpose, APTES was used as the hybrid silica source.

In a typical preparation, a solution containing 1.42 g (0.0064 moles) of APTES in 3 mL of ethanol was added to a suspension of 700 mg of MSNs in 2,5 mL of ethanol. The synthesis was left under stirring at room temperature for 2 days.

The resulting suspension was filtered and washed once with ethanol and twice with ultrapure water. The **MSN-AP** were then placed in an oven at 70°C for 24 hours.

Synthesis of CD38-PEP-MSN

Firstly, the CD38-PEP-(0.27 mmoles, 1 equivalent) was dissolved in 10 mL of a mixture of anhydrous DCM and DMF (1: 1 by volume) with DIC (0.27 mmoles, 1 equivalent) and DIPEA (0.54 mmol, 2 equivalents) to activate the carboxylic function, and the mixture was left to stir for 2 hours at room temperature. Subsequently, 0.1 g of AP-MSNs were added and the reaction was carried out for 48 hours, at room temperature and protected from light. The suspension was then filtered and washed three times with DMF and finally with anhydrous DCM to remove the unbound reagents. The so-obtained nanoparticles were dried at room temperature.

Subsequently, the surfactant within the pores was removed by two extractions of 12 h each, using 0.11 g of PEP-MSN in 0.33 l of ultrapure water at room temperature. The nanocarrier was filtered and washed two times with anhydrous 1,4-dioxane and 3 times with anhydrous DCM.

***N*-Fmoc deprotection reaction**

The removal of *N*-Fmoc group from the *N*-terminal cysteine was performed using 10 mL of a solution of 20% piperidine in DMF. Two deprotection cycles of 30 minutes each were carried out and at the end of each cycle, the obtained nanoparticles were filtered and washed with DMF and anhydrous DCM. The nanoparticles were dried at room temperature and stored under inert atmosphere.

3.3.6. Transmission electron microscopy (TEM) and electron immunocytochemistry

For conventional TEM analysis and electron immunocytochemistry, cells were treated as described for growth experiments and harvested either right after 1h MSNs treatment (to detect MSNs uptake) or after 36h following the 1h exposure to MSNs (to individuate cell death and/or cell injury in treated cells). All samples have been routinely fixed, dehydrated, and resin embedded using heat polymerization. Indirect immunolabeling has been performed on ultrathin sections (60 nm) collected on Formvar carbon-coated nickel grids. Grids with sections were floated on drops of 1% bovine serum albumin (BSA) in PBS containing 0.02-M glycine at room temperature for 30min to reduce nonspecific binding. Sections were then incubated with a rabbit polyclonal antibody against FR- β cat#PA5-45768 (1:10) (Invitrogen, ThermoFisher) in PBS 0.1% BSA at 4°C overnight. The grids were then washed in four drops of PBS for a total of 15 min, transferred to 50 μ L drops of secondary antibody conjugated to 10-nm gold particles for 1 h at room temperature. After immunolabeling, the sections were rinsed with PBS and distilled water. Control staining to demonstrate the specificity of the immunolabeling was carried out with the same steps as above, but the primary antibody was replaced by PBS. All the observations were performed under an electron microscope operating at 80 kV (Jeol JEM -1400 Plus Jeol Ltd., Tokyo, Japan)

Peptide structure and all related experimental data are not reported since a new patent application is going to be filed for the CD38-PEP-MSN-BTZ prototype.

3.4. Conclusion and future work

An oligopeptide sequence able to interact with the CD38 receptor over-expressed by multiple myeloma cells was designed and synthesized.

The peptide was synthesized, characterized and conjugated to the external surface of mesoporous silica nanoparticles as targeting molecule with the aim to achieve a more specific and efficient bortezomib delivery system (CD38-PEP-MSN-BTZ).

The uptake of the system containing on the external surface the new targeting peptide molecule was evaluated by TEM analysis. TEM images showed that the system is internalized by CD38+ RPMI MM cells. TEM studies on normal cells, expressing low levels of CD38, needed.

The synthesis of the complete system with the targeting peptide molecule on the MSNs external surface and with the bortezomib linked inside the pores via pH sensitive bond and its *in vitro/in vivo* evaluation is ongoing.

The new synthesized CD38 peptide ligand might be an excellent substitute of folic acid for the MSN-BTZ prototype, since CD38 receptor is highly expressed on MM cells.

References

1. X-X. Zhang, H.S. Eden, X. Chen, *J Control Release.*, **2012**, 159, 1: 2–13.
2. E. Vivès, J. Schmidt, A. Pèlegri, *Biochimic Biophys Acta*, **2008**, 1786, 126–138.
3. E. Ruoslahti, *Adv Drug Deliv Rev*, **2017**, 3, 12, 110–111
4. K. N. Sugahara , T. Teesalu , P.P. Karmali , V.R. Kotamraju , L. Agemy , D.R. Greenwald , E. Ruoslahti , *Science*, **2010** , 328 , 1031
5. N. Tsomaia, *Eur J Med Chem.*, **2015**, 13, 94:459-470.
6. S-H. Wang, J. Yu, *Biomaterials*, **2018**, 156, 1-15.
7. S.V. Rajkumar, *Am J Hematol*, **2016**, 91, 7: 719-734.
8. W.A. Sodeman, M.D. Sodeman, *Instructions for Geriatric Patients (Third Edition)*, **2005**, Page 324.
9. K.A. Sarosiek, L.E. Cavallin, S. Bhatt, N.L. Toomey, Y. Natkunam, W. Blasini, A.J. Gentles, J.C. Ramos, E.A. Mesri, I.S. Lossos, *Proc. Natl. Acad. Sci. U. S. A.*, **2010**, 107, 13069–13074.
10. J. Adams, V.J. Palombella, E.A. Sausville, J. Johnson, A. Destree, D.D. Lazarus, J. Maas, C.S. Pien, S. Prakash, P.J. Elliott, *Cancer Res*, **1999**, 59:2615-2622.
11. C.M. Pickart, M.J. Eddins, *Biochim Biophys Acta*. **2004**,1695(1-3):55-72.
12. T. Hideshima, P. Richardson, D. Chauhan, V.J. Palombella, P.J. Elliott, J. Adams, K.C. Anderson, *Cancer Res*, **2001**, 61:3071-3076.
13. T. Hideshima, C. Mitsiades, M. Akiyama, T. Hayashi, D. Chauhan, P. Richardson, R. Schlossman, K. Podar, N.C. Munshi, N. Mitsiades, K.C. Anderson, *Blood*, **2003**, 101:1530-1534.
14. N. Mitsiades, C.S. Mitsiades, V. Poulaki, D. Chauhan, G. Fanourakis, X. Gu, C. Bailey, M. Joseph, T.A. Libermann, S.P. Treon, N.C. Munshi, P.G. Richardson, T. Hideshima, and K.C. Anderson, *Proc Natl Acad Sci U S A*, **2002**, 99, 14374-14379.
15. R. LeBlanc, L.P. Catley, T. Hideshima, S. Lentzsch, C.S. Mitsiades, N. Mitsiades, D. Neuberg, O. Goloubeva, C.S. Pien, J. Adams, D. Gupta, P.G. Richardson, N.C. Munshi, K.C. Anderson, *Cancer Res*, **2002**, 62, 4996-5000.
16. J. Su, F. Chen, V. L. Cryns, P.B. Messersmith, *J. Am. Chem. Soc.*, **2011**, 133, 11850–11853.
17. W. Xu, J. Ding, L. Li, C. Xiao, X. Zhuang, X. Chen, *Chem. Commun.*, **2015**, 51, 6812–6815
18. G. Unsoy, S. Yalcin, R. Khodadust, P.Mutlu, O. Onguru, U.Gunduz, *Biomed Pharmacother*, **2014**, 68, 5 , 641-648.
19. J.D. Ashley, J.F. Stefanick, V.A. Schroeder, M.A. Suckow, T. Kiziltepe, B. Bilgicer, *J. Med. Chem.*, **2014**, 57, 12, 5282-5292.
20. G. Zuccari, A. Milelli, F. Pastorino, M. Loi, A. Petretto, A. Parise, C. Marchetti, A. Minarini, M. Cilli, L. Emionite, D. DiPaolo, C. Brignole, F. Piaggio, P. Perri, V. Tumiatti, V. Pistoia, G. Pagnan, M. Ponzoni, *J Control Release*, **2015**, 211, 44–52.

21. C. Argyo, V. Weiss, C. Braeuchle, T. Bein, *Chem. Mater.*, **2014**, 26, 435.
22. F. Tang, L. Li, D. Chen, *Adv. Mater.*, **2012**, 24, 1504-1534.
23. Y. Du, L. Xia, A. Jo, R.M. Davis, P. Bissel, M.F. Ehrich, D.G.I. Kingston, *Bioconjug Chem.*, **2018**, 21, 92:420-430.
24. M. Vallet-Regi, F. Balas, D. Arcos, *Angew. Chem.*, **2007**, 46, 7548–7558.
25. C.P. Silveira, L.M. Apolinario, W.J. Favaro, A.J. Paula, N. Duran, *ACS Biomater. Sci. Eng.*, **2016**, 2, 1190–1199.
26. G. Cavallaro, P. Pierro, F.S. Palumbo, F. Testa, L. Pasqua, R. Aiello, *Drug Deliv.* **2004**, 11, 41–46.
27. I.S. Carino, L. Pasqua, F. Testa, R. Aiello, F. Puoci, F. Iemma, N. Picci, *Drug Deliv.* **2007**, 14, 491–495.
28. M. Martinez-Carmona, A. Baeza, M.A. Rodriguez-Milla, J. Garcia-Castro, M. Vallet-Regi, *J. Mater. Chem. B*, **2015**, 3, 5746–5752.
29. L. Pasqua, A. Leggio, A. Liguori, C. Morelli, S. Andò, (2016) "Bortezomib-Based Delivery System". EP3288955B1, Publication number, WO2016174693 A1. Application number PCT/IT2016/000111. Owned by NanoSilical Devices Srl, spin-off of the University of Calabria.
30. R. Aiello, U. Maione, L. Pasqua, F. Testa EP2001514B1 (PCT/IT2006/000167);
31. L. Pasqua, F. Testa, R. Aiello, S. Cundari, J.B. Nagy, *Micropor Mesopor Mat*, **2007**, 103, 166-173.
32. C. Morelli, P. Maris, D. Sisci, E. Perrotta, E. Brunelli, I. Perrotta, M. L. Panno, A. Tagarelli, C. Versace, M. F. Casula, F. Testa, S. Andò, J.B. Nagya and L. Pasqua, *Nanoscale*, **2011**, 3, 3198–3207.
33. S.J. Rowan, S.J. Cantrill, G.R.L. Cousins, J.K.M. Sanders, J.F. Stoddart, *Angew. Chem.*, **2002**, 41, 898–952.
34. N.W. Van de Donk, M.L. Janmaat, T. Mutis, J.J. Lammerts van Bueren, T. Ahmadi, A.K. Sasser, H.M. Lokhorst, P.W. Parren, *Immunol Rev*, **2016**, 270, 1: 95-112.
35. Q. Liu, I.A. Kriksunov, R. Graeff, C. Munshi, H.C. Lee, Q. Hao, *Structure*, **2005**, 13, 9: 1331-9.
36. C.B. Munshi, K.B. Fryxell, H.C. Lee, W.D. Branton, *Methods Enzymol*, **1997**, 280: 318-30
37. A. Funaro, M. Reinis, O. Trubiani, S. Santi, R. Di Primio, F. Malavasi, *J Immunol*, **1998**, 160:2238-2247.
38. A. Chillemi, G. Zaccarello, V. Quarona, M. Ferracin, C. Ghimenti, M. Massaia, A.L. Horenstein, F. Malavasi, *Mol Med*, **2013**, 19: 99-108.
39. M-K. Han, S-J. Kim, Y-R. Park, Y-M. Shin, H-J. Park, K-J. Park, K-H. Park, H-K. Kim, S-I. J., N-H. An, and U-H. Kim, *J. Biol. Chem.* **2002**, 277:5315-5321.
40. N. Garofalo, A. Comandé, I. Perrotta, M. Davoli, G. Niceforo, L. Pasqua, *Adv. Sci. Lett.*, **2017**, 23, 6026-6028.

Synthesis of novel PSMA-targeted tracers as diagnostic tools for prostate cancer

[Ongoing work 3]

Abstract

Prostate cancer is the second most prevalent cancer for men worldwide. The progression of this type of cancer is very slow and can take up to 15 years for its full development into metastatic lesions. However, it is difficult to diagnose prostate cancer at an early stage due to the little symptoms that it expresses. Therefore, screening for early signs of prostate cancer is of clinical importance to detect it before it metastases and spreads to areas where it will be too difficult to eradicate. The aim of this study has been to develop four novel PSMA tracers for improved (early) diagnosis of prostate cancer. The inhibitors have been linked to a tris-hydroxypyridinone (THP) chelator to produce a total of four new THP-PSMA molecular probes for prostate cancer imaging via PET.

4.1. Introduction

Prostate cancer (PCa) is the most common one in European men and the first cancer-related cause of mortality and it was estimated that its incidence is constantly increasing.¹ The survival rate increases if this cancer is diagnosed in its early stage when still confined to the prostate gland. Nevertheless, the diagnosis of the tumor often occurs in already advanced stages of metastasis when chances of survival are drastically decreased.² In addition, in these stages its identification and treatment are made difficult by the lack of highly specific markers on the metastatic cells in circulation.³

Currently, diagnosis tools commonly used for PCa are prostate-specific antigen (PSA) level in blood, digital rectal examination, and prostate gland biopsies. Among these, the measurement of serum PSA level is the most used, even if its accuracy is not widely accepted across the scientific community⁴. In fact, dosage often gives high false-positives that can instead be related to other pathological conditions. Given the complexity of this neoplasia, new diagnostic tools that allow improving the prostate patient outcome and overcoming the limits of current ones are urgently needed. Over the last few years, molecular imaging-based techniques have seen a remarkable development in the nuclear oncology field. Used mainly as a diagnostic tool, these techniques are able to target specific molecules in a safe and non-invasive way providing high levels of earlier diagnostic accuracy and improving the overall management of the disease.

Single photon-emission computed tomography (SPECT) and positron emission tomography (PET) are the two most widely used, the latter, combined with the use of radiolabelled compounds, being the most efficient in detecting molecular and cellular biological processes.⁵ In PET imaging clinical practice, ⁶⁸Ga is widely used as a radionuclide because of its good decay properties, half-life of 68 minutes and the availability of the positron-emitting isotope.⁶⁻⁹

PSMA, prostate-specific membrane antigen, also known as glutamate carboxypeptidase (GCPII) is a type II transmembrane exopeptidase consisting of 750 amino acids, presenting an intracellular moiety (amino acids 1-18), a transmembrane domain (amino acids 19-43) and an extracellular portion (amino acids 44-750).¹⁰

Under physiological conditions, this protein is expressed in the nervous system where it performs the function of hydrolyzing the endogenous *N*-acetylaspartyl glutamate

(NAAGa) in *N*-acetylaspartate and glutamate, and is also expressed to a lesser extent in small intestine and kidneys.¹¹

PSMA has gained considerable interest in PCa research as it is over-expressed on cancer cells and its expression levels are related to tumor progression.^{12, 13} The up-regulation of PSMA expression on the cell surface together with the wide extracellular target make PSMA an excellent molecular marker for the development of small radiopharmaceuticals molecules.¹⁴

PSMA crystal structure analysis allowed to define important structural elements such as the interactions between the active site and potential inhibitors, useful for the design of PSMA ligands. PSMA contains a binuclear Zn^{2+} site which catalyzes the hydrolysis of α or γ -linked glutamates into peptide structures, and an S1 to S1' (pharmacophore) subpockets.¹⁵ Site S1' is the one preferentially implicated in the bind of inhibitors, in particular with structures containing a glutamate or glutamate-like structures in the C terminal portion.¹⁶ A fundamental element is the presence of a urea group that is planar as a peptide bond, but can resist to enzyme hydrolysis and increases the lipophilicity of the system.¹⁷

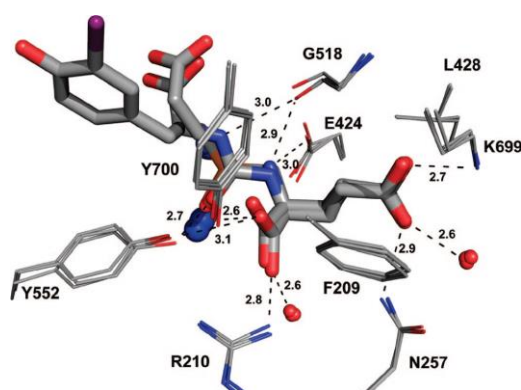


Figure 2. Structural similarity of the glutamate binding in the S1' pocket. The X-ray structures of rhGCPII/EPE (PDB code 3bi0), rhGCPII/glutamate complex (PDB code 2c6g), and the rhGCPII/2 complexes are superimposed using corresponding CR-atoms. The active site ligands are in stick representation, residues shaping the S1' pocket are shown as lines, Zn^{2+} ions as blue spheres, and conserved water molecules as red spheres. The H-bonds are indicated by dashed lines with distances shown in Ångströms (from the rhGCPII/2 complex). Adapted from 17

The binding of glutamic acid through a urea linker group via alpha amine makes available three carboxylic acids, which are fundamental for binding to the active site of the enzyme.

Therefore, the use of a lysine with the amine group in the side chain available for the formation of the urea linker is an excellent building block for the design of PSMA inhibitors.¹⁸

The main purpose of this work has been to develop new PSMA inhibitor ligands with variations in their linker region lengths starting from the previously developed ⁶⁸Ga radiolabeled probe (⁶⁸Ga-THP-PSMA, Figure 1) as model compound.¹⁹

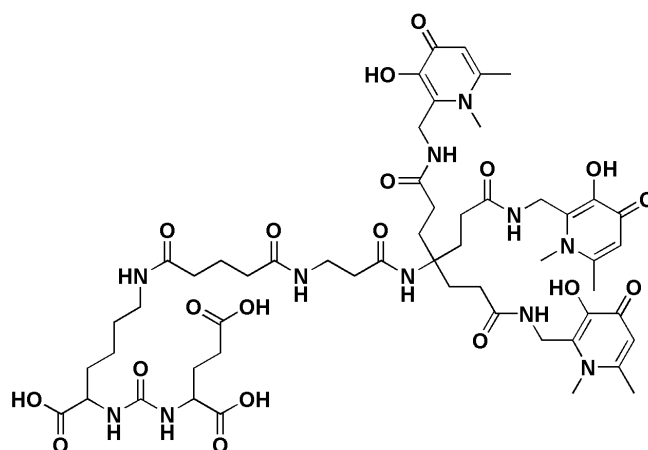
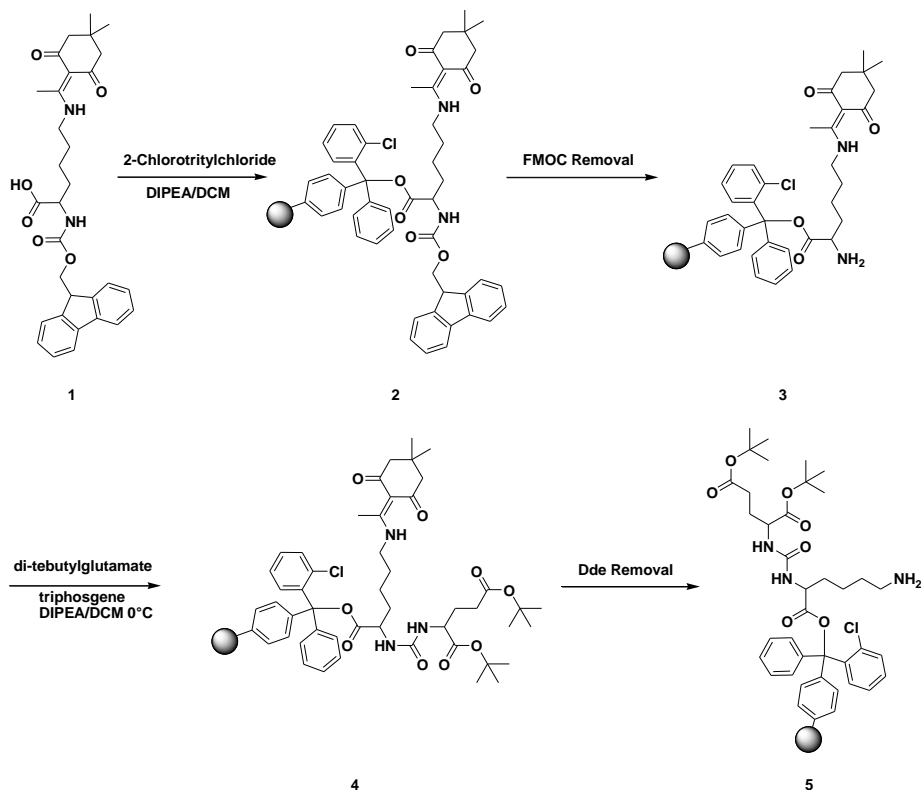


Figure 1. ⁶⁸Ga-THP-PSMA chelator.

Although the molecule has given excellent results *in vitro* and *in vivo*, binding affinity studies have shown an affinity similar or somewhat weaker than to other PSMA-targeted bioconjugates examined. Accordingly, new PSMA ligands of different sizes and lengths have been synthesized to improve the affinity binding of the system up to the (sub)nanomolar level.

4.2. Results and Discussion

The Solid-phase dipeptide synthesis was carried out using a 2-chlorotrytil chloride resin to which the Fmoc-Lysine(Dde)-OH was loaded as the first amino acid (**1**, Scheme 1).



Scheme 1. Synthesis of PSMA

The *N* α -Fmoc ((9-fluorenyl) methoxycarbonyl) group was removed using a 20% solution of piperidine in DMF (dimethylformamide) to unmask the NH₂ group **3**.

The synthesis of the urea-based structure was performed using triphosgene, which allowed the bis (tert-butyl) glutamate isocyanate formation in situ for the coupling with lysine **4**. The Dde (1-(4,4-Dimethyl-2,6-dioxocyclohex-1-ylidene)-3-ethyl) group was removed by hydrazinolysis and the reaction was monitored by LC/MS (Figure 2) doing a cleavage on a small amount of sample (10 mg) using trifluoroacetic acid with water (5% v/v), phenol (5% w/v) and triisopropylsilane (TIS) (5% v/v) as scavengers.

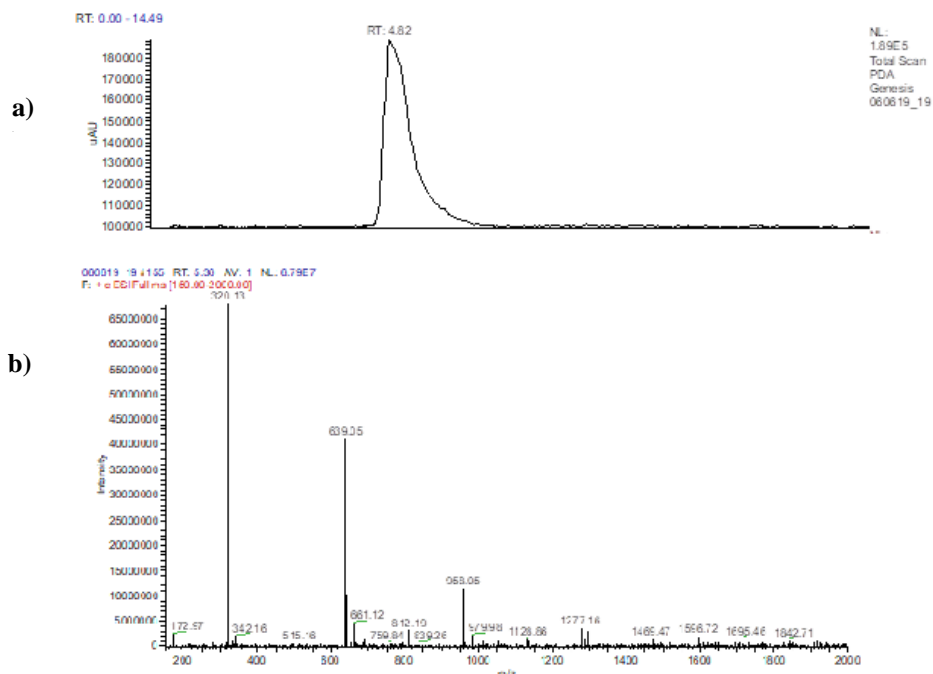


Figure 2. Liquid chromatography/mass spectrometry (LC-MS) of the compound **5**.

As depicted in Fig. 2 a) UV Chromatogram displayed a single signal with a retention time =4.82 minutes was observed corresponding to cleaved product from compound **5**, and the associated mass spectrum (Fig. 2 b) shows the m/z 320.13 ($M+H$)⁺ and 639.05 ($2M+H$)⁺ 958.06 ($3M+H$)⁺ of the MH ⁺ precursor ion. Synthesized urea-based PSMA inhibitor was then conjugated with four different tris(hydroxypyridinone) (py-THP) chelators derivatives to give the final conjugates (Figures 3, compounds **22c-d**, **28c-d**).

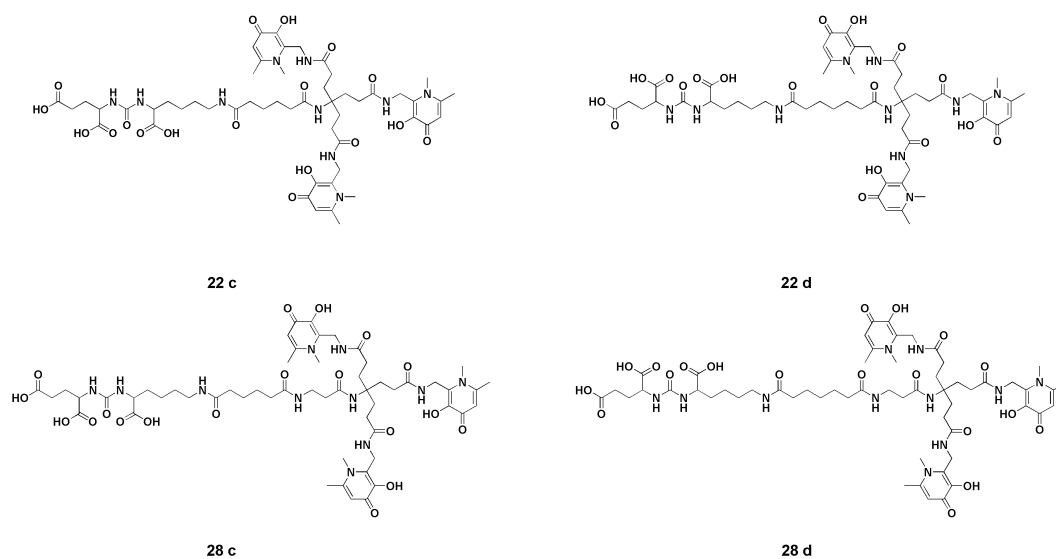


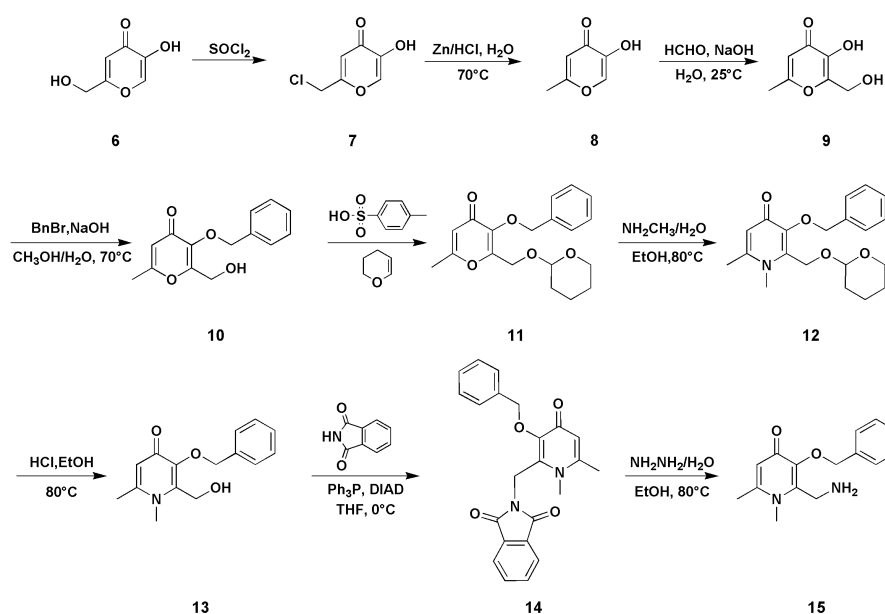
Figure 3. Structure of novel THP-PSMA ligands

The py-THP chelators have been previously synthesized in such a way to exhibit three linked bidentate 3-hydroxy-4-pyridinones able to chelate ^{68}Ga under mild conditions, with the formation of a complex with good kinetic stability.²⁰

Hydroxypyridinones have shown exceptional chelating capacities towards Fe^{3+} (high pFe^{3+} values) and given the chemical similarities between Fe^{3+} and Ga^{3+} it was predicted that these chelators would bind gallium. This would allow the development of PET radiopharmaceuticals based on ^{68}Ga .²¹⁻²⁴

The four chelator derivatives (Fig. 3) are therefore composed of a portion of peptide nature for targeting, a variable scaffold structure and portions that create coordination complexes with the ^{68}Ga .

Pyridinones were synthesized in nine steps (**6-15**, Scheme 2) starting from the commercial available kojic acid **6**, reaction with neat thionyl chloride yields the chloro-derivative, according to an established procedure.²³⁻²⁵

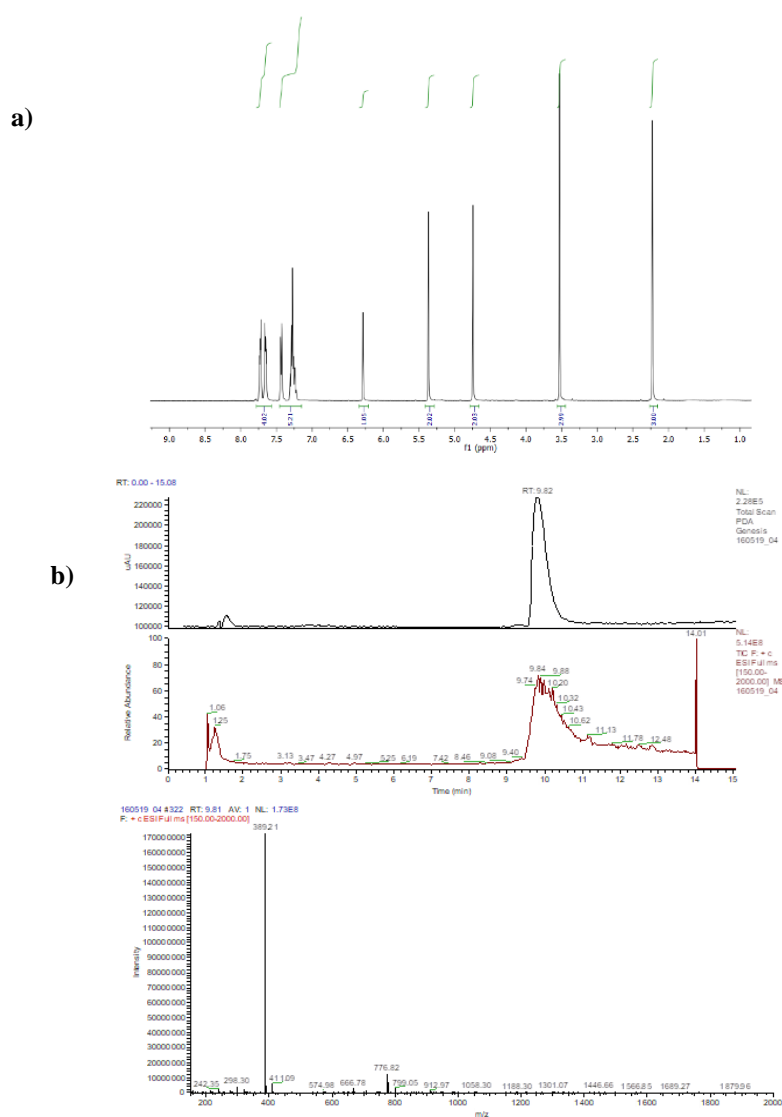


Scheme 2. Synthesis of bidentate pyridinone

A reduction reaction was then made using Zinc dust in HCl at 60 °C, affording compound **8** in a moderate yield (55%). The 2-hydroxymethyl group was subsequently introduced on the ring with a reaction similar to an aldol condensation obtaining compound **9**.

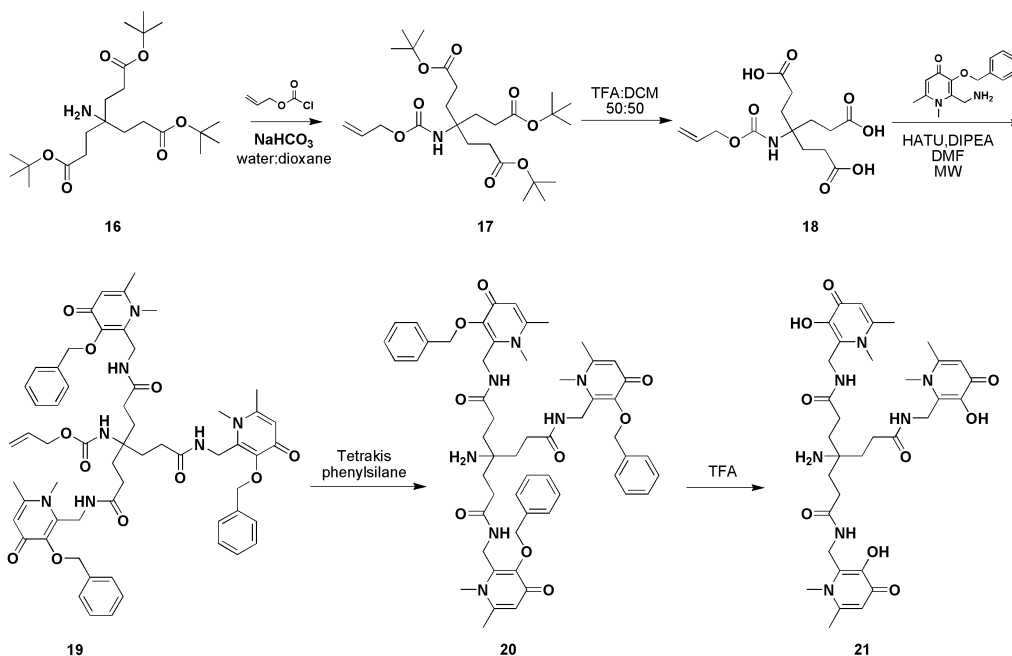
To mask the 3-hydroxyl chelator unit, a benzylation reaction was performed using benzyl bromide under alkaline conditions. The introduced benzyl group will be removed only in

the last phase of the synthesis of the final compounds to avoid any metal binding and consequently, contamination. Then 3,4-dihydro-2-H-pyran was introduced on the 2-hydroxymethyl function in position 2 (**11**) and treatment with methylamine at 70 °C allowed the subsequent conversion from pyranone to pyridinone (**12**). Thus, the protecting group was removed in acid conditions, and a Mitsunobu reaction with phthalimide. The crude was purified by column chromatography on silica gel, using chloroform: methanol 90:10 v/v as eluent mixture, so a pure white powder was obtained in a good yield (**14**, 74%) and characterized by NMR and LC/MS (Figure 4).



The ^1H NMR spectrum (Fig 4 a) shows the N-CH₃ signals at 3.53 ppm that confirms the conversion from pyranone to pyridinone, and the phthalimide signals at 7.75-7.62 ppm are present. Furthermore, the major peak in the mass spectrum m/z 389.21 [M+H]⁺ corresponds to the monpositive specie of compound **14**.

The desired product **15** was then prepared by converting phthalimide into a primary amine with which pyridinone was conjugated to tripodal tricarboxylic acid (**16**, Scheme 3).



Scheme 3. Synthesis of tris(hydroxypyridinone)

Tripodal (**16**) was first protected on the amino function with the alloc group using allyl chloroformate so that compound **17** was obtained after 4 hours and purified by column chromatography on silica gel, using as eluent solution hexane : ethyl acetate = 70:30, (**17**, yield 86%). Subsequently, to allow the coupling reaction with pyridinone the removal of tert-butyl groups on carboxylic acids was carried out with a mixture of trifluoroacetic acid and dichloromethane 50:50 v/v (**18**).

The amide bond formation was performed under microwave conditions, activation of the carboxylic acids was achieved using HATU as the coupling reagent and DIPEA as a base. The amide coupling performance has been improved under microwave irradiation and the reaction was completed in a very short time (30 minutes) in good yields (**19**, 62%).

The alloc group removal was carried out using the tetrakis(triphenylphosphine)palladium(0) in anhydrous conditions affording compound **20** that presents a primary amine for the attachment of linkers with different length chain. The reaction was left to stir overnight, the crude was purified and product **20** was characterized by NMR (Figure 5).

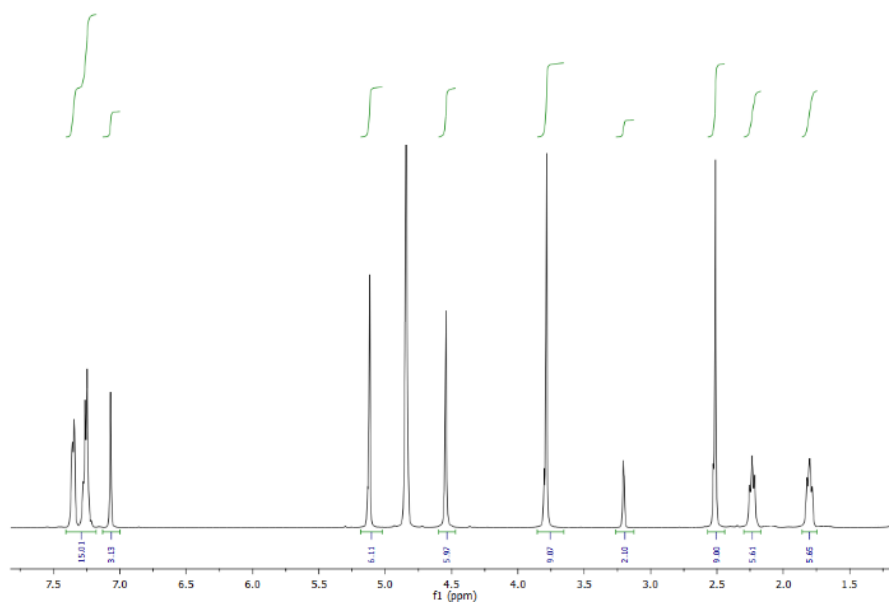
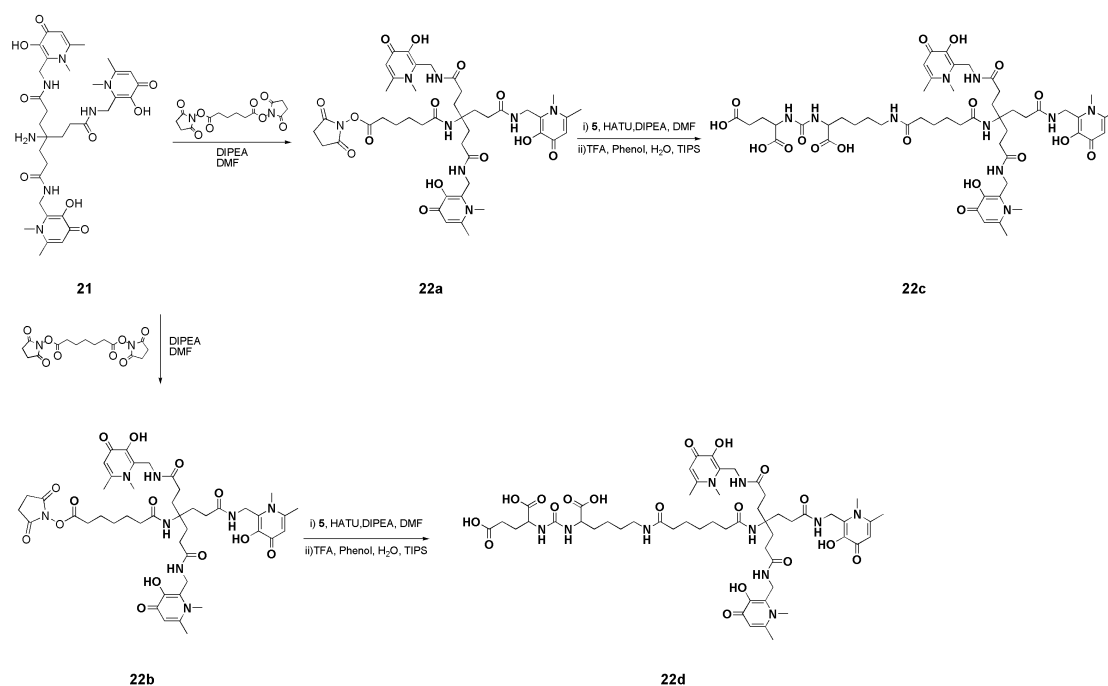


Figure 5. ^1H NMR spectrum compound **20**.

As confirmed by the spectrum, alloc group was successfully removed. Next step involves the removal of the benzyl groups that protected the pyridinones' hydroxyl group, which are directly involved in $\text{Ga}^{3+}/\text{Fe}^{3+}$ complex formation. To carry out the reaction it has been necessary to minimize the possible Fe^{3+} contamination that could come from glassware or other laboratory reagents. Therefore, the deprotection was performed in pre-treated HCl glassware.²⁶

To obtain ligands with variable length alkyl chains, compound **21** was reacted with adipic acid bis(*N*-hydroxysuccinimide ester) that incorporates a 6-atom linker (Scheme 4, **22a**, **c**), and with pimelic acid bis(*N*-hydroxy succinimide ester) that incorporates a 7-atom linker (Scheme 4, **22b**, **d**). In order to have NHS ester-activated, the two compounds have been previously synthesized starting from the corresponding chlorides and the binding reaction with the py-THP was successfully carried out without condensing agents, using DIPEA in DMF (**22a** and **22b**).

The reactions were monitored by LC-MS analysis (Figure 6 and 7) and the products were purified by preparative HPLC.



Scheme 4. Synthetic routes of final compounds **22c** and **22d**

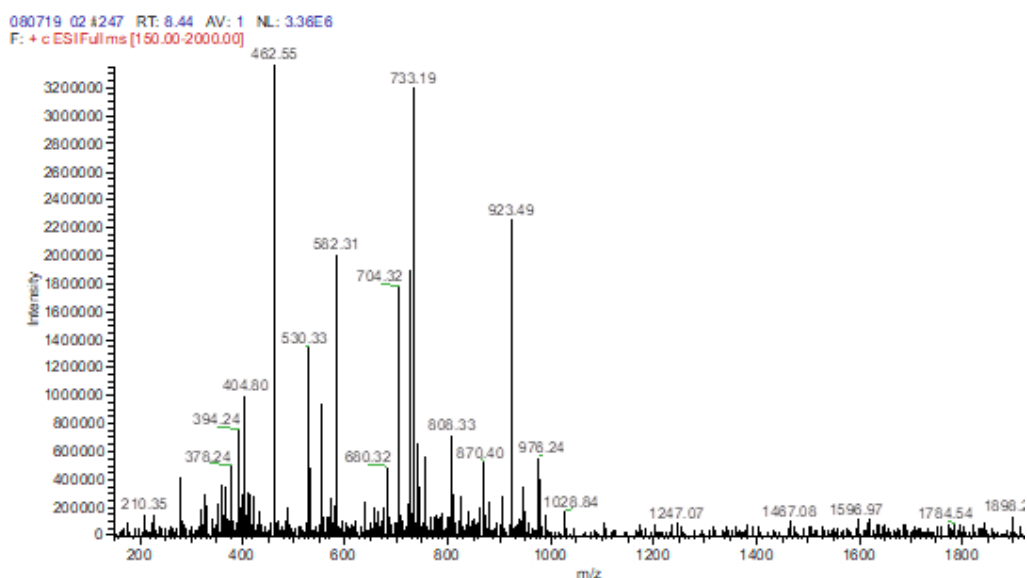


Figure 6. LC-MS analysis of the crude **22a**

The adipic acid bis(*N*-hydroxy succinimide ester) conjugation reaction was monitored by LC- MS (Figure 6) and the peak with a retention time of 8.44 belongs to compound **22a** as confirmed by the mass spectrum. When the reaction has been completed, the solvent was removed under high vacuum and the crude was purified by semipreparative reversed-phase HPLC.

The mass spectrum of the reaction crude of **22b** (Figure 7) shows the monoisotopic $[M+H]^+$ peak at m/z 937.50 (calculated $m/z = 937.42$), which is the strongest in the spectrum together with a species at m/z 469.46 $[M+2H]^+$.

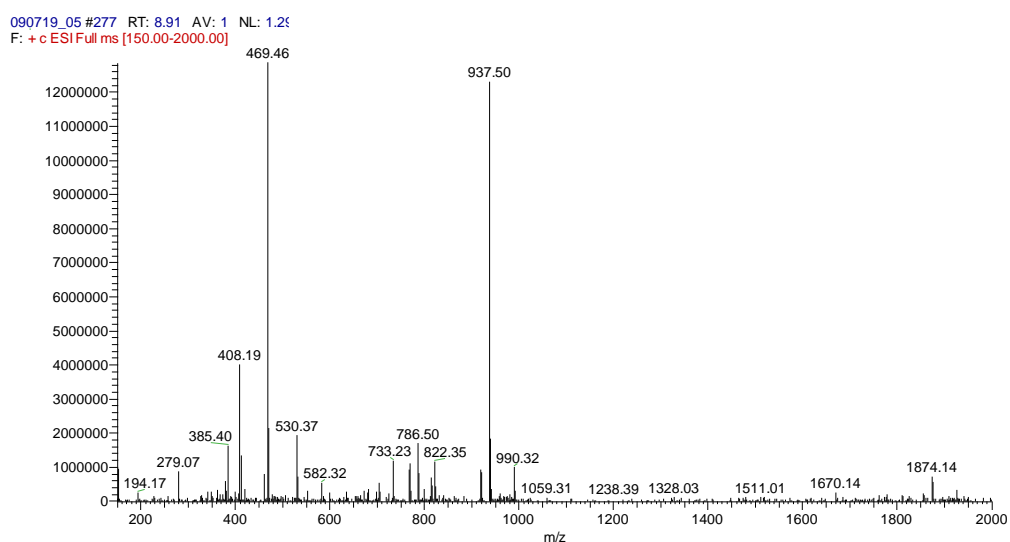


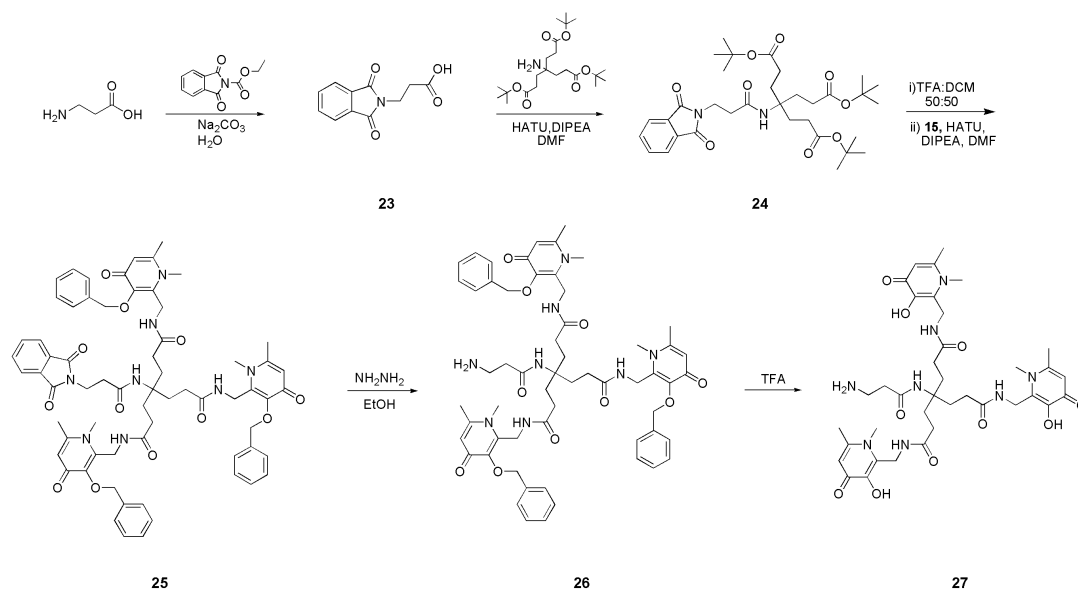
Figure 7. LC/MS analysis of the reaction crude of **22b**

The final coupling reaction between PSMA and py-THS molecules was carried out solubilizing **22a** and **22b** (0.12 mmol, 1.5 equiv) in 0.5 mL of anhydrous DMF and 0.1 mL of DMSO, HATU (0.12 mmol, 1.5 equiv), and DIPEA (0.24 mmol, 3 equiv). The solution was left to stir for 10 minutes to activate the carboxylic acids and then a suspension with **5**, previously swollen in 0.5 DMF, was added. After 36 hours the reaction mixture was filtered and washed with DMF.

Finally, the cleavage of THP-PSMA was performed using a mixture of trifluoroacetic acid, phenol, TIS, and water and after for 3 hours the reaction solution was concentrated under a nitrogen stream and products precipitated from the ice-cold ether. The crude purification by semipreparative reversed-phase HPLC and characterization of the final products **22c** and **22d** are in progress.

In order to obtain a small library of tris(hydroxypyridinone) compounds, py-THP molecules with a longer N-alkyl chain were synthesized (Scheme 5). In addition, in this case the starting material has been the tripodal that, however, has been protected on the amino group with a β -alanine-derived (**23**, Scheme 5) which has also allowed the elongation of the chain **24**.

Following the removal of the carboxylic acids protecting groups, coupling reaction with the bidentate ligand **15** was performed using HATU, DIPEA in DMF, under microwave conditions. Treatment with a 55% hydrazine solution in ethanol afforded the conversion of phthalimide into the primary amine **26**. Finally, the debenzylation was performed in neat trifluoroacetic acid and the precipitation from cold-diethyl ether allowed obtaining **27**. The reaction was monitored by LC-MS analysis (Figure 8).



Scheme 5. Synthesis of “long chain”THP

The UV chromatogram of **27** shows a single signal with a retention time of 7.58 minutes. In the correlated mass spectrum there are the two major peaks relative to the $[M+H]^+$ species at $m/z = 769.41$ and the $[M+2H]^{2+}$ at $m/z 385.47$.

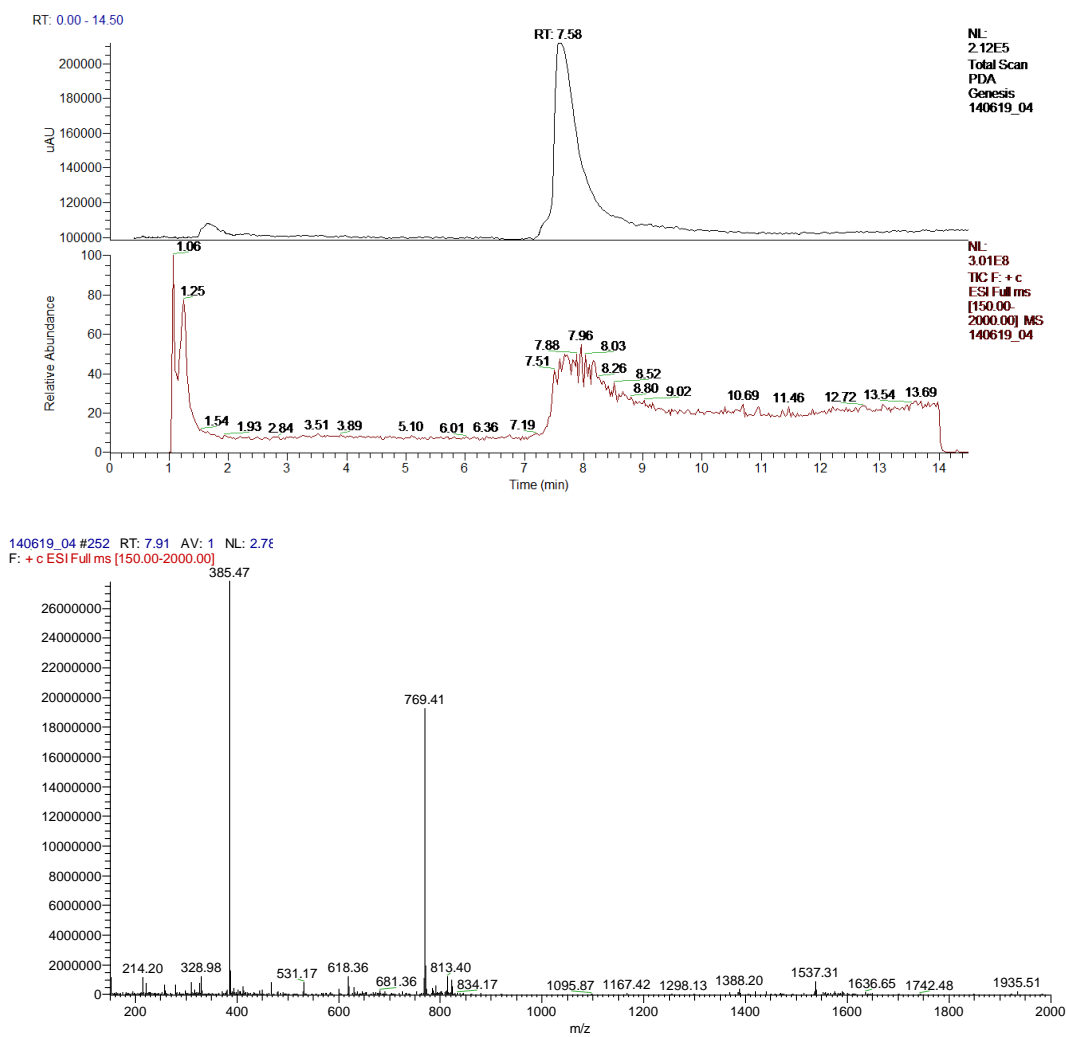
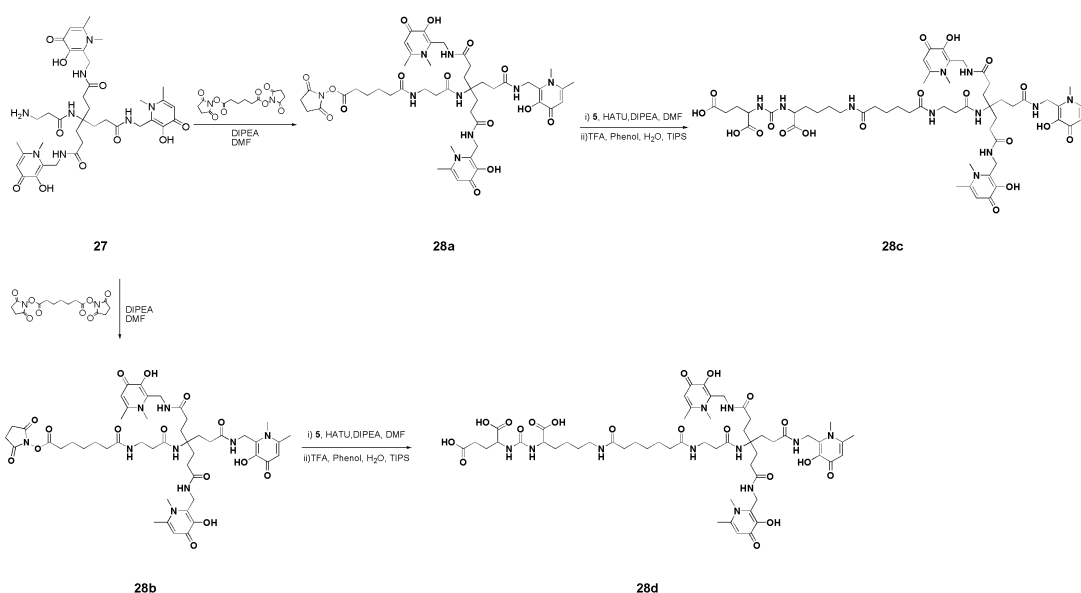


Figure 8. LC/MS analysis of debenzylated compound **27**

The debenzylated compound **27** has been reacted with adipic acid bis(*N*-hydroxysuccinimide ester) (Scheme 6, **28a, c**), and with the pimelic acid bis(*N*-hydroxysuccinimide ester) (Scheme 6, **28b, d**).



In solutions of chilled adipic acid bis(*N*-hydroxysuccinimide ester) (1.04 mmol, 10 equiv) and the pimelic acid bis(*N*-hydroxysuccinimide ester) in 2 mL of anhydrous DMF was added dropwise a mixture of **27** (0.104 mmol, 1 equiv) and DIPEA (0.156 mmol, 1.5 equiv) in 1 mL of anhydrous DMF. The reaction was carried out under inert atmosphere and was completed after 12 hours. The solvent was removed under high vacuum and the crude was purified by semipreparative reversed-phase HPLC to obtain **28a** and **28b**.

To activate groups involved in the formation of the new bond, first of all **28a** and **28b** were treated with the coupling reagent and the base, this allowed coupling reactions. After product **5** addition, the reaction in solid phase proceeded for 72 hours, and finally the resin cleavage and concurrently the removal of protecting groups in the side chains were carried out.

The reaction crudes were analyzed by LC-MS (Figures 9-10), which allowed to identify the masses of the two final products **28c** and **28d**.

The LC-MS analysis of the **28c** reaction crude (Figure 9) showed the presence of the protonated molecular ion species at m/z 600.60 of the final compound (calculated monoisotopic for $C_{55}H_{65}N_7O_9$ $m/z=$ 599.78).

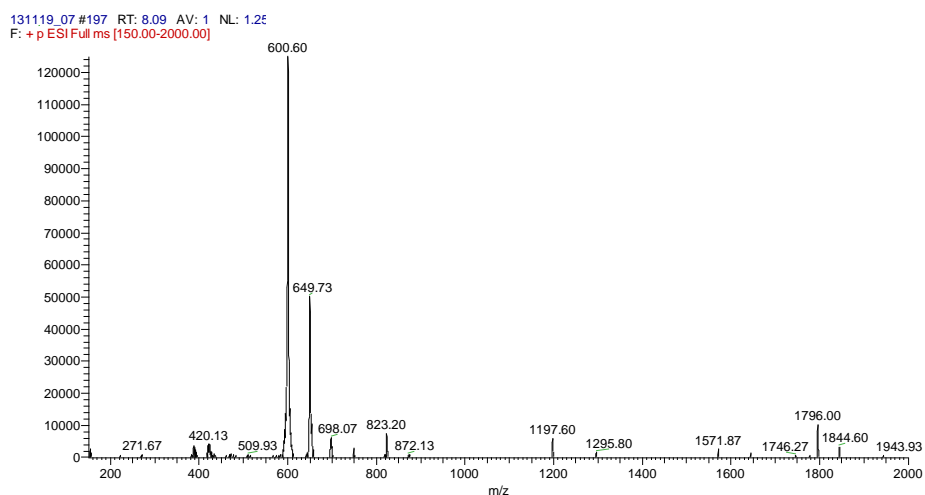
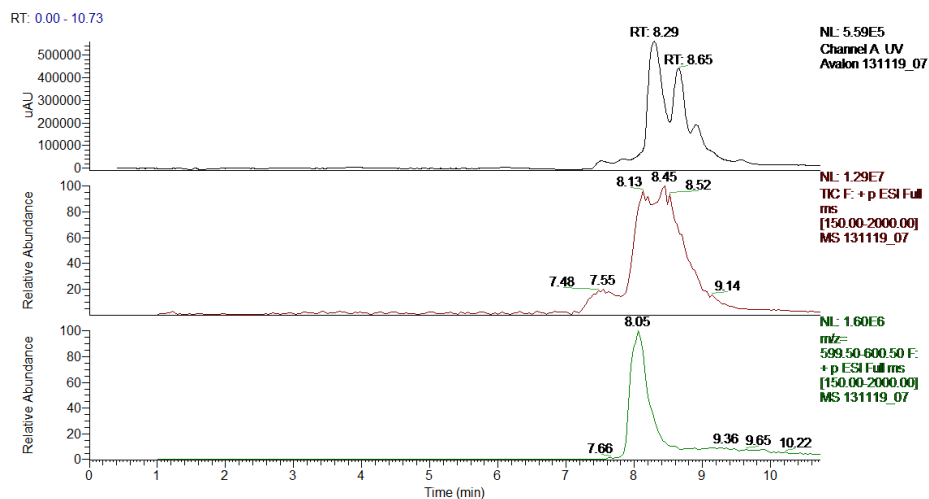


Figure 9. LC/MS analysis of reaction crude of final compound **28c**

UV-chromatogram of the **28d** crude reaction (Figure 10) shows two peaks with a retention time of 8.45 and 8.84. In particular, the first one is matching with a range mass of 605.50-606.50. The mass spectrum demonstrated the m/z 607.20 $[M+H]^+$ and corroborate the presence of the final compound in the reaction crude.

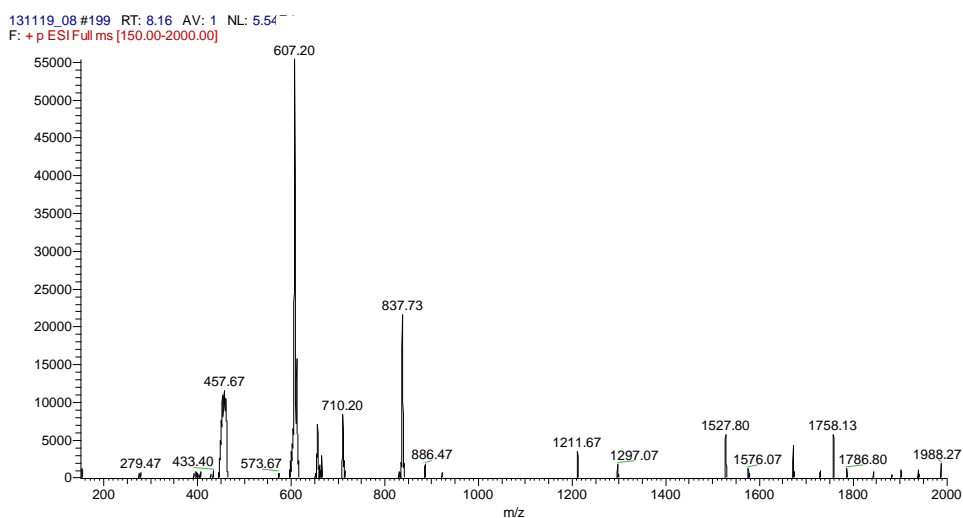
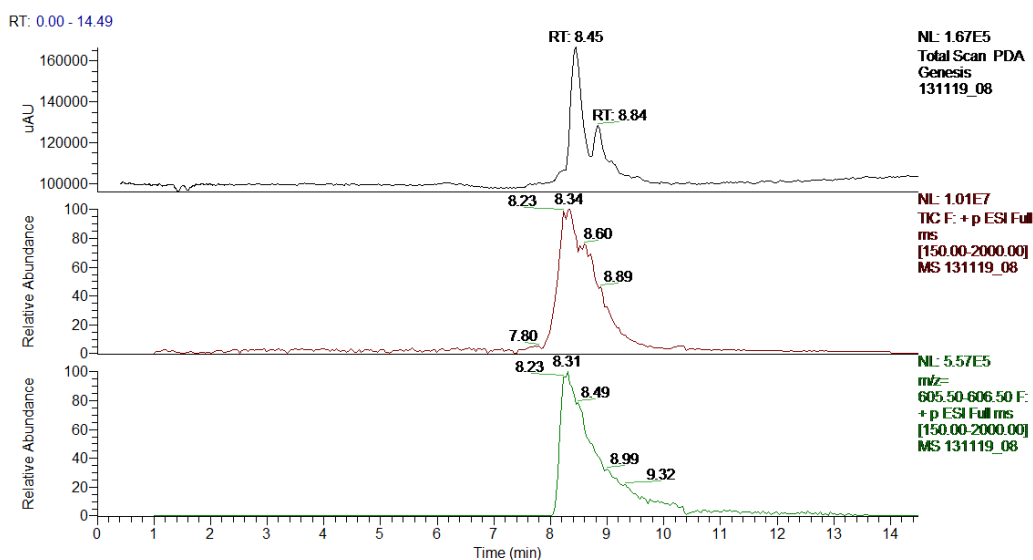


Figure 10. LC/MS analysis of reaction crude of final compound **28d**

Next steps of the synthesis, currently in progress, will be the purification of the final compounds through semi-preparative HPLC and the pure products lyophilization. We will proceed with NMR and High resolution Mass Spectrometry (HRMS) characterization and ultimately with *in vitro* binding affinity evaluation to identify the ligand with optimal characteristics.

4.3. Experimental

4.3.1. Material and instrumentation

Reagents and starting materials were obtained from commercial sources. All reactions were monitored by thin layer chromatography (TLC) using commercial plates pre-coated with Merck silica gel 60 F-254. Visualization was performed by UV fluorescence ($\lambda_{\text{max}}=254$ nm) or by staining with iodine or potassium permanganate. Chromatographic separations were performed on a silica gel column by gravity (Kieselgel 40, 0.063-0.200 mm; Merck) or flash chromatography (Kieselgel 40, 0.040-0.063 mm; Merck).

Compounds and intermediates synthesized were characterized using ^1H and ^{13}C NMR spectroscopy and mass spectrometry.

^1H NMR spectra were recorded with Avance 400 instruments (Bruker Biospin Version 002 with SGU). Chemical shifts (δ) are reported in ppm to the nearest 0.01 ppm, using the solvent as internal standard.

Analytical HPLC-MS experiments were performed on Agilent 1100 Series coupled to a Thermo LCQ DecaXP (operating in ES^+ or ES^- mode). A Phenomenex Luna C18-(2)-HST (50 \times 2 mm, 2.5 μm) column was used and the mobile phase, in linear gradient, was composed of solvent A (H_2O , +0.1% formic acid +0.05 TFA) and solvent B (acetonitrile, +0.1% formic acid +0.05 TFA). The sample solutions were prepared at a concentration of 0.1–0.01 mg/mL. The injection volume was 10–50 μL , the flow rate was 0.3 mL min^{-1} , the column temperature was 40 $^\circ\text{C}$. The values of retention time (R_t) are given in minutes. Preparative HPLC purifications were performed using a Gemini 5 μ C18 110A Axia column (100 mm \times 30 mm, 5 micron) and H_2O : CH_3CN (gradient from 98 : 2 to 5 : 95, over 45 min) as the mobile phase. The solvents were degassed and supplemented with 0.1% formic acid prior to use. The platform consisted of a Waters RP-HPLC system (Waters 2767 autosampler for sample injection and collection; Waters 2545 and 515 pumps to deliver the mobile phase to the source) coupled to a Waters Micromass ZQ mass spectrometer (with ESI in positive and negative modes) and a Waters 2996 Photodiode Array (with detection between 190–800 nm).

4.3.2. Synthesis of THP-PSMA ligands

4.3.2.1. Synthesis of Resin bound PSMA.

The dipeptide system was synthesized according to the procedure reported on J.D. Young *et al* 2017.¹⁹

Synthesis of compound 2 and 3. In a reaction vessel, 1.2 g (1 equiv) of 2-chlorotrityl chloride resin was placed in CH₂Cl₂ (dichloro methane) to swell for about 30 minutes. The first amino acid loading was carried out solubilizing 0.447g (0.7 equiv) Fmoc-Lys(Dde)-OH in anhydrous CH₂Cl₂ (dimethylformamide) and adding 440 μL of DIPEA (*N,N*-Diisopropylethylamine) (3 equiv). The reaction was allowed to stir at room temperature for 3 hours, after which it was filtered and washed with CH₂Cl₂ and DMF. In order to cap the chloride on the resin a mixture of DIPEA (20 equiv) in methanol (10 mL) was added and the reaction was left to stir for 30 minutes. Then, the resin was filtered and washed with CH₂Cl₂ and DMF (**2**).

The removal of *N*-Fmoc protecting group was performed using 15 mL of a 20% piperidine solution in DMF and stirred for 30 minutes, the resulting resin was washed with DMF (**3**).

Synthesis of compound 4. In a three-neck round bottomed flask a solution of triphosgene (300 mg, 1 mmol) in anhydrous CH₂Cl₂ (5 mL) was prepared, at 0°C under a nitrogen atmosphere. 900 mg of L-glutamic di tert-butyl ester hydrochloride was dissolved in 200 mL of anhydrous CH₂Cl₂ and 1.5 mL of DIPEA and added dropwise, over 1 hour, to the triphosgene solution. Then, the reaction solution was stirred for 1 hour, at room atmosphere and a swollen suspension of **3** (650 mg) in anhydrous CH₂Cl₂ was added and the reaction left to stir for 18 hours. The resulting resin was filtered and washed plenty with CH₂Cl₂.

Synthesis of compound 5. Removal of Dde group was carried out using a solution of 2% (v/v) hydrazine hydrate in 2 mL of DMF and the mixture was stirred for 15 minutes and filtered. The procedure was repeated four times to give compound **5**. The reaction was monitored by LC-MS doing a cleavage on a small amount (10 mg) of resin (cleavage

cocktail consisted of trifluoroacetic acid: water: TIS (triisopropylsilane): phenol 90: 2.5: 2.5: 50). LC-MS (ESI) calcd for C₁₂H₂₁N₃O₇ m/z =319.14 found m/z 320.13 [M+H]⁺, 639.05 [2M+H]⁺.

4.3.2.2. Synthesis of bidentate pyridinone

The 3-hydroxypyridin-4-ones **2-10**, were prepared following the established procedures.²³⁻²⁴

Synthesis of compound 7. Kojic acid **6** (50 g, 0.198 mol) was dissolved in distilled Thionyl Chloride (200 mL) and stirred for 1 hour. The yellow crystalline solid obtained was filtered and washed with petroleum ether. The product was recrystallized from hot water to give a colorless solid (39.8 g, 71%). ¹H NMR (400 MHz, Acetone-*d*₆) δ: 7.93 (s, 1H, 2-H), 7.69 (s, 1H, 3-OH), 6.44 (s, 1H, 5-H), 4.48 (s, 2H, Cl-CH₂).

Synthesis of compound 8. In a round-bottomed flask **7** (20g, 0.125 mol) was dissolved in water (150 mL). The mixture was stirred and heated at 40° C. Zinc dust (16.29 g, 0.25 mol) was added and then the mixture was stirred at 60°C followed by HCl 37% (37 mL) added dropwise over 1 hour. The reaction mixture was left to stir for 24 hours. The reaction progress was monitored by TLC analysis (CHCl₃ : CH₃OH 9:1 v/v, R_f=0.56), Zinc dust was removed by filtration, the pH of the filtrate was adjusted to pH=1 and extracted with CH₂Cl₂ (3×100 mL). The organic phase was dried (Na₂SO₄) and evaporated under reduced pressure to yield a brown oil. Recrystallization from isopropanol afforded a yellow crystal (13 g, 55%). ¹H NMR (400 MHz, DMSO-*d*₆) δ: 7.86 (s, 1H, 2-H), 7.57 (s, 1H, 3-OH), 6.35 (s, 1H, 5-H), 2.36 (s, 3H, 6-CH₃).

Synthesis of compound 9. The compound **8** (12g, 95 mmol) was dissolved in an aqueous solution of sodium hydroxide (4.4g, 110 mmol) and stirred at room temperature. Subsequently, 37% formaldehyde solution (9,5 mL) was added dropwise and the reaction was left to stir for 24 hours. The reaction was monitored by TLC analysis (CH₂Cl₂ : CH₃OH 8:2 v/v, R_f=0.6). When the reaction was completed, the solution was acidified to pH=1 using concentrated HCl and cooled to 5 °C then a yellow precipitate was obtained (10.9g, 70%). ¹H NMR (400 MHz, DMSO-*d*₆) δ: 8.84 (s, 1H, 3-OH), 6.22 (s, 1H, 5-H), 5.34 (s, 1H, 2-CH₂-OH), 4.40 (m, 2-CH₂-OH), 2.27 (s, 3H, 6-CH₃).

Synthesis of compound 10. To a solution of **9** (9 g, 0.57 mmol, 1 equiv) in 250 mL of methanol, sodium hydroxide (2.48 g, 0.62 mmol, 1.1 equiv) dissolved in 5 ml of distilled water was added. The reaction was stirred and heated at reflux. Benzyl bromide (9.7 g, 0.57 mmol, 1 equiv) was added dropwise over 30 min and the reaction mixture was refluxed for 24 hours. The reaction was monitored by TLC analysis (CH₂Cl₂: CH₃OH 8:2 v/v, R_f= 0.8). The solvent was evaporated under reduced pressure, the inorganic salts filtered off and the residue was dissolved in dichloromethane (200 mL). The organic phase was washed with 5% sodium hydroxide solution (1 ×100) and water (1 ×100) and dried (Na₂SO₄). The solution was then concentrated in vacuum and a brown oil was obtained. Recrystallization from dichloromethane and petroleum ether gave a white solid (18.7g, 69%). ¹H NMR (400 MHz, DMSO-d₆) δ: 7.44-7.29 (s, 5H, Ar-H), 6.26 (s, 1H, 5-H (Pyranone)), 5.01 (s, 2H, CH₂-Ph), 4.26 (s, 2H, 2-CH₂OH), 3.83 (s, 3H, N-CH₃), 2.26 (m, 3H, CH₃).

Synthesis of compound 11. The compound **10** (7g, 0.284 mmol, 1 equiv) was dissolved in CH₂Cl₂ (100 mL) in a round-bottomed flask, then 3,4-dihydro-2-H-pyran (5,20 mL, 0.561 mmol, 2 equiv) was added followed by catalytic amounts of *p*-toluensulfonic acid monohydrate (50 mg). The reaction mixture was stirred at room temperature for 6 hours and then washed with 5% aqueous sodium carbonate (10 mL) and water (1 ×10 mL). The organic fraction was dried over anhydrous sodium sulfate (Na₂SO₄) and evaporated under reduced pressure to yield a yellow/brown oil. Recrystallization with diethyl ether and petroleum ether afforded a yellow solid (2.07g, 80%). LC-MS (ESI) calcd for C₁₉H₂₂O₅ 330.37 found m/z 331.01 [M+H]⁺, 353.10 [M+Na]⁺, 660.68 [2M+H]⁺, 682.86 [2M+Na]⁺, RT = 7.14.

Synthesis of compound 12. In a sealed in a thick-walled glass tube **11** (6 g, 0.018 mmol) was dissolved in ethanol (20 mL) and 40% aqueous methylamine (20 mL). The reaction mixture was stirred at 70 °C for 16 hours. The solvent was removed under reduced pressure to give a yellow oil. Recrystallization from propan-2-ol gave a white solid (2,7 g, 45%). LC-MS (ESI) calcd for C₂₀H₂₅NO₄ m/z 343.42, found m/z 344.14 [M+H]⁺, 366.10 [M+Na]⁺, 686.77 [2M+H]⁺, RT = 6.67.

Synthesis of compound 13. The compound **12** (205g, 0.072 mmol) was dissolved in ethanol (20 mL) and 20 mL of a hydrochloric solution 2N and the reaction was heated at reflux for 12 hours. The reaction mixture was concentrated under reduced pressure, the residue was dissolved in water (50 mL) and washed with diethyl ether (2 × 20 mL). The pH of the aqueous fraction was adjusted to pH 9 with 10 N sodium hydroxide solution and was followed by extraction with dichloromethane (3×50 mL). The combined organic layers were dried over anhydrous sodium sulfate and evaporated to give a light brown solid. Recrystallization from methanol/diethyl ether afforded a white crystalline solid. ¹H NMR (400 MHz, DMSO-*d*₆) δ: 7.49-7.28 (s, 5H, Ar-H), 6.16 (s, 1H, 5-H (pyridinone)), 5.40 (s, 2H, CH₂Ph), 4.52 (s, 2H, CH₂-OH), 3.60 (s, 3H, N-CH₃), 2.35 (s, 3H, CH₃); ¹³C NMR (100 MHz, DMSO-*d*₆): δ 172.79, 148.32, 145.15, 143.26, 138.26, 128.74, 128.68, 128.25, 117.78, 73.12, 54.32, 35.92, 20.42; LC-MS (ESI) calcd for C₁₅H₁₇NO₃ m/z= 259.30 (MW), found m/z 260.12 [M+H]⁺, 282.00 [M+Na]⁺, 518.84 [2M+H]⁺, 540.98 [2M+Na]⁺, RT = 8.63.

Synthesis of compound 14. Triphenyl phosphine (2.16g, 82.6 mmol, 1.2 equiv) and phthalimide (1.21g, 82.6 mmol, 1.2 equiv) were dissolved in anhydrous tetrahydrofuran (100 mL). The compound **13** (1.79 g, 68.8 mmol, 1 equiv) was added and the mixture was cooled to 0°C in an ice bath. Diethyl azodicarboxylate (1.3 mL, 82.6 mmol, 1.2 equiv) was added dropwise over 30 min, and the reaction mixture was allowed to warm slowly to room temperature for 12 hours. The precipitate obtained was filtered, washed with THF (10 mL), and dried under reduced pressure to yield a white powder (2,4 g, 74%) ¹H NMR (400 MHz, CDCl₃) δ: 7.75-7.62 (m, 4H, phthalimide Ar-H), 7.74-7.15 (m, 5H, benzyl Ar-H), 6.29 (s, 1H, 5-H (pyridinone)), 5.37 (s, 2H, CH₂Ph), 4.74 (s, 2H, CH₂N), 3.53 (s, 3H, N-CH₃), 2.23 (s, 3H, CH₃); ¹³C NMR (100 MHz, CDCl₃) δ: 172.36, 168.58, 145.89, 145.46, 136.52, 136.01, 133.25, 130.74, 128.43, 127.15, 126.87, 122.43, 118.26, 71.12, 35.34, 33.67, 28.68, 20.08; LC-MS (ESI) calcd for C₂₃H₂₀N₂O₄ m/z= 388.42 found m/z 389.21 [M+H]⁺, 411.09 [M+Na]⁺, 776.82 [2M+H]⁺, 799.05 [2M+Na]⁺, RT = 9.82.

Synthesis of compound 15. To a solution of **14** (2.2 g, 56.7 mmol) in ethanol (20 mL) was added 4 mL of 5.5% aqueous hydrazine. The reaction was refluxed for 3 hours and after being cooled to 0 °C was acidified to pH=1 with concentrated hydrochloric acid.

The resulting precipitate was filtrated and concentrated in vacuo, and then the residue was dissolved in distilled water (50 mL), adjusted to pH 12 with 10 N sodium hydroxide, and extracted with dichloromethane (3×100 mL). The combined organic layers were dried over Na_2SO_4 , and the solvent was removed under reduced pressure to yield an orange oil. Purification by column chromatography on silica gel (chloroform: methanol 90:10 v/v) gave a white solid (1.3 g, 90%). ^1H NMR (400 MHz, $\text{DMSO}-d_6$) δ : 7.46-7.28 (m, 5H, Ar-H), 6.13 (s, 1H, 5-H (pyridinone)), 5.07 (s, 2H, CH_2Ph), 3.74 (s, 2H, $\text{CH}_2\text{-NH}_2$), 2.50 (s, 3H, N- CH_3), 2.27 (s, 3H, 6- CH_3), 1.51 (s, 2H, NH_2); ^{13}C NMR (100 MHz, $\text{DMSO}-d_6$) δ : 172.66, 147.92, 145.33, 144.53, 138.33, 129.01, 128.73, 128.31, 117.62, 72.59, 39.39, 36.92, 35.61, 20.57; LC-MS (ESI) calcd for $\text{C}_{15}\text{H}_{18}\text{N}_2\text{O}_2$ $m/z = 258.32$, found m/z 259.33 $[\text{M}+\text{H}]^+$, 517.00 $[2\text{M}+\text{H}]^+$, 539.00 $[2\text{M}+\text{Na}]^+$, RT = 4.31.

4.3.2.3. Synthesis of Tripodal tris(hydroxypyridinone) ligands

Synthesis of adipic acid bis(*N*-hydroxysuccinimide ester). *N*-Hydroxysuccinimide (690 mg, 6.0 mmol, 1.1 equiv) was dissolved in 40 mL of tetrahydrofuran and the solution was cooled at 0°C . A solution of triethylamine (607 mg, 6.0 mmol, 1.1 equiv) and adipoyl chloride (1g, 5.46 mmol, 1 equiv) was added dropwise over 10 minutes. The reaction mixture was left to stir at room temperature overnight. The solvent was removed under reduced pressure, the residue was dissolved in CH_2Cl_2 and washed 2 times with water (2×50 mL). Recrystallization with *isopropyl alcohol* afforded a white solid. ^1H NMR (400 MHz, CDCl_3) δ : 2.80-2.72 (m, 8H, $\text{COCH}_2\text{CH}_2\text{CO}$), 2.64-2.56 (m, 4H, OCOCH_2), 1.86-1.79 (m, 4H, COCH_2CH_2); LC-MS (ESI) calcd for $\text{C}_{14}\text{H}_{16}\text{N}_2\text{O}_8$ 340.29, found m/z 340.87 $[\text{M}+\text{H}]^+$, 702.56 $[2\text{M}+\text{Na}]^+$, RT = 9.90.

Synthesis of pimelic acid bis(*N*-hydroxysuccinimide ester). *N*-Hydroxysuccinimide (642 mg, 5.58 mmol, 1.1 equiv) was dissolved in 40 mL of tetrahydrofuran and the solution was cooled at 0°C . A solution of triethylamine (564 mg, 5.58 mmol, 1.1 equiv) and pimeloyl chloride (1g, 5.07 mmol, 1 equiv) was added dropwise over 10 minutes. The reaction mixture was left to stir at room temperature overnight. The solvent was removed under reduced pressure, the residue was dissolved in CH_2Cl_2 and washed 2 times

with water (2×50 mL). Recrystallization with *isopropyl alcohol* afforded a white solid. ¹H NMR (400 MHz, CDCl₃) δ: 2.91-2.77 (m, 8H, CHCH₂CH₂CO), 2.63 (t, 4H, J= 7.4 Hz, NCOCH₂), 1.86-1.75 (m, 4H, NCOCH₂CH₂), 1.63-1.52 (m, 2H, COCH₂CH₂CH₂); LC-MS (ESI) calcd for C₁₅H₁₈N₂O₈ m/z= 354.31, found m/z 354.88 [M+H]⁺, 414.86 [M+isoProp+H]⁺, RT = 10.56.

Synthesis of compound 17. Tripodal **16** (500mg, 1,20 mmol) was solubilized in 20 mL 1:1 (v/v) of water/dioxane and stirred at 0°C. A solution of Allyl chloroformate (217.54 mg, 1.80 mmol) and NaHCO₃ in 2 mL of anhydrous dioxane were added dropwise. The reaction mixture was stirred at 0°C for 2 hours and then left for other 2 hours at room temperature. The crude was extracted with dichloromethane (3 × 10 mL) treated with an aqueous 1 N HCl solution (10 mL) and extracted with methylene chloride (3 × 10 mL). The combined organic extracts were washed with a saturated aqueous solution of 1 N Hydrochloric acid (3 × 10 mL), dried (Na₂SO₄), and evaporated to dryness under reduced pressure to afford. The product was purified by silica gel chromatography (eluent solution hexane : Ethyl Acetate = 70:30, R_f = 0.68, to obtain Compound **17** (520 mg, 86%). ¹H NMR (400 MHz, CDCl₃)δ: 7.19 (s, 1H, CONH), 5.83 (m, 1H, CH=CH₂), 5.15 (m, 2H, CH=CH₂), 4.73 (s, 2H, OCH₂CH), 2.15 (m, 6H, (CH₂-CH₂-COO-tbu)₃) 1.84 (m, 6H (CH₂-CH₂-COO-tbu)₃) 1.37 (s, 27H (CH₂-CH₂-COO-tbu)₃).

Synthesis of compound 18. The reaction was carried out using 16 mL 1:1 (v/v) trifluoroacetic acid: CH₂Cl₂ and left overnight at room temperature. The trifluoroacetic acid was evaporated under a nitrogen stream and the compound was precipitated with the addition of ice-cold diethyl ether. The suspension was centrifuged and washed 3 times with diethyl ether, the solvent was removed by rotary evaporation. ¹H NMR (400 MHz, DMSO-d₆) δ: 12.04 (s, 3H, COOH), 6.85 (s, 1H, CONH), 5.88 (m, 1H, CH=CH₂), 5.21 (m, 2H, CH=CH₂), 4.42 (s, 2H, OCH₂CH), 2.12 (m, 6H, (CH₂-CH₂-COOH) 1.78 (m, 6H (CH₂-CH₂-COOH).

Synthesis of compound 19. To a solution of **18** (0.3 mmol, 1 equiv) in 5 ml anhydrous DMF, HATU (1.05 mmol, 3.5 equiv) and DIPEA (3 mmol, 10 equiv) were added and the mixture was stirred until its color changed from yellow to gold. The compound **15** (0.93 mmol, 3.1 equiv) was solubilized in 5 ml of anhydrous DMF and added to the solution

containing the THP. The microwave-assisted reaction was set at 120°C for 30 minutes. The formation of the tri-functionalized product was monitored by LCMS. DMF was removed in vacuo. The residue was dissolved in chloroform and purified by column chromatography (silica gel) with a mobile phase of 9:1 CHCl₃/CH₃OH. The fractions were combined, dried (Na₂SO₄) and the solvent was removed in vacuo to give a white solid (0.19g 62% yield). ¹H NMR (DMSO-d₆) δ: 7.41-7.22 (m, 15H [CH₂-Bnz]) 7.15 (s, 1H [CONH]) 6.2 (s, 3H [5-H pyridinone]) 5.77 (s, 1H, CH=CH₂), 5.04 (s, 6H [CH₂-Bnz]) 4.79 (m, 6H [CONH-CH₂-pyridinone]) 3.35 (s, 9H [6-CH₃ pyridinone]) 2.2 (s, 9H [N-CH₃ pyridinone]) 2.0 (m, 6H [CH₂-CH₂-CONH-pyridinone]) 1.75 (m, 6H [CH₂-CH₂-CONH-pyridinone]); LC-MS (ESI) calcd for C₅₉H₆₉N₇O₄ 1052.22 (MW), found m/z 351.84 [M+3H]⁺, 526.94 [M+2H]⁺, 1052.50 [M+H]⁺, RT = 10.39.

Synthesis of compound 20. Compound **19** (0.3 mmol, 1 equiv) was dissolved in 15 mL of anhydrous DCM under inert atmosphere. Phenylsilane (1.8 mmol, 6 equiv) and tetrakis(triphenylphosphine)palladium(0) (0.03 mmol, 0.1 equiv) were added. The reaction was left overnight at room temperature. The solvent was removed under reduced pressure and the residue was dissolved in chloroform and purified by column chromatography (silica gel) with 9:1 CHCl₃/CH₃OH as eluent solvent. The fractions were combined, dried (Na₂SO₄) and the solvent was removed in vacuo to give a yellow solid (56 %). ¹H NMR (400 MHz, methanol-d₄) δ: 7.39-7.21 (m, 15H, C3-O-CH₂-Ph). 7.07 (s, 3H, C5-H in pyridinone), 5.13 (d, 6H, J= 6.2 Hz, CH₂-CO-NH), 4.54 (s, 6H, C3-O-CH₂-Ph), 3.79 (d, 9H, J= 7.1 Hz, N-CH₃), 3.20 (m, 2H, CO-NH-CH₂-pyridinone), 2.52 (d, 9H, J= 6.0 Hz, C6-CH₃), 2.24 (t, 6H, J= 7.7 Hz, CH₂-CH₂-CO-NH-CH₂-pyridinone), 1.80 (t, 6H, J= 7.6 Hz, CH₂-CH₂-CO-NH-CH₂-pyridinone); ¹³C NMR (100 MHz, methanol-d₄) δ: 176.19 (CH₂-CH₂-CO-NH-CH₂-pyridinone) 175.34 (C4 in pyridinone), 148.65 (C6 in pyridinone), 144.86 (C3 in pyridinone), 143.42 (C2 in pyridinone), 139.47 (i-C-CH₂ in benzyl), 130.98 (m-CH in benzyl), 127.5 (p-CH in benzyl), 117.33 (C5-H in pyridinone), 72.63 (C3-O-CH₂-Ph), 58.87 (NHC-tripod), 37.76 (CH₂-CH₂-CO-NH-CH₂-pyridinone), 31.15 (CH₂-CH₂-CO-NH-CH₂-pyridinone), 30.71 (CH₂-CH₂-CO-NH-CH₂-pyridinone), 18.83 (C6-CH₃); LC-MS (ESI) calcd for C₅₅H₆₅N₇O₉ m/z= 968.15 , found m/z 323.78 [M+3H]⁺, 485.11 [M+2H]⁺, 968.52 [M+H]⁺, 990.42 [M+Na]⁺, 1936.28 [2M+H]⁺, RT = 9.82.

Synthesis of compound 21. Removal of Benzyl groups from **20** was performed using neat trifluoroacetic acid. The reaction carried out in a round bottom flask pre-treated with HCl. The mixture was monitored by LC/MS until the complete removal of all three benzyl groups. Trifluoroacetic Acid was removed under a nitrogen stream and Iced-cold diethyl ether was added to precipitate compound **21**. The suspension was centrifuged, the solvent decanted off and the precipitate washed with diethyl ether. Volatiles were evaporated under reduced pressure. ¹H NMR (400 MHz, Methanol-d₄) δ: 6.93 (s, 3H, C5-H in pyridinone), 4.01 (d, 6H, CO-NH-CH₂-pyridinone), 2.47 (s, 9H, C6-CH₃), 2.17 (m, 6H, CH₂-CH₂-CO-NH-CH₂-pyridinone), 1.87 (m, 6H, CH₂-CH₂-CO-NH-CH₂-pyridinone); ¹³C NMR (100 MHz, MeOD) δ:174.80, 160.23, 149.05, 143.58, 138.85, 112.67, 57.18, 34.97, 30.67, 29.60, 28.40, 19.69; LC-MS (ESI) calcd for C₃₄H₄₇N₇O₉ m/z= 697.78,found m/z 349.86 [M+2H]⁺, 698.31 [M+H]⁺, 1395.22 [2M+H]⁺, RT = 8.09.

Synthesis of compound 22a. In a round-bottomed flask 288 mg (0.848 mmol, 10 equiv) of adipic acid bis(*N*-hydroxysuccinimide ester) were solubilized in 2 mL of anhydrous DMF and cooled in an ice bath. A solution of **21** (65 mg, 0.084 mmol, 1 equiv), and DIPEA (1.27 mmol, 1.5 equiv) in 1 mL of anhydrous DMF was added dropwise. The reaction was carried out under inert atmosphere and monitored by LC/MS. The solvent was removed under high vacuum and the crude purification by semipreparative reversed-phase HPLC. LC-MS (ESI) calcd for C₄₃H₅₆N₈O₁₄ m/z= 922.41, found m/z 923.46 [M+H]⁺, 462.55 [M+2H]⁺, RT = 8.44.

Synthesis of compound 22b. In a round-bottomed flask 300 mg (0.848 mmol, 10 equiv) of pimelic acid bis(*N*-hydroxysuccinimide ester) were solubilized in 2 mL of anhydrous DMF and cooled in an ice bath. A solution of **21** (65 mg, 0.084 mmol, 1 equiv) and DIPEA (1.27 mmol, 1.5 equiv) in 1 mL of anhydrous DMF was added dropwise. The reaction was carried out under inert atmosphere and monitored by LC/MS. The solvent was removed under high vacuum and the crude purification by semipreparative reversed-phase HPLC. LC-MS (ESI) calcd for C₄₅H₆₀N₈O₁₄ m/z= 937.42, found m/z 937.44 [M]⁺, 469.54 [M+2H]⁺, 530.36, [M+3ACN+2H]⁺, RT = 8.91.

Synthesis of compound 22 c. In a polypropylene syringe **22a** (110 mg, 0.12 mmol, 1.5 equiv) was dissolved in 1 mL of anhydrous DMF and 0.5 mL of DMSO (dimethyl sulfoxide). Subsequently, HATU (48 mg, 0.12 mmol, 1.5) and DIPEA (86 μ L, 0.24 mmol, 3 equiv) were added and the mixture was left to stir for 10 minutes. A suspension with **5** (80 mg, corresponding to a loading of 0.08, 1 equiv) in 2 mL of anhydrous DMF was added and the reaction carried out for 72 hours at room temperature.

The reaction mixture was filtered and washed 3 times with DMF. In order to perform cleavage and removal of side-chain protecting groups a mixture of TFA, phenol (5% w/v), water (5% v/v) and TIS (2% v/v) was prepared and added to the resin. The reaction was stirred at room temperature for 3 hours. The filtrate containing **22c** collected and the resin was washed with TFA: CH₂Cl₂. The solution was concentrated under a nitrogen stream and ice-cold diethyl ether was added to precipitate **22c**. The suspension was centrifuged, the solvent was decanted off and the precipitate washed four times with diethyl ether. The crude purification with semipreparative HPLC and further characterization are *in itinere*.

Synthesis of compound 22 d. In a polypropylene syringe, **22b** (112 mg, 0.12 mmol, 1.5 equiv) was dissolved in 1 mL of anhydrous DMF and 0.5 mL of DMSO. Subsequently, HATU (48 mg, 0.12 mmol, 1.5) and DIPEA (86 μ L, 0.24 mmol, 3 equiv) were added and the mixture was left to stir for 10 minutes. A suspension with **5** (80 mg, corresponding to a loading of 0.08, 1 equiv) in 2 mL of anhydrous DMF was added and the reaction carried out for 72 hours at room temperature.

The reaction mixture was filtered and washed 3 times with DMF. In order to perform cleavage and removal of side-chain protecting groups a mixture of TFA, phenol (5% w/v), water (5% v/v) and TIPS (2% v/v) was prepared and added to the resin. The reaction was stirred at room temperature for 3 hours. The filtrate containing **22d** collected and the resin was washed with TFA: CH₂Cl₂. The solution was concentrated under a nitrogen stream and ice-cold diethyl ether was added to precipitate **22d**. The suspension was centrifuged, the solvent was decanted off and the precipitate washed four times with diethyl ether. The crude purification with semipreparative HPLC and further characterization are *in itinere*.

Synthesis of compound 23. The synthesis was carried out following published procedure.²⁷

A solution of β -alanine (4.46 g, 50 mmol) and sodium carbonate (5.35 g, 50.5 mmol) in water (100 mL) was treated with *N*-carbethoxyphthalimide (11.51 g, 52.5 mmol). The solution was filtered and acidified to pH 2-3 with 6 M HCl. Filtration was followed by washing with water and drying in air affording a white solid (6.35 g, 57 % yield). ¹H NMR (400 MHz, DMSO-*d*₆) δ : 7.85-7.78 (m, 4H, Ar-H), 3.80 (t, *J* = 7.3 Hz, 2H, NCH₂), 2.61 (t, *J* = 7.3 Hz, 2H, CH₂CO).

Synthesis of compound 24. A mixture of **23** (2.19 g, 10 mmol), DIPEA (2.27 g, 11 mmol), HATU (1.49 g, 11 mmol), and anhydrous DMF (5 mL) was stirred at room temperature for 1 hour. A solution of **13** in 2 mL of anhydrous DMF was added and the reaction mixture was left to stir at room temperature for 72 hours. DMF was removed in vacuo and the residue was purified on a silica gel column (Ethyl Acetate/MeOH 9.5:0.5). The compound **24** (3.21 g, 52%) was obtained and characterized ¹H NMR (400 MHz, CDCl₃) δ : 7.87-7.73 (m, 4H, Ar-H), 6.13 (s, 1H, NH), 3.97 (t, *J* = 7.5 Hz, 2H, NCH₂), 2.56 (t, *J* = 7.5 Hz, 2H, CH₂CO), 2.31–2.21 (m, 6H, CH₂CH₂CO), 2.02-1.95 (m, 6H, CH₂CH₂CO), 1.56-1.42 (m, 27H, C(CH₃)₃).

Synthesis of compound 25. The reaction was carried out using 16 mL of trifluoroacetic acid: CH₂Cl₂ 1:1 (v/v) and left overnight at room temperature. The trifluoroacetic acid was evaporated under a nitrogen stream and ice-cold diethyl ether was added to precipitate a white solid. The obtained product (0.3 mmol, 1 equiv) was dissolved in 5 mL of anhydrous DMF, and then HATU (1.05 mmol, 3.5 equiv) and DIPEA (3 mmol, 10 equiv) were added. The mixture was stirred until its color changed from yellow to gold. The compound **15** (0.93 mmol, 3.1 equiv) was solubilized in 5 mL of anhydrous DMF and added to the solution containing the THP. The microwave-assisted reaction was set at 120°C for 30 minutes. The DMF was removed in vacuo and the residue was dissolved in chloroform, and purified by column chromatography (eluent solvent 9:1 CHCl₃/CH₃OH). The combined fractions were dried (Na₂SO₄) and the solvent was removed by rotary evaporation to give 0.2 g of a white solid in 58% yield. ¹H NMR (DMSO-*d*₆): δ 7.86-7.71 (m, 4H [Ar-H]), 7.56-7.45(m, 15H [CH₂-Bnz]), 7.18 (s, 1H [CONH]) 6.51 (s, 3H [5-H])

pyridinone]), 5.11 (s, 6H [$\text{CH}_2\text{-Bnz}$]), 4.79 (m, 6H [$\text{CONH-CH}_2\text{-pyridinone}$]), 3.84 (t, $J=7.5$ Hz, 2H, NCH_2), 3.38 (s, 9H [6- CH_3 pyridinone]), 2.58 (t, $J=7.5$ Hz, 2H, CH_2CO), 2.31 (s, 9H [N-CH_3 pyridinone]) 2.23-1.98 (m, 6H [$\text{CH}_2\text{-CH}_2\text{-CONH-pyridinone}$]) 1.75 (m, 6H [$\text{CH}_2\text{-CH}_2\text{-CONH-pyridinone}$]).

Synthesis of compound 26. Compound **25** (3.51 g, 3 mmol) was dissolved in ethanol (40 mL) and 5.5% aqueous hydrazine (3 mL) was added. The reaction was heated at reflux for 3 hours and after was cooled to 0 °C, acidified to pH 1 with concentrated HCl, and filtered. The filtrate was concentrated in vacuo, and the residue was dissolved in distilled water (40 mL), adjusted to pH 12 with 10 M NaOH, and extracted with dichloromethane (5 \times 100 mL). The combined organic extracts were dried over anhydrous Na_2SO_4 under reduced pressure to furnish a brown oil. Purification by column chromatography on silica gel (chloroform: methanol 90:10 v/v) gave a white solid **26** (3.20 g, 87%). ^1H NMR (400 MHz, DMSO-d_6) δ : 8.11 (s, 3H, NH), 7.62-7.31 (m, 6H, PhH), 7.55-7.36 (m, 9H, PhH), 6.23 (s, 3H, pyridinone-5H), 5.03 (s, CH_2 , 6H), 4.43 (d, 6H, $J = 4.78$ Hz, CH_2), 3.32 (s, 9H, CH_3), 2.68 (t, 2H, $J = 6.42$ Hz, CH_2), 2.17 (s, 9H, CH_3), 2.06 (t, 2H, $J = 6.42$ Hz, CH_2), 2.03-1.93 (m, 6H, CH_2), 1.80-1.73 (m, 6H, CH_2), ^{13}C NMR (100 MHz, DMSO-d_6) δ : 176.6, 176.4, 172.1, 146.1, 145.1, 140.6, 136.2, 128.7, 128.4, 116.3, 70.8, 39.5, 38.6, 35.3, 34.4, 31.2, 28.7, 20.3.

Synthesis of compound 27. Benzyl groups were removed using neat trifluoroacetic acid. The reaction carried out in a round-bottomed flask pre-treated with HCl. The mixture was monitored by LC/MS until the complete removal of all three benzyl groups. Trifluoroacetic acid was removed under a nitrogen stream. Precipitation from ice-cold diethyl ether afforded a white solid. LC-MS (ESI) calcd for $\text{C}_{37}\text{H}_{52}\text{N}_8\text{O}_{10}$ $m/z = 768.86$, found m/z 385.47 [$\text{M}+2\text{H}$] $^+$, 769.41 [$\text{M}+\text{H}$] $^+$. RT = 7.91.

Synthesis of compound 28a. In a round-bottomed flask 288 mg (1.04 mmol, 10 equiv) of adipic acid bis(*N*-hydroxysuccinimide ester) were solubilized in 2 mL of anhydrous DMF and cooled in an ice bath. A solution of **27** (80 mg, 0.104 mmol, 1 equiv), and DIPEA (0.156 mmol, 1.5 equiv) in 1 mL of anhydrous DMF was added dropwise. The reaction was carried out under inert atmosphere for 12 hours, and monitored by LC/MS.

The solvent was removed under high vacuum and the crude purification by semipreparative reversed-phase HPLC. LC-MS (ESI) calcd for $C_{47}H_{63}N_9O_{15}$ $m/z=994.05$, found m/z 332.41 $[M+3H]^+$, 497.88 $[M+2H]^+$, 994.54 $[M]^+$, 1987.48 $[2M+H]^+$, RT = 8.50.

Synthesis of compound 28b. In a round bottomed flask 288 mg (0.848 mmol, 10 equiv) of pimelic acid bis(*N*-hydroxysuccinimide ester) were solubilized in 2 mL of anhydrous DMF and cooled in an ice bath. A solution of **27** (65 mg, 0.084 mmol, 1 equiv), and DIPEA (1.27 mmol, 1.5 equiv) in 1 mL of anhydrous DMF was added dropwise. The reaction was carried out under inert atmosphere for 12 hours, and monitored by LC/MS. The solvent was removed under high vacuum and the crude purification by semipreparative reversed-phase HPLC. LC-MS (ESI) calcd for $C_{48}H_{65}N_9O_{15}$ $m/z=1007.46$, found m/z 504.70 $[M+2H]^+$, 1008.43 $[M+H]^+$, RT = 9.09.

Synthesis of compound 28c. In a polypropylene syringe **28a** (110 mg, 0.12 mmol, 1.5 equiv) was dissolved in 1 mL of anhydrous DMF and 0.5 mL of DMSO. Subsequently, HATU (48 mg, 0.12 mmol, 1.5) and DIPEA (86 μ L, 0.24 mmol, 3 equiv) were added and the mixture was left to stir for 10 minutes. A suspension with **5** (80 mg, corresponding to a loading of 0.08, 1 equiv) in 2 mL of anhydrous DMF was added and the reaction carried out for 72 hours at room temperature.

The reaction mixture was filtered and washed 3 times with DMF. In order to perform cleavage and removal of side-chain protecting groups a mixture of TFA, phenol (5% w/v), water (5% v/v) and TIS (2% v/v) was prepared and added to the resin. The reaction was stirred at room temperature for 3 hours. The filtrate containing **28c** collected and the resin was washed with TFA: CH_2Cl_2 . The solution was concentrated under a nitrogen stream and ice-cold diethyl ether was added to precipitate **28c**. The suspension was centrifuged, the solvent was decanted off and the precipitate washed four times with diethyl ether. LC-MS (ESI) calcd for $C_{55}H_{65}N_7O_9$ $m/z= 599.78$, found m/z 600.60 $[M+H]^+$, RT = 8.09. The crude purification with semipreparative HPLC and further characterization are *in itinere*.

Synthesis of compound 28d. In a polypropylene syringe, **28b** (110 mg, 0.12 mmol, 1.5 equiv) was dissolved in 1 mL of anhydrous DMF and 0.5 mL of DMSO. Subsequently, HATU (48 mg, 0.12 mmol, 1.5) and DIPEA (86 μ L, 0.24 mmol, 3 equiv) were added and

the mixture was left to stir for 10 minutes. A suspension with **5** (80 mg, corresponding to a loading of 0.08, 1 equiv) in 2 mL of anhydrous DMF was added and the reaction carried out for 72 hours at room temperature.

The reaction mixture was filtered and washed 3 times with DMF. In order to perform cleavage and removal of side-chain protecting groups a mixture of TFA, phenol (5% w/v), water (5% v/v) and TIPS (2% v/v) was prepared and added to the resin. The reaction was stirred at room temperature for 3 hours. The filtrate containing **28d** collected and the resin was washed with TFA: CH₂Cl₂. The solution was concentrated under a nitrogen stream and ice-cold diethyl ether was added to precipitate **28d**. The suspension was centrifuged, the solvent was decanted off and the precipitate washed four times with diethyl ether. LC-MS (ESI) calcd for C₅₅H₆₅N₇O₉ m/z= 606.79, found m/z 607.20 [M+H]⁺, RT = 8.16. The crude purification with semipreparative HPLC and further characterization are *in itinere*.

4.4. Conclusions and outlook

New ⁶⁸Ga-Tris(hydroxypyridinone)-PSMA ligands useful for the prostate cancer diagnosis were designed and synthesized.

Two final compounds with a longer chain have been synthesized, and will be purified through semi-preparative HPLC, characterized and then will be performed *in vitro* experiments to evaluate the cellular uptake and binding affinity.

The characterization of the two ligands consisting of a shorter chain is currently underway. The systems thus composed may act as ⁶⁸Ga radiotracer for imaging PSMA expression.

References

1. J. Ferlay, M. Colombet, I. Soerjomataram, T. Dyba, G. Randi, M. Bettio, A. Gavin, O. Visser, F. Bray, *Eur J Cancer*, **2018**, 103, 356-387.
2. N. Borley, M.R. Feneley, *Asian J. Androl*, **2009**, 11: 74–80.
3. S. Wang, D. Diamond, G.M. Hass, R. Sokoloff and R. Vessella, *Int. J. Cancer*, **2001**, 92, 871–876.
4. P.F. Pinsky, E. Miller, P. Prorok, R. Grubb, E.D. Crawford and G. Andriole, *BJU Int*, **2019**, 123: 854–860.
5. S. M. Okarvi, *Clin Transl Imaging*, **2019**, 7:189-208.
6. A. Roivainen, T. Tolvanen, S. Salomäki, G. Lendvai, I. Velikyan, P. Numminen, M. Vällilä, H. Sipilä, M. Bergström, P. Härkönen, H. Lönnberg, B. Långström, *J Nucl Med*, **2004**, 45, 2, 347-355.
7. N.P. Lenzo, D. Meyrick, J.H. Turner, *Diagnostics*, **2018**, 8, 16-32.
8. M. Morais, M. Ma, *Drug Discov. Today Technol.*, **2018**, 30, 91-104.
9. A. Afshar-Oromieh, C.M. Zechmann, A. Malcher, M. Eder, M. Eisenhut, H.G. Linhart, T. Holland-Letz, B.A. Hadaschik, F.L. Giesel, J. Debus, U. Haberkorn, *Eur J Nucl Med Mol Imaging*, **2014**, 41: 11-20.
10. A. Ghosh, W.D.W. Heston, *J Cell Bioch*, **2004**, 91:528–539.
11. P. Mhawech-Fauceglia, S. Zhang, L. Terracciano, G. Sauter, A. Chadhuri, F.R. Herrmann, R. Penetrante, *Histopathology*, **2007**, 50, 472–483.
12. S.S. Chang, *Rev Urol.*, **2004**, 6 (Suppl 10): S13–S18.
13. A. Ghosh, X. Wang, E. Klein, and W.D.W. Heston, *Cancer Res*, **2005**, 65, 727-731.
14. S. Lütje, S. Heskamp, A.S. Cornelissen, T.D. Poeppel, S.A.M.W. van den Broek, S. Rosenbaum-Krumme, A. Bockisch, M. Gotthardt, M. Rijpkema, and O.C. Boerman, *Theranostics.*, **2015**, 5, 12, 1388–1401.
15. M.I. Davis, M.J. Bennett, L.M. Thomas, and P.J. Bjorkman, *PNAS*, **2005**, 102, 17:5981–5986.
16. C. Barinka, K. Hlouchova, M. Rovenska, P. Majer, M. Dauter, N. Hin, Y-S. Ko, T. Tsukamoto, B.S. Slusher, J. Konvalinka and J. Lubkowski, *J. Mol. Biol.*, **2008**, 376, 1438–1450.
17. C. Barinka, Y. Byun, C. L. Dusich, S.R. Banerjee, Y. Chen, M. Castanares, A.P. Kozikowski, R.C. Mease, M.G. Pomper and J. Lubkowski, *J. Med. Chem.*, **2008**, 51, 7737-7743.
18. K.P. Maresca, S.M. Hillier, F.J. Femia, D. Keith, C. Barone, J.L. Joyal, C.N. Zimmerman, A.P. Kozikowski, J.A. Barrett, W.C. Eckelman, and J.W. Babich, *J. Med. Chem.*, **2009**, 52, 347-357.
19. J.D. Young, V. Abbate, C. Imberti, L. K. Meszaros, M.T. Ma, S.Y.A. Terry, R.C. Hider, G.E. Mullen, P.J. Blower, *J Nucl Med*, **2017**, 58: 1270-1277.
20. D.J. Berry, Y. Ma, J.R. Ballinger, R.Tavaré, A. Koers, K. Sunassee, T. Zhou, S. Nawaz, G.E.D. Mullen, R.C. Hider, P.J. Blower, *Chem. Commun.*, **2011**, 47, 7068–7070.

21. S. Piyamongkol, Y.M. Ma, X.L. Kong, Z.D. Liu, M.D. Aytemir, D. van der Helm, and R.C. Hider, *Chem. Eur. J.*, **2010**, 16, 6374-6381.
22. R. Cusnir, C. Imberti, R.C. Hider, P. J. Blower and M. Ma, *Int. J. Mol. Sci.*, **2017**, 18, 116-139.
23. Z.D. Liu, S. Piyamongkol, D.Y. Liu, H.H. Khodr, S.L. Lu, R.C. Hider, *Bioorg. Med. Chem.*, **2001**, 9, 563-573.
24. Z.D. Liu, R. Kayyali, R.C. Hider, J.B. Porter, and A.E. Theobald, *J. Med. Chem.* **2002**, 45, 631-639.
25. C. Imberti, Y-L. Chen, C.A. Foley, M.T. Ma, B.M. Paterson, Y. Wang, J.D. Young, R.C. Hider and P.J. Blower, *Dalton Trans.*, **2019**, 48, 4299-4313.
26. A. Cilibrizzi, V. Abbate, Y-L- Chen, Y. Ma, T. Zhou, and R.C. Hider, *Chem. Rev.*, **2018**, 118, 7657-7701.
27. T. Zhou, H. Neubert, D. Y. Liu, Z.D. Liu, Y.M. Ma, X. L. Kong, W. Luo, S. Mark, and R.C. Hider, *J Med Chem*, **2006**, 49, 14, 4171-4182.

Formation of amides: One-pot condensation of carboxylic acids and amines mediated by TiCl₄

Antonella Leggio, Jessica Bagalà, Emilia Lucia Belsito, Alessandra Comandè, Marianna Greco and Angelo Liguori

[Paper 1]

Published on: *Chemistry Central Journal*, **2017**, 11:87-98.

DOI: 10.1186/s13065-017-0318-9

Abstract

A general procedure for the synthesis of amides via the direct condensation of carboxylic acids and amines in the presence of TiCl₄ is reported. The amidation reaction was performed in pyridine at 85 °C with a wide range of substrates providing the corresponding amide products in moderate to excellent yields and high purity. The reaction proceeds with low yields when both the carboxylic acid and the amine are sterically hindered. The process takes place with nearly complete preservation of the stereochemical integrity of chiral substrates.

5.1. Introduction

Amide is a key functional group in organic chemistry for its widespread occurrence in peptide and non-peptide natural products, therapeutic small molecules, and new polymeric materials.¹⁻⁴

The most general way for obtaining amides involves the activation of the carboxylic function by means the conversion of carboxylic acids into the corresponding acid chlorides.⁵⁻⁸ Subsequently this reactive derivative is coupled with the appropriate amine to yield the corresponding amide.

Alternatively, carboxylic acids, by the use of activating reagents, can be transformed into reactive acylating intermediates (acyl chlorides, anhydrides, activated esters) which directly react in situ with the suitable amines without their preliminary isolation and purification.⁹⁻¹²

The use of coupling reagents is the only practicable way when the reagents useful for obtaining acid chlorides from carboxylic acids are not compatible with other chemical functions or protecting groups present on the substrate.

The importance of amides has promoted the development of new protocols and reagents based on these approaches and alternative methods for amide bond formation.¹³⁻¹⁶

The direct formation of amides by condensing non-activated carboxylic acids and amines is extremely attractive because of its low environmental impact. Using metal-based catalysis in direct amide preparation, as an alternative to coupling reagents, has been reported.¹⁷⁻¹⁹

The main synthetic catalysts employed for direct amidation are boronic acids and esters together with Lewis acid metal complexes.

Boron-based compounds are reported as catalysts promoting the condensation of carboxylic acids and amines in refluxing toluene.²⁰⁻²¹

In addition amidation reaction protocols by using boronic acid and ester catalysts were also developed for the formation of dipeptide systems.²²⁻²⁴

Under homogeneous conditions, the most used metal catalysts for direct coupling of carboxylic acids with amines are group IV metals.

In 1972 Werdehausen et al.²⁵ developed a catalytic procedure for the direct formation of amides starting from different long chain fatty acids and amines by using 0.6–1 mol % of metal catalysts based on Ti(IV), Zr(IV) and Ta(V), at 120–200 °C.

Later carboxyamides from benzoic acids and different amines were obtained by using stoichiometric amounts of various Lewis acid catalysts in refluxing toluene.²⁶

Ti(OBu)₄ was used in catalytic amounts for obtaining amides from several carboxylic acids and anilines in refluxing o-xylene with yields ranging from 38 to 98 %), electron donating groups on the aromatic ring of anilines provided higher conversions than electron withdrawing substituents.²⁷⁻²⁸

Different amides were synthesized using titanium (IV) isopropoxide as catalyst in 10–20 mol % loading in THF.²⁹ Electronically and sterically demanding substrates provided their corresponding amides in moderate to good yields using a reaction temperature of 100 °C. The hydrolytic decomposition of the catalyst caused a drastic lowering of the reaction yields when the reaction was performed in air.

The use of Zirconium (IV) catalysts for the direct amidation of carboxylic acids and amines was also reported [17]. ZrCl₄ and ZrCp₂Cl₂ were particularly effective resulting in high conversions of the substrates after four hours of reaction time at 110 °C using a 5 mol % catalyst.

Simultaneously, Adolfsson et al. developed a ZrCl₄ catalysed amidation protocol at 70 °C in THF with molecular sieves as water scavengers.³⁰⁻³¹ Both aliphatic and aromatic carboxylic acids were converted in secondary and tertiary amides in 62–99 % yield with 2–10 mol% catalyst loading. Aromatic carboxylic acids required reaction temperatures of 100 °C and 10 % catalyst loading in order to increase the yields after 24 hours reaction time.

The sandwich complex bis(dicyclopentadienyl)hafnium dichloride ([Hf(Cp)₂Cl₂]) was used as catalyst for direct amidation of nonactivated carboxylic acids at 26 °C.³² The method provided different amides in a reaction time of 48 h and using a 10 %

catalyst loading. Some substrates were converted in the corresponding amides before this time.

In our research activity, in which titanium tetrachloride was employed, it was observed the oxophilic character of this transition metal towards carbonyl and hydroxyl groups.³³⁻³⁸

On the base of these observations, we became interested into investigating the direct coupling of carboxylic acids and amines using TiCl_4 as condensing agent.

Here, we report the successful TiCl_4 -mediated synthesis of secondary and tertiary amides starting from various carboxylic acid and amine precursors.

5.2. Results and discussion

Optimization of reaction conditions was performed by choosing benzoic acid as model substrate.

The reaction was previously investigated under catalytic conditions. Benzoic acid (1mmol) and a catalytic amount of TiCl_4 (30 mol %) were treated with aniline (1 mmol) in refluxing dry dichloromethane. During the addition of TiCl_4 to the carboxylic acid, the production of hydrochloric acid was observed. After 12 h of reaction small amounts of amide (12 %) were obtained. Then the reaction was repeated for a longer reaction time (24 h). Also in this case the reaction did not proceed and the amide product was recovered with low yield (15 %). The poor outcome of the reaction prompted us to use a base to convert the carboxylic acid into the corresponding carboxylate. Pyridine was chosen as base to form the pyridinium carboxylate. It was not possible to use non-nucleophilic tertiary nitrogen bases such as triethylamine for the known reactivity of the trialkyl amines with TiCl_4 .³⁹⁻⁴⁰ The reaction was designed in dichloromethane excluding ethereal solvents such as THF because, in the presence of TiCl_4 , O-heterocycle ring opening reaction occurs.⁴¹⁻⁴² Therefore the amidation reaction was carried out in dichloromethane under reflux by treating benzoic acid (1mmol) with pyridine (1 mmol) and TiCl_4 (1.5 mmol), then aniline was added (1mmol). In the reaction mixture, during the adding of pyridine the formation of an insoluble salt, probably relating to the pyridinium salt, was observed. After a reaction time of 12 h benzanilide was recovered in 38 % yield.

In the light of these results it was chosen to carry out the reaction in pyridine, which performs the function of solvent and base also by neutralizing the hydrochloric acid that develops during the reaction, using a higher temperature and an excess of TiCl_4 to accelerate the reaction.

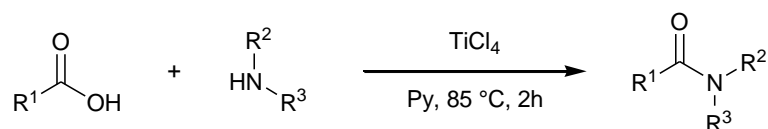
Benzoic acid (1 mmol) was dissolved in pyridine (10 mL) in a screw capped vial. Then, to the resulting solution heated at 85 °C, were added TiCl_4 (3 mmol) and aniline (1 mmol). After about 2 h reacting, the reaction was completed and the reaction mixture was acidified with 1N HCl aqueous solution and extracted with methylene chloride.

The organic phase provided the *N*-phenylbenzamide in 98 % yield and high purity as confirmed by GC/MS and NMR analyses.

Previously, TiCl₄ was used in stoichiometric amounts to form carboxamides from carboxylic acids.¹⁸ In this case the reaction was performed in THF or hexane as solvent and the nucleophilic amine was used in large excess to neutralize the hydrochloric acid produced during the reaction. The reported procedure is poorly applicable as the reaction times are very long (8 h - 7 days) also when heating is required.

Our result was particularly good and interesting, as the product was recovered pure in short times and in excellent yield without requiring the use of complex purification procedures.

Encouraged by the success of this preliminary study, the adopted procedure was applied for the preparation of a series of *N*-phenylamides. Different alkyl and aryl carboxylic acids were tested under the developed reaction conditions using aniline, the amine component, as a constant (Scheme 1).

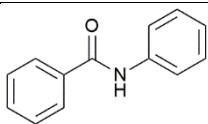
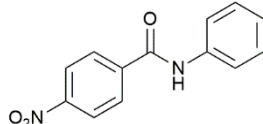
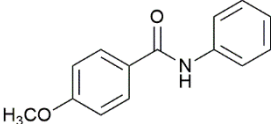
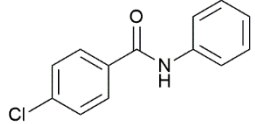
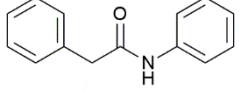
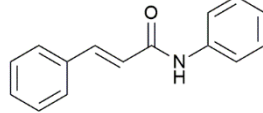
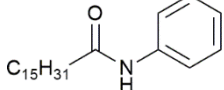


Scheme 1. Direct formation of amides assisted by TiCl₄.

Aliphatic and aromatic carboxylic acids performed well, delivering the desired amides (**1-7**) in excellent yields (entry **a-g**, Table 1).

The molecular structure of the obtained amides was assigned by ¹H NMR, ¹³C NMR and GC/MS analyses.

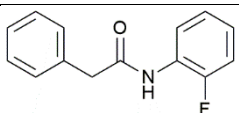
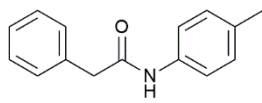
Table 1. Synthesis of *N*-phenylamides 1-7.

Entry	R ¹	R ²	R ³	Product	Yield (%) ^a
a	C ₆ H ₅	H	C ₆ H ₅	1 	98
b	4-NO ₂ -C ₆ H ₄	H	C ₆ H ₅	2 	98
c	4-CH ₃ O-C ₆ H ₄	H	C ₆ H ₅	3 	95
d	4-Cl-C ₆ H ₄	H	C ₆ H ₅	4 	95
e	C ₆ H ₅ CH ₂	H	C ₆ H ₅	5 	95
f	C ₆ H ₅ CH=CH	H	C ₆ H ₅	6 	91
g	C ₁₅ H ₃₁	H	C ₆ H ₅	7 	88

^a isolated yields

Additional experiments, that employed 2-fluoroaniline and 4-methylaniline as amine components, were carried out in order to investigate the electronic effect of the substituent on the aniline nucleophilicity and consequently on the reaction course. The reactions went to completion in short times (2h) and afforded the corresponding amides **8-9** in high yields (Scheme 1; Table 2).

Table 2. Synthesis of substituted anilides 8-9.

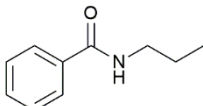
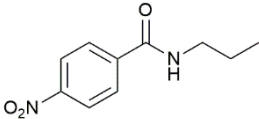
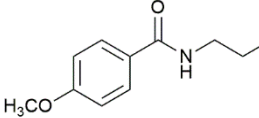
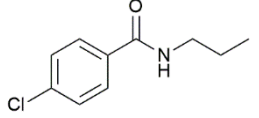
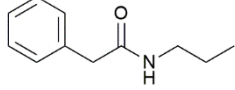
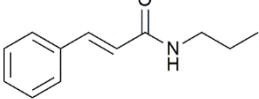
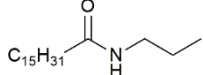
Entry	R ¹	R ²	R ³	Product	Yield (%) ^a
h	C ₆ H ₅ CH ₂	H	2-F-C ₆ H ₄	8 	72
i	C ₆ H ₅ CH ₂	H	4-CH ₃ -C ₆ H ₄	9 	98

^a isolated yields

The lower nucleophilicity of 2-fluoroaniline resulted in a lower yield of the corresponding amide (**8**) (72%, Table 2).

We explored also the reactivity of the more nucleophilic alkyl amines by choosing, as amine substrate, the propylamine. The standard protocol applied to the reaction of propylamine with aliphatic and aromatic carboxylic acids provided the corresponding amides **10-16** with yields higher than 90 %. (Scheme 1, Table 3).

Table 3. Synthesis of *N*-propylamides 10-16.

Entry	R ¹	R ²	R ³	Product	Yield (%) ^a
j	C ₆ H ₅	H	C ₃ H ₇	10 	91
k	4-NO ₂ -C ₆ H ₄	H	C ₃ H ₇	11 	92
l	4-CH ₃ O-C ₆ H ₄	H	C ₃ H ₇	12 	78
m	4-Cl-C ₆ H ₄	H	C ₃ H ₇	13 	96
n	C ₆ H ₅ CH ₂	H	C ₃ H ₇	14 	95
o	C ₆ H ₅ CH=CH	H	C ₃ H ₇	15 	97
p	C ₁₅ H ₃₁	H	C ₃ H ₇	16 	94

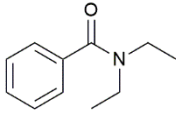
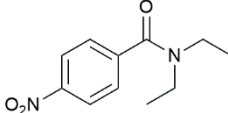
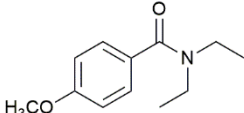
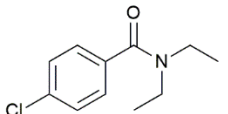
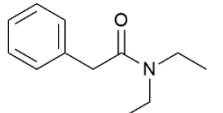
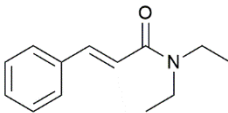
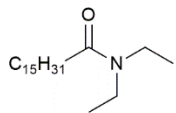
^a isolated yields

Amide formation, by using the developed reaction protocol, was also studied with disubstituted amines that are often more difficult substrates since they exhibit a significant steric hindrance.

Diethylamine was chosen as a representative dialkyl amine for studying the influence of steric hindrance on the course of the reaction (Scheme 1, Table 4).

The desired tertiary *N,N*-diethylamides were obtained with satisfactory yields even though lower than secondary amides probably due to the steric hindrance of diethylamine. (Table 4).

Table 4. Synthesis of *N,N*-diethylamides 17-23.

Entry	R ¹	R ²	R ³	Product	Yield (%) ^a
q	C ₆ H ₅	C ₂ H ₅	C ₂ H ₅		64
r	4-NO ₂ -C ₆ H ₄	C ₂ H ₅	C ₂ H ₅		80
s	4-CH ₃ O-C ₆ H ₄	C ₂ H ₅	C ₂ H ₅		56
t	4-Cl-C ₆ H ₄	C ₂ H ₅	C ₂ H ₅		77
u	C ₆ H ₅ CH ₂	C ₂ H ₅	C ₂ H ₅		85
v	C ₆ H ₅ CH=CH	C ₂ H ₅	C ₂ H ₅		87
w	C ₁₅ H ₃₁	C ₂ H ₅	C ₂ H ₅		91

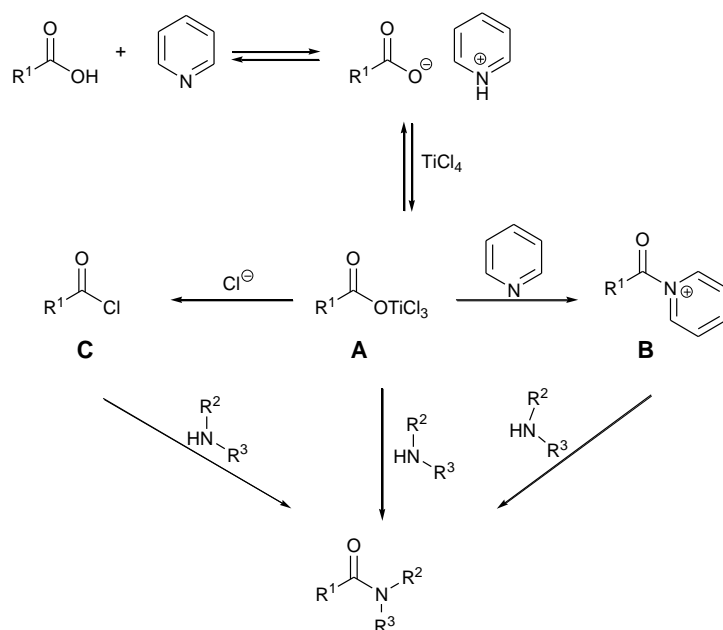
^a isolated yields

The results reported in Table 4 also suggested that, when diethyl amine is used as amine component, the reaction is affected by the electronic nature of the substituent on the aromatic ring of the benzoic acid (entry **r**, entry **t** Table 4) which probably characterize the reactivity of the reaction intermediates.

In fact, the presence of chlorine and nitro group on the aromatic ring of carboxylic acids results in higher yields in amide (**18**, **20**, Table 4) than substrates that have no substituents or have electron donor groups on the aromatic ring. (**17**, **19**, Table 4). This is consistent with the higher reactivity of the involved intermediates in the formation of **18** and **20**.

In many experiments in which benzoic acid was used, such as in the synthesis of *N,N*-diethylbenzamide (**17**), traces of benzoyl chloride were found in the crude product. This observation suggested that the acyl chloride could be the reaction intermediate.

The amidation reaction could proceed through the formation of an adduct (**A**) between the carboxylate ion, generated by the reaction of the carboxylic acid with pyridine, and TiCl_4 (Scheme 2) as reported in literature with other metals.³⁰ The adduct **A** is characterized by the presence of a good leaving group that could lead to: a) the direct formation of the amide; b) the formation of the acyl pyridinium ion (**B**); c) the formation of the acyl chloride (**C**) (Scheme 2). **B** and **C** could act as additional reaction intermediates for the formation of the amide.



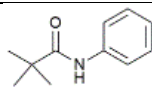
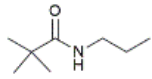
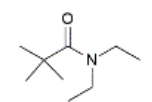
Scheme 2 Proposed mechanism for the TiCl_4 assisted direct amidation

The reaction of the sterically hindered pivalic acid with diethylamine resulted with very low conversions and provided, after 2 h, the corresponding amide **26** in 9 % yield (entry **z**, Table 5). When the reaction was performed by treating pivalic acid with aniline and propylamine (entry **x-y**, Table 5), the amides **24** and **25** were recovered

respectively with 90 % and 75 % yield (Table 5) demonstrating that the steric effect of the alone carboxylic acid has minor impact on the reaction course.

In these reactions, steric effects play a key role when both amine and carboxylic acid are sterically hindered.

Table 5. Synthesis of pivalic acid amides 24-26.

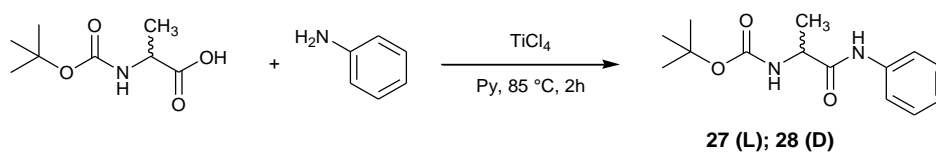
Entry	R ¹	R ²	R ³	Product	Yield (%) ^a
x	(CH ₃) ₃ C	H	C ₆ H ₅		90
y	(CH ₃) ₃ C	H	C ₃ H ₇		75
z	(CH ₃) ₃ C	C ₂ H ₅	C ₂ H ₅		9

^a isolated yields

We also explored the stereochemical outcome of the adopted procedure by synthesizing a couple of anilide enantiomers **27** and **28** starting from (*S*)-2-(*N*-tert-butoxycarbonylamino)propanoic acid (*N*-Boc-L-Alanine) and (*R*)-2-(*N*-tert-butoxycarbonylamino)propanoic acid (*N*-Boc-D-Alanine) as acid substrates (Scheme 3). Gratifyingly, we were able to synthesize the two enantiomers with high enantioselectivity.

N-Boc-L-alanine and *N*-Boc-D-Alanine reacted with aniline in the presence of TiCl₄ affording the corresponding amides **27** and **28** respectively in 88 and 87% % yield (Scheme 3).

This result demonstrates that this reaction works well also with carboxylic acids bearing acid-labile protecting groups.



Scheme 3. Direct formation of enantiomeric amides **27-28** assisted by TiCl₄

The enantiomeric purity of each crude product **27** and **28** was assessed by analyzing them by chiral GC/MS and comparing the resulting chromatograms with that of a suitably prepared mixture (approx. 1 : 1) of the two enantiomers (Figure 1). The two enantiomers of the mixture, after finding the optimal conditions for achieving good selectivity, were resolved by chiral GC/MS: two peaks with retention times of 223.46 and 224.55 minutes corresponding to **28** and **27** respectively appeared in the chromatogram (Figure 1B).

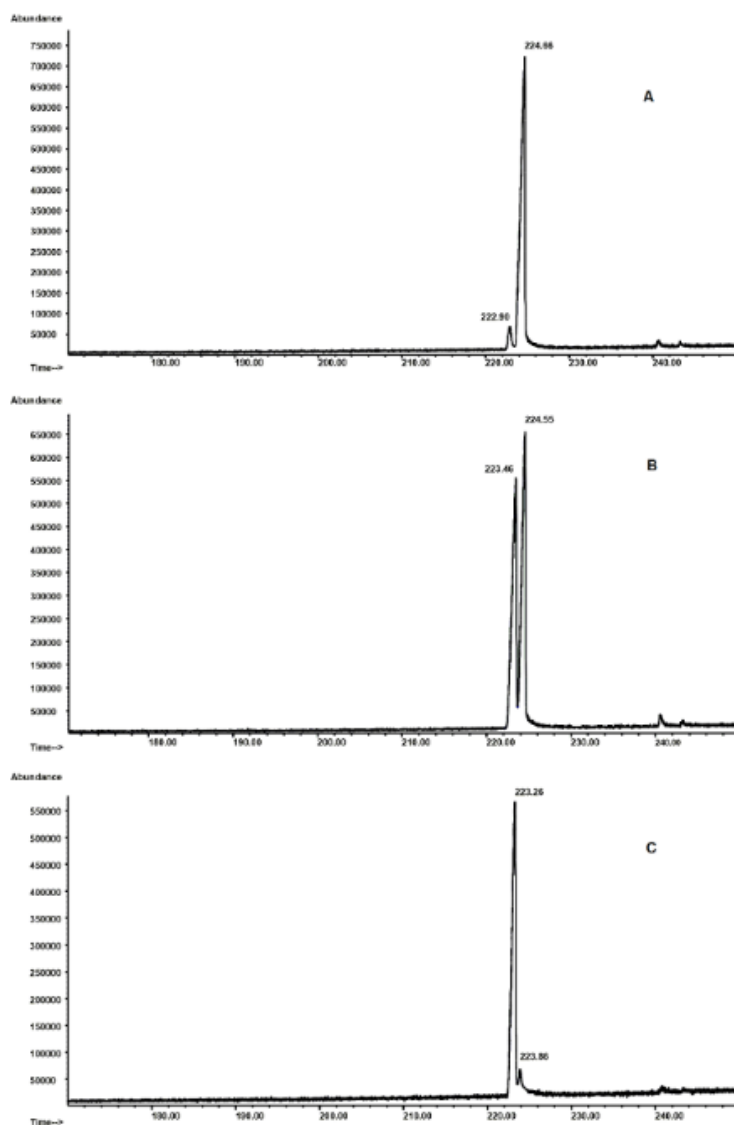


Figure 1. Chiral GC/MS analyses of crude amides **27** and **28**: (A) (S)-2-(*N*-*tert*-butoxycarbonylamino)-*N*-phenylpropanamide (**28**); (B) a mixture of **27** and **28** (approx. 1:1); (C) (R)-2-(*N*-*tert*-butoxycarbonylamino)-*N*-phenylpropanamide (**28**).

The comparison of the chromatograms of the single crude enantiomers **27** and **28** (Figure 1A and Figure 1C) with the mixture and the integration gave the data for the enantiomeric excess (ee) calculation, which was 95% for the D-isomer and 93 % for the L-isomer. The calculated enantiomeric excess was for both enantiomers satisfactory.

5.3. Experimental

5.3.1. General experimental details

All reagents were purchased commercially without further purification. Solvents were purified according to well-known laboratory methods and freshly distilled prior to use. Reaction were carried out in a tightly sealed screw-capped vial. Reactions were magnetically stirred and monitored by thin layer chromatography using Merck-Kieselgel 60 F254 plates. ^1H and ^{13}C NMR spectra were recorded on a Bruker Avance 300 instrument at 300 MHz and 75 MHz, respectively. Spectroscopic analysis was performed at 293 K on diluted solutions of each compound by using CDCl_3 and DMSO-d_6 as the solvents. Chemical shifts (δ) are reported in ppm. Coupling constants (J) are reported in Hertz (Hz). GC-MS analyses were performed with a DB-35MS (20 m \times 0.18 mm, 35% Phenyl 65% dimethylpolysiloxane) capillary column. The mass detector was operated in the electron impact ionization mode (EI/MS) with an electron energy of 70 eV. The injection port was heated to 250 $^\circ\text{C}$. The oven temperature program was initially set at 70 $^\circ\text{C}$ with a hold of 2 min and ramped to 280 $^\circ\text{C}$ at 20 $^\circ\text{C}/\text{min}$ with a hold of 10 min. Chiral GC-MS analyses of enantiomeric compounds 27-28 were performed by using a 25 m \times 0.25 mm, Diethyl tertbutyldimethylsilyl- β -cyclodextrine chiral capillary column. The injection port was heated to 250 $^\circ\text{C}$. The oven temperature program was initially set at 50 $^\circ\text{C}$, with a hold of 2 min, ramped to 250 $^\circ\text{C}$ at 0.5 $^\circ\text{C}/\text{min}$ with a hold of 5 min.

5.3.2. General procedure for the synthesis of amides 1-28.

TiCl_4 (3 mmol) and the amine (1 mmol) were added to a solution of carboxylic acid (1 mmol) in pyridine (10 mL). The tightly sealed screw-capped vial containing the reaction mixture was then heated at 85 $^\circ\text{C}$. After magnetic stirring for about 2 h, TLC analysis (chloroform/methanol 90:10 v/v) of the reaction mixture showed complete conversion of the carboxylic acid precursor. The reaction mixture was then cooled, and after removing pyridine by co-evaporation with toluene, was treated with an aqueous 1N HCl solution (10 mL) and extracted with methylene chloride (3 \times 10 mL). The combined organic extracts were washed with a saturated aqueous solution of sodium bicarbonate (3 \times 10 mL), dried (Na_2SO_4), and evaporated to dryness under reduced pressure to afford the corresponding amides **1-28** with yields ranging from 56-98 %.

N-phenylbenzamide (**1**) Solid (98 %); mp = 163-165 °C; Rf = 0.70; ¹H NMR (300 MHz, DMSO-d₆) δ: 10.23 (s, 1H), 7.99-7.95 (m, 2H), 7.81-7.78 (m, 2H), 7.56-7.52 (m, 3H), 7.38-7.32 (m, 2H), 7.12-7.07 (m, 1H); ¹³C-NMR (75 MHz, DMSO-d₆) δ: 166.0, 139.7, 135.5, 131.9, 129.0, 128.8, 128.1, 124.1, 120.9; GC/MS (EI) *m/z* (% rel.): 197 [M⁺] (46), 105 (100), 77 (46); 65 (4), 51 (9).

4-nitro-*N*-phenylbenzamide (**2**) Solid (98 %); mp = 218-220 °C; Rf = 0.65; ¹H NMR (300 MHz, DMSO-d₆) δ: 10.53 (s, 1H), 8.35 (d, J = 9.0 Hz, 2H), 8.18 (d, J = 9.0 Hz, 2H), 7.78 (d, J = 7.5 Hz, 2H), 7.46-7.27 (m, 2H), 7.13 (t, J = 7.4 Hz, 1H); ¹³C-NMR (75 MHz, DMSO-d₆) δ: 164.3, 149.6, 141.1, 139.2, 129.7, 129.1, 124.6, 124.0, 121.0; GC/MS (EI) *m/z* (% rel.): 242 [M⁺] (75), 150 (100), 120 (21), 104 (32), 92 (20), 76(25).

4-methoxy-*N*-phenylbenzamide (**3**) Solid (95 %); mp = 177-179 °C; Rf = 0.69; ¹H NMR (300 MHz, DMSO-d₆) δ: 10.06 (s, 1H), 7.99-7.88 (m, 2H), 7.80-7.74 (m, 2H), 7.39-7.24 (m, 2H), 7.13-6.99 (m, 3H), 3.83 (s, 3H); ¹³C-NMR (75 MHz, DMSO-d₆) δ: 165.4, 162.4, 139.9, 130.0, 129.0, 127.5, 123.9, 120.9, 114.1, 55.9; GC/MS (EI) *m/z* (% rel.): 227 [M⁺] (21), 135 (100), 107 (6), 92 (11), 77(12).

4-chloro-*N*-phenylbenzamide (**4**) Solid (95 %); mp = 205-207 °C; Rf = 0.78; ¹H NMR (300 MHz, DMSO-d₆) δ: 10.28 (s, 1H), 8.06-7.88 (m, 2H), 7.82-7.71 (m, 2H), 7.64-7.53 (m, 2H), 7.40-7.28 (m, 2H), 7.10 (t, J = 7.4 Hz, 1H); ¹³C-NMR (75 MHz, DMSO-d₆) δ: 164.9, 139.5, 136.9, 134.1, 130.1, 129.1, 128.9, 124.3, 120.9; GC/MS (EI) *m/z* (% rel.): 231 [M⁺] (31), 139 (100), 111 (31), 75 (12).

N,2-diphenylacetamide (**5**) Solid (95 %); mp = 105-107 °C; Rf = 0.73; ¹H NMR (300 MHz, CDCl₃) δ: 7.63 (s_{broad}, 1H), 7.49-7.42 (m, 2H), 7.39-7.21 (m, 7H), 7.09 (t, J = 7.4 Hz, 1H), 3.70 (s, 2H); ¹³C-NMR (75 MHz, CDCl₃) δ: 169.4, 137.8, 134.6, 129.5, 129.1, 128.9, 127.6, 124.4, 120.0, 44.7; GC/MS (EI) *m/z* (% rel.): 211 [M⁺] (49), 119 (11), 91(68), 93 (100), 77 (11), 65 (21).

N-phenylcinnamamide (**6**) Solid (91 %); mp = 155-157 °C; Rf = 0.72; ¹H NMR (300 MHz, CDCl₃) δ: 8.09 (s, 1H), 7.75 (d, J = 15.6 Hz, 1H), 7.69-7.59 (m, 2H), 7.52-7.39 (m,

2H), 7.38–7.23 (m, 5H), 7.12 (t, $J = 7.4$ Hz, 1H), 6.66 (d, $J = 15.6$ Hz, 1H); ^{13}C -NMR (75 MHz, CDCl_3) δ : 164.7, 142.2, 138.2, 134.6, 129.9, 129.1, 128.8, 128.0, 124.5, 121.2, 120.4; GC/MS (EI) m/z (% rel.): 223 [M^+] (25), 131 (100) 103 (36), 93 (19), 77 (24).

N-phenylpalmitamide (**7**) Solid (88 %), mp = 88-90 °C; Rf = 0.81; ^1H NMR (300 MHz, CDCl_3) δ : 7.53 (d, $J = 8.3$ Hz, 2H), 7.40 (s, 1H), 7.36-7.22 (m, 2H), 7.11 (m, 1H), 2.42-2.29 (m, 2H), 1.80-1.60 (m, 2H), 1.41-1.13 (m, 24H), 0.89 (t, $J = 6.7$ Hz, 3H); ^{13}C -NMR (75 MHz, CDCl_3) δ : 171.7, 137.9, 129.0, 124.2, 119.8, 37.8, 31.9, 29.7, 29.6, 29.5, 29.4, 29.3, 25.7, 22.7, 14.2; GC/MS (EI) m/z (% rel.): 331 [M^+] (2), 135 (19), 93 (100), 77 (2).

N-(2-fluorophenyl)-2-phenylacetamide (**8**) Solid (72 %), mp = 100-102 °C; Rf = 0.85; ^1H NMR (300 MHz, CDCl_3) δ : 8.29 (t, $J = 8.0$ Hz, 1H), 7.53-7.30 (m, 6H), 7.16-7.06 (m, 1H), 7.06-6.95 (m, 2H), 3.78 (s, 2H); ^{13}C -NMR (75 MHz, CDCl_3) δ : 169.2, 152.1 (d, $J = 242.5$ Hz), 134.1, 129.5, 129.3, 127.8, 126.2 (d, $J = 10.3$ Hz), 124.54 (d, $J = 3.8$ Hz), 124.51 (d, $J = 7.6$ Hz), 121.7, 114.7 (d, $J = 19.4$ Hz), 44.8; GC/MS (EI) m/z (% rel.): 229 [M^+] (25), 118 (24), 111 (100), 91 (76), 65 (13).

2-phenyl-*N*-(*p*-tolyl)acetamide (**9**) Solid (98 %), mp = 108-110 °C; Rf = 0.73; ^1H NMR (300 MHz, CDCl_3) δ : 7.52 (s_{broad} , 1H), 7.43-7.28 (m, 7H), 7.07 (d, $J = 8.3$ Hz, 2H), 3.69 (s, 2H), 2.29 (s, 3H); ^{13}C -NMR (75 MHz, CDCl_3) δ : 169.3, 135.2, 134.7, 134.0, 129.5, 129.4, 129.1, 127.5, 120.1, 44.6, 20.9; GC/MS (EI) m/z (% rel.): 225 [M^+] (49), 133 (12), 107 (100), 91 (46), 77 (9), 65 (12).

N-propylbenzamide (**10**) Solid (91 %); mp = 83-85 °C; Rf = 0.64; ^1H NMR (300 MHz, CDCl_3) δ : 7.82-7.69 (m, 2H), 7.52-7.27 (m, 3H), 6.60 (s_{broad} , 1H), 3.42-3.31 (m, 2H), 1.70-1.51 (m, 2H), 0.93 (t, $J = 7.4$ Hz, 3H); ^{13}C -NMR (75 MHz, CDCl_3) δ : 167.6, 134.8, 131.1, 128.4, 126.8, 41.7, 22.8, 11.3; GC/MS (EI) m/z (% rel.): 163 [M^+] (28), 134 (7), 105 (100), 77 (30).

4-nitro-*N*-propylbenzamide (**11**) Solid (92 %); mp = 102-104 °C; Rf = 0.50; ^1H NMR (300 MHz, CDCl_3) δ : 8.21 (d, $J = 8.8$ Hz, 2H), 7.92 (d, $J = 8.8$ Hz, 2H), 6.74 (s_{broad} , 1H), 3.44-3.34 (m, 2H), 1.74-1.53 (m, 2H), 0.95 (t, $J = 7.4$ Hz, 3H); ^{13}C -NMR (75 MHz,

CDCl₃) δ : 165.6, 149.5, 140.5, 127.6, 123.5, 41.96, 22.6, 11.3; GC/MS (EI) m/z (% rel.): 208 [M⁺] (21), 193 (12), 179 (12), 150 (100), 104 (23), 76 (15).

4-methoxy-N-propylbenzamide (12) Solid (78 %); mp = 58-60 °C; Rf = 0.54; ¹H NMR (300 MHz, CDCl₃) δ : 7.74 (d, J = 8.8 Hz, 2H), 6.87 (d, J = 8.8 Hz, 2H), 6.45 (s_{broad}, 1H), 3.81 (s, 3H), 3.42-3.28 (m, 2H), 1.70-1.50 (m, 2H), 0.94 (t, J = 7.4 Hz, 3H); ¹³C-NMR (75 MHz, CDCl₃) δ : 167.1, 162.0, 128.7, 127.1, 113.6, 55.4, 41.7, 22.9, 11.5; GC/MS (EI) m/z (% rel.): 193 [M⁺] (19), 151 (10), 135 (100), 107 (5), 92 (10), 77 (12).

4-chloro-N-propylbenzamide (13) Solid (96 %); mp = 96-98 °C; Rf = 0.58; ¹H NMR (300 MHz, CDCl₃) δ : 7.75-7.65 (m, 2H), 7.41-7.28 (m, 2H), 6.55 (s_{broad}, 1H), 3.43-3.28 (m, 2H), 1.70-1.50 (m, 2H), 0.94 (t, J = 7.4 Hz, 3H); ¹³C-NMR (75 MHz, CDCl₃) δ : 166.5, 137.4, 133.2, 128.6, 128.3, 41.8, 22.7, 11.3; GC/MS (EI) m/z (% rel.): 197 [M⁺] (25), 168 (6), 139 (100), 111 (23), 75 (11).

2-phenyl-N-propylacetamide (14) Solid (95 %); mp = 66-69 °C; Rf = 0.68; ¹H NMR (300 MHz, CDCl₃) δ : 7.42-7.17 (m, 5H), 5.65 (s_{broad}, 1H), 3.55 (s, 2H), 3.22-3.07 (m, 2H), 1.58-1.31 (m, 2H), 0.82 (t, J = 7.4 Hz, 3H); ¹³C-NMR (75 MHz, CDCl₃) δ : 171.0, 135.1, 129.4, 129.0, 127.3, 43.8, 41.3, 22.7, 11.2; GC/MS (EI) m/z (% rel.): 177 [M⁺] (18), 92 (100), 91 (87), 86 (10), 65 (13), 43 (23).

N-propylcinnamamide (15) Solid (97 %); mp = 75-77 °C; Rf = 0.71; ¹H NMR (300 MHz, CDCl₃) δ : 7.62 (d, J = 15.6 Hz, 1H), 7.54-7.41 (m, 2H), 7.38-7.25 (m, 3H), 6.50 (d, J = 15.6 Hz, 1H), 6.34 (s_{broad}, 1H), 3.47-3.26 (m, 2H), 1.71-1.49 (m, 2H), 0.94 (t, J = 7.4 Hz, 3H); ¹³C-NMR (75 MHz, CDCl₃) δ : 166.1, 140.5, 134.9, 128.7, 127.7, 127.7, 121.1, 41.4, 22.8, 11.4; GC/MS (EI) m/z (% rel.): 189 [M⁺] (27), 131 (100), 174 (5), 146 (24), 103 (40), 77 (24).

N-propylpalmitamide (16) Solid (94 %), mp = 74-76 °C; Rf = 0.81; ¹H NMR (300 MHz, CDCl₃) δ : 5.49 (s_{broad}, 1H), 3.27-3.14 (m, 2H), 2.20-2.09 (m, 2H), 1.73-1.58 (m, 2H), 1.57-1.41 (m, 2H), 1.40-1.11 (m, 24H), 0.98-0.78 (m, 6H); ¹³C-NMR (75 MHz, CDCl₃)

δ : 173.1, 41.2, 37.0, 31.9, 29.7, 29.6, 29.5, 29.4, 29.3, 25.9, 22.9, 22.7, 14.1, 11.4; GC/MS (EI) m/z (% rel.): 297 [M^+] (3), 268 (3), 239 (3), 114 (24), 101 (100), 43 (14).

N,N-diethylbenzamide (**17**) Viscous oil (64 %); R_f = 0.75; 1H NMR (300 MHz, $CDCl_3$) δ : 7.41-7.10 (m, 5H), 3.43 (S_{broad} , 2H), 3.14 (S_{broad} , 2H), 1.27-0.89 (m, 6H); ^{13}C -NMR (75 MHz, $CDCl_3$) δ : 171.1, 137.1, 128.9, 128.2, 126.1, 43.1, 39.1, 14.0, 12.7; GC/MS (EI) m/z (% rel.): 177 [M^+] (21), 162 (2), 148 (7), 176 (61), 105 (100), 77 (27).

N,N-diethyl-4-nitrobenzamide (**18**) Solid (80 %); mp = 54-56 °C; R_f = 0.73; 1H NMR (300 MHz, $CDCl_3$) δ : 8.26 (d, J = 8.8 Hz, 2H), 7.53 (d, J = 8.8 Hz, 2H), 3.73-3.36 (m, 2H), 3.34-3.01 (m, 2H), 1.25 (t, J = 6.9 Hz, 3H), 1.11 (t, J = 6.9 Hz, 3H); ^{13}C -NMR (75 MHz, $CDCl_3$) δ : 168.9, 148.3, 143.4, 127.3, 123.9, 43.3, 39.5, 14.2, 12.8; GC/MS (EI) m/z (% rel.): 222 [M^+] (17), 221 (42), 205 (7), 175 (4), 150 (100), 120 (13), 104 (25), 92 (8), 76 (14).

N,N-diethyl-4-methoxybenzamide (**19**) Oil (56 %); R_f = 0.65; 1H NMR (300 MHz, $CDCl_3$) δ : 7.22 (d, J = 8.7 Hz, 2H), 6.77 (d, J = 8.7 Hz, 2H), 3.68 (s, 3H), 3.29 (S_{broad} , 4H), 1.05 (S_{broad} , 6H); ^{13}C -NMR (75 MHz, $CDCl_3$) δ : 171.1, 160.1, 129.3, 128.0, 113.5, 55.1, 43.0, 39.7, 13.5; GC/MS (EI) m/z (% rel.): 207 [M^+] (15), 206 (34), 135 (100), 107 (4), 92 (11), 77 (9).

4-chloro-*N,N*-diethylbenzamide (**20**) Oil (77 %); R_f = 0.65; 1H NMR (300 MHz, $CDCl_3$) δ : 7.41-7.24 (m, 4H, ArH), 3.50 (S_{broad} , 2H), 3.22 (S_{broad} , 2H), 1.31-0.98 (m, 6H); ^{13}C -NMR (75 MHz, $CDCl_3$) δ : 170.2, 135.6, 135.1, 128.7, 127.8, 43.1, 39.1, 14.1, 12.7; GC/MS (EI) m/z (% rel.): 211 [M^+] (15), 210 (34), 139 (100), 111 (23), 75 (9).

N,N-diethyl-2-phenylacetamide (**21**) Oil (85 %); R_f = 0.73; 1H NMR (300 MHz, $CDCl_3$) δ : 7.36-7.15 (m, 5H), 3.69 (s, 2H), 3.38 (q, J = 7.1 Hz, 2H), 3.28 (q, J = 7.1 Hz, 2H), 1.16-1.02 (m, 6H); ^{13}C -NMR (75 MHz, $CDCl_3$) δ : 170.2, 135.5, 128.7, 128.6, 126.6, 42.4, 40.9, 40.1, 14.2, 12.9; GC/MS (EI) m/z (% rel.): 191 [M^+] (38), 118 (3), 100 (100), 91 (46), 72 (50).

N,N-diethylcinnamamide (**22**) Solid (87 %); mp = 58-60 °C; Rf = 0.73; ¹H NMR (300 MHz, CDCl₃) δ: 7.55 (d, J = 15.4 Hz, 1H), 7.41-7.27 (m, 2H), 7.24-7.04 (m, 3H), 6.68 (d, J = 15.4 Hz, 1H), 3.42-3.15 (m, 4H), 1.16-0.92 (m, 6H); ¹³C-NMR (75 MHz, CDCl₃) δ: 165.4, 141.9, 135.3, 129.2, 128.6, 127.5, 117.7, 42.1, 40.9, 14.9, 13.0; GC/MS (EI) *m/z* (% rel.): 203 [M⁺] (32), 188 (8), 131 (100), 126 (8), 103 (35), 77 (12).

N,N-diethylpalmitamide (**23**) Oil (91 %); Rf = 0.73; ¹H NMR (300 MHz, CDCl₃) δ: 3.42-3.21 (m, 4H), 2.35-2.19 (m, 2H), 1.71-1.51 (m, 2H), 1.39-0.99 (m, 30H), 0.87 (t, J = 6.7, 3H); ¹³C-NMR (75 MHz, CDCl₃) δ: 172.4, 41.9, 40.0, 33.2, 31.9, 29.7, 29.6, 29.5, 29.4, 25.5, 22.7, 14.4, 14.1, 13.1; GC/MS (EI) *m/z* (% rel.): 311 [M⁺] (8), 128 (26), 115 (100), 100 (23).

N-phenylpivalamide (**24**) Solid (90 %); mp = 133-135 °C; Rf = 0.82; ¹H NMR (300 MHz, CDCl₃) δ: 7.57-7.50 (m, 2H), 7.43 (s_{broad}, 1H), 7.36-7.25 (m, 2H), 7.14-7.04 (m, 1H), 1.32 (s, 9H); ¹³C-NMR (75 MHz, CDCl₃) δ: 176.6, 138.0, 128.9, 124.2, 120.0, 39.6, 27.6; GC/MS (EI) *m/z* (% rel.): 177 [M⁺] (90), 120 (7), 93 (100), 77 (12), 57 (95).

N-propylpivalamide (**25**) Oil (75 %); Rf = 0.84; ¹H NMR (300 MHz, CDCl₃) δ: 5.73 (s, 1H), 3.23-3.11 (m, 2H), 1.58-1.40 (m, 2H), 1.16 (s, 9H), 0.88 (t, J = 7.4 Hz, 3H); ¹³C-NMR (75 MHz, CDCl₃) δ: 178.4, 41.2, 38.6, 27.6, 22.8, 11.3; GC/MS (EI) *m/z* (% rel.): 143 [M⁺] (54), 128 (19), 114 (7), 100 (14), 86 (41), 85 (26), 57 (100), 43 (59).

N,N-diethylpivalamide (**26**) oil (9 %); Rf = 0.65; ¹H NMR (300 MHz, CDCl₃) δ: 3.48-3.32 (m, 4H), 1.29-1.18 (m, 15H); GC/MS (EI) *m/z* (% rel.): 157 [M⁺] (25), 142 (7); 100 (100), 72 (62), 57 (53).

(*S*)-2-(*N*-tert-Butoxycarbonylamino)-*N*-phenylpropanamide (**27**) Oil (88 %); Rf = 0.80; ¹H NMR (300 MHz, CDCl₃) δ: 8.86 (s_{broad}, 1H), 7.58-7.45 (m, 2H), 7.36-7.19 (m, 2H), 7.13-7.01 (m, 1H), 5.50 (d, J = 7.5 Hz, 1H), 4.53-4.31 (m, 1H), 1.48-1.38 (m, 12H); ¹³C-NMR (75 MHz, CDCl₃) δ: 171.2, 155.9, 137.9, 128.9, 124.2, 119.9, 80.4, 50.4, 28.3, 17.8; GC/MS (EI) *m/z* (% rel.): 264 [M⁺] (17), 208 (25), 191 (29), 144 (18), 120 (28), 93 (100), 77 (25), 57 (87).

(*R*)-2-(*N*-*tert*-Butoxycarbonylamino)-*N*-phenylpropanamide (**28**) oil (87 %); R_f = 0.80; ¹H NMR (300 MHz, CDCl₃) δ: 8.69 (s_{broad}, 1H), 7.61-7.42 (m, 2H), 7.33-7.21 (m, 2H), 7.11-7.02 (m, 1H), 5.31 (d, J = 8.0 Hz, 1H), 4.49-4.27 (m, 1H), 1.51-1.38 (m, 12H); ¹³C-NMR (75 MHz, CDCl₃) δ: 171.1, 156.1, 137.8, 128.9, 124.2, 119.9, 80.7, 51.7, 28.3, 17.5; GC/MS (EI) *m/z* (% rel.): 264 [M⁺] (17), 208 (24), 191 (28), 144 (18), 120 (28), 93 (100), (77 (25), 57 (92)).

5.4. Conclusion

A general approach to generate amides has been established using TiCl₄-induced direct condensation of carboxylic acids with amines.

Our procedure was successfully applied to a broad spectrum of readily available carboxylic acids and amines affording, in short times and after a simple work up, the corresponding amides in high purity and yields.

By using *N*-Boc-*L*-alanine and its enantiomer *N*-Boc-*D*-alanine as chiral carboxylic acids, and aniline as amine component, highly enantiomerically enriched anilides were synthesized, demonstrating that the developed procedure does not generate any significant loss of the optical integrity of the precursors.

The current investigation showed also that this approach works well also with carboxylic acids bearing acid-sensitive groups.

References

1. J.S. Carey, D. Laffan, C. Thomson, M.T. Williams, *Org Biomol Chem*, **2006**, 4:2337–2347.
2. X. Yu, D. Sun, *Molecules*, **2013**, 18:6230–6268.
3. S.D. Roughley, A.M. Jordan, *J Med Chem*, **2011**, 54:3451–3479.
4. T.J. Deming, *Adv Drug Deliver Rev*, **2002**, 54:1145–1155.
5. C.A.G.N. Montalbetti, V. Falque, *Tetrahedron*, **2005**, 61:10827–10852.
6. A. Leggio, M.L. Di Gioia, F. Perri, A. Liguori, *Tetrahedron*, **2007**, 63:8164–8173.
7. E.L. Belsito, M.L. Di Gioia, A. Greco, A. Leggio, A. Liguori, F. Perri, C. Siciliano, M.C. Viscomi, *J Org Chem*, **2007**, 72:4798–4802.
8. M.L. Di Gioia, A. Leggio, A. Liguori, F. Perri, C. Siciliano, M.C. Viscomi, *Amino Acids*, **2010**, 38:133–143.
9. J.D. Goodreid, P.A. Duspara, C. Bosch, R.A. Batey, *J Org Chem*, **2014**, 79:943–954.
10. J.R. Dunetz, J. Magano, G.A. Weisenburger, *Org Process Res Dev*, **2016**, 20:140–177.
11. E. Valeur, M. Bradley, *Chem Soc Rev*, **2009**, 38:606–631.
12. A. Leggio, E.L. Belsito, G. De Luca, M.L. Di Gioia, V. Leotta, E. Romio, C. Siciliano, A. Liguori, *RSC Adv*, **2016**, 6:34468–34475.
13. A. El-Faham, F. Albericio, *Chem Rev*, **2011**, 111:6557–6602.
14. H. Lundberg, F. Tinnis, N. Selander, H. Adolfsson, *Chem Soc Rev*, **2014**, 43:2714–2742.
15. V.R. Pattabiraman, J.W. Bode, *Nature*, **2011**, 480:471–479.
16. H. Charville, D. Jackson, G. Hodges, A. Whiting, *Chem Commun*, **2010**, 46:1813–1823.
17. C.L. Allen, A.R. Chhatwal, J.M.J. Williams, *Chem Commun*, **2012**, 48:666–668.
18. J.D. Wilson, H. Weingarten, *Can J Chem*, **1970**, 48:983–986.
19. C.L. Allen, J.M.J. Williams, *Chem Soc Rev*, **2011**, 40:3405–3415.
20. K. Ishihara, S. Ohara, H. Yamamoto, *J Org Chem*, **1996**, 61:4196–4197.
21. K. Ishihara, S. Ohara, H. Yamamoto, *Macromolecules*, **2000**, 33:3511–3513.
22. S. Liu, Y. Yang, X. Liu, F.K. Ferdousi, A.S. Batsanov, A. Whiting, *Eur J Org Chem*, **2013**, 25:5692–5700.
23. R.M. Lanigan, P. Starkov, T.D. Sheppard, *J Org Chem*, **2013**, 78:4512–4523.
24. W. Huang, W.B. Sha, *J Chem Res*, **2013**, 37:460–463.
25. A. Werdehausen, H. Weiss, Patent Application Pub. No.: DE2110060; Pub. Date: Sep. 07, **1972**.
26. A. Nordahl, R. Carlson, *Acta Chem Scand B*, **1988**, 42:28–34.
27. L.Y. Shteinberg, S.A. Kondratov, S.M. Shein, *Zh Org Khim*, **1988**, 24:1968–1972.
28. L.Y. Shteinberg, S.A. Kondratov, S.M. Shein, *Zh Org Khim*, **1989**, 25:1945–1949.
29. H. Lundberg, F. Tinnis, H. Adolfsson, *Synlett*, **2012**, 23:2201–2004.
30. H. Lundberg, F. Tinnis, H. Adolfsson, *Chem Eur J*, **2012**, 18:3822–3826.

31. F. Tinnis, H. Lundberg, T. Kivijärvi, H. Adolfsson, *Org Synth*, **2015**, 92:227-236.
32. H. Lundberg, H. Adolfsson, *ACS Catal*, **2015**, 5:3271-3277.
33. A. Leggio, E.L. Belsito, S. Gallo, A. Liguori, *Tetrahedron Letters*, **2017**, 58:1512-1514.
34. M.L. Di Gioia, A. Leggio, A. Le Pera, A. Liguori, C. Siciliano, *Eur J Org Chem*, **2004**, 463-467.
35. M.L. Di Gioia, A. Leggio, A. Le Pera, A. Liguori, A.F. Pitrelli, C. Siciliano, *Protein Pept Lett*, **2005**, 12:357-362.
36. A. Leggio, E.L. Belsito, M.L. Di Gioia, V. Leotta, E. Romio, C. Siciliano, A. Liguori, *Tetrahedron Letters*, **2015**, 56:2062-2066.
37. M.L. Di Gioia, A. Leggio, A. Le Pera, A. Liguori, F. Perri, C. Siciliano, *Eur J Org Chem*, **2004**, 21:4437-4441.
38. M.L. Di Gioia, A. Leggio, I.F. Guarino, V. Leotta, E. Romio, A. Liguori, *Tetrahedron Lett*, **2015**, 56:5341-5344.
39. M. Shi, J-K. Jiang, Y-S. Feng, *Organic Letters*, **2000**, 16:2397-2400.
40. M. Periasamy, *Arkivok*, **2002**, 6:151-166.
41. S.A. Weissman, D. Zewge, *Tetrahedron*, **2005**, 61:7833-7863.
42. P. Rajakumar, V. Murali, *Synth Commun*, **2003**, 33:3891-3896.

A titanium tetrachloride-based effective methodology for the synthesis of dipeptides

Alessandra Comandè, Marianna Greco, Emilia Lucia Belsito, Angelo Liguori, Antonella Leggio

[Paper 2]

Published on: RSC Advances, 2019, 9, 22137-22142

DOI: 10.1039/c9ra04058g

Abstract

A series of dipeptide systems have been easily achieved through TiCl_4 -assisted condensation reaction. The reaction of N-protected amino acids with amino acid methyl esters in pyridine and in the presence of TiCl_4 furnished the corresponding dipeptides in high yields and diastereoselectivity. The reaction was successfully applied to amino acids protected on the α -amino function with different protecting groups. The adopted experimental conditions allowed preserving both the protecting groups on the α -amino function and on the side chain functionalities. Furthermore, the preservation of the stereochemical integrity at the amino acid chiral centres has been verified.

6.1. Introduction

Dipeptide systems, although are widely used in medicinal and pharmacological field as well as in synthetic chemistry,¹ have been poorly investigated compared to single amino acids and long chain peptides.²

The biological functions of dipeptides may be due to dipeptides as such or to the single amino acids deriving from them as a result of hydrolysis processes.

Several dipeptide systems show antitumor,³ antioxidant,⁴ and antihypertensive activity.⁵

Commercially available dipeptides such as aspartame (L-aspartyl-L-phenylalanine methyl ester) and sustamine (L-Alanyl-L-Glutamine) are used as artificial sweetener and nutritional supplement respectively.² The dipeptide L-alanyl-L-glutamine is much more stable and soluble than the free amino acid L-glutamine (L-Gln) consequently the dipeptide system has more efficacy than the single amino acid L-glutamine. In fact, when L-Gln is supplied as L-Alanyl-L-Glutamine a greater transfer of L-Gln from the gut to plasma occurs compared to when the same dose is provided as the free amino acid.⁶

Histidine containing dipeptides, such as carnosine (β -alanyl-L-histidine) and anserine (β -alanyl-methyl-L-histidine), are easily obtained by controlled hydrolysis of animal proteins and have been proposed as food supplements able of sequestering reactive carbonyl species originating from lipid oxidative processes or from the oxidation of the sugars. These dipeptides also seem to be able to prevent the glycosylation of proteins and in particular of hemoglobin, a process that characterizes the metabolic syndrome.⁷ Other dipeptides are then widely used in the formulation of cosmetic products for instance cysteine-containing dipeptides,⁸ L-Tyr-L-Arg⁹ and aspartyl dipeptides, the latter possess highly effective skin and hair caring properties.¹⁰

Amide bond formation is an extremely important reaction in organic chemistry.¹¹ Numerous synthetic strategies to synthesize organic molecules containing amide bonds and peptides have been reported.¹²

The development of solid-phase peptide synthesis (SPPS), also automated, has made easily available polypeptides and of great interest for food, pharmaceutical and biomedical purposes.¹³

Solution phase peptide synthesis (commonly referred to as ‘liquid phase’) is the method of choice for preparing dipeptides and more generally small peptides. This strategy, although is not well suited for making longer peptides, is much more scalable, and allows to produce larger quantities of high-quality peptides, and at a lower cost than solid phase.

Peptide synthesis strategies in solution, but also in solid phase, require the protection of chemical functions not involved in the formation of the peptide bond. The formation of this bond is of particular importance for the purposes of stereochemistry preservation of the chiral centres of the amino acids that participate in the condensation reaction.

Therefore, the development of new methods of peptide bond formation in liquid phase is particularly attractive in order to obtain dipeptides or small peptides since this methodology can also be used with non-natural or unusual amino acids.

In this context, titanium tetrachloride could assume great importance as, due to its great affinity for the oxygen atom, it is used in organic synthesis for the transformation of various functional groups.¹⁴

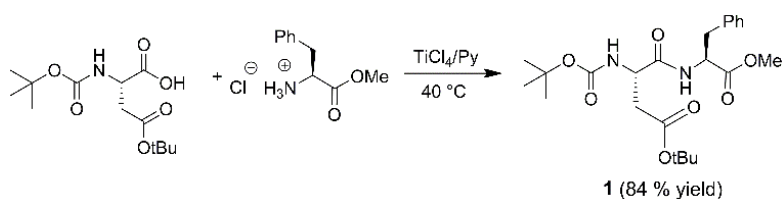
In this study, we explored the applicability of titanium tetrachloride for the formation of the peptide bond. Our results have shown the successful use of titanium tetrachloride as condensing agent for the synthesis of dipeptide systems. Furthermore, the preservation of stereochemical integrity at the amino acid chiral centres has been verified.

6.2. Results and discussion

The possibility of using titanium tetrachloride (TiCl_4) for the formation of the peptide bond was by no means obvious. In fact, TiCl_4 could deprotect not only the amino functions of *N*-protected amino acids as it occurs with other Lewis acids¹⁵ but also the amino acid side chain functional groups.

Accordingly, we thought to carry out the reaction in a pyridine-buffered medium. We proceeded preliminarily with the synthesis of the dipeptide Asp-Phe-OMe (Aspartame), via the Boc-based solution-phase approach.

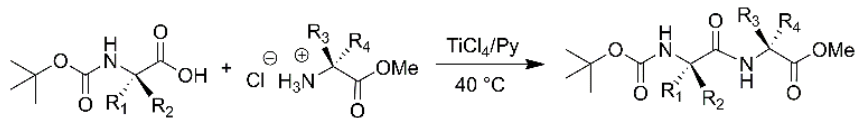
In this perspective, L-phenylalanine methyl ester hydrochloride (1 mmol) was preliminary treated with pyridine (5 mL), then *N*-Boc-L-aspartic acid- β -*t*-butyl ester (1 mmol) and TiCl_4 (2 mmol) were added to the resulting solution (Scheme 1). The reaction was carried out in a screw-capped vial at 40 °C and was complete within about 5 h. After removal of pyridine by co-evaporation with toluene, the resulting crude product was suspended in chloroform and purified by elution through a silica gel column using chloroform as mobile phase. After evaporation of chloroform the dipeptide *N*-Boc-Asp-(OtBu)-Phe-OMe (**1**) was recovered in 84 % yield and high purity as confirmed by ^1H and ^{13}C NMR analyses. Spectroscopic data analysis excluded side-chain and N-terminal amino function deprotection.



Scheme 1. Synthesis of dipeptide *N*-Boc-Asp-(OtBu)-Phe-OMe (**1**)

Afterwards Aspartame (Asp-Phe-OMe) (**1a**) was readily obtained in 95 % yield by treating the *N*-Boc-protected dipeptide **1** with trifluoroacetic acid in dichloromethane (1:1 v/v).

The developed procedure was applied successfully for the synthesis of various *N*-Boc-protected dipeptides (Scheme 2, Table 1).



2-6

Scheme 2. Synthesis of *N*-Boc protected dipeptides **2-6**

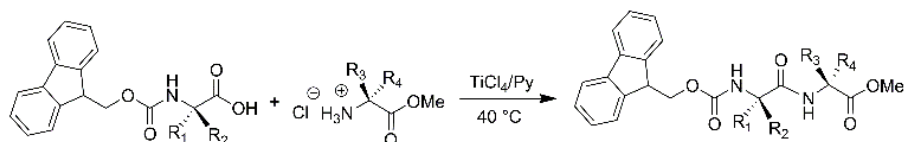
Table 1. Results of the synthesis of *N*-Boc-dipeptides **2-6**

Dipeptide	R ₁	R ₂	R ₃	R ₄	Yield (%) ^a
2	CH ₂ C ₆ H ₅	H	CH ₃	H	75
3	CH ₃	H	CH ₃	H	71
4	H	CH ₃	CH ₃	H	80
5	CH ₃	H	CH ₂ S-(Bzl)	H	80
6	CH ₃	H	(CH ₂) ₄ NH-(Boc)	H	80

^a isolated yield

All the *N*-Boc-dipeptides **2-6** were characterized by GC/MS (EI), ¹H NMR and ¹³C NMR analyses. *N*-Boc-Ala-Cys-(SBzl)-OMe (**5**) and *N*-Boc-Ala-Lys-(Boc)-OMe (**6**) kept unchanged the masking groups on the amino acid side-chains.

The successful outcomes obtained with the synthesis of dipeptides **1-6** prompted us to extend the developed methodology to the preparation of dipeptide systems protected on the α-amino function with the base-labile protecting group fluorenylmethoxycarbonyl (Fmoc) (Scheme 3). *N*-Fmoc-dipeptide systems (**7-17**) were prepared in high yields without observing the formation of reaction products deprotected on the α-amino function (Table 2).



7-17

Scheme 3. Synthesis of *N*-Fmoc protected dipeptides **7-17**

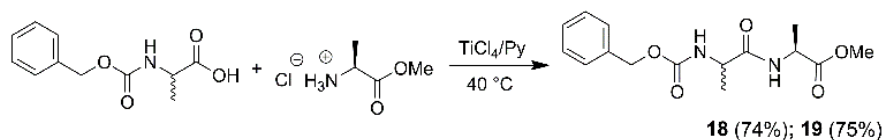
Tabella 2. Results of the synthesis of *N*-Fmoc-dipeptides **7-17**

Dipeptide	R ₁	R ₂	R ₃	R ₄	Yield (%) ^a
7	(CH ₂)COO-(<i>t</i> Bu)	H	CH ₂ Ph	H	84
8	CH ₃	H	CH ₃	H	71
9	CH ₂ CH(CH ₃) ₂	H	CH ₃	H	80
10	H	CH ₂ CH(CH ₃) ₂	CH ₃	H	80
11	H	H	CH ₃	H	80
12	CH ₂ CH(CH ₃) ₂	H	CH(CH ₃)CH ₂ CH ₃	H	87
13	CH ₂ O-(<i>t</i> Bu)	H	CH ₃	H	76
14	CH ₃	H	CH ₂ S-(Bzl)	H	78
15	CH ₃	H	(CH ₂) ₄ NH-(Boc)	H	60
16	CH ₂ S-(Bzl)	H	CH ₃	H	78
17	H	CH ₂ S-(Bzl)	CH ₃	H	74

^a isolated yield

The stability of side-chain protecting groups was also investigated by carrying out the synthesis of dipeptides *N*-Fmoc-Asp-(*Ot*Bu)-Phe-OMe (**7**), *N*-Fmoc-Ser-(*Ot*Bu)-Ala-OMe (**13**), *N*-Fmoc-Ala-Cys-(SBzl)-OMe (**14**) and *N*-Fmoc-Ala-Lys-(Boc)-OMe (**15**). In these cases, the reaction occurred without removal of the side-chain protecting groups and afforded the corresponding dipeptides in high yields (Scheme 3, Table 2). In particular, the *t*-butyl group on the serine side-chain, the benzyl group on the cysteine side-chain and the Boc group on the lysine side-chain were preserved during the condensation reaction. Therefore using pyridine as reaction solvent has proved useful not only to convert the ammonium group of amino acid methyl ester hydrochloride into the free amino function able to react as nucleophile in the condensation reaction, but also to preserve the protecting groups on the masked functionalities.

The coupling reaction mediated by TiCl₄ gave excellent results also when it was employed to get dipeptides protected on the amino terminal function with the benzyloxycarbonyl (Cbz) protecting group in fact, *N*-Cbz-L-Ala-L-Ala-OMe (**18**), and *N*-Cbz-D-Ala-L-Ala-OMe (**19**) were obtained in good yields (Scheme 4).



Scheme 4. Synthesis of *N*-Cbz protected dipeptides **18-19**

For completeness, we applied the developed procedure to the synthesis of a dipeptide system protected on the amine function with the 4-nitrobenzenesulfonyl (nosyl) group.¹⁶

Nosyl group (Ns) is an interesting protecting group as it simultaneously protects and activates the NH₂ moiety of amines,¹⁷ in fact, it is widely used for the site-selective *N*-alkylation of amino acids and peptides both in solution and solid phase.¹⁸

The condensation reaction mediated by TiCl₄ proceeded in a different way when the amino function of the N-terminal amino acid was protected with the nosyl group.

The reaction between *N*-Ns-L-phenylalanine and alanine methyl ester hydrochloride for obtaining the dipeptide *N*-Ns-L-Phe-L-Ala-OMe (**20**) was particularly slow.

After 7 hours, the TLC analysis (chloroform–methanol, 90 : 10, v/v) of reaction mixture still showed the presence of *N*-Ns-L-phenylalanine, then the reaction was stopped. After applying to the reaction mixture the previously described workup, the reaction product, recovered in 48 % yield, was analyzed by GC/MS (EI). The resulting chromatogram gave two peaks at *tr* = 46.42 min and *tr* = 46.87 min in about 3:1 ratio respectively with identical mass spectra both characterized by the presence of the molecular ion *m/z* 376 consistent with that of dipeptide *N*-Ns-Phe-L-Ala-OMe (**20**) and its corresponding diastereoisomer.

The ¹H NMR spectrum of the product also provided evidence of the presence of a mixture of two diastereoisomers in fact it showed, only for a few types of protons, the presence of two close signals of different intensity corresponding to the two stereoisomers.

Therefore, when *N*-nosyl amino acids are used as *N*-terminal residues the reaction is incomplete, probably because of the presence of the sulfonamide function, and the stereochemical integrity of the chiral centers is not completely retained.

This result prompted us to verify, also in the cases of Boc-, Cbz- and Fmoc-protected dipeptides, the configuration preservation of the amino acids chiral centers.

To this aim, we designed and carried out the synthesis of couples of diastereoisomeric dipeptides protected on the amino function with the above-cited urethane protecting groups.

Under the typical reaction conditions by using TiCl₄/pyridine reagent system, the dipeptide *N*-Boc-L-Ala-L-Ala-OMe (**3**) and its epimer *N*-Boc-D-Ala-L-Ala-OMe (**4**) were synthesized. Samples of the crude dipeptides **3** and **4** were analyzed by ¹H NMR and ¹³C NMR and the resulting spectra were compared with that obtained analyzing a mixture, of the same two epimers.

¹H NMR spectra of both single products **3** and **4** showed the presence of signals attributable to only one diastereomer and the absence of epimerized products at least within the sensibility limits of the NMR technique. The chemical shifts of the signals generated by the NH amide protons were different in the two diastereoisomers and readily resolved in the ¹H NMR spectrum of the mixture of **3** and **4**, prepared for this purpose, with a ratio 4 : 6 respectively (Figure 1).

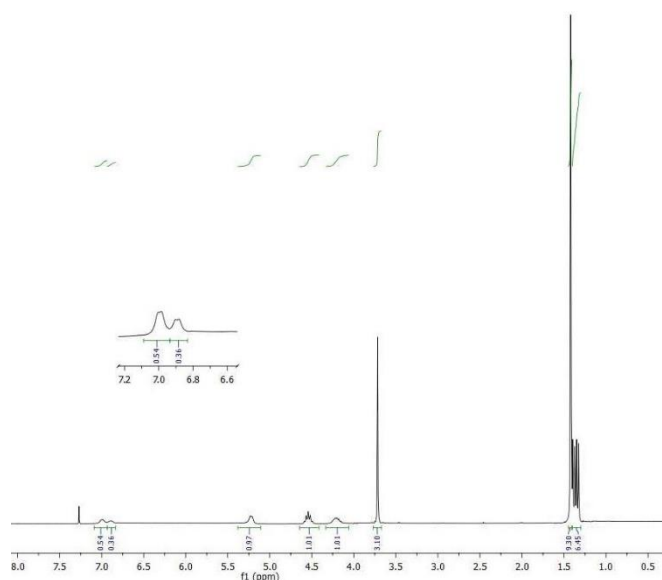


Figure 1. ¹H NMR spectrum of a mixture of **3** and **4** (approx. 4 : 6).

The GC/MS analysis of the two epimers *N*-Boc-L-Ala-L-Ala-OMe dipeptides (**3**) and *N*-Boc-D-Ala-L-Ala-OMe (**4**) instead, indicated the presence in both chromatogram of a very small amount of the other epimer, the calculated diastereomeric excess was for both epimers satisfactory ($\geq 95\%$).

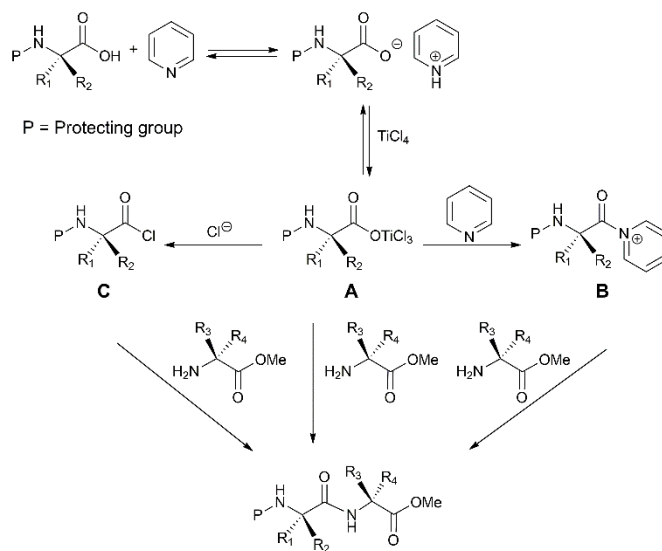
A diastereomeric excess $\geq 96\%$ was measured by analyzing by GC/MS the single dipeptides *N*-Cbz-L-Ala-L-Ala-OMe (**18**) and its epimer *N*-Cbz-D-Ala-L-Ala-OMe (**19**).

The ^1H NMR spectra of the single products **18** and **19** did not show residual signals attributable to the other diastereomer while, in the ^1H NMR analysis of a mixture of **18** and **19**, approximately 4.2 : 5.8 respectively, the signals corresponding to the amide proton (6.89 ppm, 6.83 ppm) and to the methyl ester protons (3.72 ppm, 3.73 ppm) of the two epimers resulted separated.

Finally, also the dipeptides *N*-Fmoc-L-Leu-L-Ala-OMe (**9**) and *N*-Fmoc-D-Leu-L-Ala-OMe (**10**), obtained through the developed methodology, showed no detectable loss of stereointegrity. In fact ^1H NMR spectra of both single products **9** and **10** indicated the presence of signals corresponding to only one diastereomer while in the ^1H NMR spectrum of a mixture of both epimers **9** and **10** the chemical shifts of amide and urethanic protons were resolved.

Additional experiments have been performed in order to test the epimerization process when sensitive Cys(Bzl)OH is used as *N*-terminal residue. To this aim we synthesized a couple of diastereomeric dipeptide systems *N*-Fmoc-L-Cys(Bzl)-L-Ala-OMe (**16**) and *N*-Fmoc-D-Cys(Bzl)-L-Ala-OMe (**17**) (Scheme 3, Table 2). In the crude ^1H NMR spectra of both systems (**16** and **17**) the presence of about 10% of the other diastereoisomer has been detected indicating in this case a higher epimerization level. In particular, we observed in both spectra two different signals corresponding to the NH amide proton in a ratio of about 0.9:0.1.

The formation of peptide bond under the adopted reaction conditions could occur through the mechanism depicted in Scheme 5. We hypothesized that TiCl_4 interacts with the *N*-protected amino acid pyridinium salt by forming the intermediate **A**. This could react with the amino acid methyl ester directly or after conversion into the corresponding chloride (**C**) or acyl pyridinium ion (**B**) to form the dipeptide system.



Scheme 5. Proposed mechanism for the TiCl_4 -mediated synthesis of dipeptides

6.3. Experimental

6.3.1. General experimental details

Reagents were commercially available with analytical grade and used as purchased without further purification. Solvents were purified according to well-known laboratory methods and freshly distilled prior to use. Reaction were carried out in a tightly sealed screw-capped vial. Reactions were magnetically stirred and monitored by thin layer chromatography using Merck-Kieselgel 60 F254 plates. Spots on the TLC plates were visualized with a UV lamp (254 nm) and by spraying with 0.2% ninhydrin in ethanol and charring after elution. ^1H and ^{13}C NMR spectra were recorded on a Bruker Avance 300 instrument at 300 MHz and 75 MHz, respectively. Spectroscopic analysis was performed at 293 K on diluted solutions of each compound by using CDCl_3 or DMSO-d_6 as solvents. Chemical shifts (δ) are reported in ppm. Coupling constants (J) are reported in Hertz (Hz). GC–MS analyses were performed with a DB-35MS (20 m \times 0.18 mm, 35% Phenyl 65% dimethylpolysiloxane) capillary column. The mass detector was operated in the electron impact ionization mode (EI/MS) with an electron energy of 70 eV. The injection port was heated to 250 °C. The oven temperature program was initially set at 70 °C with a hold of 2 min and ramped to 280 °C at 20 °C/min with a hold of 10 min. In order to obtain a good separation of diastereoisomers the oven temperature program was initially set at 40 °C with a hold of 2 min and ramped to 280 °C at 5 °C/min with a hold of 10 min.

6.3.2. General procedure for the synthesis of dipeptides 1-18

α -amino acid methyl ester hydrochloride (1 mmol) is first solubilized in 5 ml of anhydrous pyridine by magnetic stirring. After about 5 minutes the *N*-protected- α -amino acid (1 mmol) and TiCl_4 (2 mmol) are added. The tightly sealed screw-capped vial containing the reaction mixture is left under magnetic stirring at 40 °C, maintaining the pH at values as close as possible to neutrality by adding further amounts of pyridine. The reaction, monitored by TLC analysis (chloroform–methanol, 90 : 10, v/v), is completed after about 5 hours. After removal of pyridine by co-evaporation with toluene, the resulting crude product is suspended in chloroform and purified by elution through a silica gel column also containing a

layer of NaHCO₃ and one of NaHSO₄ separated by a silica gel one and using chloroform as mobile phase. The evaporation of chloroform under reduced pressure affords the corresponding *N*-protected dipeptide **1-18** with yields ranging from 60 to 87 %.

***N*-Boc-L-Phe-L-Ala-OMe (2)** White solid (0.140 g), 75 % yield; mp = 95-97 °C; R_f = 0,85; ¹H NMR (300 MHz, CDCl₃) δ: 7.34 – 7.13 (m, 5H, ArH), 6.66 (s_{broad}, 1H, CONH), 5.14 (d, *J* = 7.9 Hz, 1H, OCONH), 4.51 (m, 1H, CHCOOCH₃), 4.40 (m, 1H, CHCONH), 3.70 (s, 3H, OCH₃), 3.05 (d, *J* = 6.2 Hz, 2H, CH₂Ph), 1.39 (s, 9H, (CH₃)₃C), 1.33 (d, *J* = 7.2 Hz, 3H, CH₃CH); ¹³C NMR (75 MHz, CDCl₃) δ: 172.82, 170.82, 155.38, 136.58, 129.35, 128.56, 126.88, 80.14, 55.53, 52.33, 48.08, 38.36, 28.22, 18.25; GC/MS (EI, 70eV) *m/z* (% rel.): 294 (11), 277 (7), 263 (4), 248 (1), 233 (18), 220 (10), 191 (3,7), 178 (15), 164 (41,5), 159 (27), 146 (9), 120 (100), 91 (52), 57 (94). Found: C, 61.49; H, 7.45; N, 7.96. C₁₈H₂₆N₂O₅ requires C, 61.70; H, 7.48; N, 7.99 %.

***N*-Boc-L-Asp(OtBu)-Phe-OMe (1)** Oil (0.133 g), 84 % yield; R_f = 0.90; ¹H NMR (300 MHz, CDCl₃) δ: 7.34 – 7.21 (m, 3H, ArH), 7.18 – 7.07 (m, 2H, ArH), 7.01 (d, *J* = 6.9 Hz, 1H, CONH), 5.66 (d, *J* = 8.2 Hz, 1H, OCONH), 4.80 (m, 1H, CHCOOCH₃), 4.46 (m, 1H, CHCONH), 3.68 (s, 3H, OCH₃), 3.12-3.07 (m, 2H, CH₂Ph), 2.86 (dd, *J* = 16.9, 4.5 Hz, 1H, CH₂COOtBu), 2.58 (dd, *J* = 16.9, 6.5 Hz, 1H, CH₂COOtBu), 1.43 (s, 18H, (CH₃)₃C); ¹³C NMR (75 MHz, CDCl₃) δ: 173.59, 171.39, 170.61, 157.14, 135.82, 129.29, 128.53, 127.05, 81.64, 80.19, 53.51, 52.13, 50.68, 37.91, 37.28, 28.25, 28.00; GC/MS (EI, 70eV) *m/z* (% rel.): 281 (6), 276 (10), 262 (4), 207 (19), 162 (24), 131 (16), 91 (55), 86 (49), 71 (69), 57 (100). Found: C, 61.53; H, 7.63; N, 6.27. C₂₃H₃₄N₂O₇ requires C, 61.32; H, 7.61; N, 6.22 %.

***N*-Boc-L-Ala-L-Ala-OMe (3)** White solid (0.167 g), 87 % yield; mp = 110-111 °C; R_f = 0,70; ¹H NMR (300 MHz, CDCl₃) δ: 6.94 (s_{broad}, 1H, CONH), 5.28 (d, *J* = 6.7 Hz, 1H, OCONH), 4.53 (p, *J* = 7.2 Hz, 1H, CHCOOCH₃), 4.18 (m, 1H, CHCONH), 3.71 (s, 3H, OCH₃), 1.40 (s, 9H, (CH₃)₃C), 1.36 (d, *J* = 7.2 Hz, 3H, CH₃CH); 1.33 (d, *J* = 7.1 Hz, 3H, CH₃CH); ¹³C NMR (75 MHz, CDCl₃) δ: 173.14, 172.37, 155.44, 79.91, 52.32, 52.31, 47.96, 28.25, 18.30, 18.13; GC/MS (EI, 70eV) *m/z* (% rel.): 218 (2), 201 (23), 187 (6), 172

(3), 159 (5), 144 (60), 102 (40), 88 (48), 57 (100). Found: C, 52.68; H, 8.05; N, 10.16. C₁₂H₂₂N₂O₅ requires C, 52.54; H, 8.08; N, 10.21 %.

N-Boc-D-Ala-L-Ala-OMe (4) White solid (0.176 g), 87 % yield; mp = 67-68 °C; Rf = 0.80; ¹H NMR (300 MHz, CDCl₃) δ: 6.93 (s_{broad}, 1H, CONH), 5.15 (d, J = 6.8 Hz, 1H, OCONH), 4.55 (p, J = 7.2 Hz, 1H, CHCOOCH₃), 4.20 (m, 1H, CHCONH), 3.72 (s, 3H, OCH₃), 1.51 – 1.27 (m, 15H, (CH₃)₃C, CH₃CH); ¹³C NMR (75 MHz, CDCl₃) δ: 173.22, 172.27, 155.24, 80.19, 52.34, 52.33, 47.98, 28.27, 18.17, 18.16. GC/MS (EI, 70eV) m/z (% rel.): 218 (2), 201 (23), 187 (6), 172 (3), 159 (5), 144 (60), 102 (40), 88 (48), 57 (100). Found: C, 52.65; H, 8.03; N, 10.18. C₁₂H₂₂N₂O₅ requires C, 52.54; H, 8.08; N, 10.21 %.

N-Boc-L-Ala-L-Cys(Bzl)-OMe (5) Oil (0.250 g), 80 % yield; Rf = 0.76; ¹H NMR (300 MHz, CDCl₃) δ: 7.40 – 7.21 (m, 5H, ArH), 6.89 (d, J = 6.5 Hz, 1H, CONH), 5.06 (d, J = 7.1 Hz, 1H, OCONH), 4.77 (m, 1H, CHCOOCH₃), 4.18 (m, 1H, CHCONH), 3.73 (s, 3H, OCH₃), 3.70 (s, 2H, CH₂Ph), 2.95-2.78 (m, 2H, CH₂S), 1.44 (s, 9H, (CH₃)₃C), 1.36 (d, J = 7.1 Hz, 3H, CH₃CH); ¹³C NMR (75 MHz, CDCl₃) δ: 172.56, 171.02, 155.45, 137.69, 128.96, 128.61, 127.27, 80.34, 52.67, 51.31, 49.81, 36.55, 32.84, 28.32, 18.12. GC/MS (EI, 70eV) m/z (% rel.): 322 (4), 296 (1), 281 (3), 231 (11), 208 (31), 175 (9), 124 (5), 101 (2), 91 (100), 73 (5). Found: C, 57.76; H, 7.09; N, 7.03; S, 8.06. C₁₉H₂₈N₂O₅S requires C, 57.55; H, 7.12; N, 7.07; S, 8.09 %.

N-Boc-L-Ala-L-Lys(Boc)-OMe (6) Oil (0.176 g), 80 % yield; Rf = 0.85; ¹H NMR (300 MHz, CDCl₃) δ: 6.78 (d, J = 7.3 Hz, 1H, CONH), 5.15 (m, 1H, OCONH), 4.75 (m, 1H, CH₂NHCOO), 4.58 (m, 1H, CHCOOCH₃), 4.19 (m, 1H, CHCONH), 3.73 (s, 3H, OCH₃), 3.15 – 3.02 (m, 2H, CH₂NHCOO), 1.96 – 1.78 (m, 2H, CHCH₂), 1.68 (m, 1H, CHCH₂CH₂), 1.56 – 1.39 (m, 21H, CHCH₂CH₂CH₂, (CH₃)₃C), 1.36 (d, J = 7.1 Hz, 3H, CH₃CH); ¹³C NMR (75 MHz, CDCl₃) δ: 172.71, 172.61, 156.17, 155.52, 80.00, 79.00, 52.38, 51.77, 49.81, 39.97, 31.88, 29.68, 29.19, 28.43, 28.29, 22.29, 17.93. GC/MS (EI, 70eV) m/z (% rel.): 331 (3), 321 (8), 258 (18), 187 (25), 158 (24), 145 (100), 128 (36), 84 (98), 73 (26), 57 (70). Found: C, 55.58; H, 8.62; N, 9.72. C₂₀H₃₇N₃O₇ requires C, 55.67; H, 8.64; N, 9.74 %.

N-Fmoc-L-Asp(tBu)-L-Phe-OMe (7) Oil (0.245 g), 84 % yield; $R_f = 0.80$; $^1\text{H NMR}$ (300 MHz, CDCl_3) δ : 7.78 (d, $J = 7.4$ Hz, 2H, ArH), 7.59 (d, $J = 7.3$ Hz, 2H, ArH), 7.42 (t, $J = 7.4$ Hz, 2H, ArH), 7.36-7.11 (m, 7H, ArH), 7.06 (d, $J = 7.3$ Hz, 1H, CONH), 5.97 (d, $J = 8.0$ Hz, 1H, OCONH), 4.83 (m, 1H, CHCOOCH_3), 4.55 (m, 1H, CHCONH), 4.38 (m, 2H, $\text{CH}_2\text{-Fmoc}$), 4.22 (m, 1H, CH-Fmoc), 3.70 (s, 3H, OCH_3), 3.22-2.99 (m, 2H, CH_2Ph), 2.90 (dd, $J = 17.1$, $J = 4.1$ Hz, 1H, CH_2COOtBu), 2.62 (dd, $J = 17.1$, $J = 6.6$ Hz, 1H, CH_2COOtBu), 1.45 (s, 9H, $(\text{CH}_3)_3\text{CH}$); $^{13}\text{C NMR}$ (75 MHz, CDCl_3) δ : 171.38, 170.20, 170.14, 160.17, 143.73, 141.32, 135.75, 129.25, 128.59, 127.77, 127.11, 125.05, 120.01, 81.90, 67.18, 53.57, 52.18, 49.95, 47.13, 37.18, 31.57, 28.03. Found: C, 69.47; H, 6.36; N, 4.91. $\text{C}_{33}\text{H}_{36}\text{N}_2\text{O}_7$ requires C, 69.21; H, 6.34; N, 4.89 %.

N-Fmoc-L-Ala-L-Ala-OMe (8) White solid (0.285 g), 71 % yield; mp = 192-194 °C; $R_f = 0.54$; $^1\text{H NMR}$ (300 MHz, CDCl_3) δ : 7.68 (d, $J = 7.5$ Hz, 2H, ArH), 7.50 (d, $J = 7.3$ Hz, 2H, ArH), 7.31 (t, $J = 7.5$ Hz, 2H, ArH), 7.27 – 7.16 (m, 2H, ArH), 6.73 (d, $J = 7.1$ Hz, 1H, CONH), 5.55 (d, $J = 7.5$ Hz, 1H, OCONH), 4.50 (p, $J = 7.1$ Hz, 1H, CHCOOCH_3), 4.37-4.17 (m, 3H, $\text{CH}_2\text{-Fmoc}$, CHCONH), 4.13 (t, $J = 7.0$ Hz, 1H, CH-Fmoc), 3.65 (s, 1H, OCH_3), 1.41-1.22 (m, 6H, CH_3CH); $^{13}\text{C NMR}$ (75 MHz, CDCl_3) δ : 173.13, 171.96, 156.11, 143.74, 141.31, 127.74, 127.09, 125.08, 120.00, 67.14, 52.48, 50.46, 48.12, 47.14, 18.87, 18.22. Found: C, 66.41; H, 6.07; N, 7.04. $\text{C}_{22}\text{H}_{24}\text{N}_2\text{O}_5$ requires C, 66.65; H, 6.10; N, 7.07 %.

N-Fmoc-L-Leu-L-Ala-OMe (9) White solid (0.256 g), 80 % yield; mp = 162-163 °C; $R_f = 0.65$; $^1\text{H NMR}$ (300 MHz, CDCl_3) δ : 7.81 – 7.71 (m, 2H, ArH), 7.64 – 7.52 (m, 2H, ArH), 7.45-7.35 (m, 2H, ArH), 7.34 – 7.22 (m, 2H, ArH), 6.91 (d, $J = 7.2$ Hz, 1H, CONH), 5.65 (d, $J = 8.7$ Hz, 1H, OCONH), 4.57 (p, $J = 7.2$ Hz, 1H, CHCOOCH_3), 4.46 – 4.26 (m, 3H, $\text{CH}_2\text{-Fmoc}$, CHCONH), 4.20 (m, 1H, CH-Fmoc), 3.72 (s, 3H, OCH_3), 1.79 – 1.51 (m, 3H, $\text{CH}_2\text{CH}(\text{CH}_3)_2$), 1.39 (d, $J = 7.2$ Hz, 3H, CH_3CH), 1.02-0.83 (m, 6H, $\text{CH}(\text{CH}_3)_2$); $^{13}\text{C NMR}$ (75 MHz, CDCl_3) δ : 173.11, 171.93, 156.17, 143.84, 141.31, 127.70, 127.07, 125.04, 119.97, 67.10, 53.44, 52.40, 48.07, 47.18, 41.65, 24.64, 22.88, 18.14. Found: C, 68.21; H, 6.85; N, 6.37. $\text{C}_{25}\text{H}_{30}\text{N}_2\text{O}_5$ requires C, 68.47; H, 6.90; N, 6.39 %.

N-Fmoc-D-Leu-L-Ala-OMe (10) White solid (0.326 g), 80 % yield; mp = 141-144 °C;

$R_f = 0.66$; $^1\text{H NMR}$ (300 MHz, CDCl_3) δ : 7.79-7.72 (m, 2H, ArH), 7.65 – 7.53 (m, 2H, ArH), 7.44-7.35 (m, 2H, ArH), 7.34 – 7.25 (m, 2H, ArH), 6.78 (d, $J = 7.1$ Hz, 1H, CONH), 5.39 (d, $J = 8.5$ Hz, 1H, OCONH), 4.58 (p, $J = 7.2$ Hz, 1H, CHCOOCH_3), 4.50 – 4.34 (m, 2H, $\text{CH}_2\text{-Fmoc}$), 4.33-4.16 (m, 2H, CHCONH , CH-Fmoc), 3.71 (s, 3H, OCH_3), 1.75 – 1.49 (m, 3H, $\text{CH}_2\text{CH}(\text{CH}_3)_2$), 1.40 (d, $J = 7.1$ Hz, 3H, CH_3CH), 0.99-0.85 (m, 6H, $\text{CH}(\text{CH}_3)_2$); $^{13}\text{C NMR}$ (75 MHz, CDCl_3) δ : 173.11, 171.75, 158.44, 143.74, 141.32, 127.71, 127.06, 125.02, 119.98, 66.71, 53.37, 52.44, 48.07, 47.21, 41.47, 24.73, 22.94, 18.22. Found: C, 68.23; H, 6.84; N, 6.35. $\text{C}_{25}\text{H}_{30}\text{N}_2\text{O}_5$ requires C, 68.47; H, 6.90; N, 6.39 %.

N-Fmoc-Gly-L-Ala-OMe (11) Oil (0.191 g), 80 % yield; $R_f = 0.80$; $^1\text{H NMR}$ (300 MHz, CDCl_3) δ : 7.76 (d, $J = 7.4$ Hz, 2H, ArH), 7.60 (d, $J = 7.3$ Hz, 2H, ArH), 7.40 (t, $J = 7.3$ Hz, 2H, ArH), 7.35-7.28 (m, 2H, ArH), 6.78 (d, $J = 6.1$ Hz, 1H, CONH), 5.70 (s_{broad} , 1H, OCONH), 4.59 (m, 1H, CHCOOCH_3), 4.41 (d, $J = 7.0$ Hz, 2H, $\text{CH}_2\text{-Fmoc}$), 4.22 (t, $J = 7.0$ Hz, 1H, CH-Fmoc), 3.88 (s_{broad} , 2H, CH_2CONH), 3.73 (s, 3H, OCH_3), 1.41 (d, $J = 7.1$ Hz, 3H, CH_3CH); $^{13}\text{C NMR}$ (75 MHz, CDCl_3) δ : 173.27, 168.65, 155.64, 143.74, 141.30, 127.76, 127.10, 125.07, 120.02, 67.28, 52.59, 48.12, 47.07, 44.34, 18.24. Found: C, 66.22; H, 5.77; N, 7.29. $\text{C}_{21}\text{H}_{22}\text{N}_2\text{O}_5$ requires C, 65.96; H, 5.80; N, 7.33 %.

N-Fmoc-L-Leu-L-Ile-OMe (12) Oil (0.120 g), 87 % yield; $R_f = 0.80$; $^1\text{H NMR}$ (300 MHz, CDCl_3) δ : 7.77 (d, $J = 7.5$ Hz, 2H, ArH), 7.59 (d, $J = 7.3$ Hz, 2H, ArH), 7.40 (t, $J = 7.4$ Hz, 2H, ArH), 7.34 – 7.28 (m, 2H, ArH), 6.58 (d, $J = 8.4$ Hz, 1H, CONH), 5.36 (d, $J = 8.4$ Hz, 1H, OCONH), 4.58 (dd, $J = 8.4$, $J = 4.9$ Hz, 1H, CHCOOCH_3), 4.47-4.35 (m, 2H, $\text{CH}_2\text{-Fmoc}$), 4.31-4.17 (m, 2H, CH-Fmoc , CHCONH), 3.73 (s, 3H, OCH_3), 1.98-1.74 (m, 2H, CH_3CH , $(\text{CH}_3)_2\text{CH}$), 1.73-1.61 (m, 2H, $(\text{CH}_3)_2\text{CHCH}_2$), 1.41 (m, 1H, CH_3CH_2), 1.15 (m, 1H, CH_3CH_2), 1.02 – 0.83 (m, 12H, $(\text{CH}_3)_2\text{CH}$, CH_3CH , CH_3CH_2); $^{13}\text{C NMR}$ (75 MHz, CDCl_3) δ : 172.05, 171.93, 156.16, 143.73, 141.31, 127.71, 127.06, 125.02, 119.97, 67.10, 56.46, 53.53, 52.02, 47.19, 41.32, 37.86, 25.14, 24.67, 22.86, 22.01, 15.40, 11.48. Found: C, 69.77; H, 7.51; N, 5.79. $\text{C}_{28}\text{H}_{36}\text{N}_2\text{O}_5$ requires C, 69.98; H, 7.55; N, 5.83 %.

N-Fmoc-L-Ser(tBu)-L-Ala-OMe (13) White solid (0.114 g), 76 % yield; mp = 86-87 °C;

Rf = 0.83; ^1H NMR (300 MHz, CDCl_3) δ : 7.78 (d, $J = 7.4$ Hz, 2H, ArH), 7.65 – 7.58 (m, 2H, ArH), 7.51 (d, $J = 6.9$ Hz, 1H, CONH), 7.41 (t, $J = 7.2$ Hz, 2H, ArH), 7.37 – 7.29 (m, 2H, ArH), 5.84 (d, $J = 6.0$ Hz, 1H, OCONH), 4.60 (m, 1H, CHCOOCH_3), 4.40 (d, $J = 7.1$ Hz, 2H, $\text{CH}_2\text{-Fmoc}$), 4.32 – 4.19 (m, 2H, CH-Fmoc, CHCONH), 3.83 (dd, $J = 8.5$, $J = 4.1$ Hz, 1H, CH_2OtBu), 3.77 (s, 3H, OCH_3), 3.41 (t, $J = 8.5$ Hz, 1H, CH_2OtBu), 1.44 (d, $J = 7.2$ Hz, 3H, CH_3CH), 1.25 (s, 9H, $(\text{CH}_3)_3\text{C}$); ^{13}C NMR (75 MHz, CDCl_3) δ : 172.99, 170.04, 160.96, 143.90, 141.30, 127.71, 127.07, 125.14, 119.98, 80.89, 67.01, 61.87, 52.02, 50.66, 48.03, 47.16, 27.35, 18.15. Found: C, 66.88; H, 6.86; N, 5.95. $\text{C}_{26}\text{H}_{32}\text{N}_2\text{O}_6$ requires C, 66.65; H, 6.88; N, 5.98 %.

***N*-Fmoc-L-Ala-L-Cys(Bzl)-OMe (14)** Oil (0.170 g), 78 % yield; Rf = 0.76 ; ^1H NMR (300 MHz, CDCl_3) δ : 7.77 (d, $J = 7.5$ Hz, 2H, ArH), 7.67-7.54 (m, 2H, ArH), 7.41 (t, $J = 7.3$ Hz, 2H, ArH), 7.36 – 7.21 (m, 7H, ArH), 6.82 (sbroad, 1H, CONH), 5.50 (sbroad, 1H, OCONH), 4.78 (m, 1H, CHCOOCH_3), 4.40 (d, $J = 7.0$ Hz, 2H, $\text{CH}_2\text{-Fmoc}$), 4.31 (m, 1H, CHCONH), 4.22 (t, $J = 7.0$ Hz, 1H, CH-Fmoc), 3.73 (s, 3H, OCH_3), 3.66 (s, 2H, CH_2Ph), 2.89 (d, $J = 4.9$ Hz, 2H, CHCH_2S), 1.40 (d, $J = 6.8$ Hz, 3H, CH_3CH); ^{13}C NMR (75 MHz, CDCl_3) δ : 172.15, 170.89, 156.01, 143.99, 141.31, 137.67, 128.90, 128.62, 127.72, 127.30, 127.09, 125.08, 119.98, 67.00, 52.64, 51.81, 50.40, 47.16, 36.65, 33.34, 18.57. Found: C, 66.98; H, 5.80; N, 5.36; S, 6.16. $\text{C}_{29}\text{H}_{30}\text{N}_2\text{O}_5\text{S}$ requires C, 67.16; H, 5.83; N, 5.4; S, 6.18%.

***N*-Fmoc-L-Ala-L-Lys(Boc)-OMe (15)** Yellow solid (0.227 g), 74 % yield; mp = 140-143 °C; Rf = 0.66; ^1H NMR (300 MHz, CDCl_3) δ 7.81-7.71 (m, 2H, ArH), 7.65-7.52 (m, 2H, ArH), 7.40 (t, $J = 7.0$ Hz, 2H, ArH), 7.35-7.27 (m, 2H, ArH), 6.86 (d, $J = 7.6$ Hz, 1H, CONH), 5.73 (d, $J = 7.3$ Hz, 1H, OCONH), 5.29 (s, 1H, NHCH_2), 4.77 (m, 1H, CHCOOCH_3), 4.57 (m, 1H, CHCONH), 4.37 (d, $J = 7.1$ Hz, 2H, $\text{CH}_2\text{-Fmoc}$), 4.21 (t, $J = 7.1$ Hz, 1H, CH-Fmoc), 3.73 (s, 3H, OCH_3), 3.18-2.95 (m, 2H, NHCH_2CH_2), 1.83 (m, 1H, CHCH_2), 1.66 (m, 1H, CHCH_2), 1.49 – 1.19 (m, 16H, CH_3CH , $(\text{CH}_3)_3\text{C}$, $\text{CH}_2\text{CH}_2\text{CH}_2\text{CH}_2$); ^{13}C NMR (75 MHz, CDCl_3) δ 172.56, 172.36, 161.52, 157.67, 143.69, 141.28, 127.73, 127.10, 125.10, 119.98, 79.28, 67.22, 56.70, 52.24, 50.46, 47.05, 41.54, 29.37, 28.42, 22.22, 16.03. Found: C, 64.87; H, 7.06; N, 7.55. $\text{C}_{30}\text{H}_{39}\text{N}_3\text{O}_7$ requires C, 65.08; H, 7.10; N, 7.59 %.

***N*-Fmoc-*L*-Cys(Bzl)-*L*-Ala-OMe (16)** Yellow solid (0.296 g), 78 % yield; mp = 155-157 °C; R_f = 0.86; ¹H NMR (300 MHz, CDCl₃) two diastereoisomers (90*:10) δ 7.80 (d, J = 7.5 Hz, 2H, ArH), 7.63 (d, J = 7.3 Hz, 2H, ArH), 7.44 (t, J = 7.4 Hz, 2H, ArH), 7.40-7.20 (m, 7H, ArH), 6.89* and 6.81 (2_Sbroad, 1H, CONH), 5.72 (S_{broad}, 1H, OCONH), 4.59 (p, J = 7.2 Hz, 1H, CH₂COOCH₃), 4.53 – 4.39 (m, 2H, CH₂-Fmoc), 4.39-4.15 (m 2H, CHCONH, CH-Fmoc), 3.92-3.63 (m, 5H, SCH₂Ph, OCH₃), 2.92 (dd, J = 13.5 Hz, J = 5.4 Hz, 1H, CHCH₂S), 2.79 (dd, J = 13.5 Hz, J = 6.9 Hz, 1H, CHCH₂S), 1.44 (d, J = 7.1 Hz, 3H); ¹³C NMR (75 MHz, CDCl₃) δ 172.96, 169.88, 156.01, 143.72, 141.32, 137.94, 129.78, 128.78, 128.19, 126.26, 124.06, 121.09, 119.03, 67.09, 54.90, 51.67, 49.07, 47.90, 36.56, 34.23, 17.28. Found: C, 66.89; H, 5.81; N, 5.35; S, 6.17. C₂₉H₃₀N₂O₅S requires C, 67.16; H, 5.83; N, 5.4; S, 6.18%.

***N*-Fmoc-*D*-Cys(Bzl)-*L*-Ala-OMe (17)** Yellow solid (0.310 g), 74 % yield; mp = 147-148 °C; R_f = 0.86; ¹H NMR (300 MHz, CDCl₃) two diastereoisomers (90*:10) δ 7.80 (d, J = 7.5 Hz, 2H, ArH), 7.63 (d, J = 7.3 Hz, 2H, ArH), 7.44 (t, J = 7.4 Hz, 2H, ArH), 7.40-7.23 (m, 7H, ArH), 6.91 and 6.82* (2 S_{broad}, 1H, CONH), 5.73 (S_{broad}, 1H, OCONH), 4.61 (p, J = 7.1 Hz, 1H, CH₂COOCH₃), 4.53 – 4.30 (m, 3H, CH₂-Fmoc, CHCONH), 4.26 (t, J = 7.0 Hz, 1H, CH-Fmoc), 3.89-3.61 (m, 5H, SCH₂Ph, OCH₃), 2.92 (dd, J = 13.4 Hz, J = 4.7 Hz, 1H, CHCH₂S), 2.81 (dd, J = 13.4 Hz, J = 7.1 Hz, 1H, CHCH₂S), 1.44 (d, J = 7.1 Hz, 3H); ¹³C NMR (75 MHz, CDCl₃) δ 172.96, 169.77, 156.03, 143.68, 141.30, 137.89, 129.76, 128.68, 128.18, 126.28, 124.05, 121.07, 119.03, 67.19, 54.91, 51.66, 49.06, 47.95, 36.52, 34.33, 17.26. Found: C, 66.87; H, 5.78; N, 5.38; S, 6.16. C₂₉H₃₀N₂O₅S requires C, 67.16; H, 5.83; N, 5.4; S, 6.18%.

***N*-Cbz-*L*-Ala-*L*-Ala-OMe (18)** White solid (0.243 g), 74 % yield; mp = 104-106 °C; R_f = 0.84; ¹H NMR (300 MHz, CDCl₃) δ: 7.40 – 7.20 (m, 5H, ArH), 6.78 (d, J = 7.2 Hz, 1H, CONH), 5.54 (d, J = 7.5 Hz, 1H, OCONH), 5.10 (s, 2H, CH₂Ph), 4.55 (p, 1H, J = 7.2 Hz, CH₂COOCH₃), 4.30 (m, 1H, _ 173.12, 171.86, 155.67, 136.26, 128.50, 128.14, 128.00, 66.99, 52.39, 50.36, 48.07, 18.61, 18.17. GC/MS (EI, 70eV) m/z (% rel.): 308 [M⁺] (2), 249 (2), 206 (3), 178 (9), 134 (16), 102 (9), 91 (100), 88 (13), 70 (6), 59 (2). Found: C, 58.51; H, 6.53; N, 9.07. C₁₅H₂₀N₂O₅ requires C, 58.43; H, 6.54; N, 9.09 %.

***N*-Cbz-*D*-Ala-*L*-Ala-OMe (19)** White solid (0.197 g), 75 % yield; mp = 136-137 °C; Rf = 0.85; ¹H NMR (300 MHz, CDCl₃) δ: 7.44 – 7.18 (m, 5H, ArH), 7.01 (d, J = 7.1 Hz, 1H, CONH), 5.71 (d, J = 7.6 Hz, 1H, OCONH), 5.09 (s, 2H, CH₂Ph), 4.55 (p, J = 7.1 Hz, 1H, CHCOOCH₃), 4.33 (m, 1H, CHCONH), 3.70 (s, 3H, OCH₃), 1.37 (d, J = 7.0 Hz, 6H, CH₃CH); ¹³C NMR (75 MHz, CDCl₃) δ: 173.35, 172.01, 155.96, 136.19, 128.54, 128.20, 128.06, 67.01, 52.52, 50.74, 48.01, 18.66, 18.08. GC/MS (EI, 70eV) m/z (% rel.): 308 [M⁺] (2), 249 (2), 206 (3), 178 (9), 134 (16), 102 (9), 91 (100), 88 (13), 70 (6), 59 (2). Found: C, 58.53; H, 6.51; N, 9.07. C₁₅H₂₀N₂O₅ requires C, 58.43; H, 6.54; N, 9.09 %.

***N*-Ns-*L*-Phe-*L*-Ala-OMe (20)** Yellow solid (0.169 g), 48 % yield; mp = 168-172 °C; Rf = 0.85; ¹H NMR (300 MHz, CDCl₃), two diastereoisomers (74*:26) δ: 8.14 (d, J = 8.2 Hz, 2H, ArH), 7.77 (d, J = 8.2 Hz, 2H, ArH), 7.20-7.07 (m, 3H, ArH), 7.07-6.94 (m, 3H, ArH), 6.89* and 6.66 (2d, J = 6.8 Hz, 1H, ArSO₂NH), 6.19 (d, J = 7.6 Hz, 1H, CONH), 4.44 (m, 1H, CHCOOCH₃), 4.03 (m, 1H, CHCONH), 3.73* and 3.72 (2s, 3H, OCH₃), 3.09 (dd, J = 13.5, J = 4.5 Hz, 1H, CH₂Ph), 2.91 (dd, J = 13.5, 8.8 Hz, 1H, CH₂Ph), 1.32* and 1.26 (2d, J = 7.0 Hz, 3H, CH₃CH); ¹³C NMR (75 MHz, CDCl₃) two diastereoisomers (74*:26) δ: 172.64, 169.65, 149.93, 145.21, 135.45, 129.27, 128.78, 128.19, 127.28, 124.17, 58.48, 53.30 and 52.36*, 48.41, 38.92, 19.29 and 18.01*. GC/MS (EI, 70eV) m/z (% rel.): 376 (7), 344 (8), 305 (100), 233 (43), 186 (23), 174 (63), 156 (10), 130 (32), 122 (36), 118 (45), 91 (63), 76 (14), 59 (9). Found: C, 52.32; H, 4.87; N, 9.67; S, 7.35. C₁₉H₂₁N₃O₇S requires C, 52.41; H, 4.86; N, 9.65; S, 7.36%.

Synthesis of *L*-Asp-*L*-Phe-OMe (1a)

To a solution of *N*-Boc-Asp-(OtBu)-Phe-OMe (**1**) (0.1 g, 0.22 mmol), in dry CH₂Cl₂ (1,5 mL), trifluoroacetic acid (TFA) (1,5 mL) was added and stirred for 2 h at room temperature. The progress of the reaction was followed by TLC analysis with chloroform–methanol 80 : 20, (v/v) as eluent and visualization with 0.2% ninhydrin in ethanol. Then excess reagent and solvent were removed under vacuum. The resulting oil was stirred in cold diethyl ether (15 mL) and *L*-Asp-*L*-Phe-OMe (**1a**) was recovered by filtration as a white solid (0.086 g) in 95 % yield. mp = 244-245 °C; Rf = 0.20; ¹H NMR (300 MHz, DMSO-d₆) δ: 8.86 (d, J = 6.9 Hz, 1H,

CONH), 7.39 – 7.09 (m, 5H, ArH), 4.52 (m, 1H, $\underline{\text{C}}\text{HCOOCH}_3$), 4.01 (m, 1H, $\underline{\text{C}}\text{HCONH}$), 3.61 (s, 3H, OCH_3), 3.07 (dd, $J = 13.9, 5.3$ Hz, 1H, CH_2Ph), 2.93 (dd, $J = 13.9, 9.1$ Hz, 1H, CH_2Ph), 2.78 (dd, $J = 17.5, 3.4$ Hz, 1H, $\underline{\text{C}}\text{H}_2\text{COOH}$), 2.65 (dd, $J = 17.5, 8.4$ Hz, 1H, $\underline{\text{C}}\text{H}_2\text{COOH}$); ^{13}C NMR (75 MHz, DMSO-d_6) δ : 171.74, 171.50, 168.84, 137.28, 129.50, 128.82, 127.17, 54.52, 52.50, 50.63, 38.14, 36.82. Found: C, 56.98; H, 6.14; N, 9.49. $\text{C}_{14}\text{H}_{18}\text{N}_2\text{O}_5$ requires C, 57.13; H, 6.16; N, 9.52 %.

6.4. Conclusions

Here we developed a synthetic process mediated by TiCl_4 that yields dipeptide systems having high stereochemical and chemical purity. TiCl_4 /pyridine reagent system represents a valuable tool for synthesizing peptides. Dipeptide systems were synthesized easily and in high yields through a TiCl_4 -assisted condensation reaction between *N*-protected amino acids and amino acid methyl esters in pyridine.

The reaction was applied successfully to amino acids protected on the α -amino function with different protecting groups. The adopted experimental conditions allowed preserving not only the α -amino protecting groups but also the acid-labile side chain protecting groups.

The recovery of the dipeptide products has been achieved by simple filtration through a silica gel column, which greatly simplifies the reaction work-up and avoids the formation of emulsions and product losses.

The maintenance of amino acids stereochemical integrity is almost complete for dipeptides protected on the amino function with urethane protecting groups (Fmoc, Z, Boc). A non-negligible loss of stereochemical integrity was instead observed in *N*-nosyl-protected dipeptides.

Notes and references

1. (a) M. S. Iyer, K.M. Gigstad, N. D. Namdev and M. Lipton, *J. Am. Chem. Soc.*, **1996**, *118*, 4910-4911; (b) J. Oku, N. Ito and S. Inoue, *Makromol. Chem.*, **1979**, *180*, 1089-1091.
2. (a) M. Yagasaki and S. Hashimoto, *Appl. Microbiol. Biotechnol.*, **2008**, *81*, 13-22; (b) J. Arima, Y. Uesugi, M. Uraji, M. Iwabuchi and T. Hatanaka, *Appl. Environ. Microbiol.*, **2006**, *72*, 4225-4231.
3. (a) V. K. Khavinson and V. N. Anisimov, *Dokl. Akad. Nauk*, **2000**, *372*, 421-423; (b) M. Nath, S. Pokharia, G. Eng, X.Q. Song and A. Kumar, *Spectrochim. Acta A.*, **2006**, *63*, 66-75.
4. A. Guiotto, A. Calderan, P. Ruzza and G. Borin, *Curr. Med. Chem.*, **2005**, *12*, 2293-2315.
5. D. D. Kitts and K. Weiler, *Curr. Pharm. Des.*, **2003**, *9*, 1309-1323.
6. R. C. Harris, J. R. Hoffmanb, A. Allsoppc and N. B. H. Routledge, *Nutr. Res.*, **2012**, *32*, 272-277.
7. B. C. Song, N.-S. Joo, G. Aldini and K.-J. Yeum, *Nutr. Res. Pract.* **2014**, *8*, 3-10.
8. T.-S. Tseng, K.-C. Tsai, W.-C. Chen, Y.-T. Wang, Y.-C. Lee, C.-K. Lu, M.-J. Don, C.-Y. Chang, C.-H. Lee, H.-H. Lin, H.-J. Hsu and N.-W. Hsiao, *J. Agric. Food Chem.*, **2015**, *63*, 6181-6188.
9. K. Lintner and O. Peschard, *Int. J. Cosmet. Sci.*, **2000**, *22*, 207-218.
10. A. Sallam, M. Krehenbrink, D. Kalkandzhiev WO 2017/162879 A1.
11. (a) F. Albericio, *Curr. Opin. Chem. Biol.*, **2004**, *8*, 211-221; (b) T. Kimmerlin and D. Seebach, *J. Pept. Res.*, **2005**, *65*, 229-260.
12. (a) V. R. Pattabiraman and J. W. Bode, *Nature*, **2011**, *480*, 471-479; (b) A. El-Faham and F. Albericio, *Chem. Rev.*, **2011**, *111*, 6557-6602; (c) R. De Marco, M. Spinella, A. De Lorenzo, A. Leggio and A. Liguori, *Org. Biomol. Chem.*, **2013**, *11*, 3786-3796; (d) A. Leggio, E. L. Belsito, G. De Luca, M. L. Di Gioia, V. Leotta, E. Romio, C. Siciliano and A. Liguori, *RSC Adv.*, **2016**, *6*, 34468-34475; (e) A. Leggio, A. Comandè, E. L. Belsito, M. Greco, L. Lo Feudo and A. Liguori, *Org. Biomol. Chem.*, **2018**, *16*, 5677-5683.

13. (a) R. B. Merrifield, *J. Am. Chem. Soc.*, **1963**, 85, 2149–2154; (b) M. L. Di Gioia, A. Leggio, A. Liguori and F. Perri, *J. Org. Chem.*, **2007**, 72, 3723–3728; (c) D. M. M. Jaradat, *Amino Acids*, **2018**, 50, 39–68.
14. (a) M. T. Reetz, *Organotitanium Reagents in Organic Synthesis*, Springer-Verlag, Berlin, **1986**; (b) M. L. Di Gioia, A. Leggio, A. Le Pera, A. Liguori, A.F. Pitrelli and C. Siciliano, *Protein Pept. Lett.*, **2005**, 12, 357–362; (c) A. Leggio, E. L. Belsito, M. L. Di Gioia, V. Leotta, E. Romio, C. Siciliano and A. Liguori, *Tetrahedron Lett.*, **2015**, 56, 2062–2066; (d) M. L. Di Gioia, A. Leggio, I.F. Guarino, V. Leotta, E. Romio and A. Liguori, *Tetrahedron Lett.*, **2015**, 56, 5341–5344; (e) A. Leggio, E.L. Belsito, S. Gallo and A. Liguori, *Tetrahedron Lett.*, **2017**, 58, 1512–1514; (f) A. Leggio, J. Bagalà, E. L. Belsito, A. Comandè, M. Greco and A. Liguori, *Chem. Cent. J.*, **2017**, 11:87, 1–12.
15. (a) A. Leggio, A. Liguori, A. Napoli, C. Siciliano, and G. Sindona, *Eur. J. Org. Chem.*, **2000**, 5732575; (b) M. L. Di Gioia, A. Leggio, A. Le Pera, A. Liguori, F. Perri and Siciliano, C., *Eur. J. Org. Chem.*, **2004**, 4437–4441; (c) M. L. Di Gioia, A. Leggio, A. Le Pera, C. Siciliano, G. Sindona and A. Liguori, *J. Peptide Res.*, **2004**, 63, 383–387.
16. (a) A. Leggio, M. L. Di Gioia, F. Perri and A. Liguori, *Tetrahedron*, **2007**, 63, 8164–8173; (b) R. De Marco, M. L. Di Gioia, A. Leggio, A. Liguori and M. C. Viscomi, *Eur. J. Org. Chem.* **2009**, 3795–3800.
17. (a) T. Fukuyama, C.-K. Jow and M. Cheung, *Tetrahedron Lett.*, **1995**, 36, 6373–6374; (b) A. Le Pera, A. Leggio and A. Liguori, *Tetrahedron*, **2006**, 62, 6100–6106.
18. (a) S. C. Miller and T. S. Scanlan, *J. Am. Chem. Soc.*, **1997**, 119, 2301–2302; (b) M. L. Di Gioia, A. Leggio, A. Liguori, F. Perri, C. Siciliano and M. C. Viscomi, *Amino Acids*, **2010**, 38, 133–143; (c) E. Biron and H. Kessler, *J. Org. Chem.*, **2005**, 70, 5183–5189; (d) C. Aroulanda, G. Celebre, G. De Luca and M. Longeri, *J. Phys. Chem. B*, **2006**, 110, 10485–10496; (e) E. L. Belsito, M. L. Di Gioia, A. Greco, A. Leggio, A. Liguori, F. Perri, C. Siciliano and M. C. Viscomi, *J. Org. Chem.*, **2007**, 72, 4798–4802; (f) A. Leggio, E. L. Belsito, R. De Marco, A. Liguori, F. Perri and Viscomi M. C., *J. Org. Chem.*, **2010**, 75, 1386–1392; (g) R. De Marco, A. Leggio, A. Liguori, T. Marino, F. Perri, N. Russo, *J. Org. Chem.*,

2010, 75, 3381-3386; (h) M. L. Di Gioia, A. Leggio and A. Liguori, *J. Org. Chem.*,
2005, 70, 3892-3897.

Alternative formation of amides and β -enaminones from aroyl chlorides using the TiCl_4 -trialkylamine reagent system

Antonella Leggio, Alessandra Comandè, Emilia Lucia Belsito, Marianna Greco, Lucia Lo Feudo, and Angelo Liguori

[Paper 3]

Published on: Organic & Biomolecular Chemistry, 2018, 16, 5677-5683.

DOI: 10.1039/c8ob01536h

Abstract

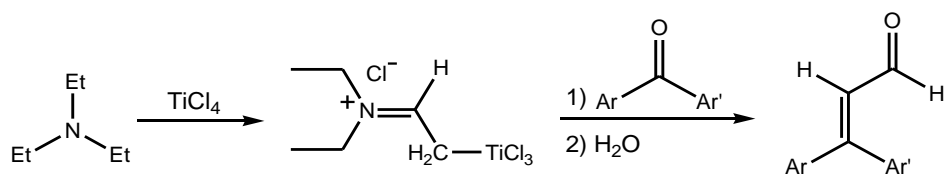
The $\text{TiCl}_4/\text{NR}_3$ reagent system has been successfully employed for the synthesis of amides and β -enaminones. The reaction of variously substituted benzoyl chlorides with $\text{TiCl}_4/\text{NR}_3$ reagent system, by using two different experimental procedures (Method A and Method B), afforded alternatively the corresponding amides and β -enaminones as unique or major products. The two developed protocols were investigated with a series of tertiary amines. The reactions, modulated by the presence of TiCl_4 , provided the corresponding amides or β -enaminones with satisfactory yields. This paper reports a new method for carbon-carbon bond formation via the reaction of aroyl chlorides with $\text{TiCl}_4/\text{NR}_3$ reagent system.

7.1. Introduction

Various kinds of Lewis acid are employed in organic synthesis to promote reactions.¹ In particular titanium tetrachloride is a reagent widely used in organic synthesis for accelerating many reactions and transforming different functional groups.² Titanium tetrachloride (TiCl_4) used in combination with a tertiary amine (NR_3) represents a useful reagent system ($\text{TiCl}_4\text{-NR}_3$) for the formation of carbon-carbon bonds, also with high stereoselectivity, such as in aldol and other condensation reactions.³ Titanium enolates can be generated by the action of trimethylamine (Et_3N) and TiCl_4 with aldehydes or ketones through the removal of an acidic hydrogen atom and used in conjugate addition reactions to α,β -unsaturated carbonyl compounds.⁴ The $\text{TiCl}_4/\text{Et}_3\text{N}$ reagent system is also used to promote the Baylis-Hilman type reaction in which arylaldehydes react with α,β -unsaturated carbonyl compounds to provide the corresponding chlorinated condensation product.⁵ Complex processes occur when TiCl_4 and Et_3N react with esters generating titanium enolates. In these cases, oxidation-reduction reactions involve dimerization of the enolates.⁶

Furthermore, the reaction of the $\text{TiCl}_4/\text{Et}_3\text{N}$ reagent system with ketimines and ketoximes allows the formation of heterocycle systems.⁷ Organotitanium compounds are also obtained by the reaction of 1-alkynes with the $\text{TiCl}_4\text{-NR}_3$ system. These reagents react with carbonyl compounds to give the corresponding enynones.⁸ In all cases, the reaction is driven by the amine that generates a carbanion by deprotonation. This carbanion by interaction with TiCl_4 originates species such as titanium enolates or simple organotitanium compounds. In the absence of organic substrates containing acidic hydrogens, the tertiary amine reacts with titanium tetrachloride to give an ammonium ion adduct which evolves producing an oxidation product with iminium ion structure and a titanium(III) specie.

The iminium ion intermediate containing acidic hydrogen atoms is converted into an organotitanium compound by the consecutive action of the amine and titanium tetrachloride. Such organotitanium intermediates are not isolated but react in situ with aromatic ketones by giving the corresponding unsaturated aldehydes (Scheme 1).⁹

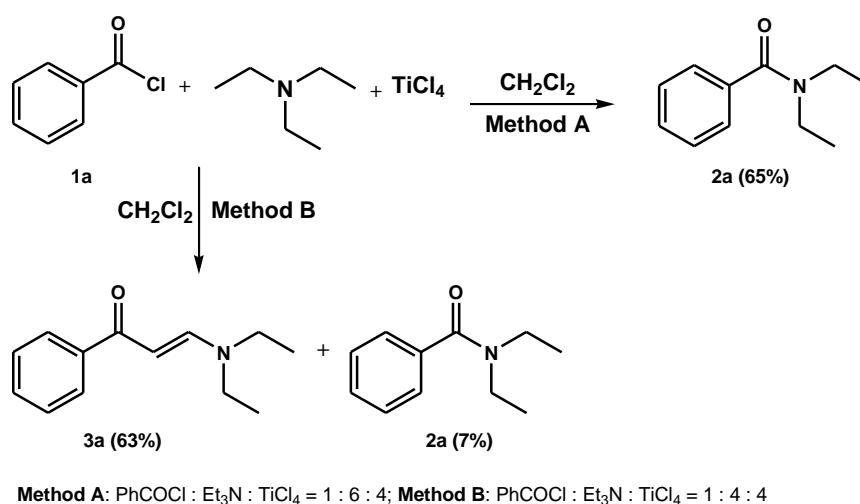


Scheme 1. Conversion of diaryl ketones into α, β -unsaturated aldehydes.

Herein we report an interesting study on the reactivity of acyl chlorides, lacking of hydrogen atoms at the carbon atom alpha to the carbonyl group, with organotitanium compounds obtained from the reaction of trialkylamines with TiCl_4 . On this base we developed two different experimental procedures that lead to the exclusive or prevalent formation of amides and β -enaminones that are of great importance in organic synthesis.

7.2. Results and discussion

We began the investigation by testing the model reaction between benzoyl chloride and the reagent system consisting of triethylamine (Et_3N) and titanium tetrachloride (Scheme 2). The amount of amine used proved to be critical to the outcomes of the reaction. Two different ways of performing the reaction were established leading to the formation of completely different main products as the result of two diverse reaction pathways (Method A and Method B) (Scheme 2). The reaction via Method A is characterized by the presence of an excess of amine and the rapid consecutive addition of the reagents. Benzoyl chloride (1 mmol) and TiCl_4 (4 mmol) are added to a solution of Et_3N (6 mmol) in methylene chloride (15 mL). The reaction mixture is kept under magnetic stirring at room temperature for about 12 h until complete conversion of the benzoyl chloride. *N,N*-Diethylbenzamide (2a) is recovered in 65% yield after purification of the crude reaction mixture by column chromatography (Scheme 2). In the Method B a solution of Et_3N (4 mmol) in methylene chloride (15 mL) is added dropwise, by means of a pressure equalized dropping funnel, over a period of 1 hour to a solution of benzoyl chloride (1 mmol) and TiCl_4 (4 mmol) in methylene chloride (20 mL). The reaction is complete within about 12 h. The purification of crude reaction product by column chromatography afforded as main reaction product the corresponding β -enaminone, (*E*)-3-(diethylamino)-1-phenylprop-2-en-1-one (3a), in 63% yield and *N,N*-diethylbenzamide (2a) in 7% yield (Scheme 2).



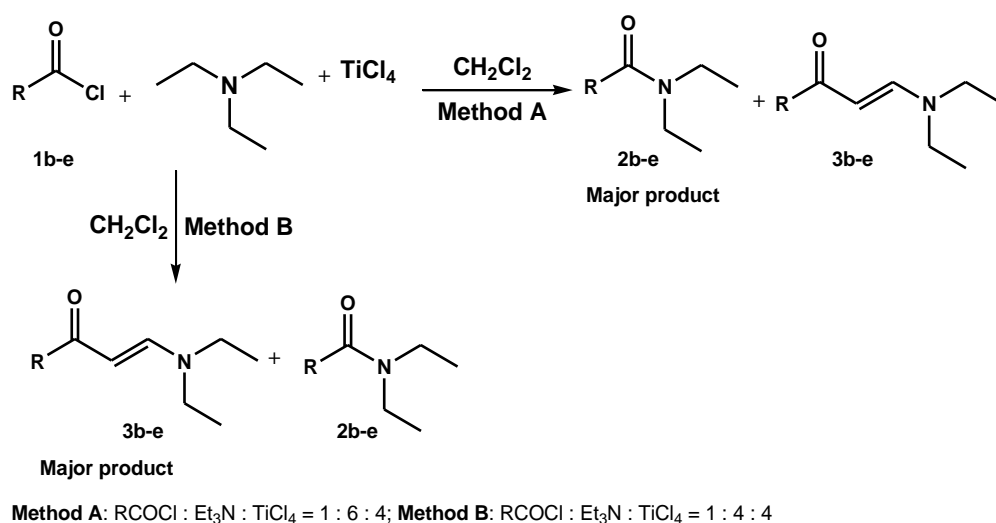
Scheme 2. Conversion of benzoyl chloride into the corresponding *N,N*-diethylamide (method A) and *N,N*-diethyl- β -enaminone (method B).

Under the Method B experimental conditions, the reaction occurs in the presence of a low concentration of base.

In the light of these results, in order to confirm the outcome of the reaction via the two methods we decided to

apply the adopted procedures (Method A and Method B) to a series of differently substituted benzoyl chlorides (Scheme 3, Table 1). *N,N*-Diethylamides (2) are the predominant reaction products by the reaction pathway A while β -enaminones (3) are the main ones by the reaction pathway B. However, with both protocols (Method A and Method B), no particular electronic effects of the substituents on the aromatic ring of the starting substrates are observed. The reaction of benzoyl chloride with the reagent system consisting of tripropylamine (Pr_3N) and TiCl_4 (Scheme 4) leads to results consistent with those obtained with trimethylamine and TiCl_4 . In fact, with the method A, *N,N*-dipropylbenzamide (4a) is obtained in 68% yield as unique reaction product, whereas with method B the amide (4a) is recovered only in 4% yield and the β -enaminone (5a) is the prevalent product (71% yield) (Scheme 4).

Additional experiments were performed by using tertiary amines with different alkyl substituents. To this aim, *N,N*-diisopropylethylamine (DIPEA) and *N,N*-dimethylisopropylamine (DMIPA), chosen as model systems, were treated with *p*-chlorobenzoyl chloride (1d) and TiCl_4 under the reaction conditions of both Method A and Method B.



Scheme 3 Synthesis of *N,N*-diethylamides (method A) and *N,N*-diethyl- β -enaminones (method B).

N,N-diethylamides (**2**) are the predominant reaction products by the reaction pathway A while β -enaminones (**3**) are the main ones by the reaction pathway B.

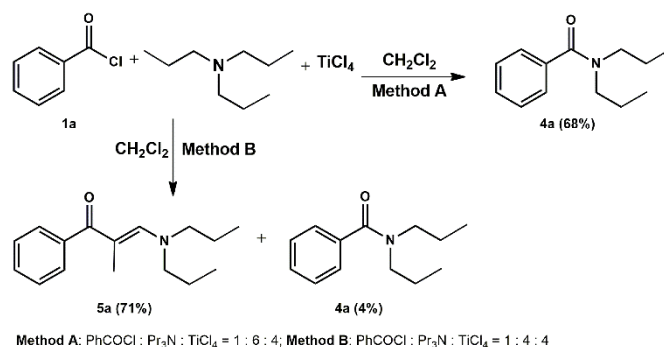
However, with both protocols (Method A and Method B), no particular electronic effects of the substituents on the aromatic ring of the starting substrates are observed.

Table 1. Results of the reactions reported in Scheme 3.

	R	Method	Amide ^a 2	β -Enaminone ^a 3
b	<i>p</i> -H ₃ COC ₆ H ₄	A	62 %	8 %
b	<i>p</i> -H ₃ COC ₆ H ₄	B	8 %	65 %
c	<i>m</i> -ClC ₆ H ₄	A	70 %	
c	<i>m</i> -ClC ₆ H ₄	B	7 %	69 %
d	<i>p</i> -ClC ₆ H ₄	A	67 %	4 %
d	<i>p</i> -ClC ₆ H ₄	B	6 %	60 %
e	<i>p</i> -O ₂ NC ₆ H ₄	A	62 %	5 %
e	<i>p</i> -O ₂ NC ₆ H ₄	B	7 %	61 %

^a Isolated yield

The reaction of benzoyl chloride with the reagent system consisting of tripropylamine (Pr₃N) and TiCl₄ (Scheme 4) leads to results consistent with those obtained with triethylamine and TiCl₄. In fact, with the method A, *N,N*-dipropylbenzamide (**4a**) is obtained in 68% yield as unique reaction product, whereas with method B the amide (**4a**) is recovered only in 4% yield and the β -enaminone (**5a**) is the prevalent product (71% yield) (Scheme 4).

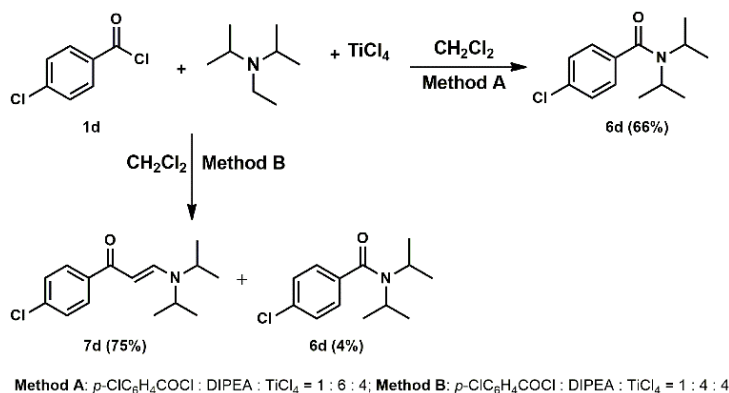


Scheme 4 Synthesis of *N,N*-dipropylamides (Method A) or *N,N*-dipropyl- β -enaminones (Method B).

Additional experiments were performed by using tertiary amines with different alkyl substituents. To this aim, *N,N*-diisopropylethylamine (DIPEA) and *N,N*-dimethylisopropylamine (DMIPA), chosen as model systems, were treated with *p*-chlorobenzoyl chloride (**1d**) and TiCl_4 under the reaction conditions of both Method A and Method B.

It is interesting to note that by using the reagent system consisting of DIPEA and TiCl_4 the two isopropyl groups of the amine are kept in the reaction products obtained through both reaction pathways (Scheme 5).

Method A leads to the exclusive formation of *N,N*-diisopropyl-*p*-chlorobenzamide (**6d**) (66% yield) while method B provides the corresponding β -enaminone (*E*)-1-(4-chlorophenyl)-3-(diisopropylamino)prop-2-en-1-one (**7d**) in 75% yield and traces of amide (**6d**) (4% yield) (Scheme 5).

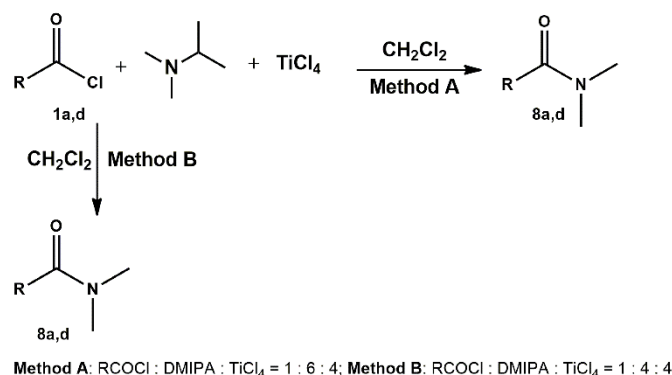


Scheme 5 Synthesis of *N,N*-diisopropylamides (Method A) or *N,N*-diisopropyl- β -enaminones (Method B).

These results offer evidence that the ethyl group of DIPEA is involved in the formation of the reactive intermediates and is lost during the reaction. On the other hand, the

isopropyl groups of DIPEA do not participate in the reaction and are preserved in the reaction products of both reaction pathways.

Instead, the reaction driven by the reagent system DMIPA/TiCl₄ under both methods A and B provides a single reaction product consisting of *N,N*-dimethyl-*p*-chlorobenzamide (**8d**) in 63% and 70 % yield respectively (Scheme 6, Table 2).



Scheme 6 Synthesis of *N,N*-dimethylamides (Method A, Method B).

The outcome of the reaction of *p*-chlorobenzoyl chloride (**1d**) with the reagent system DMIPA/TiCl₄ shows that the formation of the β -enaminone requires that at least one of the alkyl groups of the amine has, in alpha position with respect to nitrogen atom, a primary carbon atom with not sterically hindered hydrogens and also a chain of at least two carbon atoms.

This finding is confirmed by the reaction of the same reagent system DMIPA/TiCl₄ with benzoyl chloride (**1a**) (Scheme 6, Table 2). Also in this case, in fact, both method A and B provide exclusively *N,N*-dimethylbenzamide (**8a**) with yields close to 65%.

Table 2. Results of the reactions reported in Scheme 6.

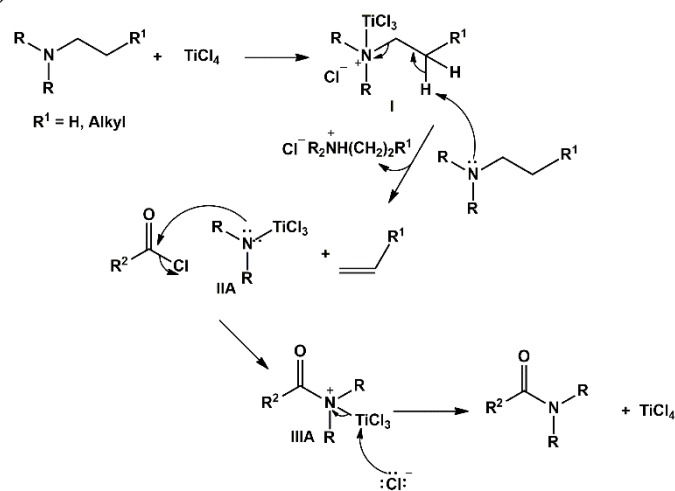
	R	Method	Amide ^a 8	β -Enaminone ^a
a	C ₆ H ₅	A	65 %	–
a	C ₆ H ₅	B	63 %	–
d	<i>p</i> -ClC ₆ H ₅	A	63 %	–
d	<i>p</i> -ClC ₆ H ₅	B	70 %	–

^a Isolated yield

On the basis of the collected experimental data using differently substituted tertiary amines under the reaction conditions of the two diverse reaction pathways, and of the available literature data⁹ on the reactivity of the $\text{TiCl}_4/\text{Et}_3\text{N}$ reagent system, adequate reaction mechanisms for the formation of the amides and β -enaminones were hypothesized.

The key intermediate could be the ammonium ion (Adduct I) (Scheme 7, Scheme 8) that is generated from the reaction between the tertiary amine and titanium tetrachloride.

The reaction path, which provides the amide as the predominant product, is favoured when an excess of amine is present in the reaction medium (Method A). Under these conditions, the ammonium ion (Adduct I) reacts with the amine in excess through an elimination process with the loss of an alkene (Hoffmann elimination) and the formation of a nucleophile intermediate (IIA) that reacts with the acyl chloride thus generating the amide (Scheme 7).

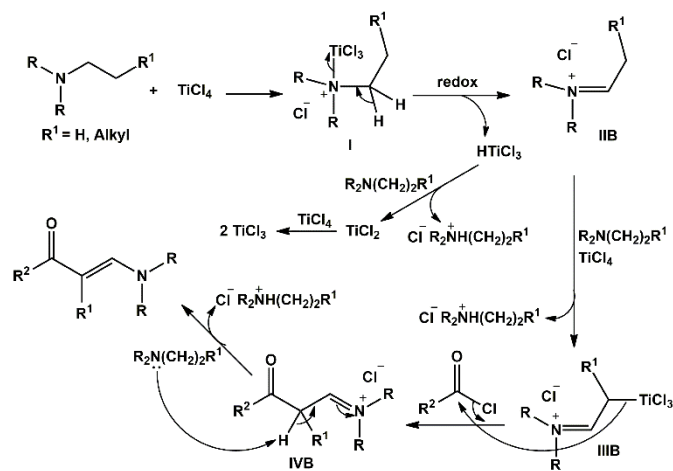


Scheme 7 Proposed mechanism for amide formation (Method A)

The reaction path, which provides the amide as the predominant product, is favoured when an excess of amine is present in the reaction medium (Method A). Under these conditions, the ammonium ion (Adduct I) reacts with the amine in excess through an elimination process with the loss of an alkene (Hoffmann elimination) and the formation of a nucleophile intermediate (IIA) that reacts with the acyl chloride thus generating the amide (Scheme 7).

When the amine is added slowly (Method B) to the reaction mixture containing TiCl_4 and the acyl chloride, the produced ammonium ion (adduct I), in the presence of limited amount of amine, is oxidized generating the iminium ion (IIB) which then reacts with the

amine and TiCl_4 to give the imminioalkyl titanium ion (IIIB) (Scheme 8). The reaction of acyl chloride with the organotitanium compound (IIIB) generates the adduct IVB, that evolves to β -enaminone, and TiCl_4 that is converted in titanium dioxide (TiO_2) during the final hydrolytic workup (Scheme 8).



Scheme 8 Proposed mechanism for β -enaminone formation (Method B)

7.3. Experimental

7.3.1. General experimental details

All reagents were purchased commercially without further purification. Solvents were purified according to well-known laboratory methods and freshly distilled prior to use. Reaction were carried out in a tightly sealed screw-capped vial. Reactions were magnetically stirred and monitored by thin layer chromatography using Merck-Kieselgel 60 F254 plates. ^1H and ^{13}C NMR spectra were recorded on a Bruker Avance 300 instrument at 300 MHz and 75 MHz, respectively. Spectroscopic analysis was performed at 293 K on diluted solutions of each compound by using CDCl_3 as the solvent. Chemical shifts (δ) are reported in ppm. Coupling constants (J) are reported in Hertz (Hz). GC-MS analyses were performed with a DB-35MS (20 m \times 0.18 mm, 35% Phenyl 65% dimethylpolysiloxane) capillary column. The mass detector was operated in the electron impact ionization mode (EI/MS) with an electron energy of 70 eV. The injection port was heated to 250 $^\circ\text{C}$. The oven temperature program was initially set at 70 $^\circ\text{C}$ with a hold of 2 min and ramped to 280 $^\circ\text{C}$ at 20 $^\circ\text{C}/\text{min}$ with a hold of 10 min.

7.3.2. General procedures for the synthesis of amides and β -enaminones.

General procedure Method A

Benzoyl chloride or substituted benzoyl chloride (1 mmol) and TiCl_4 (4 mmol) were added in rapid succession to a solution of trialkylamine (6 mmol) in anhydrous dichloromethane (15 mL). The resulting mixture was maintained under an inert atmosphere (N_2) and stirred at room temperature for about 12 hours monitoring the reaction progress by TLC (chloroform/methanol 90:10 v/v). After adding dichloromethane (20 mL) the mixture was washed first with aqueous HCl 1N (3 \times 10 mL) and then with a saturated aqueous solution of NaHCO_3 (3 \times 10 mL) and dried over anhydrous Na_2SO_4 . The evaporation of the organic solvent under reduced pressure afforded a crude reaction product that was purified by flash column chromatography (chloroform/methanol 95:5 v/v) to provide the corresponding *N,N*-dialkylamide (62-70 % yield) and *N,N*-dialkyl- β -enaminone (0-8 % yield).

General procedure Method B

To a solution of benzoyl chloride or substituted benzoyl chloride (1 mmol) in anhydrous dichloromethane (20 mL), under an inert atmosphere (N₂), TiCl₄ (4 mmol) was added. To the resulting solution trialkylamine (4 mmol), dissolved in anhydrous dichloromethane (15 mL), was added dropwise over a period of an hour. The mixture was stirred at room temperature for about 12 hours monitoring the reaction progress by TLC (chloroform/methanol 90:10 v/v). Then the mixture was washed with aqueous HCl 1N (3×10 mL) and with a saturated aqueous solution of NaHCO₃ (3 × 10 mL) and dried (Na₂SO₄). The organic solution was concentrated in vacuo and the crude residue was purified by flash column chromatography (chloroform/methanol 95:5 v/v) to provide the corresponding *N,N*-dialkyl-β-enaminone (61-75 % yield) and *N,N*-dialkylamide (0-7 % yield).

***N,N*-diethylbenzamide (2a)** Oil (65%); R_f = 0.70; ¹H NMR (300 MHz, CDCl₃) δ: 7.45-7.30 (m, 5H, ArH), 3.67-3.43 (m, 2H, CH₂), 3.40-3.15 (m, 2H, CH₂), 1.25 (t, *J* = 6.0 Hz, 3H, CH₃), 1.11 (t, *J* = 6.0 Hz, 3H, CH₃); ¹³C NMR (75 MHz, CDCl₃) δ: 171.14, 137.12, 128.94, 128.23, 126.09, 43.13, 39.12, 14.02, 12.74; GC/MS (EI, 70 eV) *m/z* (% rel.): 177 [M⁺] (15), 176 (42), 162 (1), 148 (3), 105 (100), 77 (32), 51 (6). Found: C, 74.62; H, 8.56; N, 7.86. C₁₁H₁₅NO requires C, 74.54.13; H, 8.53; N, 7.90%

(*E*)-3-(diethylamino)-1-phenylprop-2-en-1-one (3a) Oil (63%); R_f = 0.62; ¹H-NMR (300 MHz, CDCl₃) δ: 7.93-7.77 (m, 3H, ArH, CHN), 7.56-7.30 (m, 3H, ArH), 5.75 (d, *J* = 12.5 Hz, 1H, COCH), 3.42-3.13 (m, 4H, CH₂), 1.43-1.02 (m, 6H, CH₃); ¹³C NMR (75 MHz, CDCl₃) δ: 188.80, 152.46, 140.78, 130.73, 128.07, 127.44, 91.77, 50.52, 42.91, 14.59, 11.39 (prof); GC/MS (EI, 70 eV) *m/z* (% rel.): 203 [M⁺] (97), 186 (100), 174 (40), 146 (17), 126 (18), 105 (95), 98 (32), 77 (45). Found: C, 76.56; H, 8.48; N, 6.81. C₁₃H₁₇NO requires C, 76.81; H, 8.43; N, 6.89%.

***N,N*-diethyl-4-methoxybenzamide (2b)** Oil (62%); R_f = 0.71; ¹H NMR (300 MHz, CDCl₃) δ: 7.22 (d, *J* = 8.7 Hz, 2H, ArH), 6.77 (d, *J* = 8.7 Hz, 2H, ArH), 3.68 (s, 3H, OCH₃), 3.49-3.06 (m, 4H, CH₂), 0.90-1.26 (m, 6H, CH₃); ¹³C NMR (75 MHz, CDCl₃) δ: 171.06, 160.15, 129.30, 127.99, 113.48, 55.08, 42.40, 39.81, 13.30; GC/MS (EI, 70 eV) *m/z* (% rel.): 207 [M⁺] (12), 206 (28), 135 (100), 107 (5), 92 (10), 77 (11). Found: C, 69.61; H, 8.21; N, 6.65. C₁₂H₁₇NO₂ requires C, 69.54; H, 8.27; N, 6.76%.

(E)-3-(diethylamino)-1-(4-methoxyphenyl)prop-2-en-1-one (3b) Oil (65%); Rf = 0.64; ¹H NMR (300 MHz, CDCl₃) δ: 7.87 (d, *J* = 8.9 Hz, 2H, ArH), 7.79 (d, *J* = 12.5 Hz, 1H, CHN), 6.89 (d, *J* = 8.9 Hz, 2H, ArH), 5.74 (d, *J* = 12.5 Hz, 1H, COCH), 3.82 (s, 3H, OCH₃), 3.30 (q, *J* = 7.2 Hz, 4H, CH₂), 1.20 (t, *J* = 7.2 Hz, 6H, CH₃); ¹³C NMR (75 MHz, CDCl₃) δ: 187.57, 161.84, 152.02, 133.30, 129.39, 113.26, 91.15, 55.33, 45.51, 14.67; MS (EI, 70 eV) *m/z* (% rel.): 233 [M⁺] (54), 216 (46), 204 (10), 190 (5), 176 (7), 161 (3), 135 (100), 107 (5), 98 (26), 77 (15). Found: C, 72.33; H, 8.29; N, 5.93. C₁₄H₁₉NO₂ requires C, 72.07; H, 8.21; N, 6.00%.

3-chloro-*N,N*-diethylbenzamide (2c) Oil (70%); Rf = 0.50; ¹H NMR (300 MHz, CDCl₃) δ: 8.01-7.89 (m, 1H, ArH), 7.55-7.50 (m, 1H, ArH), 7.59-7.47 (m, 1H, ArH), 7.41-7.31 (m, 1H, ArH), 7.28-7.20 (m, 1H, ArH), 3.66-3.45 (m, 2H, CH₂), 3.35-3.18 (m, 2H, CH₂), 1.33-1.18 (m, 3H, CH₃), 1.21-0.99 (m, 3H, CH₃); ¹³C NMR (75 MHz, CDCl₃) δ: 169.88, 138.71, 134.49, 129.85, 129.37, 126.55, 124.41, 45.85, 33.44, 14.12, 12.70; GC/MS (EI, 70 eV) *m/z* (% rel.): 211 [M⁺] (13), 210 (38), 182 (5), 139 (100), 111 (25), 75 (11). Found: C, 62.47; H, 6.65; N, 6.54. C₁₁H₁₄ClNO requires C, 62.41; H, 6.67; N, 6.62%.

(E)-1-(3-chlorophenyl)-3-(diethylamino)prop-2-en-1-one (3c) Oil (69%); Rf = 0.34; ¹H NMR (300 MHz, CDCl₃) δ: 7.99-7.53 (m, 3H, ArH, CHN), 7.46-7.07 (m, 2H, ArH), 5.67 (d, *J* = 12.5 Hz, 1H, COCH), 3.51-2.99 (m, 4H, CH₂), 1.36-0.89 (m, 6H, CH₃); ¹³C NMR (75 MHz, CDCl₃) δ: 186.88, 152.78, 142.49, 134.12, 130.53, 129.35, 127.50, 125.48, 91.16, 50.58, 42.82, 14.64, 11.48; GC/MS (EI, 70 eV) *m/z* (% rel.): 237 [M⁺] (87), 222 (39), 220 (92), 208 (41), 190 (15), 180 (16), 165 (8), 154 (6), 139 (100), 126 (36), 111 (52), 98 (56), 75 (23), 56 (38). Found: C, 65.55; H, 6.85; N, 5.84. C₁₃H₁₆ClNO requires C, 65.68; H, 6.78; Cl, 14.91; N, 5.89%.

4-chloro-*N,N*-diethylbenzamide (2d) Oil (67%); Rf = 0.63; ¹H NMR (300 MHz, CDCl₃) δ: 7.41-7.24 (m, 4H, ArH), 3.63-3.37 (m, 2H, CH₂), 3.34-3.11 (m, 2H, CH₂), 1.35-0.97 (m, 6H, CH₃); ¹³C NMR (75 MHz, CDCl₃) δ: 170.21, 135.58, 135.11, 128.67, 127.82, 43.22, 39.11, 14.29, 12.82; GC/MS (EI, 70 eV) *m/z* (% rel.): 211 [M⁺] (13), 210 (35), 139 (100), 111 (24), 75 (10). Found: C, 62.46; H, 6.64; N, 6.54. C₁₁H₁₄ClNO requires C, 62.41; H, 6.67; Cl, 16.75; N, 6.62%.

(E)-1-(4-chlorophenyl)-3-(diethylamino)prop-2-en-1-one (3d) Oil (60%); Rf = 0.47; ¹H NMR (300 MHz, CDCl₃) δ: 7.92-7.77 (m, 3H, ArH, CH-N), 7.45-7.32 (m, 2H, ArH),

5.71 (d, $J = 12.4$ Hz, 1H, COCH), 3.51-3.18 (m, 4H, CH₂), 1.38-1.13 (m, 6H, CH₃); ¹³C NMR (300 MHz, CDCl₃) δ : 187.17, 152.62, 139.12, 136.79, 128.88, 128.26, 91.28, 50.70, 42.95, 14.62, 11.60; GC/MS (EI, 70 eV) m/z (% rel.): 237 [M⁺] (73), 220 (78), 208 (29), 180 (13), 139 (100), 111 (35), 98 (40), 75 (14), 56 (19). Found: C, 65.81; H, 6.71; N, 5.96. C₁₃H₁₆ClNO requires C, 65.68; H, 6.78; Cl, 14.91; N, 5.89%.

***N,N*-diethyl-4-nitrobenzamide (2e)** Oil (62%); R_f = 0.43; ¹H NMR (300 MHz, CDCl₃) δ : 8.35-8.12 (m, 2H, ArH), 7.58-7.38 (m, 2H, ArH), 3.64-3.38 (m, 2H, CH₂), 3.29-3.05 (m, 2H, CH₂), 1.25 (t, $J = 7.0$ Hz, 3H, CH₃), 1.11 (t, $J = 7.0$ Hz, 3H, CH₃); ¹³C NMR (75 MHz, CDCl₃) δ : 168.94, 148.02, 143.38, 127.35, 123.87, 43.28, 39.48, 14.19, 12.85; GC/MS (EI, 70 eV) m/z (% rel.): 222 [M⁺] (14), 221 (34), 193 (3), 150 (100), 120 (27), 104 (31), 92 (14), 76 (19). Found: C, 59.38; H, 6.44; N, 12.70. C₁₁H₁₄N₂O₃ requires C, 59.45; H, 6.35; N, 12.60%.

(*E*)-3-(diethylamino)-1-(4-nitrophenyl)prop-2-en-1-one (3e) Solid (61%); mp = 85.0-86.6 °C; R_f = 0.30; ¹H NMR (300 MHz, CDCl₃) δ : 8.23 (d, $J = 8.8$ Hz, 2H, ArH), 7.99 (d, $J = 8.8$ Hz, 2H, ArH), 7.86 (d, $J = 12.4$ Hz, 1H, CHN), 5.72 (d, $J = 12.4$ Hz, 1H, COCH), 3.51-3.21 (m, 4H, CH₂), 1.34-1.17 (m, 6H, -CH₃); ¹³C NMR (75 MHz, CDCl₃) δ : 185.82, 153.32, 148.92, 146.23, 128.23, 123.32, 91.44, 50.80, 43.02, 14.64, 11.52; GC/MS (EI, 70 eV) m/z (% rel.): 248 [M⁺] (75), 231 (100), 219 (43), 173 (16), 150 (49), 98 (49), 76 (21), 56 (34). Found: C, 63.04; H, 6.45; N, 11.19. C₁₃H₁₆N₂O₃ requires C, 62.89; H, 6.50; N, 11.28%.

***N,N*-dipropylbenzamide (4a)** Oil (68%); R_f = 0.77; ¹H NMR (300 MHz, CDCl₃) δ : 7.48-7.29 (m, 5H, ArH), 3.57-3.35 (m, 2H, NCH₂), 3.25-3.07 (m, 2H, NCH₂), 1.80-1.61 (m, 2H, CH₂), 1.61-1.42 (m, 2H, -CH₂), 1.08-0.91 (m, 3H, CH₃), 0.83-0.65 (m, 3H, CH₃); ¹³C NMR (75 MHz, CDCl₃) δ : 170.90, 136.42, 128.36, 127.52, 125.61, 49.89, 45.48, 21.05, 19.85, 10.65, 10.18; GC/MS (EI, 70 eV) m/z (% rel.): 205 [M⁺] (15), 204 (20), 176 (8), 162 (2), 134 (7), 105 (100), 77 (23). Found: C, 75.98; H, 9.35; N, 6.75. C₁₃H₁₉NO requires C, 76.06; H, 9.33; N, 6.82%.

(*E*)-3-(dipropylamino)-1-phenylbut-2-en-1-one (5a) Oil (71%); R_f = 0.66; ¹H NMR (300 MHz, CDCl₃) δ : 7.62-7.20 (m, 6H, ArH, CHN), 3.28-3.02 (m, 4H, NCH₂), 2.08 (s, 3H, CH₃), 1.69-1.46 (m, 4H, CH₂CH₃), 1.09-0.70 (m, 6H, CH₂CH₃); ¹³C NMR (75 MHz, CDCl₃) δ : 197.00, 155.43, 142.35, 128.83, 128.25, 127.71, 105.12, 55.05, 22.59, 10.87,

10.83; GC/MS (EI, 70 eV) m/z (% rel.): 245 [M^+] (37%), 228 (100), 216 (45), 202 (17), 168 (11), 160 (12), 145 (8), 140 (30), 105 (84), 91 (50), 77 (56). Found: C, 78.18; H, 9.38; N, 5.65. $C_{16}H_{23}NO$ requires C, 78.32; H, 9.45; N, 5.71%.

4-chloro-*N,N*-diisopropylbenzamide (6d) Solid (66%); mp= 81.6-83.7 °C; Rf = 0.70; 1H NMR (300 MHz, $CDCl_3$) δ : 7.42-7.32 (m, 2H, ArH), 7.30-7.21 (m, 2H, ArH), 3.98-3.34 (m, 2H, $NCH(CH_3)_2$), 1.61-1.02 (m, 12H, $NCH(CH_3)_2$); ^{13}C NMR (75 MHz, $CDCl_3$) δ : 169.88, 137.30, 134.61, 128.70, 127.13, 51.99, 20.69; GC/MS (EI, 70 eV) m/z (% rel.): 239 [M^+] (6), 224 (5), 196 (18), 139 (100), 111 (19). Found: C, 65.22; H, 7.64; N, 5.79. $C_{13}H_{18}ClNO$ requires C, 65.13; H, 7.57; Cl, 14.79; N, 5.84%.

(*E*)-1-(4-chlorophenyl)-3-(diisopropylamino)prop-2-en-1-one (7d) Oil (75%); Rf = 0.63; 1H NMR (300 MHz, $CDCl_3$) δ : 7.97 (d, $J = 12.5$ Hz, 1H, CHN), 7.82 (d, 2H, $J = 8.7$ Hz, ArH), 7.35 (d, 2H, $J = 8.7$ Hz, ArH), 5.83 (d, $J = 12.5$ Hz, 1H, -CO-CH=CH), 4.08-3.90 (m, 1H, $NCH(CH_3)_2$), 3.73-3.51 (m, 1H, - $NCH(CH_3)_2$), 1.30-1.20 (m, 12H, - $NCH(CH_3)_2$); ^{13}C NMR (75 MHz, $CDCl_3$) δ : 186.49, 149.31, 139.19, 136.65, 128.87, 128.23, 91.29, 49.51, 48.19, 23.68, 19.68; GC/MS (EI, 70 eV) m/z (% rel.): 265 [M^+] (33), 250 (8), 222 (56), 139 (100), 126 (20), 111 (21), 43 (18). Found: C, 68.04; H, 7.67; N, 5.16. $C_{15}H_{20}ClNO$ requires C, 67.79; H, 7.58; Cl, 13.34; N, 5.27%.

***N,N*-dimethylbenzamide (8a)** Oil (65% yield method A, 63% yield method B); Rf = 0.64; 1H -NMR (300 MHz, $CDCl_3$) δ : 7.51-7.30 (m, 5H, ArH), 3.11 (s, 3H, CH_3), 2.97 (s, 3H, CH_3); ^{13}C -NMR (75 MHz, $CDCl_3$) δ : 171.62, 136.37, 129.45, 128.29, 127.01, 39.23, 35.11; GC/MS (EI, 70 eV) m/z (% rel.): 149 [M^+] (21), 148 (64), 105 (100), 77 (53), 51 (12). Found: C, 72.50; H, 7.40; N, 9.34. $C_9H_{11}NO$ requires C, 72.46; H, 7.43; N, 9.39%.

4-chloro-*N,N*-dimethylbenzamide (8d) Oil (63% yield method A, 70% yield method B); Rf = 0.53; 1H NMR (300 MHz, $CDCl_3$) δ : 7.42-7.24 (m, 4H, ArH), 3.08 (s, 3H, CH_3), 2.96 (s, 3H, CH_3); ^{13}C NMR (75 MHz, $CDCl_3$) δ : 170.51, 135.57, 134.68, 128.62, 128.59, 39.50, 35.55; GC/MS (EI, 70 eV) m/z (% rel.): 183 [M^+] (18), 182 (51), 139 (100), 111 (38), 75 (16). Found: C, 58.97; H, 5.53; N, 7.58. $C_9H_{10}ClNO$ requires C, 58.86; H, 5.49; Cl, 19.31; N, 7.63%.

7.4. Conclusions

In this work, we have devised two methodologies that can constitute alternative procedures for the synthesis of amides and β -enaminones. The reported study represents a new example of reactivity of $\text{TiCl}_4\text{-NR}_3$ reagent system with aroyl chlorides involving carbon-carbon bond formation.

The reactions according to method A and method B, both modulated by the presence of TiCl_4 , lead to the formation, with satisfactory yields, of amides or β -enaminones that are of great importance in organic synthesis.

Amides in fact are very important functional groups in organic chemistry and the formation of amide bond is one of the most used transformations in organic synthesis.¹⁰ Amides are also biologically interesting compounds because of their presence in molecules such as peptides, pharmaceutical agents, naturally occurring molecules, proteins.¹¹

β -enaminones represent useful synthons for the synthesis of various heterocyclic compounds and biologically active molecules.¹² β -enaminones possess the nucleophilicity of an enamine and the electrophilicity of an enone, therefore they are important intermediates in organic synthesis.

Titanium tetrachloride forms with the alkyl tertiary amine an ammonium ion adduct. In the presence of an excess of amine this adduct generates, through an elimination process, the amide (Method A). The formation of the amide with the proposed method A is quite general.

In the absence of further amine the adduct leads to the formation of β -enaminone (Method B). This mechanism operates when the amine is added slowly.

The formation of the β -enaminone with the method B, however, does not occur when the amine has a secondary carbon directly linked to the nitrogen atom. This situation evidently prevents the oxidation process of the amine to the iminium ion by TiCl_4 . Iminium ion, in fact, constitutes the key intermediate for the formation of the β -enaminone.

The formation of alkyltitanium species seems to be favoured at primary carbon atoms rather than secondary ones. When β -enaminone, for the reasons mentioned above, does not form, the channel leading to the formation of the amide is activated.

Notes and references

1. a) H. Yamamoto, *Lewis Acids in Organic Synthesis*, Ed.; Wiley-VCH: New York, **2000**; b) M.L. Di Gioia, A. Leggio, A. Le Pera, C. Siciliano, G. Sindona, A. Liguori, *J. Pept. Res.*, **2004**, *63*, 383; c) M.L. Di Gioia, A. Leggio, A. Le Pera, A. Liguori, F. Perri, C. Siciliano, *Eur. J. Org. Chem.*, **2004**, 4437, d) M.L. Di Gioia, A. Leggio, A. Le Pera, A. Liguori, C. Siciliano, *J. Org. Chem.*, **2005**, *70*, 10494; e) O. M. Singh, L. R. Devi, *Mini Rev Org Chem*, **2013**, *10*, 84.
2. a) M. T. Reetz, *Organotitanium Reagents in Organic Synthesis*, Springer-Verlag: Berlin, **1986**; b) T. Mukaiyama, *Angew. Chem., Int. Ed.* **1977**, *16*, 817; c) A. Leggio, E. L. Belsito, S. Gallo and A. Liguori, *Tetrahedron Letters*, **2017**, *58*, 1512; d) M. L. Di Gioia, A. Leggio, A. Le Pera, A. Liguori, and C. Siciliano, *Eur. J. Org. Chem.*, **2004**, 463; e) M. L. Di Gioia, A. Leggio, I. F. Guarino, V. Leotta, E. Romio and A. Liguori, *Tetrahedron Lett.*, **2015**, *56*, 5341; f) A. Leggio, J. Bagalà, E. L. Belsito, A. Comandè, M. Greco, A. Liguori, *Chemistry Central Journal*, **2017**, *11*, 87;
3. a) C. R. Harrison, *Tetrahedron Letters*, **1987**, *28*, 4135; b) D. A. Evans, D. L. Rieger, M. T. Bilodeau, F. Urpi, *J. Am. Chem. Soc.*, **1991**, *113*, 1047; c) D. A. Evans, F. Urpi, T. C. Somers, J. S. Clark, M. T. Bilodeau, *J. Am. Chem. Soc.*, **1990**, *112*, 8215.
4. D. A. Evans, M. T. Bilodeau, T. C. Somers, J. Clardy, D. Cherry, Y. Kato, *J. Org. Chem.*, **1991**, *56*, 5750.
5. a) M. Shi, J.-K. Jiang, Y.-S. Feng, *Org. Lett.*, **2000**, *2*, 2397; b) M. Shi, J.-K. Jiang, Y.-S. Feng, *Org. Lett.*, **2000**, *2*, 617; c) M. Shi, J.-K. Jiang, SC. Cui, *Molecules*, **2001**, *6*, 852; d) M. Shi, Y.-S. Feng, *J. Org. Chem.*, **2001**, *66*, 466; e) T. Kataoka, T. Iwama, S. Tsujiyama, *Chem. Commun.*, **1998**, 197; f) D. Basavaiah, K. Muthukumar, B. Sreenivasulu, *Synlett* **1999**, 1249.
6. Y. Matsumara, M. Nishimura, H. Hiu, M. Watanabe, N. Kise, *J. Org. Chem.* **1996**, *61*, 2809.
7. a) M. Periasamy, G. Srinivas, P. Bharathi, *J. Org. Chem.*, **1999**, *64*, 4204; b) M. Periasamy, G. Srinivas, M. Seenivasaperumal, *J. Chem. Res.*, **2004**, 270; c) M. Periasamy, *Arkivoc*, **2002**, vii, 151.
8. M. Periasamy, G. V. Karunakar, P. Bharathi, *J. Chem. Res.* **2006**, 566.
9. P. Bharathi, M. Periasamy, *Org. Lett.* **1999**, *1*, 857.
10. a) V. R. Pattabiraman, J. W. Bode, *Nature*, **2011**, *480*, 471; b) A. Leggio, M. L. Di Gioia, F. Perri, A. Liguori, *Tetrahedron*, **2007**, *63*, 8164; c) A. Leggio, E. L. Belsito, G. De Luca, M. L. Di Gioia, V. Leotta, E. Romio, C. Siciliano, A. Liguori, *RSC Adv.*, **2016**, *6*, 34468; d) A. Leggio, E. L. Belsito, R. De Marco, A. Liguori, C. Siciliano, M. Spinella, *J. Chromatogr. A*, **2012**, 1241, 96.
11. a) H. Lundberg, F. Tinnis, N. Selander, H. Adolfsson, *Chem. Soc. Rev.* **2014**, *43*, 2714; b) A. Ojeda-Porrás, D. Gamba-Sánchez, *J. Org. Chem.*, **2016**, *81*, 11548; c) S. Catalano, A. Leggio, I. Barone, R. De Marco, L. Gelsomino; A. Campana, R. Malivindi, S. Panza, C. Giordano, A. Liguori, D. Bonfiglio, A. Liguori, S.

- Andò, *J. Cell. Mol. Med.* **2015**, *19*, 1122; d) M. L. Di Gioia, A. Leggio, A. Liguori, F. Perri, C. Siciliano, M. C. Viscomi, *Amino Acids*, **2010**, *38*, 133.
12. a) H. M. Gaber, M. C. Bagley, Z. A. Muhammada, S. M. Gomha, *RSC Adv.*, **2017**, *7*, 14562.; b) B. Govindh, B. S. Diwakar, Y. L. N. Murthy, *Org. Commun.*, **2012**, *5*, 105; c) V. N. Charushin, N. N. Mochulskaya, A. A. Andreiko, V. I. Filyakova, M. I. Kodess, O. N. Chupakhin, *Tetrahedron Lett.*, **2003**, *44*, 2421; d) D. E. Natalie, S. C. Donna, M. Khurana, N. S. Noha, P. S. James, J. H. Sylvia, N. Abraham, S. T. Robert, A. M. Jacqueline, *Eur. J. Med. Chem.* **2003**, *38*, 49.

Synthesis and Characterization of Large Pore MSU-Type Mesoporous Silica

Nicoletta Garofalo, Alessandra Comandé, Ida Perrotta, Mariano Davoli, Giancarlo Niceforo and Luigi Pasqua

[*Paper 4*]

Published on: *Advanced Science Letters*, 2017, 23, 9:6026-6028.

DOI: 10.1166/asl.2017.9099

Abstract

The syntheses and characterization of mesoporous silica obtained by neutral polyoxiethylene surfactants are reported. Syntheses were carried out according to a previously-reported interfacial approach based on a slow-rate not-catalyzed tetraethylortosilicate (TEOS) hydrolysis but using different organic phases. Synthesis systems are constituted by a two-level biphasic emulsion and mesoporous silica particles grow at the interface of the organic (upper) and the inorganic (lower) regions. The newly-formed particles migrate because of the gravity force to the bottom of the synthesis vessel, far from the upper silica-feeding solution. Typical particle size is at the nanometer scale. Solids with very large mesopores, high pore volume and specific surface SBET up to 400 m²/g are obtained at room temperature starting from synthesis systems not including a mineralizing agent such as H⁺, OH⁻ or F⁻ ions.

8.1. Introduction

Silica-based mesoporous materials have been proposed for several applications such as drug targeting,¹ sampling of peptide mixtures for mass spectrometry,² and enzyme immobilization.³ The regular nanostructure, large surface areas, large void volumes, the high homogeneity in pore diameter and the high versatility of the procedures to modify the external and/or internal silica surface allow to consider these materials as a promising tool for the biomedicine-applied nanotechnology.

Mesoporous macroscale structures were obtained by oil-water interface templating systems at acid pH. TEOS is used as silica source and is hydrolyzed just at the oil-water interface where mesostructures are formed reflecting, on a larger scale, size and shape of the oil spheres because the inorganic materials condense around them. Stirring is one of the mechanism for controlling emulsion properties through modification of long-range hydrodynamic forces. Under slow stirring fiber-type morphologies are predominantly observed while with increasing stirring rate more and more sphere-like particles are formed. The two level by-phase control was also used on a larger scale to produce self-supporting membranes at a static interface between an aqueous and an inorganic phase.⁴

Successively, a method has been described in which mesoporous silica particles of macroscopic dimensions functionalized with organic ligands can be produced from alkaline medium in a one-step emulsion process.⁵ Furthermore, hard mesoporous silica spheres have been described according to a procedure closely related to that initially reported for the synthesis of MCM-41;⁶⁻⁷ the primary difference is that phase separation and emulsion chemistry which result from the hydrophobic nature of tetrabutylorthosilicate and butanol are used in order to create the desired morphology.⁸ More recently, the conditions favoring the formation of mesoporous film over bulk material through the separation of the ingredients into two stratified phases, both in acid and in basic media, have been defined.⁹ Mesoporous materials and functionalized mesoporous materials are obtained from two-level biphasic emulsions. The upper one is an organic phase and contains the silica source; the lower phase is a water or water-ethylene glycol solution of the neutral surfactant. Micelles are feed by the silicon alkoxide, precursor of the inorganic coverage, in the interfacial region and, after condensation, the particles move to the bottom part of the synthesis vessel.¹⁰ In this work

the same approach has been applied employing emulsions with different organic phases with the aim of producing mesoporous silica provided with ultra large porosity for engineering multifunctional devices.

8.2. Materials and methods

The neutral surfactant, named Triton x-100, was used as received by Sigma-Aldrich, Tetraethylortosilicate (Aldrich) was used as silica source. The molar compositions of the synthesis mixtures investigated are shown in Table 1.

Table 1. Molar ratios in two-level biphasic emulsions used for the synthesis of mesoporous materials.

System	Upper Phase				Lower Phase		
	TEOS	Cyclohexane	Decane	Dodecane	Triton 100	x-	H ₂ O
1	1		1.01		0,32		120
2(15 days)	1	1.08			0,32		120
3(10 days)	1	1.08			0,32		120
4	1			1.08	0,32		120

In a typical preparation of a mesoporous silica (Synthesis system for MSN-3) 21,0 g of the surfactant are completely dissolved in 230 g of distilled H₂O at room temperature. A solution of TEOS (22,0 g) in cyclohexane (9,8 g) had slowly run along the vessel wall of the aqueous solution so that the upper organic phase is easily established. The mixture is aged at room temperature for 15 days (MSN-1 and MSN-2) or 10 days (MSN-3 and MSN-4) under slow magnetic stirring. The organic phase is finally removed and the resulting suspension is filtered, washed and dried for 8 hours at 80° C.

Solvent extraction is carried out by refluxing 1,0 g of the as-synthesized mesoporous silica in 600 ml of a 1/1 V/V water-ethanol mixture under stirring for 50 hours at 70°C.

X-Ray powder diffraction patterns were measured on a Bruker D8 Advance diffractometer using Cu-K α radiation (40 Kv, 20 mA) over the range $0.5 < 2\theta < 10$. The N₂ adsorption-desorption volumetric isotherms at 77 K were measured on a Micromeritics Asap 2010 apparatus. Samples were pre-treated under vacuum at 573 K to a residual pressure of 2 μ m Hg. Surface area of the samples was calculated by BET linearization in the pressure range 0.05 to 0.2 P/P₀. Lattice pore volume was obtained from the amount of nitrogen gas adsorbed at the top of the rising section of the isotherms of type I or IV. The amount of surfactant was measured by TG analysis. The measurements were carried out with a Netzsch STA 409 instrument between 20 °C and 850 °C at a ramp of 10 °C/min in air with a flow rate of 10 ml/min. SEM micrographs were collected by a Field Emission Scanning Electron Microscope (FESEM) mod. Quanta 200F - FEI Company while TEM images were obtained on JEM-1400 PLUS (JEOL Ltd./Japan) operating at 80 kV accelerating voltage.

8.3. Results and Discussion

In this work cyclohexane, decane and dodecane have been used as organic phases. The upper organic phase dissolves the silica source while the lower inorganic phase contains the surfactant so that the composite material is assembled in the interfacial region.

The particle growth process stops when silica particles move by sedimentation to the bottom of the synthesis vessel far from the upper organic silica-feeding solution. Table 2 shows the reticular plane distance d-spacing values, d_0 , for as-made samples, d_{0ex} , for extracted samples (from XRD analysis), specific surface areas S_{BET} , pore volume and organic content data of obtained mesoporous silica samples.

Table 2. d-spacing values, d_0 , for as-made samples, d_{0ex} for extracted samples (from XRD analysis), specific surface areas S_{BET} and pore volume of obtained mesoporous silica samples.

System	d_o (Å)	d_{0ex} (Å)	S_{BET}	Pore Volume	Organic/SiO ₂ +Organic %
	As made	Extracted	(m ² /g)	(0,95 P/P ₀ , cm ³ /g)	nic % mass ratio
1	120.8-98.3				44,7
2	119.4-97.9				58.1
3	125.9-99.5	125.1-100	376	0.88	70,5
4	123.3-99.7	125.0-100.0	355	0,88	62,6

In **Figure 1** X-ray powder diffraction patterns of the different samples are presented. It can be noted that a main reflection is present composed of two reticular plane distance for all the samples that are reported in **Table 2**. Higher order reflections are completely

absent for all the obtained samples as it is usual with MSU-type mesoporous materials.¹¹ Surfactant removal carried out by solvent extraction (see materials and methods) does not induce shift in d_{0ex} position (Table 2). The higher values obtained for d_o and d_{0ex} , if compared with the results presented in ref. 10,

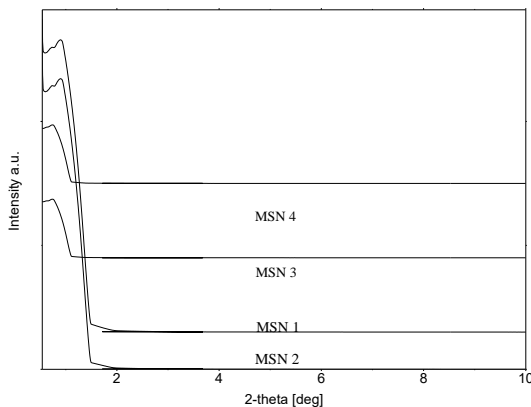


FIGURE 1. X-ray powder diffraction patterns of the different samples obtained.

can be explained with the different ability of the organic phases employed in this work to be included in the cores of the surfactant micelles, so-producing, micelles with very large diameters. Nitrogen adsorption-desorption isotherms have been carried out on samples MSN-3 and MSN-4 (Figure 2). The isotherms, in both cases type IV, present a mesopore-filling step at very high relative pressures. The materials show S_{BET} specific surface around $400 \text{ m}^2/\text{g}$ and high pore volumes up to $0.9 \text{ cm}^3/\text{g}$. BJH adsorption average pore diameters resulted to be 121.5 and 91.0 \AA for samples MSN-3 and MSN-4 respectively that are at the upper limit for MSU-type materials. S_{BET} specific surface area values are lower if compared to the samples obtained in reference 10, this reduction can be explained with the relevant increase of pore diameters. All the samples includes very large organic amounts (Table 2).

In Figure 3 Scanning Electron (SEM) and Transmission Electron (TEM) micrographs of sample MSN-4 are shown. SEM micrograph shows particles not larger than 300 nm in the form of aggregates while in TEM micrograph a single particle is observed. It presents the typical worm-like porosity obtained with neutral surfactant (not easily observable at this magnification) and it is comparable, in size, with the black bar (200 nm).

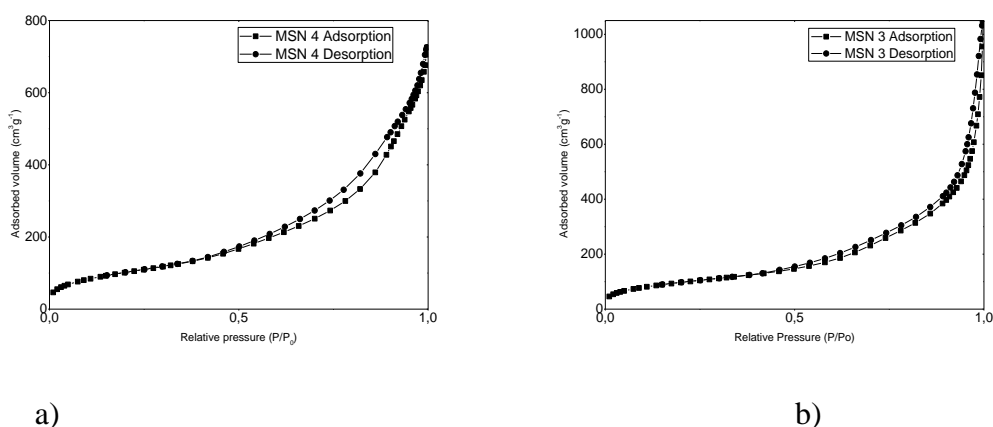


FIGURE 2. Nitrogen adsorption-desorption isotherms acquired on sample MSN-3 a) and MSN-4 b)

It presents the typical worm-like porosity obtained with neutral surfactant (not easily observable at this magnification) and it is comparable, in size, with the black bar (200 nm).

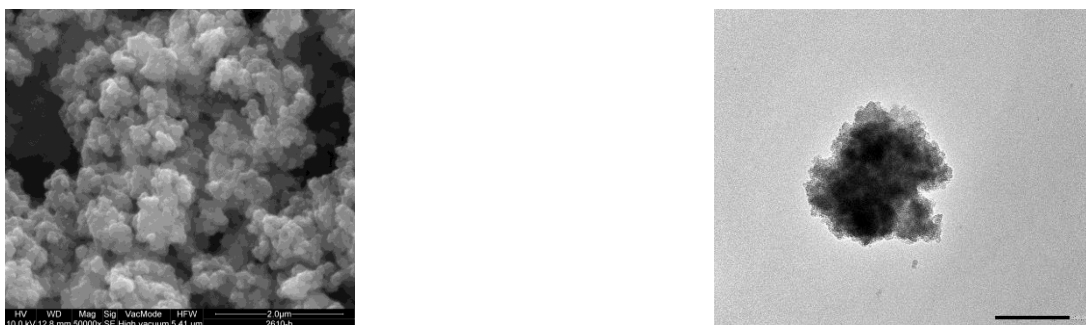


FIGURE 3. SEM a) and TEM b) micrographs of sample MSN-4.

8.4. Conclusions

In conclusion, emulsions with cyclohexane, decane and dodecane have been employed in the synthesis of mesoporous silica provided with ultra large porosity producing materials potentially useful in the engineering multifunctional devices.

References

1. C. Ceresa, G. Nicolini, R. Rigolio, M. Bossi, L. Pasqua and G. Cavaletti, *Curr. Med. Chem.*, **2013**, *20*, 2589-2600.
2. R. Terracciano, F. Casadonte, L. Pasqua, P. Candeloro, E. Di Fabrizio and A. Urbani, *Talanta*, **2010**, *80*, 1532-1538.
3. F. Casadonte, F. Casadonte, L. Pasqua, R. Savino and R. Terracciano, *Chem. Eur. J.*, **2010**, *16*, 8998-9001.
4. S. Schacht, Q. Huo, I.G. Voigt-Martin, G.D. Stucky and F. Schuth, *Science*, **1996**, *273*, 768-771.
5. R.I. Nooney, M. Kalyanaraman, G. Kennedy and E.J. Magin, *Langmuir*, **2001**, *17*, 528-533.
6. C. T. Kresge, M.E. Leonowicz, W.J. Roth, J. C Vartuli and J. S. Beck, *Nature*, **1992**, *359*, 710-712.
7. J.S. Beck, J.C. Vartuli, W.J. Roth, M.E. Leonowicz, C.T. Kresge, K.D. Schmitt, C.T. W. Chu, D.H. Olson, E.W. Sheppard, S.B. McCullen, J.B. Higgins, J.L. Schenkler, *J. Am. Chem. Soc.*, **1992**, *114*, 10834-10843.
8. Q. Huo, J. Feng, F. Schuth and G.D. Stucky, *Chem. Mater.*, **1997**, *9*, 14-17.
9. L. Faget, A Bergman and O. Regev, *Thin Solid Films*, **2001**, *386*, 6-13.
10. L. Pasqua, F. Testa, R. Aiello, *Stud. Surf. Sci. Catal.*, **2005**, *158*, 557-564.
11. C. Morelli, P. Maris, D. Sisci, E. Perrotta, E. Brunelli, I. Perrotta, M.L. Panno, A. Tagarelli, C. Versace, M.F. Casula, F. Testa, S. Andò, J. B. Nagy, L. Pasqua, *Nanoscale*, **2011**, *3*, 3198-3207.

Mesoporous silica-based nanocarriers for pH-triggered doxorubicin delivery in cancer therapy

[Ongoing work 4]

Abstract

The major limitations of antineoplastic drugs are poor bioavailability, high-dose requirements, the development of drug resistance, and adverse side effects induced by the lack of selectivity.

In this regard, the main effort of pharmaceutical research is to obtain a therapeutic strategy that addresses these drawbacks by developing drug delivery systems (DDS), that can selectively release the drug to cancer tissues avoiding normal cells.

Recently, several nanocarriers based on organic (liposomes, polymers) and inorganic (gold and silica nanoparticles) platforms have been developed as promising candidates for drug delivery.

Among the inorganic-based DDS mesoporous silica nanoparticles (MSN) have attracted great attention thanks to their unique structural characteristics such as high surface area, tunable pore diameter, easy surface modification and biocompatibility, which make them widely exploited in the biotechnological and biomedical field.

Furthermore, the abundant silanol groups (Si–OH) present in their surfaces facilitate post-synthesis modification, and allow to design versatile DDS able to host various therapeutics agents and to conjugate, on the outer MSNs surface, targeting ligands that interact selectively with specific receptors overexpressed in cancer cells.

The drugs can be adsorbed or covalently linked inside the pores of the particles through cleavable bonds and then released under specific conditions.¹

In this work, the design and synthesis of MSN-based anticancer prodrug systems for active targeting delivery of doxorubicin is described.

Doxorubicin is an antineoplastic drug clinically used in different types of malignancies but with serious limitations due to undesired systemic toxicity.

The target was the development of devices having stimuli-responsive properties and able to release the drug, exploiting the pH difference between the circulatory stream and the tumor intracellular microenvironment.

The MSN-based devices, FOL-MSN-DOXO, consist of nanometric silica frame that presents, folic acid (FOL) covalently linked to the external surface of particles as targeting function (folate receptor specific ligand) and doxorubicin (DOXO) linked within the pores by means of imine or hydrazone acid-labile bonds.

For our purpose, we have used folic acid as targeting molecule to mediate specific uptake by cancer cells.

In the present study, our aim was to design, synthesize FOL-MSN-DOXO conjugates, evaluate their cytotoxic effect in vitro and understand the structure-biological activity relationship of the obtained systems, with the intention of creating effective DOXO delivery systems as chemotherapeutics for tumor targeting.

The developed systems will constitute a model for the development of similar devices for the delivery of DOXO in which the targeting function is a peptide molecule that is tailored toward specific receptors, which are overexpressed or exclusively expressed in cancer cells and that recognize tumors with high specificity.

9.1. Introduction

Anthracyclines are an important class of chemotherapeutic agents used in the treatment of various malignancies such as Lymphoma and Leukaemia,² furthermore, they represent a cornerstone in early and metastatic breast cancer treatment.^{3,4}

Doxorubicin and Daunomycin have been the firsts Anthracyclines drugs discovered in the early 1960s from *Streptomyces peucetius* and being drugs with a wide-spectrum of action they continue to attract considerable interest in today pharmaceutical research field.^{5,6}

Doxorubicin (DOXO), and in general anthracyclines, perform their cytotoxic action through different proposed mechanisms i.e. by inhibiting Topoisomerase II (enzyme involved in DNA repair), acting as a DNA intercalating agent and generating free radicals.^{7,8} However, doxorubicin therapy is also associated with serious adverse effects such as cardiomyopathy, myelosuppression and other effects on the gastrointestinal tract.⁹⁻¹³

The mechanism by which DOXO causes cardiotoxicity has not been well clarified. Initially, the main cause of this side effect was attributed to reactive oxygen species generation.¹⁴ Recently, however, the hypothesis of an involvement of Topoisomerase II present in cardiac tissues seems to take hold.¹⁵ Noteworthy is that cardiotoxicity level is also related to the age of the patient, the heart state of health and above all to the drug dosage received.¹⁵

Considering the therapeutic importance of anthracyclines, various approaches have been proposed to limit cardiotoxicity.^{16,17}

The use of carrier systems e.g. polymeric nanoparticles, liposomes, micelles and more able to control DOXO release and lower down the administered dose represents an important approach to overcome these limits.¹⁸⁻²⁰

In the last few years among drug delivery systems, mesoporous silica-based nanoparticles (MSNs) have gained considerable interest thanks to their attractive structural and morphological properties. Furthermore, due to their biocompatibility and the presence on their surfaces of silanol groups (SiOH) that can be appropriately functionalized, they have been extensively investigated for therapeutic and diagnostic purposes, especially in oncology.²¹⁻²⁵

Nowadays, several delivery systems for DOXO based on mesoporous silica nanoparticles have been developed. M. Martinez-Carmona *et al.* 2015 have designed a nanocarrier with Transferrin (Tf) molecules anchored through a UV-sensitive cross-linker on the surface of Doxorubicin (DOXO)-loaded MSNs.²⁶

In order to improve the selectivity of the system and the cytotoxicity of DOXO has been also synthesized MSNs conjugated with cRGD peptide and loaded with the antineoplastic drug.²⁷ Another interesting device are the magnetic nanocarriers DOX-conjugated (MMCNCs-DOX) and stabilized by polysaccharose (agarose) with a facile solvothermal method, that exhibited the pH-sensitive behavior (targeted drug release in tumor cells) and the ability to be driven externally through magnetic manipulation.²⁸

As part of our research activity, smart mesoporous silica nanostructured devices, able to overcome the main limitations currently associated with conventional antineoplastic agents, have been developed.

Specifically, these systems present a targeting molecule (ligand) on the outer surface able to target, bind and penetrate cells that express the specific receptor for the ligand and an anticancer drug conjugated to the pore walls, through a pH-sensitive bond, that is stable at physiological pH but that it can be hydrolyzed at slightly acid pHs.²⁹⁻³⁴

In such a way, the drug is protected inside the nanocarrier during the plasmatic distribution, until when it enters the target cells, where it leaves the system because of the lower pH of the intracellular compartments and it can exert its effects on the cells.

Folic acid was chosen as targeting function since its use as tumour-homing agent is widespread recognised.³⁵

This essential vitamin has a high affinity for folate receptor (FR), a tumour associated anchored protein which is expressed at high to moderate levels in a large number of tumours³⁶ while it occurs at very low levels in most normal tissues and that can actively internalize folates and folate conjugated compounds via receptor-mediated endocytosis.³⁷

The anticancer drug doxorubicin was conjugated to the nanoparticles through a carboxylic hydrazone linker or by means the formation of an imine bond both cleavable under acidic conditions.

The obtained MSN-based conjugates have been characterized by FT-IR spectroscopy, powder X-ray diffraction, thermogravimetric analysis (TGA).

The effect of FOL-MSN-DOXO prototypes on cell proliferation was evaluated on FR+ and FR- cell lines aimed at obtaining informations regarding their cytotoxic activity.

9.2. Results and Discussion

We designed and constructed pH-sensitive mesoporous silica nanocarriers with diverse functional components, such as tumor-targeting unit to mediate specific uptake by cancer cells, and pH-sensitive linkers to get the acid-responsive drug release at the desired site. In the present work, drug doxorubicin (DOX)-loaded MSN-based systems were developed using MSU-Type Mesoporous Silica nanoparticles.

The MSU-type MSNs were obtained by using an interfacial synthesis procedure at room temperature (RT), introducing cyclohexane as the organic phase in which TEOS is dissolved, that we developed to obtain large pore nanoparticles (*Paper 5*).³² Specifically, the cyclohexane usage as a solvent has led to the formation of micelles with a wider diameter. The micelles acting as a templating agent for the mesostructured material formation led to the synthesis of MSNs with a large pore diameter (the BJH adsorption average pore diameter was 121.5 Å). The synthesized MS particles have an average diameter between 100 and 200 nm as shown in the SEM image (**Figure 1**).

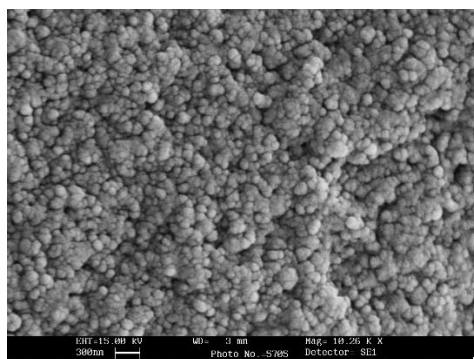


Figure 1 Electron scanning microscopy (SEM)

This structural feature has made these nanoparticles the ideal carriers for the binding of drugs within the pores.

Furthermore, to prevent a dramatic pore volume reduction in the final systems, the obtained materials were externally functionalized before surfactant extraction to preferentially address the siloxane modifying agent on the external surface of the particles. In this way, a considerable pore volume is recovered after surfactant extraction and folic acid targeting molecule is anchored preferentially on the external surface since allowing a consistent drug loading.

An important feature for a stimuli-responsive device is to respond with physicochemical changes to specific stimuli such as pH gradients, different temperatures, magnetic field etc.³⁸

In physiological and pathological states is present a pH gradient among subcellular organelles, organs, and human tissues,³⁹ the pH of normal tissues and blood is approximately 7.4, while the pH value is lower in the tumor microenvironment such as in the endosomal (pH = 5.9-5.5) and lysosomal (pH<5) compartments.⁴⁰

These aspects can be exploited to create systems that allow the anticancer drug release only after the system is internalized by cells through endocytosis. To achieve this goal, in these systems the drug should be conjugated to the nanoparticles by means a bond that is stable at physiological pH and easily cleavable inside the endosomal compartments where the pH is slightly acid. To this aim, a widely used procedure in the design of DDS is to anchor the drug to the vehicle by means acid-sensitive bonds.

It is largely reported the use of acid-sensitive acetals,⁴¹⁻⁴² imines,⁴³⁻⁴⁵ hydrazones⁴⁶⁻⁴⁸ or ortho-ester linkers⁴⁹ that could be stable at physiological pH (pH 7.4) but degraded effectively at the lower pH of endosomes and lysosomes (pH 4.5-6) to release drug.

The silanol groups (Si-OH) present on the inner surface of the nanoparticles can be suitably derivatized in order to bind Doxorubicin covalently. It is interesting to note that Doxorubicin presents, in its structure, different groups (carbonyl, hydroxyl and amine functions) that can be exploited for the formation of acid-sensitive bonds (**Figure 2**).

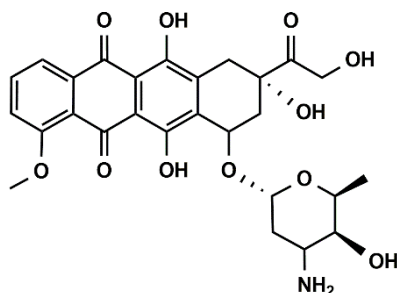


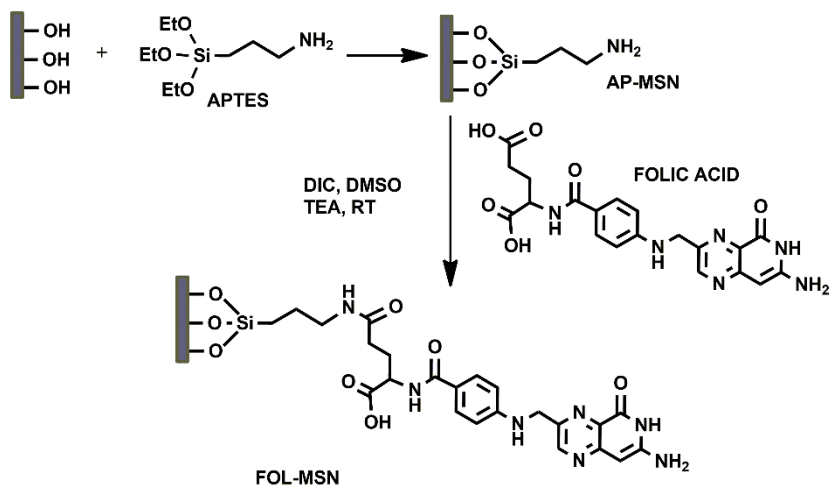
Figure 2. Doxorubicin structure

To our aims, we focused on the formation of imine and hydrazone linkages therefore the inner pore walls of nanoparticles were decorated with different chemical functionalities to incorporate doxorubicin through imine or hydrazone bonds.

9.2.1. MSNs conjugated with DOXO via pH-sensitive imine bond.

Firstly, the targeting ligand folic acid was covalently attached to the MSNs external surface through amide bond formation between the amino group of AP-MSN and folic acid using DIC as condensing agent (Scheme 1). Then, after removal of templating agent from the pores, the nanoparticles were functionalized with 3-aminopropyltrimethoxysilane (APTES) to afford the amine functionalized mesoporous silica nanoparticles (FOL-MSN-AP_{in}) that were recovered by filtration and analyzed by thermogravimetric analysis and FT-IR spectroscopy.

Thermogravimetric analysis of the sample before and after functionalization with APTES shows an increment of the organic compound mass on the sample by 6.53%.



Scheme 1 Synthesis of FOL-MSN

The anticancer drug DOXO was conjugated to the nanoparticles through an imine bond thus the MSN-based targeted prodrug (FOL-MSN-IM-DOXO) was obtained.

The formation of imine bond occurs between the carbonyl group of hydroxymethyl ketone side chain at C-9 of doxorubicin and the amino functions present on the inner pore walls of the nanoparticles (**Figure 3**).

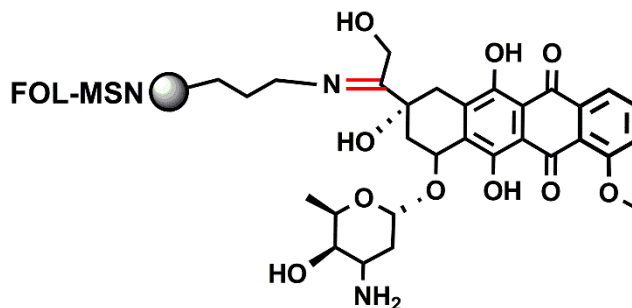


Figure 3. FOL-MSN-IM-DOXO system

The obtained intense red colored FOL-MSN-IM-DOXO powder was exhaustively washed with solvent, dried and then characterized by FT-IR spectroscopy (**Figure 4**) and Thermogravimetric analysis.

In the IR spectrum of FOL-MSN-IM-DOXO the absorbance bands related to the C = N group of hydrazone and those characteristics of the amide bonds overlap at 1640 cm^{-1} and at about 1540 cm^{-1} , while the characteristic peaks at 1725 , 1607 and 1580 cm^{-1} are assigned to quinone and ketone carbonyl groups of doxorubicin molecule.⁵⁰

Some additional absorption bands are observed in the range of $800\text{-}700\text{ cm}^{-1}$ corresponding to the primary amine NH₂ wagging and N-H deformation bonds from DOXO. These observations confirm the loading of DOX to the nanocarrier.

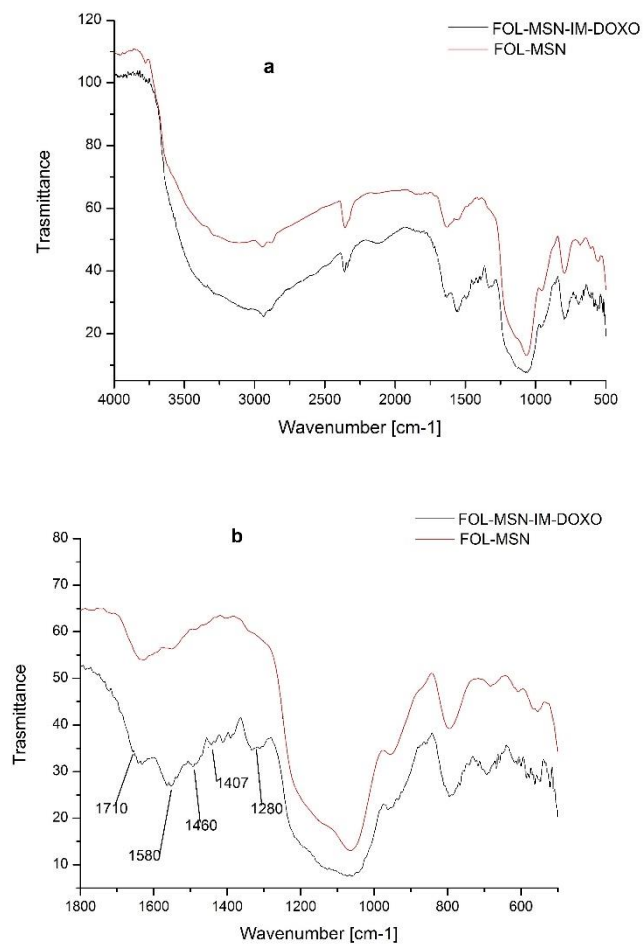


Figure 4. a) FT-IR spectra of **FOL-MSN** and **FOL-MSN-IM-DOXO**, b) magnification of a) between 1800 and 550 cm^{-1} .

In addition, the cytotoxicities of the FOL-MSN-IM-DOXO, FOL-MSN nanoparticles and free-DOXO were investigated *in vitro* and compared using HeLa cervical cancer cells (FR +), RPMI-8226 human multiple myeloma cells (FR+) and human normal fibroblast BJhTERT (FR-) (**Figure 5**).

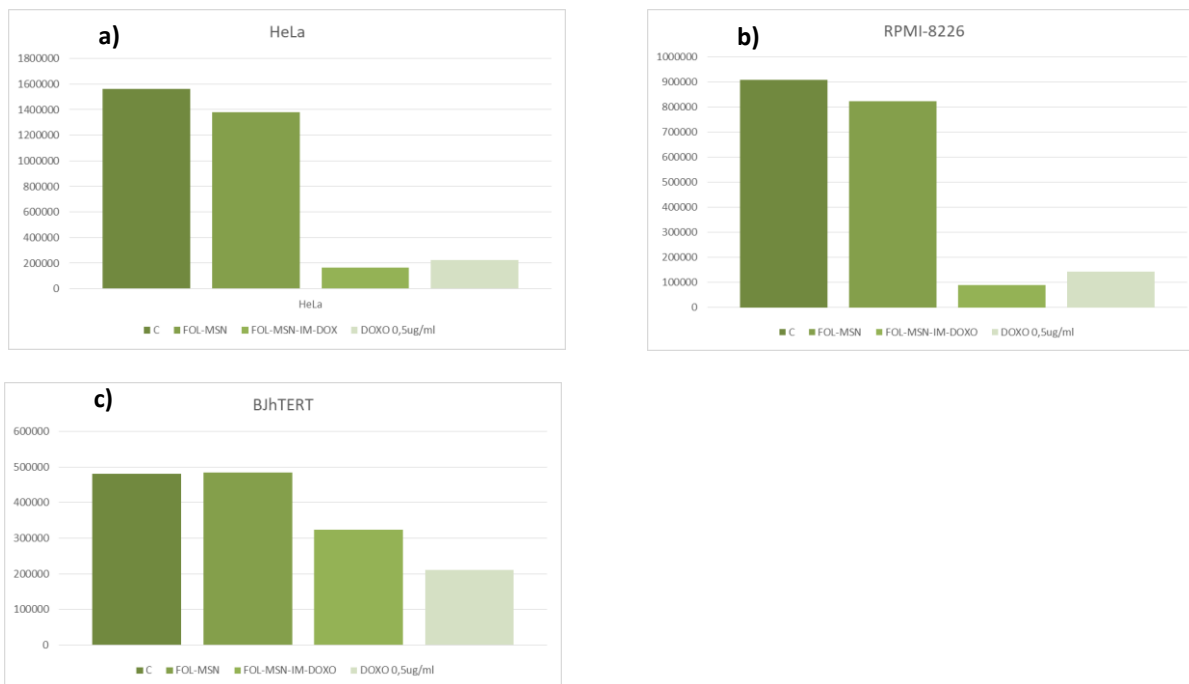


Figure 5. Growth curves of **a)** cancerous FR+ HeLa, **b)** cancerous FR+ RPMI-8626 human myeloma cells, **c)** Normal FR- BJhTERT cells treated with FOL-MSN-IM-DOXO, FOL-MSN and free-DOXO; C = control

Normal FR- BJhTERT cells, cancerous FR+ RPMI cells and cancerous FR+ HeLa, were left untreated (C= control) or treated for 1h with FOL-MSN-IM-DOXO, FOL-MSN and with an equivalent concentration of free-DOX. Free-DOXO was used as positive control. Cell viability has been evaluated after 1, 2 or 3 days after treatment.

Figure 5a and **5b** shows how FOL-MSN-IM-DOXO significantly reduced the viability in HeLa and RPMI-8226 cells respectively. The cytotoxicity of the sample is comparable to that determined by the free DOX. However, FOL-MSN-IM-DOXO showed some toxicity even on normal FR- BJhTERT cells (**Fig. 5c**). FOL-MSN system was also tested to demonstrate the biocompatibility of the device.

The detected toxicity of FOL-MSN-IM-DOXO on FR- BJhTERT cells is probably due to the premature release of the drug at neutral pH without cellular uptake. Therefore the imine bond between DOXO and nanoparticles could be unstable at pH 7 and result in undesired drug leakage and cell toxicity.

While certain types of imine bonds are known to be stable at pH 7.4 and degrade at low pH (i.e., < 6.0), chemistries adjacent to both hydrazine and ketone functionality can

greatly affect pH and hydrolytic stability. Hence, imine bonds can present different bond cleavage rates and pH sensitivities.

In light of these results, we performed DOXO in vitro release studies at different pH values in order to investigate the stability of the imine linker.

9.2.1.1. In vitro DOXO release tests

The system FOL-MSN-IM-DOXO was incubated in phosphate or acetate buffer (pH 7.4 and 5.0, respectively), to verify its stability at physiological pH (pH 7.4) and evaluate the release of the drug at endolysosomal compartment pH (pH ~ 5) (**Figure 6**).

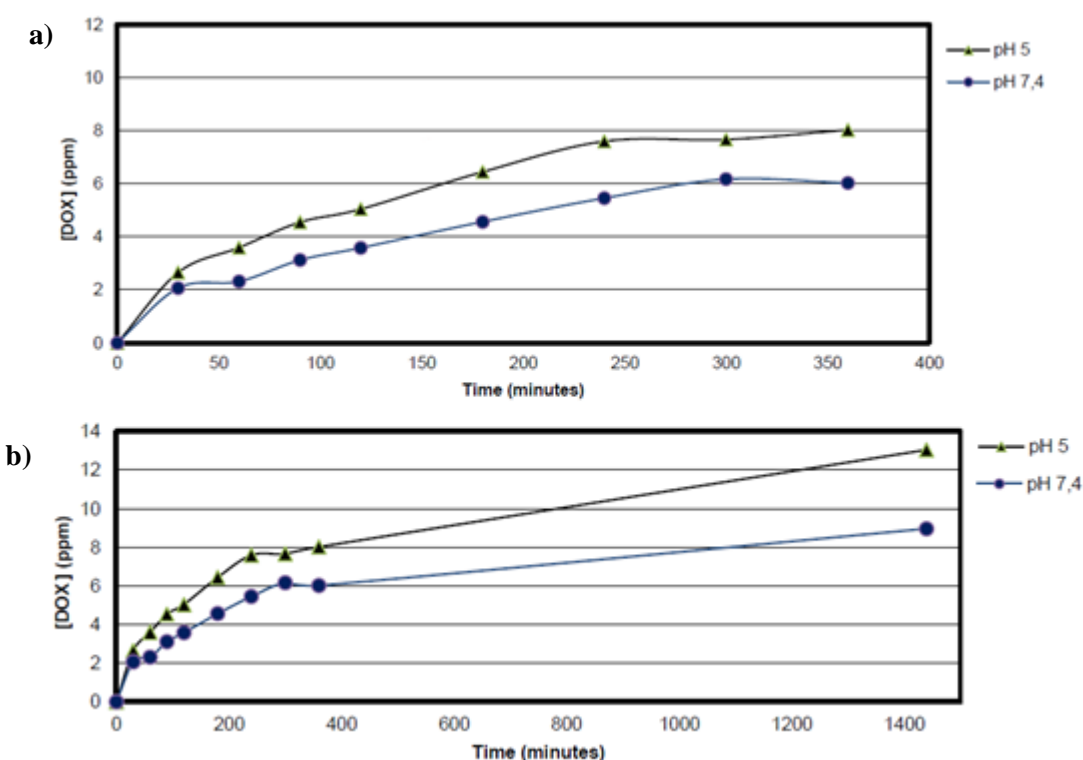


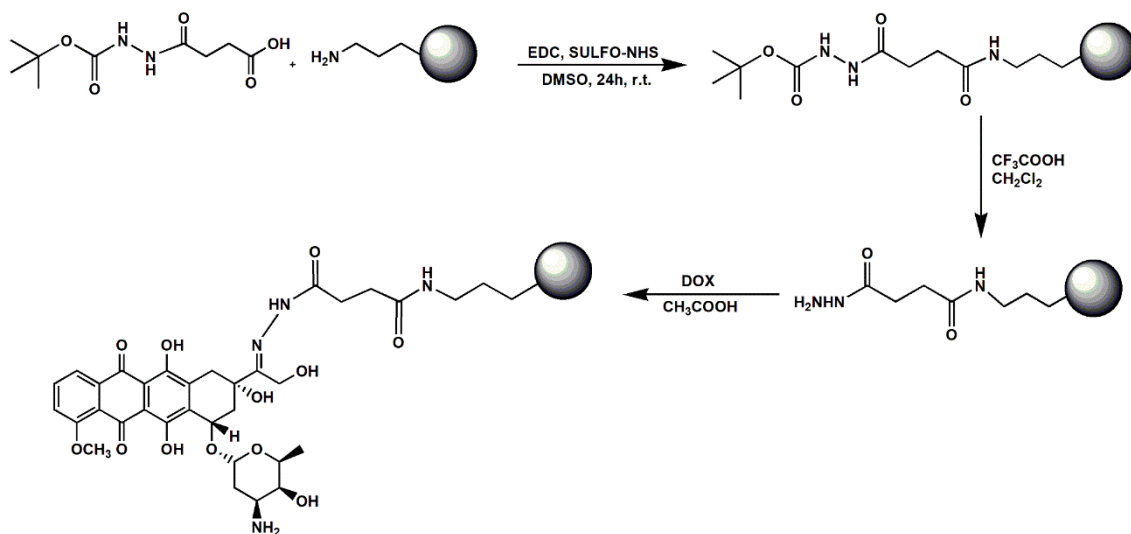
Figure 6. Doxorubicin release at pH=5 and 7.4. **a)** Drug release profile within 6 hours **b)** Drug release profile within 24 hours.

DOXO release profile from the carrier (Figure 5) shows a linear and gradual trend over time. The release is higher at pH =5 and this demonstrates that the imine bond between Doxorubicin and FOL-MSNs undergoes hydrolysis preferably at acid pH values. However, although the released amount is lower, some not negligible release occurred even at pH=7.4. This result indicates that the designed imine bond is not sufficiently stable at neutral pH, and justify

es the toxicity observed on FR- BJhTERT cells.

9.2.2. MSNs conjugated with DOXO via pH-sensitive hydrazone bond.

The applied synthetic route for obtaining FOL-MSN-HYD-DOXO is shown in **Scheme 2**. The antineoplastic drug DOXO was conjugated to the pores of nanoparticles by condensation of DOXO side chain carbonyl group with the hydrazide linker anchored to MSNs. To incorporate the hydrazine group on the pore surface, a linker molecule (*N*-Boc succinic acid monohydrazide) was synthesized and anchored to the MSNs through an amide bond.



Scheme 2. Synthesis of FOL-MSN-HYD-DOXO

After removal of Boc group from the hydrazide function with trifluoroacetic acid, doxorubicin was covalently linked to the particles via hydrazone bond (Scheme 2).

FOL-MSN-AP_{in}, FOL-MSN-HYD and FOL-MSN-HYD-DOXO samples were analysed by XRD (**Figure 7**). The XRD analysis shows how the presence of new chemical species within the pores attenuates the intensity of the diffraction.⁵¹ Therefore with the progression of the pore filling the interference is increasing. All samples show ample single reflection due to the lack of long-range crystalline order.

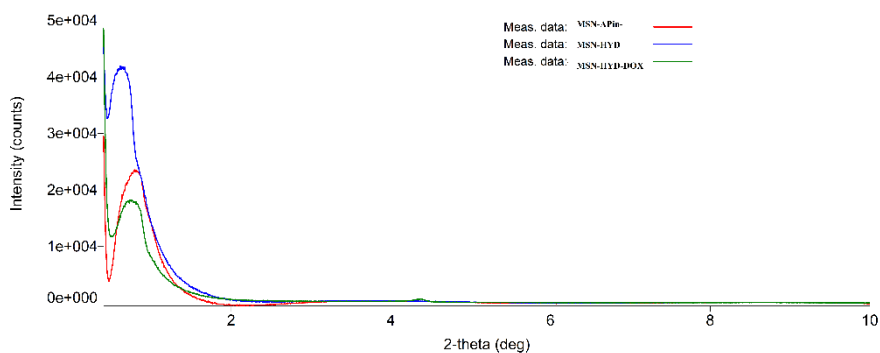


Figure 7. XRD analysis with an overlay of MSN-AP_{in}, MSN-HYD and MSN-HYD-DOXO samples.

FT-IR spectra of pure DOXO and FOL-MSN-HYD-DOXO are shown in Figure 8b while FT-IR spectra of the precursors FOL-MSN-AP_{in} and FOL-MSN-HYD are reported in Figure 8b.

In the IR spectrum of FOL-MSN-HYD-DOXO is possible to observe some of the typical bands of Doxorubicin, which demonstrate the nanoparticle drug loading. In FOL-MSN-HYD-DOXO spectrum (Figure 8b) the bands at 3524 cm⁻¹ and 3327 cm⁻¹ assigned to the stretching vibration of OH and NH₂ groups of DOXO are evident, furthermore, in the spectral range 3100–2900 cm⁻¹, are present new absorption bands respect to the spectrum of the precursor FOL-MSN-HYD (Fig. 8a) that correspond to the stretching of aromatic and aliphatic C-H bonds. In the spectral range 1700-1500 cm⁻¹, the band ascribable to the hydrazone stretching vibration overlaps with the absorption peaks corresponding to the stretching vibrations of amide and ketone carbonyl groups of the different chemical entities conjugated to the carrier. The loading of DOXO was also confirmed by the appearance, in FT-IR spectrum of FOL-MSN-HYD-DOXO (Fig. 8b), of a new absorption band at about 830 cm⁻¹, ascribable to the out-of-plane bending of aromatic C-H bonds.

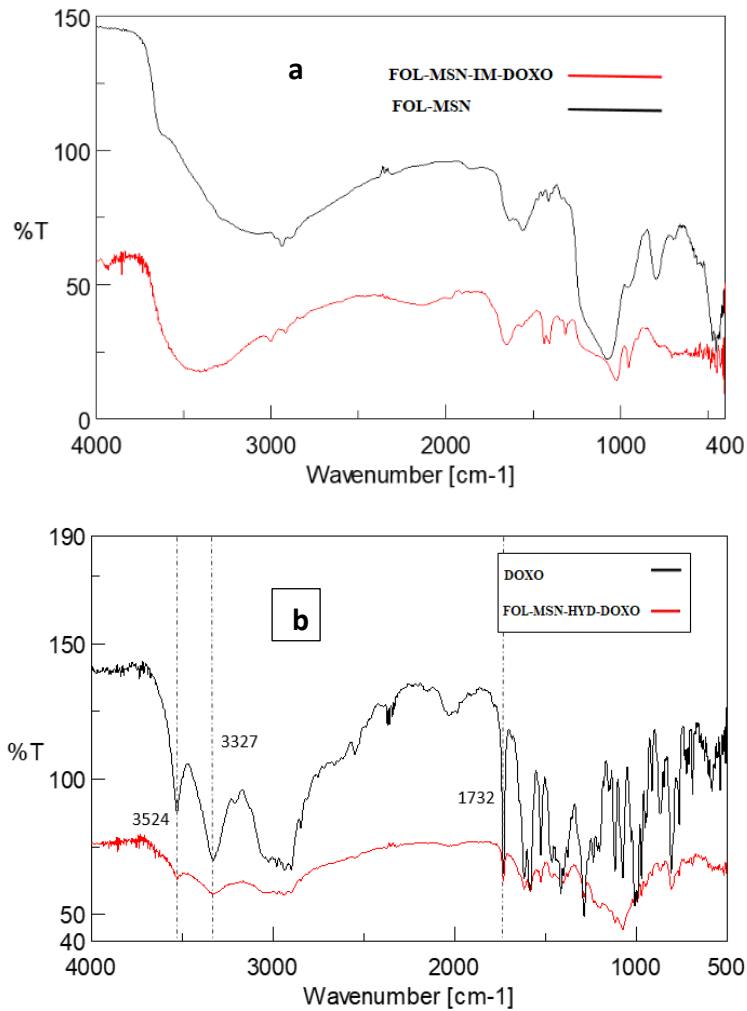


Figure 8. FT-IR spectra of a) FOL-MSN-AP_{in}, FOL-MSN-HYD, b) FOL-MSN-HYD-DOXO and DOXO

The effect of MSN-HYD-DOXO nanoparticles on cell proliferation was evaluated on normal FR- BJhTERT cells and cancerous FR+ HeLa cells (**Figure 9**). Cells have been treated with FOL-MSN-DOXO, left untreated (C=control), FOL-MSN (used as negative control) and the free drug DOXO (positive control).

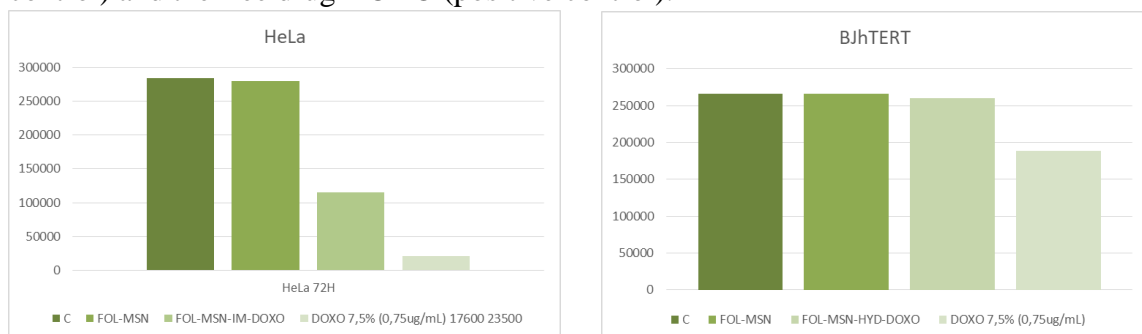


Figure 9. Growth curves of a) cancerous FR+ HeLa, b) Normal FR- BJhTERT cells treated with FOL-MSN-HYD-DOXO, FOL-MSN and free-DOXO; C = control

FOL-MSN-HYD-DOXO nanoparticles cause significant cell death only in HeLa cervical cancer cells (FR+ cells) (Figure 8a) but not in FR- normal cells (Figure 9b).

Furthermore, the device bearing the receptor-specific ligand folic acid (FOL-MSN) is not cytotoxic.

Compared to the antineoplastic drug doxorubicin alone (DOXO), MSN with folic acid (FOL-MSN) and DOXO (FOL-MSN-DOXO), induce death only in cancer cells expressing folate receptor (FR), but not in normal cells (FR-). This means that, when doxorubicin is conjugated to MSNs, drug toxicity on healthy cells is almost completely abrogated.

9.3. Experimental

9.3.1. Materials and experimental details

Triton X-100, neutral polyoxyethylene(10) octylphenyl ether, tetraethylorthosilicate (TEOS), (3-aminopropyl)-triethoxysilane (APTES), Folic acid (FOL), Diisopropylcarbodiimide (DIC) Doxorubicin hydrochloride European Pharmacopoeia (EP) Reference Standard, Tert-butyl carbazate, 1-ethyl-3-(3-dimethylaminopropyl)carbodiimide hydrochloride (EDC), N-Hydroxysulfosuccinimide sodium salt (sulfo-NHS), succinic anhydride, 4-dimethylamino pyridine (DMAP), water (HPLC grade), Acetone (HPLC grade) were purchased from Sigma Aldrich. Ethanol, Diethyl ether, 1,4-Dioxan, Dimethylformamide (DMF), Tetrahydrofuran (THF), trifluoroacetic acid (TFA), Acetic Acid from VWR. Dimethyl sulfoxide (DMSO) and Cyclohexane from Merck and Triethylamine from Carlo Erba. Solvents were purified according to well-known laboratory methods and freshly distilled prior to use. Ultrapure water was distilled with the MilliQ® water, Millipore. Triethoxysilylbutyraldehyde, tech-90 was purchased from Gelest, Inc.

Fourier transform infrared (FTIR) spectra were recorded with an infrared spectrometer (FT/IR-4600 FT-IR, Jasco; Germany). The ordered mesoporous framework of the synthesized materials was studied by small angle powder X-ray diffraction (XRD) on a MiniFlex 600 Rigaku diffractometer operating at 40 kV and 15 mA, employing Ni b-filtered Cu K α radiation in the 2θ range of 0.3–10° with a scan speed of 0.3 deg per min. The TG analysis were carried out with a Netzsch STA 409 instrument between 20 °C and 850 °C at a ramp of 10 °C/min in air with a flow rate of 10 ml/min. Doxorubicin amount was determined using a 300 UV-Vis Evolution, Thermo Fisher Scientific.

¹H and ¹³C NMR spectra were recorded on a Bruker Avance 300 instrument at 300 MHz and 75 MHz, respectively. Spectroscopic analysis was performed at 293 K on diluted solutions of each compound by using CDCl₃ as the solvent. Chemical shifts (δ) are reported in ppm. Coupling constants (J) are reported in Hertz (Hz).

GC-MS analyses were performed with a DB-35MS (20 m \times 0.18 mm, 35% Phenyl 65% dimethylpolysiloxane) capillary column. The mass detector was operated in the electron impact ionization mode (EI/MS) with an electron energy of 70 eV. The injection port was

heated to 250 °C. The oven temperature program was initially set at 70 °C with a hold of 2 min and ramped to 280 °C at 20 °C min⁻¹ with a hold of 10 min.

9.3.2. General synthesis of Folic acid-targeted MSNs (FOL-MSN)

9.3.2.1. Synthesis of Mesoporous Silica Nanoparticles (MSNs)

MSU-type MSNs were synthesized through an assembly mechanism at neutral pH of non-ionic poly(ethylene oxide)-based surfactants and silica sources we developed (*Paper 5*).³² The surfactant Triton X-100 (21 g) was dissolved in ultrapure water (230 g) in about four hours at room temperature. In order to create two phases, along the vessel it was slowly added a solution of TEOS (22 g) in cyclohexane (9.8 g) (molar composition TEOS: Cyclohexane: Triton X-100: H₂O 1: 1.08: 0.32: 120).

The synthesis was carried out at room temperature and aged for 15 days. The upper phase was removed and the resulting precipitate was collected by filtration and washed three times with ultrapure water. Finally, the sample was dried in the oven at 70 °C for 24 h thus a white powder was obtained.

9.3.2.2. Synthesis of AP-MSN

The external surface of the nanoparticles was functionalized with aminopropyl groups necessary for the subsequent reaction. For the purpose, (3-aminopropyl)-triethoxysilane (APTES) was used as the hybrid silica source.

In a typical preparation, a solution of APTES (19.46 g) in ethanol (34 ml) was added to a dispersion of MSNs (8 g) in ethanol (28,57 ml). The synthesis was left under stirring at room temperature for 2 days.

The resulting suspension was filtered and washed once with ethanol and twice with ultrapure water. The resulting aminopropyl functionalized mesoporous silica nanospheres (AP-MSN) were then placed in oven at 70 °C for 24 hours.

9.3.2.3. Synthesis of FOL-MSN

All the prototypes used for this study were externally functionalized with Folic acid.

For FOL-MSN preparation Folic acid (0.60 g, 1,35 mmol) was completely dissolved in DMSO (15 mL). After that, triethylamine (0.301 mL, 2,16 mmol) and **AP-MSN** (4.3 g) were added.

The amide bond formation between the folic acid carboxylic group and the amine groups on the nanoparticles was carried out adding of DIC (0.746 mL, 4,7 mmol).

The so-obtained suspension was stirred at room temperature for 40 hours. Finally, the mixture was filtered and washed with dimethylformamide, dioxane, diethyl ether and ultrapure water (once for every solvent). The resultant yellow powder (6.2 g) was dried and stored in sealed containers protected from light.

Subsequently, the surfactant within the pores was removed by two extractions of 12 h each, using 1 g of material in 0.33 L of ultrapure water at room temperature.

The number of extractions to perform to reach a complete surfactant removal was established by monitoring (TG analysis) the total mass loss of little amounts of samples subjected to additional extraction steps, until a constant value was reached.

Then, the solution of the last extraction was filtered, and the obtained nanoparticles **FOL-MSN** were washed with 1,4-dioxane and dried at 45 °C overnight.

9.3.3. Synthesis of MSNs conjugated with DOXO via pH-sensitive imine bond (FOL-MSN-IM-DOXO)

9.3.3.1. Synthesis of MSN-AP_{in} (inner surface functionalization)

The inner pores of **FOL-MSN** were functionalized with APTES in order to decorate the walls with amino functions useful to anchor the drug to MSNs by an imine bond.

FOL-MSN (0.70 g) was dissolved in 1,4-dioxane (20 mL) and then APTES (1.54 g) was added. After 18 hours under stirring the suspension was filtered and the solid washed with 1,4-dioxane and tetrahydrofuran (THF). The nanoparticles (**MSN-AP_{in}**) were dried at 45°C overnight.

9.3.3.2. Synthesis of FOL-MSN-IM-DOXO

For FOL-MSN-DOXO preparation doxorubicin was loaded using a MSN: DOXO ratio of 1:1.5 on the base of the aminopropyl amount determined by TGA analysis. The reaction was carried out under an inert atmosphere.

Doxorubicin Hydrochloride (0.060 g) was dissolved in anhydrous THF (20 mL) then, **FOL-MSN-AP_{in}** (0.260 g) was added and the pH was adjusted to pH~5 with acetic acid. The reaction proceeded for 24 hours at room temperature and then the nanoparticles were filtered and washed with anhydrous THF. The obtained red solid was suspended again in 10 mL of anhydrous THF and a second drug loading was carried out in order to maximize DOXO interaction with mesoporous silica. The second loading step was performed under the same operating conditions of the first one.

After 24 hours, the reaction was filtered and washed plenty with anhydrous THF and CH₂Cl₂. The red powder (**FOL-MSN-DOXO**) was stored at -20 °C, under an inert atmosphere and protected from light. The amount of DOXO loaded (5 %) was quantified by UV-VIS ($\lambda_{\text{abs}} = 485 \text{ nm}$).

9.3.4 Synthesis of MSNs conjugated with DOXO via pH-sensitive hydrazone bond (FOL-MSN-HYD-DOXO)

The starting system for the synthesis of this prototype consists of MSNs decorated on the external surface with folic acid and functionalized on the pore walls with aminopropyl groups (**FOL-MSN-AP_{in}**).

The synthesis of **FOL-MSN-AP_{in}** was carried out according to the procedures above described.

9.3.4.1. Synthesis of N-tert-butyloxycarbonyl-succinic acid monohydrazide (N-Boc-succinic acid monohydrazide)

N-Boc- succinic acid monohydrazide was used as linker molecule for the hydrazone bond formation.³⁴

In a round-bottom flask succinic anhydride (0.5 g, 5.0 mmol) was dissolved in CH₂Cl₂ (20 mL), then DMAP (5 mg, 0.039 mmol) was added. Subsequently, a solution of *tert*-butyl carbazate (0.67 g, 5.0 mmol) in dichloromethane (7 ml) was added dropwise under stirring. The reaction proceeded for about 12 hour at room temperature. The solvent was removed under reduce pressure. Then the crude product was purified by flash column chromatography (chloroform/methanol 90:10 v/v).

¹H NMR (300 MHz, CDCl₃) δ: 8.83 (s, 1H), 8.28 (s, 1H), 7.43 (s, 1H), 2.74-2.58 (m, 2H, (CH₂COOH), 2.57-2.44 (m, 2H, (CH₂CONHNH), 1.43 (m, 9H, (CH₃)₃) (SPETTRO 22-3-17); ¹³C NMR (75 MHz, CDCl₃) δ: 176.07, 172.14, 156.11, 81.97, 28.97, 28.36, 28.12; GC/MS (EI, 70 eV) m/z (% rel.): 232 [M⁺] (19), 176 (39), 159 (45), 132 (26), 114 (15), 101 (9), 76 (8), 57 (100).

9.3.4.2. Synthesis of MSNs conjugated to succinic acid monohydrazide linker (FOL-MSN-hydrazine)

N-Boc-succinic acid monohydrazide was conjugated to MSNs through the formation of an amide bond between the carboxyl group of succinic acid moiety and the amino functions present on the wall of the **FOL-MSN-APin** pores. Boc group was then removed under acid conditions in order to generate the hydrazine functional group through which is formed the hydrazone bond with DOXO.

N-Boc-succinic acid monohydrazide (0.210 g, 0.90 mmol) was dissolved in 5 mL of DMSO then EDC (0.176 g, 0.91 mmol) and sulfo-NHS (0.199 g, 0.9 mmol) were added. After about 1 hour a suspension of **FOL-MSN-APin** (0.635g) in 25 mL of DMSO was added and the reaction mixture was left under stirring for 24 hours at room temperature, Finally, the suspension was filtered and washed with DMSO and diethyl ether and then dried at 45°C overnight.

The obtained powder (**FOL-MSN-hydrazine-Boc**) was dissolved in 20 mL of CH₂Cl₂/TFA (10% TFA in CH₂Cl₂ by volume), the resulting reaction mixture was left under stirring for 24 hours. Then, was centrifuged (9000 rpm for 10 minutes) and the obtained sediment was plenty washed with anhydrous CH₂Cl₂. The recovered nanoparticles (**FOL-MSN-hydrazine**) were dried at 45°C overnight.

9.3.4.3. Synthesis of FOL-MSN-HYD-DOXO

Doxorubicin hydrochloride (0.020 g) was dissolved in anhydrous tetrahydrofuran (10 mL) thus **FOL-MSN-hydrazine** (0.200 g) was added and the pH adjusted to pH~5 with acetic acid. The drug was loaded with a ratio of 1:1,5 (Linker molecule: DOXO), the linker amount was determined with TGA analysis.

The reaction was performed at room temperature under anhydrous conditions. After stirring for 24 h the drug loaded nanoparticles were filtered and then washed with anhydrous tetrahydrofuran. The resulting precipitate was suspended in anhydrous THF and a second drug loading was carried out under the same previously described reaction conditions. Then the reaction mixture was filtered and washed plenty with anhydrous THF and dichloromethane. The obtained nanomaterial **FOL-MSN-HYD-DOXO** was stored in sealed containers at -20°C, under anhydrous conditions. The amount of DOXO loaded (7,5 %) was quantified by UV-VIS ($\lambda_{\text{abs}} = 482 \text{ nm}$).

9.3.5. *In vitro* experiments

The effect of the synthesized **FOL-MSN-DOXO** systems on cell proliferation was assessed by trypan blue exclusion assay. All cell lines in the exponential growth phase were plated in the following way: BJhTERT and HeLa cells were seeded in triplicate in 12-well plates at a concentration of 105 cells/well and grown overnight.

The following day, cells were synchronized in serum free media (SFM) for 24h, so that most of the cells belonged to a population in the same cell cycle phase, to avoid growth differences among cells.

RPMI-8226 were seeded in 100mm untreated plates at the concentration of 3×10^6 cell/dish, directly in SFM where grown for 24h.

All samples were suspended (1mg) in 5ml SFM, stirred for 30'. Therefore, the suspensions were added to the cells: 10ug/well for BJhTERT, HeLa, and 300ug/dish for RPMI-8226. Whereas 1mg of doxorubicin powder were dissolved in 1ml DMSO and added to the cells at the final concentration of 0,5ug/well (BJhTERT/HeLa) and 5ug/dish (RPMI-8226).

After 1h the cells were washed twice in PBS and the medium was then replaced with fresh medium plus 1% FBS. In this phase RPMI-8226 were collected in falcon tubes and

centrifuged at 500-600 rpm to pellet only the live cells and discard most of dead cells and nanoparticles. The pellet is thus resuspended in fresh medium with 1% FBS and seeded in 12-well no-treated plates at the confluence of 100,000/well.

After 3 days, both cell lines have been counted: BJhTERT and HeLa cells were harvested by trypsinization; RPMI-8226 have been collected in eppendorf directly. Each collected sample was incubated in a 0.5% trypan blue solution for 1 min at room temperature (20ul+20ul). Cell viability was determined by Countess Automated Cell Counter (Invitrogen, Life Technology, IT).

9.3.6. *In vitro* release studies

DOXO release experiments were performed in media mimicking the physiological conditions (pH 7.4) and the acidic endolysosomal compartment (pH 5.0).

A dispersion of **FOL-MSN-IM-DOXO** (19 mg) in acetate buffer or phosphate buffer (5 mL) was loaded in a dialysis bag (cut-off 12kDa) that was immersed in 60 mL of the corresponding buffer solution and stirred.

At pre-established times, 1 mL of release medium was collected, replaced with 1 mL of fresh solution buffer and analyzed with a UV-Vis absorption spectrophotometer ($\lambda_{\text{abs}} = 485 \text{ nm}$) using standard calibration curves of DOXO (range of 5-50 ppm) prepared under the same conditions. Experiments were performed in triplicate.

9.4. Conclusion and Outlook

In this work, we designed and synthesized MSNs-based nanodevices (FOL-MSN-DOXO) with folate-mediated cell uptake for the controlled release of the anticancer drug doxorubicin. The effect of MSNs on cell proliferation was evaluated on FR+ and FR- cell lines.

The *in vitro* test of FOL-MSN-IM-DOXO system, in which the drug is linked to the nanocarrier via an imine bond, showed some toxicity also on FR- BJhTERT cells due to the premature drug release at physiological pH demonstrating a moderate stability of imine bond at neutral pH.

The second system (FOL-MSN-HYD-DOXO), in which the drug is conjugated to the nanoparticles through a hydrazone bond gave interesting results since it showed a good FR+ cancer cell killing efficacy and consequently an enhanced cellular uptake by FR positive cancer cells and a negligible cytotoxicity to FR- negative cells.

The developed system FOL-MSN-HYD-DOXO represents a versatile drug delivery system useful as template for the development of a highly selective and efficient targeted DOXO delivery systems in which the targeting function is a peptide molecule that, interacting with specific receptors overexpressed on cancer cells, addresses the drug exclusively to cancer cells avoiding the normal ones.

References

1. Lee C H, Cheng S H, Huang I P, Souris J S, Yang C S, Mou C Y and Lo L W 2010 *Angew. Chem. Int. Edn.* 49:214–9)
2. P.A. Henriksen, *Heart*, **2017**, 0:1–7.
3. L. Gianni, L. Norton, N. Wolmark, T.M. Suter, G. Bonadonna, G.N. Hortobagyi, *J Clin Oncol* , **2009**, 27:4798-4808.
4. S. Beslija, *Breast Cancer Res Treat*, **2003**, 81(Suppl 1): 25.
5. J. V. McGowan, R. Chung, A. Maulik, I. Piotrowska, J. M. Walker, D. M. Yellon, *Cardiovasc Drugs Ther*, **2017**, 31:63–75.
6. G. Cassinelli, *Tumori.*, **2016**, 3:226-35.
7. C.F. Thorna, C. Oshiroa, S. Marshe, T. Hernandez-Boussardb, H. McLeodd, T.E. Kleina, and R.B. Altmana, *Pharmacogenet Genom*, **2011**, 21,7:, 440-446.
8. G. Minotti, P. Menna, E. Salvatorelli, G. Cairo, L. Gianni, *Pharmacol Rev*, **2004**, 56, 185-229.
9. K. Chatterjee, J. Zhang, N. Honbo, J.S. Karliner, *Cardiology*, **2010**, 115, 155-162.
10. D. L. Hershman, A. Eisenberger, J. Wang, J. Jacobson, V. Grann, R. McBride, W. Tsai, and A. Neugut, *J Clin Oncol*, **2007**, 25,18, 3159-3165.
11. L.A. Smith, V.R. Cornelius, C.J. Plummer, G. Levitt, M. Verrill, P. Canney and A. Jones, *BMC Cancer*, **2010**, 10,337.
12. Gewirtz DA, *Biochem. Pharmacol.*, **1999**, 57, 727-741.
13. M.R. Ray, C. Lakshmi, C. Deb, C. Ray and T. Lahiri, *Comp. Haematol. Int.*, **2000**, 10, 212-220.
14. T. Šimunek, M. Štirba, O. Popelová, M. Adamcová, R. Hrdina, V. Geršl, *Pharmacol Rep*, **2009**, 61, 154-171.
15. S. Zhang, X. Liu, T. Bawa-Khalfe, L.S. Lyu, L.F. Liu, E.T. Yeh, *Nat Med*, **2012**, 18, 1639-1642.
16. G. Akolkar, N. Bhullar, H. Bews, B. Shaikh, S. Premecz, K.-A. Bordun, D.Y.C. Cheung, V. Goyal, A. K Sharma, P. Garber, P.K. Singal, and D.S. Jassal, *Cardiovasc Ultrasound.*, **2015**, 13, 18.
17. J.H. Doroshov, *Biochem. Biophys. Res. Commun.*, **1986**, 135, 1, 330-335.
18. L. Brannon-Peppas, J.O. Blanchette, *Adv Drug Deliv Rev*, **2012**, 64, 206-212.
19. N. Zhao, M.C Woodle, and A.J. Mixson, *J Nanomed Nanotechnol.*, **2018**, 9, 5: 519.
20. D. N. Waterhouse, P.G. Tardi, L.D. Mayer, M. B. Bally, *Drug-Safety*, **2001**, 24: 903.
21. I. Slowing, J.L. Vivero-Escoto, C-W. Wu, VS-Y. Lin, *Adv. Drug Deliv.Rev.*, **2008**, 60, 1278-1288.
22. A. Nigro, M. Pellegrino, M. Greco, A. Comandè, D. Sisci, L. Pasqua, A. Leggio, and C. Morelli, *Pharmaceutics*, **2018**, 10, 250.

23. L. Pasqua, I.E. De Napoli, A. Leggio, C. Morelli, A. Comandè, A. Nigro, M. Greco, G. Montera, "Engineered Stimuli-Responsive Nanoparticles for the Interaction With Biological Structures", *Chemistry of Silica and Zelite-based Materials: Synthesis, Characterization and Applications*, Elsevier, Chapter 21, 399-412, **2019**.
24. S. Jafaria, H. Derakhshankhaha, L. Alaeib, A. Fattahia, B.S. Varnamkhashtia, A.A. Sabouryb, *Biomed Pharmacother.*, **2019**, 109, 1100-1111.
25. R. Narayan, U.Y. Nayak, A.M. Raichur, and S. Garg, *Pharmaceutics*, **2018**, 10, 3: 118.
26. M. Martinez-Carmona, A. Baeza, M.A. Rodriguez-Milla, J. Garcia-Castro, M.Vallet-Regi, *J. Mater. Chem. B*, **2015**, 3, 5746–5752.
27. J. Mo, L. He, B. Ma, T. Chen, *ACS Appl. Mater. Interfaces*, **2016**, 8, 6811–6825.
28. D. Li, J. Tang, C. Wei, J. Guo, S. Wang, D. Chaudhary, C. Wang, *Small*, **2012**, 17, 2690-2697.
29. G. Cavallaro, P. Pierro, and F. S. Palumbo, F. Testa, L. Pasqua, and R. Aiello, *Drug Delivery*, **2004**, 11:41-46.
30. L. Pasqua, F. Testa, R. Aiello, S. Cundari, J.B. Nagy, *Micropor Mesopor Mat*, **2007**, 103, 166-173.
31. C. Morelli, P. Maris, D. Sisci, E. Perrotta, E. Brunelli, I. Perrotta, M.L. Panno, A. Tagarelli, C. Versace, M.F. Casula, F. Testa, S. Andò, J. B. Nagy and L. Pasqua, *Nanoscale*, **2011**, 3, 3198.
32. N. Garofalo, A. Comandè, I. Perrotta, M. Davoli, G. Niceforo and L. Pasqua, *Adv. Sci. Lett.*, **2017**, 23, 6026-6028.
33. L. Pasqua, I.E. De Napoli, M. De Santo, M. Greco, E. Catizzone, D.Lombardo, G. Montera, A. Comandè, A. Nigro, C. Morelli and A. Leggio, *Nanoscale Adv.*, **2019**, 1, 3269-3278.
34. L. Pasqua, A. Leggio, A. Liguori, C. Morelli, S. Andò "Bortezomib-Based Delivery System". WO 2016174693 A1 3-11-2016 (PCT/IT2016/000111 29-4-2016)
35. S.D. Weitman, R.H. Lark, L.R. Coney, D.W. Fort, V. Frasca, V.R. Jr Zurawski, B.A. Kamen, *Cancer Research*, **1992**, 52, 3396-3401.
36. C.M. Paulos, J.A. Reddy, C.P. Leamon, M.J. Turk, P.S. Low, *Mol Pharmacol*, **2004**, 66,1406-1414.
37. J. Fan, G. Fang, X. Wang, F. Zeng, Y. Xiang and S. Wu, *Nanotechnol.*, **2011**, 22, 455102-455113.
38. S. Mura, J. Nicolas, P. Couvreur, *Nat. Mat.*, **2013**, 12: 991-1003.
39. A. Asokan, M.J. Cho, *J. Pharm. Sci.*, **2002**, 91, 4, 903-913.
40. C. Wang, T. Zhao, Y. Li, G.Huang, M.A. White, and J. Gao, *Adv Drug Deliv Rev.*, **2017**, 113: 87-96.
41. E.R. Gillies, A.P. Goodwin, J.M. J. Fréchet, *Bioconjugate Chem.*, **2004**, 15, 6, 1254-1263.

42. J.-K. Kim, V.K. Garripelli, U.-H. Jeong, J.-S. Park, M.A. Repka, and S. Jo, *Int J Pharm.*, **2010**, 401, 1-2: 79–86.
43. L. Matesic, J. M. Locke, K.L.Vine, M. Ranson, J.B.Bremner, D. Skropeta, *Bioorg Med Chem*, **2011**, 19, 5, 1771-1778.
44. N. Deirram, C. Zhang, S.S. Kermaniyan, A.P.R. Johnston, *Macromol. Rapid Commun.*, **2019**, 40, 1800917-1800930.
45. X. Qu, Z. Yang, *Chem. Asian J*, **2016**, 11, 2633-2641.
46. J.E. Lee, D.J. Lee, N. Lee, B. H. Kim, S. H. Choi and T. Hyeon, *J. Mater. Chem.*, **2011**, 21, 16869-16872.
47. S.J. Sonawane, R.S. Kalhapure, T. Govender, *Eur J Pharm Sci.*, **2017**, 1, 99:45-65.
48. B.D. Nkazi, E.W. Neuse, E.R. Sadik, B.A. Aderibigbe, *J Drug Deliv Sci Technol*, **2013**, 23, 6:537-545.
49. R. Tang, W. Ji, D. Panus, R.N. Palumbo, C. Wang, *J Control Release*, **2011**, 151, 1:18-27.
50. Depan, D.; Shah, J.; Misra, R.D.K. *Mater. Sci. Eng. C* 2011, 31, 1305–1312.
51. R. Kohn, M. Froba, *Catal Today*, **2001**, 68, 227-236.